POTSDAM UNIVERSITY

Quantifying Impacts of Climate Extreme Events on Vegetation

Event Coincidence Analysis and its Applications Across Scales

by

Jonatan Frederik Siegmund

A cumulative dissertation submitted in partial fulfillment
for the
degree of 'doctor rerum naturalium' (Dr. rer. nat.)

Faculty of Science
Institute for Earth- and Environmental Science

Supervisors
Prof. Dr. Gunnar Lischeid
Dr. Reik Donner

January 2018

„Anfänger bedürfen des Mutes um voranzuschreiten, Fortgeschrittene der Demut um nicht zurückzugehen.“

Wilhelm von Kügelgen, 1870

Published online at the
Institutional Repository of the University of Potsdam:
URN urn:nbn:de:kobv:517-opus4-407095
http://nbn-resolving.de/urn:nbn:de:kobv:517-opus4-407095

Abstract

Together with the gradual change of mean values, ongoing climate change is projected to increase frequency and amplitude of temperature and precipitation extremes in many regions of Europe. The impacts of such in most cases short term extraordinary climate situations on terrestrial ecosystems are a matter of central interest of recent climate change research, because it can not per se be assumed that known dependencies between climate variables and ecosystems are linearly scalable. So far, yet, there is a high demand for a method to quantify such impacts in terms of simultaneities of event time series.

In the course of this manuscript the new statistical approach of Event Coincidence Analysis (ECA) as well as it's R implementation is introduced, a methodology that allows assessing whether or not two types of event time series exhibit similar sequences of occurrences. Applications of the method are presented, analyzing climate impacts on different temporal and spacial scales: the impact of extraordinary expressions of various climatic variables on tree stem variations (subdaily and local scale), the impact of extreme temperature and precipitation events on the flowering time of European shrub species (weekly and country scale), the impact of extreme temperature events on ecosystem health in terms of NDVI (weekly and continental scale) and the impact of El Niño and La Niña events on precipitation anomalies (seasonal and global scale).

The applications presented in this thesis refine already known relationships based on classical methods and also deliver substantial new findings to the scientific community: the widely known positive correlation between flowering time and temperature for example is confirmed to be valid for the tails of the distributions while the widely assumed positive dependency between stem diameter variation and temperature is shown to be not valid for very warm and very cold days. The larger scale investigations underline the sensitivity of anthrogenically shaped landscapes towards temperature extremes in Europe and provide a comprehensive global ENSO impact map for strong precipitation events.

Finally, by publishing the R implementation of the method, this thesis shall enable other researcher to further investigate on similar research questions by using Event Coincidence Analysis.

Acknowledgements

Für die vielfältige Unterstützung während meiner Arbeit an diesem Manuskript möchte ich danken:
Zuerst natürlich meinem Betreuer Dr. Reik Donner für die umfangreiche Hilfe beim Einwerben des Stipendiums, für die geduldige Zusammenarbeit bei allen Publikationen und für das stets 'offene Ohr' bei allerlei Schwierigkeiten des wissenschaftlichen Lebens. Ich danke Prof. Dr. Gunnar Lischeid für die wissenschaftliche Betreuung meiner Promotion, für seine pragmatischen Ratschläge und seine ungewöhnlich schnelle Kommunikation. Desweiteren danke ich meinen Kollegen von 'CoSy' Marc Wiedermann, Chiranjit Mitra, Jasper Franke und Julian Maluk für die stets anregenden und konstruktiven Diskussionen, welche einen wichtigen Beitrag zu meiner Arbeit geleistet haben - stay cosy! Desweiteren danke ich Dr. Jonathan Donges für seine vielfältigen wichtigen Ratschläge und Dr. Gerd Helle sowie Tanja Sanders für die Einführung in die 'Dendro-Community'. Ich danke dem Evangelischen Studienwerk Villigst e.V. für die finanzielle Unterstützung. Schließlich und nicht zuletzt danke ich meiner lieben Frau Nicole, die mir während der gesamten Zeit eine phantastische Diskussionspartnerin und Kollegin war und ohne die ich gar nicht erst zur Klimaforschung gekommen wäre.

Contents

Abstract **ii**

Acknowledgements **iii**

Abbreviations **v**

1 Introduction **1**
1.1 Climate Change and Extreme Events 1
1.2 Contributing Publications 6

2 Manuscripts **9**
2.1 Event coincidence analysis for quantifying statistical interrelationships between event time series 9
2.2 Impact of temperature and precipitation extremes on the flowering dates of four German wildlife shrub species 27
2.3 Meteorological Drivers of Extremes in Daily Stem Radius Variations of Beech, Oak, and Pine in Northeastern Germany: An Event Coincidence Analysis 53
2.4 CoinCalc - A new R package for quantifying simultaneities of event series 75
2.5 Impacts of temperature extremes on European vegetation during the growing season 85
2.6 Differential imprints of distinct ENSO flavors in global extreme precipitation patterns 99

3 Discussion **111**

4 Summary **116**

Bibliography **118**

Abbreviations

GPP	**G**ross **P**rimary **P**roduction
ECA	**E**vent **C**oincidence **A**nalysis
ECECA	**C**onditional **E**vent **C**oincidence **A**nalysis
SCR	**S**ignificant **C**oincidence **R**ate
SRV	**S**tem **R**adius **V**ariation
ENSO	**E**l **N**iño **S**outhern Oscillation

Chapter 1

Introduction

1.1 Climate Change and Extreme Events

In the course of the last decades climate change has become a predominant matter of discussion, both in environmental sciences and environmental policy - and due to easy-to-understand linkages between climate change and modern lifestyle, the issue of climate change is nowadays an almost omnipresent part of public debate [*Schäfer* (2016)] as well as of private thinking of many European citizen [*Engels et al.* (2013); *Eurobarometer* (2008)]. Yet, the public non-scientific debate is mostly held without a clear imagination of how exactly climate change could possibly impact environmental or human life aspects [*Eurobarometer* (2008)]. This discrepancy between the awareness of climate change in general and the low knowledge about its impacts has, to a certain degree, parallels to the development of climate change research during the past decades. During the first decades of modern climate change research, starting around the te 50's of the 20th century, the main focus lay on analyses of historic trends and future projections of physical and chemical environmental parameters such as atmospheric composition, temperature, moisture and others. Due to low data availability and/or quality as well as coarse temporal and spacial resolutions of climate models, in-depth analysis of the *impacts* of historic, recent or possible future climate developments on biological elements of the earth system have been rare for long time. Just during the last few years, following on the development of a large body of climate change studies, climate research nowadays focuses to a larger degree on the possible impacts of changing climate parameters like temperature and precipitation [*IPCC* (2013)]. Meanwhile, climate impact research has

made large efforts in investigating the impact of climate change on terrestrial [*Cramer et al.* (2001); *Walther et al.* (2002)] and marine ecosystems [*Hoegh-Guldberg and Bruno* (2010)], global biodiversity [*Heller and Zavaleta* (2009)] and human health [*Patz et al.* (2005)]. Due to the large amount of climate impact studies we are now better able to understand recent and assess possible future developments of the interplay between a changing climate and the connected ecosystems.

But: to a large degree these climate impact studies have so far been focused on the impacts of gradually changing atmospheric parameters. This may have three reasons: 1) The gradual rise of global mean temperature is the predominant characteristic of climate change and therefore assessments of the impacts of this development seems an obvious necessity. 2) Climate projections have been focusing on the development of the mean behavior (*the climatology*) of atmospheric variables like temperature and precipitation without providing reliable information about climate characteristics on shorter time scales. 3) The most commonly used statistical data analysis methods to account for the common behavior of climate and environmental variables are linear correlation and regression analysis which (only) allow for the assessment of the mean common behavior (common variance) of two variables of interest.

As a consequence, our knowledge about the impacts of climate events that can not be described by a gradual change (like climate extreme events) is determined by a much smaller amount of studies. Yet, since approximately the last five years the number of new ecologic studies about extreme climate impacts exceeded the number of new studies dealing with gradual changes [*Jentsch et al.* (2007)]. This is a very important development, because the interrelationship between climate and environment can not in general be assumed to be of linear nature - impacts may also for example only occur if a certain threshold is exceeded or have other nonlinear imprints [see e.g. *Burkett et al.* (2005) or *Rockström et al.* (2009)]. Yet, by far the largest part of these studies describe experiments [e.g. *Jentsch et al.* (2009); *Nagy et al.* (2013)], are case studies only investigating the impact of one specific example event [see e.g. *Arnone et al.* (2011); *Luterbacher et al.* (2007); *Marchand et al.* (2005); *Rutishauser et al.* (2008)] or analyze model output data [see e.g. *Rammig et al.* (2015)] just to give some prominent examples. The analysis of the impacts of extreme climate events on parts of the ecosystem on larger spacial *and* longer temporal scales based on real world observational data has remained a very rarely addressed task. The number of studies providing analyses of that kind can actually be counted on two hands: *Ma et al.* (2015) and *Anderson et al.* (2015) published studies

about climate extreme impacts on vegetation for Australia and Brazil based on satellite observations, *Xu et al.* (2012) and *Liu et al.* (2013) provided important studies using remote sensing products, as well, and only *Jentsch et al.* (2009) and *Crabbe et al.* (2016) explicitly analyzed climate extreme event impacts on vegetation on a European scale, *Zscheischler et al.* (2014) analyzed the impact of climate extremes in GPP on a global scale and *Menzel et al.* (2011) analyzed the impact of cold and warm spells on plant phenology between 1950 and 2010 for central Europe.

On the background of ongoing climate change there is an urgent need for further comprehensive in depth investigations of the impacts of climate extreme events on ecosystems and/or parts of them: After having markedly increased during the last century [*Coumou and Rahmstorf* (2012); *Haylock and Goodess* (2004); *IPCC* (2013); *Luterbacher et al.* (2004); *Tank and Konnen* (2003)], frequency and amplitude of climate extreme events are for many parts of the world projected to increase on the course of the upcoming century [*Coumou and Rahmstorf* (2012); *IPCC* (2013); *Kundzewicz et al.* (2006); *Kysely et al.* (2011); *Rahmstorf and Coumou* (2011); *Rajczak et al.* (2013); *Tank and Konnen* (2003)]. Although these events normally are only of small temporal extension, extremes in meteorological conditions can be huge challenges for terrestrial ecosystems. One example would be the temporal mismatch between symbiotic species due to different reactions to the unprecedented meteorological conditions [see e.g. *Burkle et al.* (2013); *Kudo and Ida* (2013); *Law et al.* (2000); *Parmesan et al.* (2000); *Rafferty et al.* (2015)].

As mentioned above, the lag of climate extreme event impact studies is also a matter of the lag of suitable methods. Almost all of the above mentioned studies used the concept of producing composites of the environmental variable of interest out of every time step where a climate extreme was indicated. These composites were then plotted as anomalies for visual interpretation. *Anderson et al.* (2015) did not even construct composites, but plotted a large number of anomaly maps (one for every time step) in order to visually compare the time steps with extreme climate events to other time steps with normal climate conditions. The expedience of such approaches is debatable.

An important exception is given by the study of *Liu et al.* (2013) where the data analysis was performed by a kind of 'workaround': In a first step all pixels of the data sets belonging to a certain group (climate regime) were combined to a large sample. Then the quantification of extreme event impacts was achieved by applying linear correlation analysis between the climate extreme event frequencies of all members of a group on the

one hand and the environmental extreme event frequencies of the respective pixels on the other hand. As a consequence, this approach comes with a strong reduction of the spacial resolution from a global 0.5 x 0.5 degree grid to eight biome classes.
The commonly used technique of visually analyzing anomaly patterns as well as the analysis of *Liu et al.* (2013) very well illustrate the necessity for a statistical tool that is capable to quantitatively characterize statistical interdependencies between (extreme) events of two time series. Furthermore, this necessity is also evident for time series that are not given in discrete values for each time step, but only consist of time steps with event and time steps without event (in the following called binary time series). Prominent examples for this kind of data are time series of volcanic eruptions, wildfires, El Niño or flood events. Especially in the case of binary time series it would additionally be of high interest to apply a measure that enables users for interpretations about a certain directionality of the relationship between the two event time series.
Thus, the research questions of this thesis, unifying and leading through the publications listed below, are:

General questions

- How can a new statistical measure be defined that quantifies simultaneities between two event time series and that is capable to differentiate between different directions of relationship?
- Is it possible to generate new findings about the impacts of climate extreme events on parts of the terrestrial ecosystem using this new method?
- How do these new findings differ from already known extreme climate impacts and do they qualitatively differ from general interrelationships found for the variables of interest (e.g. quantified by correlation analysis)?

Specific questions

Additionally to these general research questions, the single publications follow their own and independent questions along the course of extreme climate impacts:

- How does the flowering time of different domestic shrub species react to the occurrence of unusually warm and cold temperatures? Are there differences between the species? Are there regional differences on a larger scale?

- How do the very short term stem radius variations of domestic tree species react to the occurrence of those events? Are there differences between individuals and species?
- How is the overall ecosystem productivity in terms of NDVI effected by such events? How does this reaction differ among the subregions of Europe?
- Is it possible to retrace the global impacts of El Niño/ La Niña events that have been reported in literature by applying the new method and can this application reveal new, so far unknown or undocumented El Niño/ La Niña impacts? How can the different impacts of different types of ENSO events be quantified?

In order to work on this research questions, the manuscripts listed in the following chapter have been published/submitted in/to international scientific peer-reviewed journals. Additionally to answering the research questions, another important scope of this work is to assist other researches to further contribute to the field of climate impact research by building, publishing and distributing an implementation of the used methodology in R, one of the most commonly used statistical frameworks in environmental sciences.

1.2 Contributing Publications

Donges, J., C.-F. Schleussner, J. Siegmund, and R. Donner (2016), Event coincidence analysis for quantifying statistical interrelationships between event time series, *The European Physical Journal Special Topics*, *225*(3), 471–487

Publication comprehensively describing the novel approach of Event Coincidence Analysis.
My contribution to the publication:

- participation in general methodological discussions
- introduction of the bi-directionality of ECA: the differentiation between trigger and precursor coincidence rate
- proofread of the manuscript

Siegmund, J., M. Wiedermann, J. Donges, and R. Donner (2016a), Impact of temperature and precipitation extremes on the flowering dates of four German wildlife shrub species, *Biogeosciences*, *13*, 55415555, doi: 10.5194/bg-13-5541-2016

Publication analyzing the impact of very warm/cold and very wet/dry weather conditions on different time scales on the flowering date of four wildlife shrub species in Germany using the Event Coincidence Analysis.
My contribution to the publication:

- Conception of the work
- Data analysis and interpretation
- Illustrations
- Writing the article

Siegmund, J., T. Sanders, I. Heinrich, E. van der Maaten, S. Simard, G. Helle, and R. Donner (2016b), Meteorological Drivers of Extremes in Daily Stem Radius Variations of Beech, Oak, and Pine in Northeastern Germany: An

Event Coincidence Analysis, *Frontiers in Plant Sciences*, *7:733*, doi: 10.3389/fpls.2016.00733

Publication analyzing the impact of various extraordinary weather conditions on the daily stem radius variations of three different tree species in terms of Event Coincidence Analysis *and* notion/conception of a multivariate extension of the method: the conditional event coincidence analysis.
My contribution to the publication:

- Conception of the work
- Notion of the conditional event coincidence analysis
- Data analysis and interpretation
- Illustrations
- Writing the article

Siegmund, J. F., N. Siegmund, and R. V. Donner (2017), CoinCalc - A new R package for quantifying simultaneities of event series, *Computers and Geosciences*, *98*, 64–72, doi: 10.1016/j.cageo.2016.10.004

Publication presenting the new R Package `CoinCalc`, an R implementation of the Event Coincidence Analysis plus examples of how the package can be used including one example from *Siegmund et al.* (2016a) and one example dealing with soil sample data.
My contribution to the publication:

- Conception and implementation of the R package `CoinCalc`
- intensive bug-testing of the package
- Conception of the article
- Data analysis and interpretation
- Illustrations
- Writing the article

Baumbach, L., J. Siegmund, M. Mittermeier, and R. Donner (2017), Impacts of temperature extremes on european vegetation during the growing season, *Biogeosciences*, under Review

Publication analyzing simultaneities between extreme temperature events and extreme NDVI events over Europe using MODIS satellite remote sensing data and the Event Coincidence Analysis.
My contribution to the publication:

- Conception and design of the work
- Illustrations
- Partly writing the article, especially the chapters 'Methods', 'Results' and 'Discussion'
- Critical revision of the article

Wiedermann, M., J. Siegmund, J. Donges, and R. Donner (2017), Differential imprints of distinct enso flavors in global extreme precipitation patterns, *Climate Dynamics*, under Review

Publication dealing with the impacts of two different kinds of El Niño and La Niña Events on strong positive and negative precipitation anomalies on a global scale. My contribution to the publication:

- Partly conception and design of the work
- Data analysis and interpretation
- Illustrations
- Partly writing the article, especially the chapters 'Methods' and 'Results'
- Critical revision of the article

Chapter 2

Manuscripts

2.1 Event coincidence analysis for quantifying statistical interrelationships between event time series

Eur. Phys. J. Special Topics **225**, 471–487 (2016)
© EDP Sciences, Springer-Verlag 2016
DOI: 10.1140/epjst/e2015-50233-y

THE EUROPEAN PHYSICAL JOURNAL SPECIAL TOPICS

Regular Article

Event coincidence analysis for quantifying statistical interrelationships between event time series

On the role of flood events as triggers of epidemic outbreaks

J.F. Donges[1,2,a], C.-F. Schleussner[1,3], J.F. Siegmund[1,4], and R.V. Donner[1]

[1] Potsdam Institute for Climate Impact Research, Telegrafenberg A31, 14473 Potsdam, Germany
[2] Stockholm Resilience Centre, Stockholm University, Kräftriket 2B, 114 19 Stockholm, Sweden
[3] Climate Analytics, Friedrichstr. 231, Haus B, 10969 Berlin, Germany
[4] Institute of Earth and Environmental Science, University of Potsdam, Karl-Liebknecht-Str. 24-25, 14476 Potsdam-Golm, Germany

Received 28 July 2015 / Received in final form 6 April 2016
Published online 25 May 2016

Abstract. Studying event time series is a powerful approach for analyzing the dynamics of complex dynamical systems in many fields of science. In this paper, we describe the method of event coincidence analysis to provide a framework for quantifying the strength, directionality and time lag of statistical interrelationships between event series. Event coincidence analysis allows to formulate and test null hypotheses on the origin of the observed interrelationships including tests based on Poisson processes or, more generally, stochastic point processes with a prescribed inter-event time distribution and other higher-order properties. Applying the framework to country-level observational data yields evidence that flood events have acted as triggers of epidemic outbreaks globally since the 1950s. Facing projected future changes in the statistics of climatic extreme events, statistical techniques such as event coincidence analysis will be relevant for investigating the impacts of anthropogenic climate change on human societies and ecosystems worldwide.

1 Introduction

Climate extremes and related natural disasters are of major interest for research on climate change and its impacts, because their frequency and amplitude is projected to increase significantly in the future [1–3]. However, when it comes to the quantification of impacts of associated natural disasters on ecosystems [4] and society (e.g. in terms of triggering epidemics or social unrest [5]), there are only very few studies providing

[a] e-mail: donges@pik-potsdam.de

a systematic assessment beyond individual cases. In-depth studies in this field require tailored statistical analysis tools that allow for a quantitative characterization of statistical interdependencies between event time series and are also applicable to series comprising only a few events.

Time series of events or event series, here defined as an ordered set of N event timings $\{t_1, \ldots, t_N\}$, are the subject of study in many fields of science. In this paper, such event series are considered as binary, i.e. amplitudes associated to the event timings t_i are either not available or are not taken into account in the analysis (corresponding to a description as unmarked point processes). There are many real-world examples of event series of this type, including photon arrival times in physics [6], neuronal spikes in neurosciences [7,8], exchange of messages on communication networks in social science [9] or timings of climatic extreme events [1,2] and armed civil conflicts [10–12] in climate impact studies [13]. Many recent studies have focused on investigating statistical properties of single event series or point processes such as inter-event time distributions. For example, the analysis of human online communication reveals that waiting times between text messages do not follow an exponential distribution as expected from an uncorrelated (Poissonian) random process, but include bursts of frequent events interrupted by long periods of inactivity that can be better described by power-law distributions [9].

However, less work appears to be available in the literature on quantifying and systematically studying statistical interrelationships between two or more event series, particularly when compared to the wide range of methods of this type available for standard time series such as Pearson correlation [14], mutual information [15] or synchronization measures [16]. Particularly in neuroscience, techniques have been developed for measuring the similarity or synchrony of event series of neuronal spike trains [7,8,17–19]. In climatology, measures of event synchronization have been recently applied to study statistical interrelationships between extreme precipitation events and their complex spatial structure [20] using climate network approaches [21]. More specifically, this approach has been used to unravel the complex spatio-temporal patterns of heavy rainfall events in the Indian monsoon domain [20,22], derive predictors for extreme flood events in South America [23] and study regional climatological phenomena related to extreme precipitation over Central Europe [24].

Measures of event synchronization tend to be used mostly in an explorative mode of research aiming to reveal associations in large data sets of event series from neuroscience or climatology. However, some of the currently most debated problems in climate impact research, e.g. concerning climate-related variables such as extreme temperatures or the El Niño–Southern Oscillation as potential drivers of armed civil conflicts [10,11], call for a more in-depth analysis of statistical interrelations between event series. Extending upon previously applied event synchronization approaches, in this paper we formally put forward the alternative framework of event coincidence analysis [25] for investigating in detail the statistical interrelationships between pairs of event time series and testing hypotheses on the nature of these interrelationships. Event coincidence analysis is designed to measure the strength, directionality and time lag of statistical relations between event series. The method was introduced in a less general setting to study possible statistical interrelationships between nonlinear regime shifts in African paleoclimate during the past 5 million years and events in hominin evolution such as the appearance and disappearance of species [25]. It has also been applied to investigate the impacts of climatic extremes such as droughts and heat waves on vegetation productivity based on observational data and dynamic vegetation model runs [4]. Furthermore, event coincidence analysis has been used to evaluate different hypotheses on socio-economic factors influencing the vulnerability of countries to natural disasters with a focus on the possible triggering of outbreaks of civil conflicts [5].

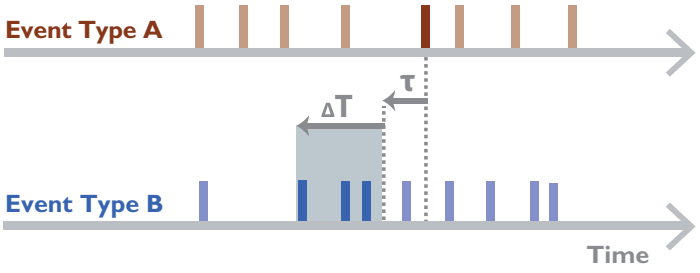

Fig. 1. Schematic illustration of event coincidence analysis for quantifying statistical interrelationships between two event time series A and B for the case of precursor coincidences. The assumption to be quantified and tested for is that events in B are precursors of events in A (under the condition that an A-event has occurred). Focusing on an event in series A (dark red bar), a (lagged) coincidence occurs with events in series B (dark blue bars) if the latter fall into the coincidence interval of width ΔT (grey bar) that can be shifted by a lag parameter τ. Coincidence rates are obtained by computing the relative frequency of occurrence of such coincidences for all events in series A (Sect. 2).

We argue that event coincidence analysis is a particularly useful tool in the area of climate impact studies, since it allows to statistically study the effects of such extreme events on other processes and explicitly takes their nature as event series into account. To illustrate the capabilities of our approach, we employ event coincidence analysis to assess extreme flood events as possible drivers of epidemics extending upon earlier work [4,5]. Applying the framework in this case study based on observational data yields evidence that, from a globally aggregated perspective, flood events have acted as drivers of epidemics in the same country in the past.

The structure of this paper is as follows: event coincidence analysis is thoroughly introduced in Sect. 2 including descriptions of the basic methodology, statistical null models for testing hypotheses and related approaches. Subsequently, the results of applying event coincidence analysis to event series of extreme floods and epidemics are reported in Sect. 3. Finally, Sect. 4 provides conclusions and perspectives for promising future extensions of the event coincidence analysis methodology.

2 Methods

In this section, we develop the method of event coincidence analysis that is concerned with quantifying the statistical interrelationships between pairs of event series, extending upon the approach introduced in [25]. A pair of *event time series* A and B is here defined as two ordered event sets with timings $\{t_1^A, \ldots, t_{N_A}^A\}$ and $\{t_1^B, \ldots, t_{N_B}^B\}$ with numbers of events N_A, N_B, respectively. Both event series are assumed to cover a time interval (t_0, t_f) of length $T = t_f - t_0$, such that $t_0 \leq t_1^A \leq \cdots \leq t_{N_A}^A \leq t_f$ and $t_0 \leq t_1^B \leq \cdots \leq t_{N_B}^B \leq t_f$. This yields event rates $\lambda_A = N_A/T$ and $\lambda_B = N_B/T$.

Event coincidence analysis is based on counting coincidences between events of different types. In the following, the assumption to be quantified and tested for is that events in B precede events in A, which is related to a possible causal influence from B- to A-type events (Fig. 1). The opposite case of assuming that events in A precede events in B can be accommodated by exchanging the labels A and B throughout the formulae and text.

An *instantaneous coincidence* is defined to occur if two events at t_i^A, t_j^B with $t_j^B < t_i^A$ are closer in time than a temporal tolerance or *coincidence interval* ΔT, i.e. if

$$t_i^A - t_j^B \leq \Delta T \tag{1}$$

holds. In turn, a *lagged coincidence* is defined as an instantaneous coincidence between the time shifted event at $t_i^A - \tau$, where $\tau \geq 0$ is a time lag parameter, and the event at $t_j^B < t_i^A - \tau$, i.e. if the condition

$$(t_i^A - \tau) - t_j^B \leq \Delta T \tag{2}$$

is satisfied.

Differing from the above problem formulation that is consistently used throughout this work, we note that event coincidence analysis can also be performed by employing coincidence intervals that are symmetric around A-events and relaxing the assumption that B-events must precede A-events. The resulting condition $|t_i^A - t_j^B| \leq \Delta T$ can be meaningful, e.g. given event series with pronounced dating uncertainties as in the case of archeological, paleontological and paleoenvironmental data [25].

In the following, we introduce the concept of the *coincidence rate* between a single pair of event series (Sect. 2.1) as well as an aggregated coincidence rate for taking into account several pairs of event series (Sect. 2.2). Section 2.3 discusses coincidence statistics for null models of stochastic point processes that can be used to test the statistical significance of coincidence rates estimated from data. Moreover, we put event coincidence analysis into the context of other related approaches for the analysis of event time series (Sect. 2.4).

Many of the measures and significance tests described below are implemented in the open source software package `CoinCalc` [26] written in the programming language R which is available at `https://github.com/JonatanSiegmund/CoinCalc`.

2.1 Coincidence rates for a pair of event series

For quantifying the strength of statistical interrelationships between two event time series A and B, we introduce two variants of coincidence rates addressing B-type events as *precursors* and *triggers* of A-type events, respectively. In the first case, the *precursor coincidence rate*

$$r_p(\Delta T, \tau) = \frac{1}{N_A} \sum_{i=1}^{N_A} \Theta \left[\sum_{j=1}^{N_B} 1_{[0,\Delta T]} \left((t_i^A - \tau) - t_j^B \right) \right], \tag{3}$$

measures the fraction of A-type events that are preceded by at least one B-type event (note that multiple B-type events within the coincidence interval are counted only once, see also Fig. 1). Here, $\Theta(\cdot)$ denotes the Heaviside function (here defined as $\Theta(x) = 0$ for $x \leq 0$ and $\Theta(x) = 1$ otherwise) and $1_I(\cdot)$ the indicator function of the interval I (defined as $1_I(x) = 1$ for $x \in I$ and $1_I(x) = 0$ otherwise). In the second case, the *trigger coincidence rate*

$$r_t(\Delta T, \tau) = \frac{1}{N_B} \sum_{j=1}^{N_B} \Theta \left[\sum_{i=1}^{N_A} 1_{[0,\Delta T]} \left((t_i^A - \tau) - t_j^B \right) \right], \tag{4}$$

measures the fraction of B-type events that are followed by at least one A-type event (note that multiple A-type events within the coincidence interval are counted only once). Distinguishing between precursor and trigger coincidence rates allows to introduce a certain notion of directionality to the method of event coincidence analysis. Furthermore, the parameter τ allows to explicitly take into account lagged relationships between event series.

2.2 Aggregated coincidence rates

In some applications, it can be relevant to have at hand an integrated measure for coincidences that occur between several pairs of event series as in the case of events that are available on a spatial grid or for different regions or countries. For example, consider multiple country-wise sets of A-type events (floods) and B-type events (epidemic outbreaks) as in the application presented in Sect. 3. In this case, coincidences can only be meaningfully counted on a per-country basis, but it is desirable to quantify the aggregated coincidence rate over all countries in the data set or a suitably filtered subset of countries to obtain a global measure of the strength of the relationship between the two event types considered and its statistical significance with respect to different null hypotheses [5]. Another motivation for considering aggregate measures of coincidence relationships is related to data quality. In some applications with small event numbers N_A, N_B, only aggregation over several pairs of event series allows to draw robust statistical conclusions.

Analogously to the case of a single pair of event series, two flavors of aggregated coincidence rates are defined as follows given a set G of pairs of A- and B-type events. The *aggregated precursor coincidence rate*

$$r_p^G(\Delta T, \tau) = \frac{\sum_{k\in G}\sum_{i=1}^{N_{A,k}} \Theta\left[\sum_{j=1}^{N_{B,k}} 1_{[0,\Delta T]}\left((t_i^{A,k}-\tau)-t_j^{B,k}\right)\right]}{\sum_{k\in G} N_{A,k}} \tag{5}$$

measures the total number of precursor coincidences occurring in all pairs of event series normalized by the maximum possible number of such coincidences. Along the same lines, the *aggregated trigger coincidence rate*

$$r_t^G(\Delta T, \tau) = \frac{\sum_{k\in G}\sum_{i=1}^{N_{B,k}} \Theta\left[\sum_{j=1}^{N_{A,k}} 1_{[0,\Delta T]}\left((t_i^{A,k}-\tau)-t_j^{B,k}\right)\right]}{\sum_{k\in G} N_{B,k}} \tag{6}$$

is the accordingly normalized total number of trigger coincidences occurring in all pairs of event series in G. Note that for both types of aggregated coincidence rates, multiple events falling within the coincidence window are counted only once, as in the definition of coincidence rates for a single pair of event series (Sect. 2.1).

Studying aggregated coincidence rates can be seen as a first step towards a systematic analysis of coincidences in more general spatio-temporal event data. Such data can be conceptionalized as being generated by spatial or spatio-temporal point processes [27,28]. More generally, events of interest for an extended event coincidence analysis can also take the form of higher dimensional objects with a nontrivial shape in terms of, e.g. latitude, longitude and time, such as the spatio-temporal extremes in the fraction of absorbed photosynthetically active radiation (fAPAR) identified by Zscheischler et al. [29].

2.3 Statistics for null models of stochastic point processes

Treating stochastic point processes as generators of event time series allows to derive distributions of coincidence rates to test the statistical significance of the results of event coincidence analysis based on a hierarchy of null hypotheses, analogously to classical statistics and the method of surrogates for standard time series analysis [15,30]. Here, we focus on Poisson processes without temporal correlations between events (Sect. 2.3.1) and point processes with a prescribed inter-event time distribution $P(\Delta t)$ that allow to consider, e.g. processes with heavy-tailed $P(\Delta t)$ that tend

to produce bursts of events (Sect. 2.3.2). More generally, classes of null models for point processes of interest include, for example, event series with higher-order memory effects such as correlations between event bursts [31] that are, however, beyond the scope of this paper. We also briefly touch upon the possibility of constructing surrogate event series from time series surrogates (Sect. 2.3.3).

Analytical results are given below where available, otherwise we rely on Monte Carlo simulations. For illustration, we restrict ourselves to a single pair of event time series, the case of sets of event series can be treated analogously. Significance tests based on the null hypothesis of Poisson processes following a Monte Carlo approach are applied in Sect. 3 to quantify the statistical interrelationships between flood events and epidemic outbreaks.

2.3.1 Poisson processes

Here, we assume that both A- and B-type events are generated by Poisson processes with event rates λ_A and λ_B, respectively. This assumption implies that both types of events are distributed randomly, independently and uniformly over the continuous time interval of length T. Since our focus is on using the derived statistics for hypothesis testing on data sets with typically small numbers of events in each series, we assume fixed event numbers $N_A = \lambda_A T$ and $N_B = \lambda_B T$. Note that the analytically derived estimators presented below are only expected to yield reliable results in the limit of sufficiently large event numbers

$$N_A \gg 1 \text{ and } N_B \gg 1. \tag{7}$$

First, we analytically derive the statistics of precursor coincidence rates extending upon [25]. The probability for a (lagged) precursor coincidence between an A-event and a preceding B-event is given by the probability

$$p = \frac{\Delta T}{T - \tau} \tag{8}$$

that a B-event occurs randomly in a segment of length ΔT of the effective time span of interest $T-\tau$. This follows from the null hypothesis of Poisson processes generating the event series, where the probability for events to occur is the same in any time instant and is independent from the occurrence of other events, resulting in a linear dependence of p on ΔT.

Then the probability of a specific A-event to coincide with *at least one* of the N_B B-events is given by

$$1 - (1-p)^{N_B} = 1 - \left(1 - \frac{\Delta T}{T - \tau}\right)^{N_B}. \tag{9}$$

Note that when counting only exactly contemporaneous coincidences with $\Delta T = 0$, $p = 0$ follows in the limit of a continuous time axis. However, in real-world data sets, the time axis is often discrete, e.g. due to finite sampling intervals or finite numerical precision. In this common case, $p = 1/(T - \tau)$ needs to be used in the following with T and τ measured in numbers of time steps instead of units of absolute time when the interest is in coincidences with zero tolerance [32].

Based on this expression, we can calculate the probability $P(K; N_A, 1-(1-p)^{N_B})$ that exactly K precursor coincidences are observed for a given realization of the two Poisson processes. Even though A-events are assumed to be distributed independently in the interval $[0, T]$, to proceed with the derivation we need to further assume that

A-type events are typically spaced much more widely than the coincidence interval ΔT, i.e.

$$\Delta T \ll T/N_A. \tag{10}$$

When this condition (Eq. 10) is fulfilled, the events that a specific A_i-event coincides with *at least one* B-event and that another specific A_j-event coincides with *at least one* B-event can be considered statistically independent. Only then, $P(K; N_A, 1-(1-p)^{N_B})$ is given by the binomial distribution with N_A trials and a success probability $1-(1-p)^{N_B}$ [33] and, hence,

$$P(K; N_A, 1-(1-p)^{N_B}) = \binom{N_A}{K} \left(1 - \left(1 - \frac{\Delta T}{T-\tau}\right)^{N_B}\right)^{K} \left(\left(1 - \frac{\Delta T}{T-\tau}\right)^{N_B}\right)^{N_A-K}. \tag{11}$$

Using the relationship $K = r_p N_A$ to substitute K by r_p in the above equation yields the distribution of precursor coincidence rates $P(r_p; N_A, 1-(1-p)^{N_B})$.

From the distribution (Eq. (11)), the expectation value $\langle K \rangle$ and standard deviation $\sigma(K)$ can be straightforwardly derived as

$$\langle K \rangle = N_A \left(1 - (1-p)^{N_B}\right) = N_A \left(1 - \left(1 - \frac{\Delta T}{T-\tau}\right)^{N_B}\right) \tag{12}$$

and

$$\begin{aligned} \sigma(K) &= \sqrt{N_A \left(1 - (1-p)^{N_B}\right) (1-p)^{N_B}} \\ &= \sqrt{N_A \left(1 - \left(1 - \frac{\Delta T}{T-\tau}\right)^{N_B}\right) \left(1 - \frac{\Delta T}{T-\tau}\right)^{N_B}}. \end{aligned} \tag{13}$$

This yields the expectation value of the precursor coincidence rate

$$\langle r_p \rangle = \frac{\langle K \rangle}{N_A} = 1 - \left(1 - \frac{\Delta T}{T-\tau}\right)^{N_B} \tag{14}$$

and its standard deviation

$$\begin{aligned} \sigma(r_p) &= \sigma(K)/N_A \\ &= \sqrt{\frac{1}{N_A} \left(1 - \left(1 - \frac{\Delta T}{T-\tau}\right)^{N_B}\right) \left(1 - \frac{\Delta T}{T-\tau}\right)^{N_B}}. \end{aligned} \tag{15}$$

The p-value of an observation K_e with respect to the test distribution (Eq. (11)), i.e. the probability to obtain a number of coincidences K larger or equal to the empirically observed number K_e, is then given by

$$P(K \geq K_e) = \sum_{K^*=K_e}^{N_A} P(K^*; N_A, 1-(1-p)^{N_B}). \tag{16}$$

The statistics of trigger coincidence rates for event series generated by Poisson processes can be derived analogously by assuming a wide enough typical spacing of B-events:

$$\Delta T \ll T/N_B. \tag{17}$$

The distribution of the number of trigger coincidences K is then given by

$$P(K; N_B, 1-(1-p)^{N_A}) = \binom{N_B}{K} \left(1-\left(1-\frac{\Delta T}{T-\tau}\right)^{N_A}\right)^{K} \left(\left(1-\frac{\Delta T}{T-\tau}\right)^{N_A}\right)^{N_B-K} \tag{18}$$

yielding the expectation value and standard deviation of the trigger coincidence rate

$$\langle r_t \rangle = 1-\left(1-\frac{\Delta T}{T-\tau}\right)^{N_A} \tag{19}$$

and

$$\sigma(r_t) = \sqrt{\frac{1}{N_B}\left(1-\left(1-\frac{\Delta T}{T-\tau}\right)^{N_A}\right)\left(1-\frac{\Delta T}{T-\tau}\right)^{N_A}}, \tag{20}$$

respectively. As above, the p-value of an empirically observed number of trigger coincidences K_e can then be written as

$$P(K \geq K_e) = \sum_{K^*=K_e}^{N_B} P(K^*; N_B, 1-(1-p)^{N_A}). \tag{21}$$

In the case that the conditions (7), (10) and (17) are not met, Monte Carlo simulations need to be applied to compute statistics of event coincidence analysis such as the mean and standard deviation of coincidence rates or the significance level (p-value) of an observed coincidence rate corresponding to the null hypothesis that the empirical coincidence rate can be explained as the result of Poisson processes. To illustrate this issue, we compare the expectation values and standard deviations of trigger coincidence rates for Poisson processes derived from analytics and Monte Carlo simulation for different relative coincidence intervals $\Delta T/T$ and numbers of B-events N_B (Fig. 2). Indeed, the statistics are only comparable if conditions (7) and (17) are met, i.e. for $N_B \gg 1$ and $N_B \ll N_B^c(\Delta T/T) = (\Delta T/T)^{-1}$ (green line in Fig. 2), where $N_B^c(\cdot)$ denotes a critical value of N_B. Otherwise, Monte Carlo simulations show that the analytical approximation tends to overestimate the expected coincidence rate and its standard deviation, even though the approximations (Eqs. (14), (15)) show the correct asymptotic behavior of $r \to 0$ and $\sigma(r) \to 0$ for $\Delta T/T \to 0$ and $r \to 1$ and $\sigma(r) \to 0$ for $\Delta T/T \to 1$.

2.3.2 Stochastic point processes with prescribed inter-event time distribution

Compared to the Poisson processes discussed above, a more general null hypothesis is that the observed values of coincidence rates can be explained by stochastic point processes with a given distribution of inter-event times $P(\Delta t)$. For example, the inter-event time distribution for Poisson processes with average event rate λ is given by the exponential distribution

$$P_1(\Delta t) = \lambda e^{-\lambda \Delta t}. \tag{22}$$

However, it has been shown that many event time series display bursting behavior associated with inter-event time distributions having more slowly decaying (heavy) tails than the exponential distribution $P_1(\Delta t)$ [9,34]. For example, human violent conflicts were reported to display universal bursting behavior [34] associated with inter-event time distributions of the form

$$P_2(\Delta t) = \lambda F(\lambda \Delta t), \tag{23}$$

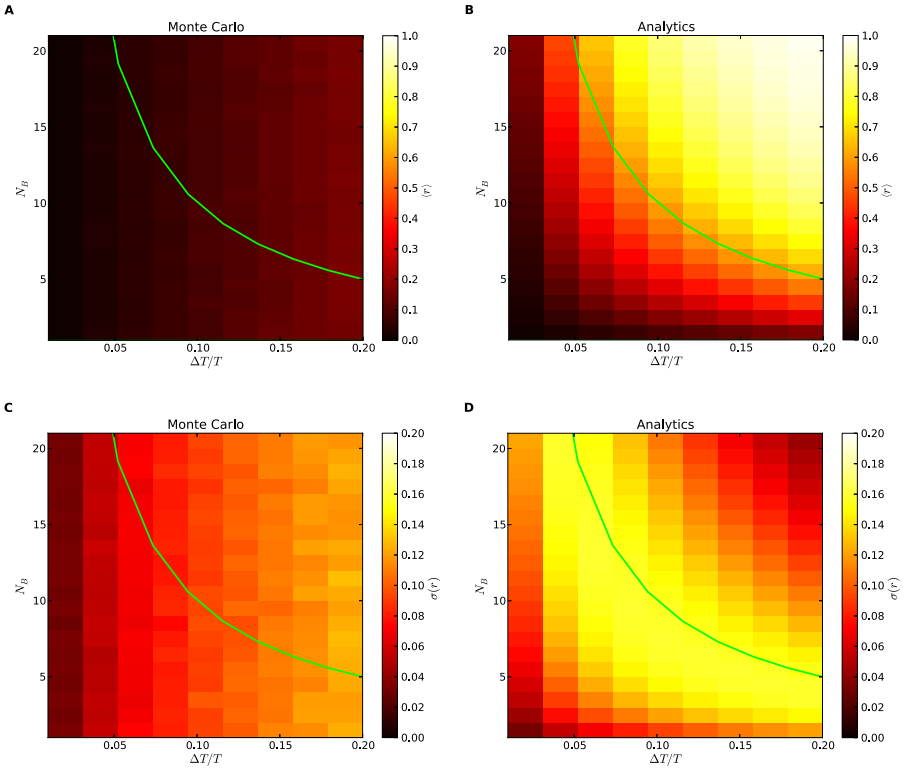

Fig. 2. Comparison of the expected trigger coincidence rate $\langle r_p \rangle$ (A,B) and its standard deviation $\sigma(r_p)$ (C,D) obtained using Monte Carlo simulation (A,C) and an analytical approximation (B,D) depending on the relative coincidence interval $\Delta T/T$ and the number of B-type events N_B. The analytical approximation is only accurate in the regime $N_B \gg 1$ and $N_B \ll N_B^c(\Delta T/T) = (\Delta T/T)^{-1}$ (green line), where $N_B^c(\cdot)$ denotes a critical value of N_B. In this example, the number of A-type events is $N_A = 10$, no lag is used ($\tau = 0$), events are distributed in the unit interval of width $T = 1$ and $m = 1,000$ trials are used in the Monte Carlo simulations for each considered combination of parameters.

where $F(\cdot)$ exhibits a power-law decay with exponent α such that

$$F(x) = ax^{-\alpha} \tag{24}$$

yielding

$$P_2(\Delta t) \propto \Delta t^{-\alpha}. \tag{25}$$

Power-law inter-event time distributions with an exponential cutoff

$$P_3(\Delta t) = C(\lambda \Delta t)^{\alpha} e^{-\lambda \Delta t/\beta} \tag{26}$$

have been reported to accurately describe the return time statistics of earthquakes [35] and other types of event series.

While deriving analytical results for coincidence statistics based on these and other classes of point processes with prescribed $P(\Delta t)$ remains the subject of future research, Monte Carlo simulations can be applied to obtain test distributions for assessing the statistical significance of empirically observed coincidence rates. Note that these tests can only be meaningfully applied in practice if either $P(\Delta t)$ can be estimated well from the empirically observed inter-event time statistics requiring a

sufficiently large number of events, or a good process understanding exists, i.e. the inter-event time distribution is known from theoretical considerations or observations from analogous systems. Alternatively, ensembles of surrogate event series can be generated by randomly shuffling inter-event time intervals given a large number of events. These conditions are not met for the application studied in Sect. 3, implying the need for restricting the analysis to the null hypothesis of Poisson processes there.

2.3.3 Surrogate event series generated from time series surrogates

In a number of relevant applications of event coincidence analysis, e.g. when studying climatological extreme events, event series are generated from underlying time series data. This transformation from time series to event data is typically achieved by thresholding to identify extreme events in the time series according to a prescribed quantile [4,32] or some other form of filtering. In this case, various types of time series surrogates [30] can be used to generate ensembles of event series for hypothesis testing by applying the same transformation to original and surrogate time series data. For example, univariate iterative amplitude adjusted Fourier transform (iAAFT) surrogates as implemented in [36] can be used to generate surrogate event series based on surrogate time series with the same amplitude distribution and autocorrelation function as the original data. This procedure is useful for constructing suitable significance tests for event coincidence analysis when extreme events in the series of interest tend to cluster due to pronounced autocorrelation in the underlying time series data, as it was found to be the case for European temperature, precipitation, tree ring width and simulated net primary productivity (NPP) [4]. Along these lines, bivariate event series surrogates derived from bivariate iAAFT time series surrogates could be used for testing the null hypothesis that observed coincidence rates can be explained by the co-occurrence of extremes due to the conserved linear cross-correlation structure of the underlying pair of time series.

2.4 Related methods

The complex systems-inspired framework of event coincidence analysis presented above is conceptually related to measures from spatial statistics for the correlation of spatial and spatio-temporal point processes [27,28] such as Ripley's cross-K [37] as well as various forms of regression analysis for point process data. Another popular related approach is considering measures of event synchronization for quantifying the similarity of event series [17,20,23]. Hence, the considerations on surrogate event series and significance tests given above could be applied to the latter concept as well, given that the requirements and basic assumptions are met. However, it should be noted that event synchronization lacks the distinction between coincidence interval ΔT and lag parameter τ provided by event coincidence analysis, and also does not allow to distinguish the cases of precursor and trigger coincidences.

While the statistical theory of temporal point processes appears generally less consolidated than the theory of standard time series [8], a multitude of methodologies for studying statistical interrelationships between event time series have been developed in the neurosciences in the last decades focussing on the specific, but important, application to neural spike trains. These techniques include methods focussing on the distributions of relative waiting times of events in series A with respect to events in series B [38], cross-correlograms and cross-intensity functions as well as frequency-domain methods, neural spike train decoding or information-theoretical methods [8].

Certainly, this wealth of alternative methodologies holds a great potential for fruitful applications in other fields of science, considering, for example, series of climatological extreme events and natural disasters.

It should also be mentioned that the statistical and mathematical literature contains a large number of less closely related studies of coincidences, e.g. considering the *birthday problem* [39]. The term *coincidence analysis* is also used in different contexts in fields such as elementary particle physics [40] or in the identification of causal dependencies in configurational data [41]. This is why we choose to use the more specific term *event coincidence analysis* when referring to the methodology introduced in this paper.

3 Application: Extreme flood events as possible drivers of epidemics

To illustrate the capabilities of event coincidence analysis, we apply it here to analyze the interrelations between two types of event time series of natural disasters, for which a causal relation is commonly assumed in the literature: hydrological flooding events (B-events) and outbreaks of epidemics (A-events) [42]. Our analysis is performed on the EmDAT data base covering the time interval 1950–2009 in a monthly time resolution [43]. This data base contains 3,468 flood events worldwide that are defined as a significant rise of water level in a stream, lake, reservoir or coastal region as well as 1,152 epidemic outbreaks, defined as either an unusual increase in the number of cases of an infectious disease that already exists in the region or population concerned, or the appearance of an infectious disease previously absent from a region. For each country k in the data base, a pair of event series is available containing $N_{f,k}$ flood events and $N_{e,k}$ epidemic outbreaks, respectively.

As described above, event coincidence analysis allows for two different test setups: in the first setup, we test on the basis of the occurrence of epidemic outbreaks and perform a coincidence test with flood events preceding epidemic outbreaks within a given coincidence interval (statistics based on precursor coincidences). Since we analyze coincidences based on the condition that an epidemic outbreak has occurred, this setup may also be termed a *risk enhancement test* [5]. In the second case, we perform the event coincidence analysis on the basis of occurrence of flood events that are followed by epidemic outbreaks (statistics based on trigger coincidences). We call this the *trigger test* [5], since it investigates a possible causal direction of flood events triggering epidemic outbreaks. In the following, we do not consider additional time lags between different types of events that are not covered already by the coincidence interval ΔT and, hence, set $\tau = 0$ (see Fig. 1). Furthermore, we compute aggregated coincidence rates covering all countries in the data base (Sect. 2.2) as well as coincidence rates on a country-wise basis (Sect. 2.1).

To test for statistical significance with the null hypothesis (NH) that the observed coincidences can be explained on the basis of event series generated by Poisson processes with the empirically observed event rates, Monte Carlo simulation is applied to generate pairs of surrogate event time series with conserved event numbers on an individual country basis by uniformly and independently drawing $N_{f,k}, N_{e,k}$, event timings over the full analysis period 1950–2009. We generate $m = 1,000$ ensemble members for each country and significance levels of 95% and 99% are applied for the rejection of the NH.

Figure 3 displays coincidence rates aggregated over all countries with available event data for coincidence intervals ΔT ranging from 0 to 24 months. While $\Delta T = 0$ implies considering coincidences within the same month, a 24-months window counts coincidences between 0 and 24 months after (before) a flooding (epidemic outbreak) event, respectively. For the risk enhancement test, we find that about 20% of all

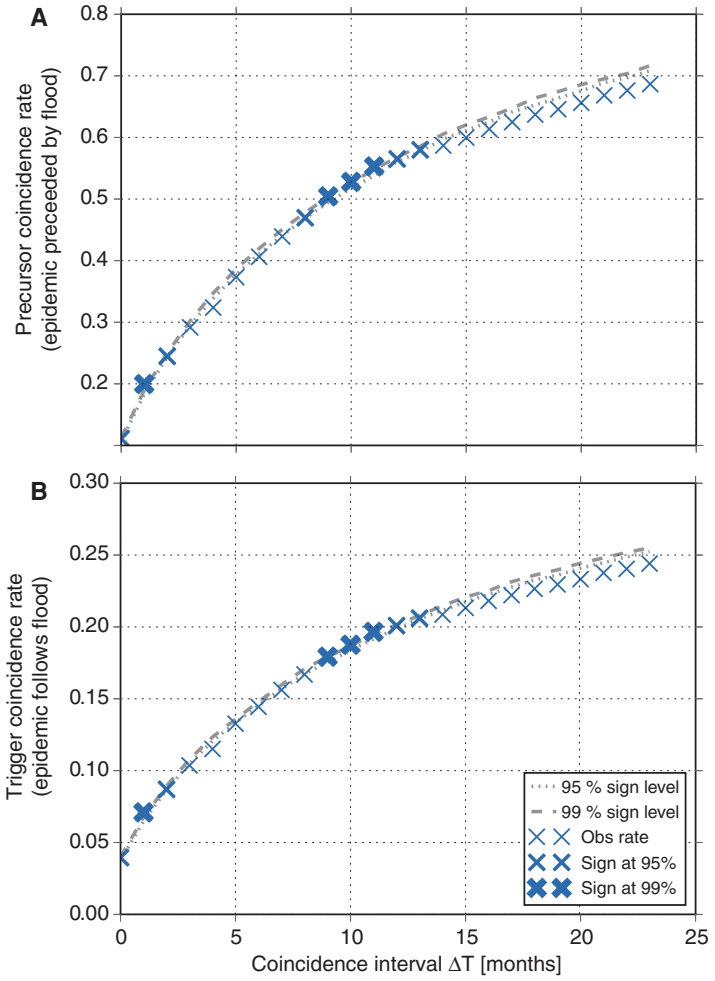

Fig. 3. Results of event coincidence analysis for the flood and epidemic outbreak event time series: Aggregated precursor (A) and trigger (B) coincidence rates. Dotted (dashed) grey lines mark the 95% (99%) significance level determined by Monte Carlo simulations. Coincidence rates that are significant at 95% (99%) levels are highlighted by bold markers.

epidemic outbreaks have been preceded by a flooding event within a month before the outbreak. Our corresponding results indicate that floods robustly contribute to the outbreak risk (Fig. 3A). While no direct causal attribution is possible based on this test, the trigger test (Fig. 3B) also robustly suggests a possible causal relationship. We find that about 7% of all flooding events have been followed by an epidemic outbreak in the next month, which is significant at the 99% level.

These results are robust also for other small coincidence intervals. In turn, for window widths ΔT exceeding 3 months, we do not find indications that the NH of the aggregated coincidence rate arising by chance can be rejected. However, this changes for window lengths between 9 and 13 months, where the NH can be rejected at least at the 95% level, indicating a robust long-range interrelation between the two types of events. In fact, more than 50% of all epidemic outbreaks have been preceded by a flooding event over a 12-months coincidence interval and about 20% of all flooding events have possibly triggered epidemic outbreaks within the 12 months following the natural disaster.

It should be noted that although we perform multiple hypothesis tests for varying coincidence intervals ΔT, standard corrections of the significance level to account for these multiple comparisons such as Bonferroni adjustments are not applicable in our case. This is particularly true for the corresponding universal null hypothesis that no statistical relationship exists between flood events and epidemic outbreaks for any of the ΔT [44,45]. In contrast, the two detected clusters of ΔT with statistically significant rates for both precursor and trigger coincidences around monthly and annual time scales indicate the existence of robust coincidence relationships that are present in the data. To further investigate the robustness of these findings, we performed Monte Carlo simulations to assess the probability that the null hypothesis is falsely rejected for fixed pairs of Poisson data surrogates for n values of ΔT. We find that the probability to observe $n = 4$ falsely rejected tests at a significance level of 99% (compare Fig. 3) in this setting is less than 0.001, implying that the results presented in Fig. 3 can be considered highly statistically significant when taking the effects of multiple testing in the specific setting of our study into account.

The global frequencies of flood events and epidemics are depicted in Fig. 4A,B, and the country-wise trigger coincidence rates for coincidences within the same month and a 12-months coincidence interval in Fig. 4C,D. While these maps give some guidance on where floods may have triggered epidemic outbreaks, they need to be interpreted with great caution, since no information about the statistical significance of these rates is conveyed. Since coincidence rates are plotted, countries with very limited statistics (e.g. only one or very few events) can still exhibit high individual coincidence rates. However, several epidemic-prone regions such as parts of South America, South-East Asia, India and Sub-Saharan Africa are highlighted as having substantial trigger coincidence rates for both coincidence intervals. At the same time, these maps also illustrate a limitation of the tests performed here, since the data is provided on a country-wise resolution, while the considered events, in particularly floods, are bound to geographical regions and water-sheds. This is in particular problematic for larger countries, where a sub-country resolution would be needed to ensure at least the possibility of a causal relation between the event time series. While this represents a clear limitation, it does not affect the significance of our results. The reason is that inclusion of causally unrelated events on a country basis can only increase the probability of coincidences occurring by chance, thereby increasing the significance levels and rendering the test more conservative.

While being the most common natural disasters, floods are the leading cause of natural disaster fatalities worldwide: Doocy *et al.* [46] estimate global fatalities due to flood events directly to exceed half a million for the period 1980–2009. At the same time, flood events are also found to increase the risk of outbreaks of fecal-oral, vector-borne and rodent-borne diseases [47]. However, the interrelation between floods and disease outbreaks is found to be complex and strongly case-dependent [47] and, as a consequence, difficult to assess in an aggregated fashion using classical statistical methods. The event-based event coincidence analysis applied here provides a methodological alternative by assessing the statistical interrelationships between the two types of event time series on a case-to-case basis. In line with a systematic review of the literature on floods and human health [48], we report robust evidence for both short-term and long-term impacts of floods on epidemic outbreaks. Specifically, we find that more than 50% (20%) of all epidemic outbreaks have been preceded by a flooding event within a 12(1)-month(s) window before the outbreak and that about 20% (7%) of all floods might have triggered such an outbreak in the 12(1) month(s) following the natural disaster. Our results indicate statistically significant coincidence rates up to three months following the disaster and then between 9 and 12 months afterwards, indicating the importance of seasonal effects, which shall be further studied in future work. In particular in tropical regions, flooding events are tied

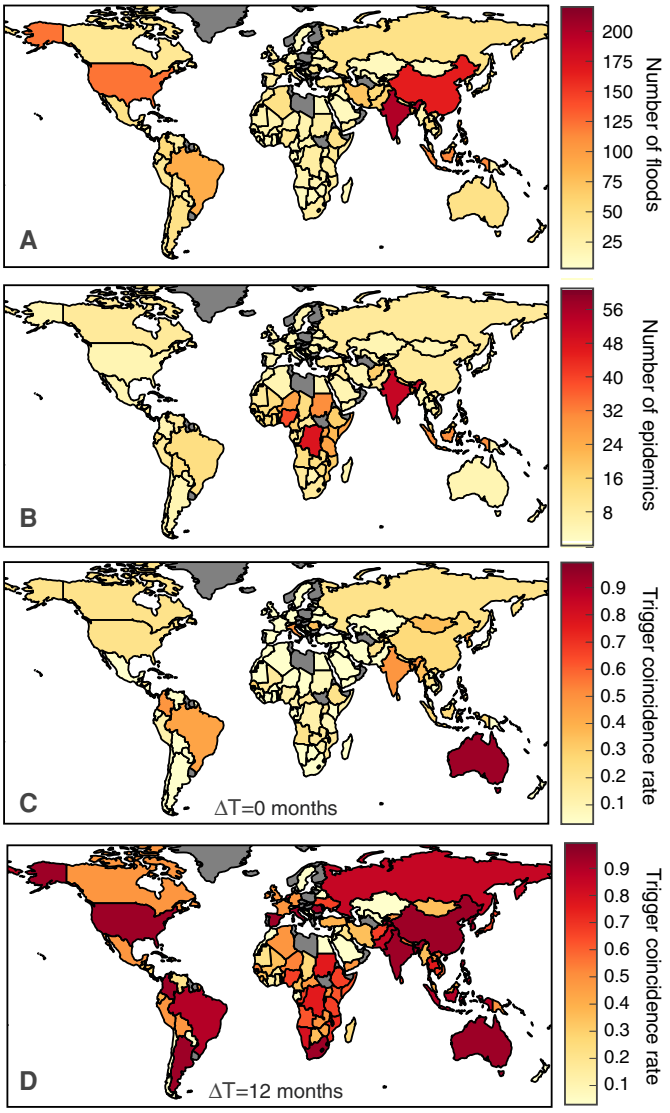

Fig. 4. Global mapping of the frequency of floods (A) and epidemics (B) between 1950 and 2009. Country-wise trigger coincidence rates are shown for coincidences occurring within the same month (C) as well as a coincidence interval of 12 months (D). Gray fillings indicate a lack of data for the corresponding countries.

to the rainy season as are major drivers in particular vector-borne diseases [49]. Thus, while the significant short-term coincidence rates might to a large extent be a direct consequence of the flooding events, indirect effects will likely dominate the long-term coincidence rates observed, e.g. through impacts on general health, food systems and livelihoods exacerbating poverty and potentially malnutrition that increase long-term susceptibility for diseases [48]. It is important to note, however, that the clustering of floods and epidemics during the rainy season in tropical countries could lead to statistically significant long-term coincidence rates due to the counting of causally unrelated events in successive rainy seasons. This effect should be controlled for in future studies.

Given the projected increase in flood risk under anthropogenic climate change [50,51], our findings highlight the risk of such natural disasters for human health and call for an integrated view on climate and health risks in adaptation efforts. As a note of caution, we would like to stress again the illustrative nature of the results of event coincidence analysis presented for this particular application. More detailed analyses including additional and independent data bases and taking into account systematic effects such as biases induced by changes in self-reporting behavior as have been reported for EmDAT and other data bases [52] are relevant subjects of future research.

4 Conclusions

In this work, we have introduced event coincidence analysis as a method for investigating statistical interrelationships between event time series such as climate extremes, natural disasters or civil conflicts and other sources of event-like data. Event coincidence analysis builds upon already established methodologies such as event synchronization or measures of correlation between spatial point processes and allows to quantify the strength (via the coincidence rate), directionality (by distinguishing precursor and trigger coincidences) and lag of such interrelationships. Statistical significance tests for these properties have been proposed based on different kinds of null hypotheses on the nature of the temporal point processes underlying the event series, including Poisson processes and stochastic point processes with a given inter-event time distribution.

As an exemplary application in the timely context of global anthropogenic climate change, we have employed event coincidence analysis for studying statistical interrelationships between flood events and epidemic outbreaks in the same country on a globally aggregated level. We have found evidence that flood events may have acted as possible drivers of epidemic outbreaks in the past, underlining this potential causal relationship as an important subject of further studies in climate impact and adaptation research.

Promising further methodological developments include the design and more detailed mathematical analysis of appropriate null hypotheses for event coincidence analysis including analytical derivations of the corresponding test statistics as well as the incorporation of event amplitude information [53], i.e. by considering marked point processes. Spatial information could be taken into account more explicitly than is the case for the aggregated coincidence rates studied in this paper, building upon a notion of spatio-temporal coincidences with links to the theory of spatial [27] and spatio-temporal point processes [28]. Furthermore, multivariate extensions such as partial or conditional event coincidence analysis [54] for measuring statistical interrelations between two event series conditional on a third or even more event series, e.g. methods extending upon the PC-algorithm and its variants [55], would allow to extract further information from rich sources of event data in hypothesis-driven as well as exploratory research modes [8].

This research was performed in the context of flagship project COPAN on Coevolutionary Pathways in the Earth system and the BMBF Young Investigators Group “Complex Systems Approaches to Understanding Causes and Consequences of Past, Present and Future Climate Change” at the Potsdam Institute for Climate Impact Research. We appreciate funding by a Humboldt University / IRI THESys fellowship, the Stordalen Foundation (via the Planetary Boundary Research Network PB.net), the Earth League’s EarthDoc program, the German Federal Ministry for Education and Research (BMBF projects GLUES and CoSy-CC^2 (grant No. 01LN1306A)) and the Evangelisches Studienwerk Villigst. The work was

supported by the German Federal Ministry for the Environment, Nature Conservation and Nuclear Safety (11-II-093-Global-A SIDS and LDCs). Jobst Heitzig, Marc Wiedermann and Miguel Mahecha are acknowledged for helpful insights and discussions at various stages of the reported research. Event coincidence analyses can be performed using the R package `CoinCalc` [26] which is available at `https://github.com/JonatanSiegmund/CoinCalc`.

References

1. S. Rahmstorf, D. Coumou, Proc. Natl. Acad. Sci. USA **108**, 17905 (2011)
2. D. Coumou, S. Rahmstorf, Nat. Clim. Change **2**, 491 (2012)
3. T.F. Stocker, D. Qin, G.K. Plattner, M. Tignor, S.K. Allen, J. Boschung, A. Nauels, Y. Xia, V. Bex, P.M. Midgley (eds.), *Climate Change 2013: The Physical Science Basis. Contribution of Working Group I to the Fifth Assessment Report of the Intergovernmental Panel on Climate Change* (Cambridge University Press, Cambridge, 2013)
4. A. Rammig, M. Wiedermann, J.F. Donges, F. Babst, W. von Bloh, D. Frank, K. Thonicke, M.D. Mahecha, Biogeosciences **12**, 373 (2015)
5. C.F. Schleussner, J.F. Donges, R.V. Donner, H.J. Schellnhuber, in review (2016)
6. A. Kuhn, M. Hennrich, G. Rempe, Phys. Rev. Lett. **89**, 067901 (2002)
7. R.Q. Quiroga, T. Kreuz, P. Grassberger, Phys. Rev. E **66**, 041904 (2002)
8. E.N. Brown, R.E. Kass, P.P. Mitra, Nat. Neurosci. **7**, 456 (2004)
9. Y. Wu, C. Zhou, J. Xiao, J. Kurths, H.J. Schellnhuber, Proc. Natl. Acad. Sci. USA **107**, 18803 (2010)
10. S.M. Hsiang, K.C. Meng, M.A. Cane, Nature **476**, 438 (2011)
11. S.M. Hsiang, M. Burke, E. Miguel, Science **341**, 1235367 (2013)
12. S.M. Hsiang, M. Burke, Clim. Change **123**, 39 (2014)
13. H.J. Schellnhuber, B. Hare, O. Serdeczny, M. Schaeffer, S. Adams, F. Baarsch, S. Schwan, D. Coumou, A. Robinson, M. Vieweg, et al., *Turn down the heat: climate extremes, regional impacts, and the case for resilience* (International Bank for Reconstruction and Development, World Bank, 2013)
14. P.J. Brockwell, R.A. Davies, *Time series: theory and methods*, 2nd edn. (Springer, New York, 2002)
15. H. Kantz, T. Schreiber, *Nonlinear time series analysis*, 2nd edn. (Cambridge University Press, Cambridge, 2004)
16. A.S. Pikovsky, M.G. Rosenblum, J. Kurths, *Synchronization: a universal concept in nonlinear sciences* (Cambridge University Press, Cambridge, 2001)
17. T. Kreuz, F. Mormann, R.G. Andrzejak, A. Kraskov, K. Lehnertz, P. Grassberger, Physica D **225**, 29 (2007)
18. T. Kreuz, J.S. Haas, A. Morelli, H.D.I. Abarbanel, A. Politi, J. Neurosci. Meth. **165**, 151 (2007)
19. J. Dauwels, F. Vialatte, T. Weber, A. Cichocki, in *Advances in Neuro-Information Processing* (Springer, Berlin Heidelberg, 2009), Vol. 5506 of Lecture Notes in Computer Science, p. 177
20. N. Malik, B. Bookhagen, N. Marwan, J. Kurths, Clim. Dyn. **39**, 971 (2012)
21. J.F. Donges, I. Petrova, A. Loew, N. Marwan, J. Kurths, Clim. Dyn. **45**, 2407 (2015)
22. V. Stolbova, P. Martin, B. Bookhagen, N. Marwan, J. Kurths, Nonlin. Proc. Geophys. **21**, 901 (2014)
23. N. Boers, B. Bookhagen, H.M.J. Barbosa, N. Marwan, J. Kurths, J.A. Marengo, Nat. Comm. **5**, 5199 (2014)
24. A. Rheinwalt, N. Boers, N. Marwan, J. Kurths, P. Hoffmann, F.W. Gerstengarbe, P. Werner, Clim. Dyn. **46**, 1065 (2015)
25. J.F. Donges, R.V. Donner, M.H. Trauth, N. Marwan, H.J. Schellnhuber, J. Kurths, Proc. Natl. Acad. Sci. USA **108**, 20422 (2011)
26. J.F. Siegmund, N. Siegmund, R.V. Donner, preprint [`arXiv:1603.05038`] [stat.ME] (2016)

27. J. Moller, R.P. Waagepetersen, *Statistical inference and simulation for spatial point processes* (CRC Press, 2003)
28. P.J. Diggle, in *Statistical methods for spatio-temporal systems*, edited by B. Finkenstädt, L. Held, V. Isham (CRC Press, 2007), Vol. 107 of Monographs on Statistics and Applied Probability, p. 1
29. J. Zscheischler, M.D. Mahecha, S. Harmeling, M. Reichstein, Ecol. Inform. **15**, 66 (2013)
30. T. Schreiber, A. Schmitz, Physica D **142**, 346 (2000)
31. H.H. Jo, J.I. Perotti, K. Kaski, J. Kertesz, Phys. Rev. E **92**, 022814 (2015)
32. J.F. Siegmund, M. Wiedermann, J.F. Donges, R.V. Donner, Biogeosci. Discuss. **12**, 18389 (2015)
33. E.T. Jaynes, G.L. Bretthorst, *Probability theory: the logic of science* (Cambridge University Press, Cambridge, 2003)
34. S. Picoli, M. del Castillo-Mussot, H.V. Ribeiro, E.K. Lenzi, R.S. Mendes, Sci. Rep. **4**, 4773 (2014)
35. Á. Corral, Phys. Rev. Lett. **92**, 108501 (2004)
36. J.F. Donges, J. Heitzig, B. Beronov, M. Wiedermann, J. Runge, Q.Y. Feng, L. Tupikina, V. Stolbova, R.V. Donner, N. Marwan, et al., Chaos **25**, 113101 (2015)
37. P.M. Dixon, in *Encyclopedia of environmetrics* (Wiley Online Library, 2006)
38. D.H. Perkel, G.L. Gerstein, G.P. Moore, Biophys. J. **7**, 419 (1967)
39. P. Diaconis, F. Mosteller, J. Am. Stat. Assoc. **84**, 853 (1989)
40. D. Zaborov, Phys. Atom. Nucl. **72**, 1537 (2009)
41. M. Baumgartner, A. Thiem, The R Journal **7**, 176 (2015)
42. D. Campbell-Lendrum, D.D. Chadee, Y. Honda, L. Qiyong, J.M. Olwoch, B. Revich, R. Sauerborn, in *Climate Change 2014: Impacts, Adaptation, and Vulnerability. Part A: Global and Sectoral Aspects. Contribution of Working Group II to the Fifth Assessment Report of the Intergovernmental Panel on Climate Change*, edited by C.B. Field, V.R. Barros, D.J. Dokken, K.J. Mach, M.D. Mastrandrea, M. Bilir, M. Chatterjee, K.L. Ebi, Y.O. Estrada, R.C. Genova, et al. (Cambridge University Press, Cambridge, UK and New York, NY, USA, 2014), Chap. 11, p. 709
43. D. Guha-Sapir, R. Below, P. Hoyois, *EM-DAT: International Disaster Database*, – `www.emdat.be` (Université Catholique de Louvain, Brussels, Belgium)
44. K.J. Rothman, Epidemiology **1**, 43 (1990)
45. T.V. Perneger, Brit. Med. J. **316**, 1236 (1998)
46. S. Doocy, A. Daniels, S. Murray, T.D. Kirsch, PLoS Curr. **5**, 1 (2013)
47. M. Ahern, R.S. Kovats, P. Wilkinson, R. Few, F. Matthies, Epidemiol. Rev. **27**, 36 (2005), ISSN 0193936X
48. K. Alderman, L.R. Turner, S. Tong, Environ. Int. **47**, 37 (2012)
49. J.T. Watson, M. Gayer, M.A. Connolly, Emerg. Infect. Dis. **13**, 1 (2007)
50. N.W. Arnell, S.N. Gosling, Clim. Change **134**, 387 (2016)
51. Y. Hirabayashi, R. Mahendran, S. Koirala, L. Konoshima, D. Yamazaki, S. Watanabe, H. Kim, S. Kanae, Nat. Clim. Change **3**, 816 (2013)
52. D.D. Saulnier, K. Brolin, Int. J. Public Health **60**, 781 (2015)
53. S. Suzuki, Y. Hirata, K. Aihara, Int. J. Bifurcation Chaos **20**, 3699 (2010)
54. J.F. Siegmund, T.G.M. Sanders, I. Heinrich, E. van der Maaten, S. Simard, G. Helle, R.V. Donner, Frontiers in Plant Science (in review) (2016)
55. J. Runge, V. Petoukhov, J.F. Donges, J. Hlinka, N. Jajcay, M. Vejmelka, D. Hartman, N. Marwan, M. Paluš, J. Kurths, Nat. Comm. **6**, 8502 (2015)

2.2 Impact of temperature and precipitation extremes on the flowering dates of four German wildlife shrub species

Biogeosciences, 13, 5541–5555, 2016
www.biogeosciences.net/13/5541/2016/
doi:10.5194/bg-13-5541-2016
© Author(s) 2016. CC Attribution 3.0 License.

Biogeosciences Open Access EGU

Impact of temperature and precipitation extremes on the flowering dates of four German wildlife shrub species

Jonatan F. Siegmund[1,2], **Marc Wiedermann**[1,3], **Jonathan F. Donges**[4,5], **and Reik V. Donner**[1]

[1]Research Domain IV, Transdisciplinary Concepts & Methods, Potsdam Institute for Climate Impact Research, Telegrafenberg A31, 14473 Potsdam, Germany
[2]Institute of Earth and Environmental Science, University of Potsdam, Karl-Liebknecht-Str. 24–25, 14476 Potsdam-Golm, Germany
[3]Department of Physics, Humboldt University of Berlin, Newtonstraße 15, 12489 Berlin, Germany
[4]Research Domain I, Earth System Analysis, Potsdam Institute for Climate Impact Research, Telegrafenberg A31, 14473 Potsdam, Germany
[5]Stockholm Resilience Centre, Stockholm University, Kräftriket 3B, 11419 Stockholm, Sweden

Correspondence to: J. F. Siegmund (jonatan.siegmund@pik-potsdam.de)

Received: 13 September 2015 – Published in Biogeosciences Discuss.: 16 November 2015
Revised: 25 August 2016 – Accepted: 20 September 2016 – Published: 6 October 2016

Abstract. Ongoing climate change is known to cause an increase in the frequency and amplitude of local temperature and precipitation extremes in many regions of the Earth. While gradual changes in the climatological conditions have already been shown to strongly influence plant flowering dates, the question arises if and how extremes specifically impact the timing of this important phenological phase. Studying this question calls for the application of statistical methods that are tailored to the specific properties of event time series. Here, we employ event coincidence analysis, a novel statistical tool that allows assessing whether or not two types of events exhibit similar sequences of occurrences in order to systematically quantify simultaneities between meteorological extremes and the timing of the flowering of four shrub species across Germany. Our study confirms previous findings of experimental studies by highlighting the impact of early spring temperatures on the flowering of the investigated plants. However, previous studies solely based on correlation analysis do not allow deriving explicit estimates of the strength of such interdependencies without further assumptions, a gap that is closed by our analysis. In addition to direct impacts of extremely warm and cold spring temperatures, our analysis reveals statistically significant indications of an influence of temperature extremes in the autumn preceding the flowering.

1 Introduction

In comparison to geological timescales, ongoing climate change is extraordinarily fast (IPCC, 2013). The associated changes in meteorological conditions, which are among the main driving factors for plant growth, are a huge challenge for terrestrial ecosystems: in some cases, the quick changes may exceed their ability to adapt to the new conditions, leading to severe temporal or spatial mismatches between interacting/symbiotic species that may cause critical disruptions of the food chain and thus affect population size and health of both species.

Beyond the gradual change in the mean climatology of Europe, the spatial extent, intensity and frequency of extreme climate events like droughts or heatwaves have also markedly increased over the past decades (Coumou and Rahmstorf, 2012; Tank and Konnen, 2003; Luterbacher et al., 2004; IPCC, 2013). Both the probability of occurrence and the amplitude of many types of climatic extremes have been rising (Fischer et al., 2007; Barriopedro et al., 2011; Petoukhov et al., 2013; Seneviratne et al., 2012) and are projected to increase further (Stott et al., 2004; Rahmstorf and Coumou, 2011; Petoukhov et al., 2013). Especially during recent years, extreme summer temperatures have been observed which were clearly beyond the limits of previously observed extreme values. Specifically, examples like the European heat-

wave in 2003 (Schaer et al., 2004; Luterbacher et al., 2004; Garcia-Herrera et al., 2010) or the Russian heatwave in 2010 (Trenberth and Fasullo, 2012) by far exceeded historical extreme values of the past 500 years.

In terms of water availability, past and ongoing trends of heavy rainfall events strongly depend on region and season (Tank and Konnen, 2003; Lupikasza et al., 2011; Coumou and Rahmstorf, 2012; Haylock and Goodess, 2004), whereas future projections suggest increases in those events' frequency and intensity for most parts of Europe (Kundzewicz et al., 2006; Kysely et al., 2011; Rajczak et al., 2013). In turn, droughts as a combination of high temperatures, low precipitation and high evapotranspiration only show low to moderate positive trends for central Europe during the last 60 years (Spinoni et al., 2015b; Gudmundsson and Seneviratne, 2015). For the future development of drought intensity and frequency over central Europe, trend estimates have provided ambiguous results (Spinoni et al., 2015a).

The effects of climate extremes on terrestrial ecosystems are diverse and highly complex and may lead to unprecedented outcomes (Frank et al., 2015; Reichstein et al., 2013). Besides direct impacts, there is a growing body of evidence that climate extremes can critically disturb sensitive ecological equilibria (Parmesan, 2006) and mutualisms (Rafferty et al., 2015). The effects of temporal displacement or even absolute failure of flowering and fruit ripening of food plants for nectarivores, small mammals and birds are important examples (Law et al., 2000; Jacobs et al., 2009). A rapid population decline up to species extinction due to phenological mismatches between plant and pollinator has already been demonstrated (McKinney et al., 2012; Burkle et al., 2013; Kudo and Ida, 2013). The resulting damage on the affected population could propagate through the ecosystem and endanger its structure, dynamics and stability (Post and Stenseth, 1999; Parmesan et al., 2000; Parmesan, 2006; Augspurger, 2009).

A widely used source of long-term observations allowing us to study the inter-annual variability of plant growth dynamics is the timing of phenological phases. From several studies, it is known that the phenological phases of most central European plant species experience systematic, gradual changes related to climate change. Especially the change in temperature plays an important role for long-term variations in the dates of foliation, flowering and leaf colouring (Ahas et al., 2000; Sparks et al., 2000; Sparks and Menzel, 2002; Menzel, 2003; Cleland et al., 2007; Schleip et al., 2012).

However, it is likely that seasonal temperature extremes can affect terrestrial ecosystems much more strongly and more directly than gradual changes (Easterling et al., 2000; Jentsch et al., 2007, 2009; Zimmermann et al., 2009; Menzel et al., 2011; Nagy et al., 2013; Reyer et al., 2013). Associated with extreme weather conditions, flowering dates of temperate species have been observed to be shifted by up to 1 month or to have even failed completely (Nagy et al., 2013).

Unlike for temperature extremes, the possible impact of drought or heavy precipitation events on plant flowering is less well understood. So far, only few studies have explicitly addressed this question, and those that have are of an experimental nature only. The experiments of Nagy et al. (2013) and Jentsch et al. (2009) found significantly delayed flowering dates of *Genistra tinctoria* after drought treatment. On the other hand, Nagy et al. (2013) also found that the average flowering date of *Calluna vulgaris* was not significantly affected by drought. In a similar study, Prieto et al. (2008) observed no shift in the flowering dates of *Erica multiflora* related to drought. Heavy rainfall did not effect flowering time at all in the experiments of both Nagy et al. (2013) and Jentsch et al. (2009).

In general, the reaction of flowering to climate extremes has so far mainly been analysed for individual events (Luterbacher et al., 2007; Rutishauser et al., 2008) or with experimental setups (Prieto et al., 2008; Jentsch et al., 2009; Nagy et al., 2013). Systematic studies exploiting existing large-scale spatially distributed data of phenological phases by means of sophisticated data analysis methods are scarce. As one notable exception, Menzel et al. (2011) presented an in-depth analysis of the influence of warm and cold spells on crop plant phenology over Europe. However, since agricultural crops are often subject to specific treatments (which have changed over the past decades), these results are not directly transferable to wildlife plants, for which a corresponding study is still missing.

In order to close this research gap, we investigate the individual influence of extremely high- and low-temperature and precipitation events on the flowering dates of four central European wildlife shrub species, using a phenological data set covering the period from 1950 to 2010. In contrast to other recent studies (e.g. Rybski et al., 2011), we intentionally focus on flowering as a single phenological phase with paramount ecological importance. Moreover, we select just four shrub species (see Sect. 2) as a case study to address the following research questions:

- Do the flowering dates of these shrub species systematically react to temperature and/or precipitation extremes?
- Which species are more/less susceptible?
- Do these effects differ by region?

The remainder of this paper is organized as follows: after a description of the phenological and meteorological data sets under investigation, the approaches of extreme-value definition as well as the methodology of event coincidence analysis are described in Sects. 2 and 3, respectively. Subsequently, the results of our study are presented in Sect. 4 and further discussed in Sect. 5. We conclude this paper with a short summary of the results in Sect. 6.

2 Data

2.1 Meteorological data

As a climatological reference data set, we use an ensemble of homogenized and expanded daily mean temperature and precipitation time series from Österle et al. (2006), which are based on meteorological stations operated by the German Weather Service (DWD; Deutscher Wetterdienst, Offenbach, 2009). While the precipitation data are directly based on observations made at all considered stations, mean temperatures partially involve a sophisticated spatial interpolation from a set of fewer stations with direct measurements (Österle et al., 2006). Both data sets are commonly employed as a benchmark data set for assessing the performance of hindcast simulations of regional climate models (German baseline scenario). The data set covers the time interval from 1950 to 2010 and comprises 1440 stations distributed across Germany as well as a set of stations located in the adjacent regions of some of its neighbouring countries.

2.2 Phenological data

As a source of information on the reactions of terrestrial ecosystems to climatic drivers, we use the German Plant Phenology Data Set, provided by DWD (http://www.dwd.de/phaenologie). This data set contains the Julian days of the occurrence of several phenological phases. Besides 22 fruit species and 22 crop types, the data cover 37 wildlife species at 6525 stations distributed over all of Germany for a period from 1951 to 2013. However, the actually available time series length strongly varies by station. While some stations have series covering the full considered time span, others contain just a few or even only one observation per plant species and phenological phase. Due to these different time series lengths, we select only those stations for our further analyses which contain at least 40 years of observation between 1951 and 2010.

In this work, we analyse the flowering dates of four of the most abundant German wildlife shrub species: lilac (*Syringa vulgaris* L.), elder (*Sambucus nigra* L.), hawthorn (*Crataegus monogyna* (Jacq.)/*Crataegus laevigata* (Poir.) DC) and blackthorn (*Prunus spinosa* L.). These four shrubs are representative of the regional vegetation. Moreover, they are characterized by a usually large amount of flowers during early to late spring and constitute important components of their local ecosystems, which are in some regions key for local insect, bird or small-mammal populations. For example, hawthorn and blackthorn are visited by 149 and 109 insect species, respectively, with around 100 lepidoptera species among them (Southwood, 1961). In contrast, elder is of lower importance for insect species (only around 20 species are known to depend on elderflowers or fruits; see Duffey et al., 1974), but it is an important food source for numerous birds during summer and autumn due to its high amount of very nutritious

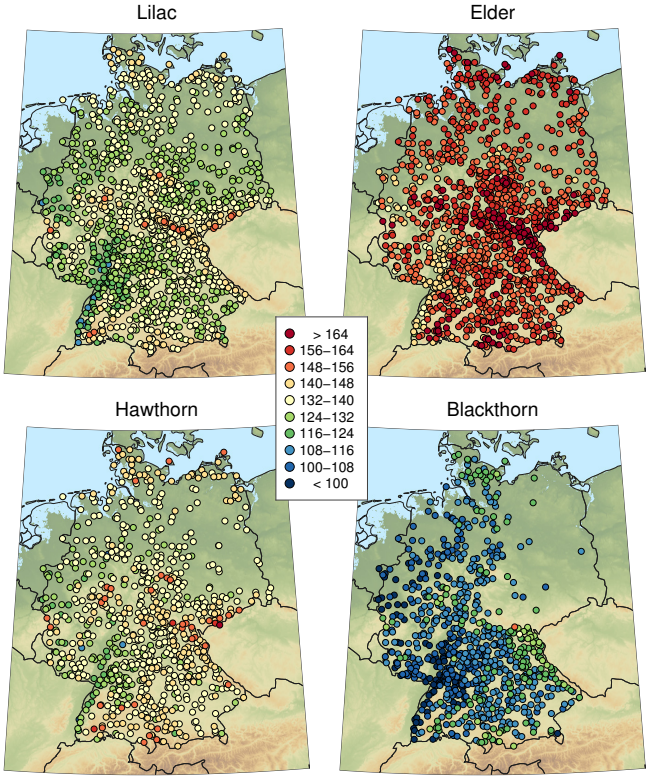

Figure 1. Mean flowering dates (Julian days) of the four analysed shrub species. The figure only shows those records that contain at least 40 observations.

berries (Atkinson and Atkinson, 2002). Other shrub species contained in the DWD data set do either not fall into the same category regarding massive flowering and spatial distribution or the available amount of data is considerably smaller. Therefore, these additional data are not used in the present study, which focuses on the aforementioned four species as illustrative examples with reliable data.

The mean flowering times of the considered shrub species range from early April (blackthorn) to May (hawthorn and lilac) to mid-June (elder); see Fig. 1. The distributions of the flowering dates of all four species are, however, very wide. Flowering can even occur 1–2 months earlier than normal under certain conditions, which shall be further explored in the course of this work. Due to the selection criterion of at least 40 years of data (at most 20 missing years of observations), the data set is strongly reduced to about 1000 recording sites per plant, and the spatial distribution of the corresponding phenological stations becomes much more heterogeneous, with larger gaps existing especially for blackthorn in northeastern Germany (Fig. 1).

3 Methodology

3.1 General relationship between flowering dates and meteorological conditions

Before explicitly focusing on the timing of extremes, it is reasonable to address the general dependency between spring temperature/precipitation and the flowering dates of the four shrub species, taking the full empirical distribution of the different observables into account.

For this purpose, the raw data described in the previous section are analysed according to the following scheme:

- The flowering dates of each individual station are normalized according to their respective mean and variance, using a classical z score approach. This normalization is necessary for the following investigations, since the individual study sites differ strongly in their year-to-year flowering date variability, so that absolute changes cannot be compared between two stations. For example, a shift of flowering by 10 days might be important for site A, while having only a minor impact (i.e. it can still be within the "normal" variability range) for station B. Hence, our normalization procedure allows for inter-comparability between the results of different phenological stations at the cost of losing explicit date information, which is otherwise practically important for common ecological studies. A combination of both viewpoints might be helpful to get as much information as possible out of the given data set. However, given the focus of the present study, we restrict ourselves to the consideration of normalized flowering dates in the following.

- For each meteorological station, the temperature and precipitation observations are consolidated to mean daily spring temperature and the sum of spring precipitation (using daily data for the Julian days 31 to 120 of each year), resulting in time series with one value per year for each station. The resulting time series are transformed into z scores following the same approach as for the flowering dates.

- The z scores of temperature and precipitation from all considered stations are categorized into 20 equiprobable groups according to the 20 inter-percentile classes of 5 % width each.

- The distribution of the flowering dates of each shrub species taken from all stations is evaluated separately for the 20 different categories according to the respective assignment of the associated meteorological observations.

3.2 Definition of extreme values

3.2.1 Phenology

In order to take a sufficiently large set of events into account that allows us to draw statistically justified conclusions, we define a flowering date earlier than the empirical 10th percentile of all recorded values at a given phenological station to be extreme. Hence, each time series of flowering dates has an individual absolute threshold date for the definition of an early flowering event. This approach is chosen since the timings of the phenological phases of every station can crucially depend on local conditions like altitude, exposition, water availability, etc. Since the time series lengths differ between the different phenological records (40 to 61 observations), this approach also leads to different numbers of extremes in each time series. The definition of extreme late flowering dates is performed in full analogy using the 90th percentile.

3.2.2 Temperature and precipitation

In order to obtain information on temperature and precipitation extremes that is directly comparable with the phenological information, a three-step treatment of the available continuous daily meteorological records is necessary, which is detailed below:

Spatial interpolation As a first step, for each phenological station used in this study, we create one daily mean temperature/precipitation series by spatial interpolation of the existing observational records. For this purpose, we apply inverse geographical distance-weighted mean interpolation, using the four closest meteorological stations surrounding each site with phenological recordings. Since we are only interested in the timing of (local and seasonal) temperature (precipitation) extremes rather than the associated explicit values of the respective variables, we do not explicitly take other covariates into account, although being aware of their actual relevance for the specific timing of flowering. Due to the different spatial coverage of phenological data for the four considered plant species, this approach results in four new temperature (precipitation) data sets to be further exploited as described in the following.

Temporal averaging Extreme climatic conditions present for just a single day may not be sufficient to trigger a detectable ecological response like an anomalous date of flowering (Menzel et al., 2011). In turn, given the common timescales of plant physiological processes, it appears reasonable to consider extremes in the mean climate conditions taken over a certain period of time. The aspect of the crucial temporal duration of a climatic extreme event to influence flowering time is of special interest for the interpretation of the impact of climate change scenarios on plant flowering. Accordingly, in

a second step of preprocessing, we calculate the average daily mean temperature (daily precipitation) for running windows in time. In order to explicitly study the effect of the averaging timescale and potentially demonstrate the robustness of the obtained results against the specific choice of windows, we consider three different window sizes of 15, 30 and 60 days. These windows are moved along the time series with a step size of 1 day. For the 15- and 30-day periods, these windows start on 1 January of the year prior to the flowering and extend up to 1 December of the subsequent year (700 steps). For the 60-day window, the last step starts on 1 November (670 steps). This procedure leads to "window-mean temperatures/precipitation", resulting in 700 (670) values for each year from 1951 to 2010 and for each phenological station. Notably, we use an unweighted averaging, giving the same weight to all observations within a given time window.

Definition of temperature/precipitation extremes

Before defining extreme window-mean temperatures/precipitation, we account for the numerous missing data values of the phenological data set by discarding the meteorological information for all those years, where the corresponding phenological information is missing. We then identify those among the remaining windows for which the corresponding value exceeds the 90th percentile (or falls below the 10th percentile) of all windows of the same size and time period at one station and consider them as extremes. By using this approach, the seasonal variability of temperature and precipitation is already included in the threshold definition, so that no further preprocessing (e.g. calculation of climatological anomalies or z scores) is necessary.

In the case of precipitation, our approach is equivalent to the calculation of the standardized precipitation index (SPI), resulting in 15-day SPI, 30-day SPI and 60-day SPI values. The application of the 10th and 90th percentile then produces (extreme) events corresponding to the SPI category "moderately dry/wet" (WMO, 2012).

3.3 Event coincidence analysis

3.3.1 Basic idea

To detect and quantify a possible statistical interrelationship between extreme seasonal temperatures (or extreme precipitation) and extreme flowering dates, we apply event coincidence analysis (Donges et al., 2011, 2016; Rammig et al., 2015), a novel statistical framework which allows the identification of non-random simultaneous occurrences of events in two series. For this purpose, for each considered phenological station we convert the two time series (window-mean temperature/precipitation and flowering date of the given

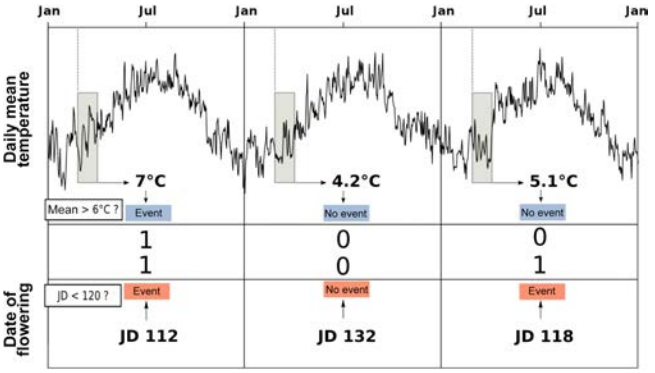

Figure 2. Schematic illustration of the event coincidence analysis used in this work. Upper and lower panels depict the approaches used for defining events based on climatological (daily mean temperature or precipitation) and phenological information (Julian day of flowering), respectively. For the climate data, windows covering the same time interval during each year are fixed for computing window-mean values. The width and location of these windows are varied throughout the analysis as described in the text. Extreme conditions are defined by the exceedance of certain quantiles of the respective variable of interest (flowering time or window-mean value of the considered meteorological variable for the specified window width and position, i.e. one value per year).

year) into binary vectors, representing time steps with or without such extreme conditions, as explained above (see Fig. 2 for a schematic illustration of the approach). Subsequently, we count the number K_{obs} of simultaneous events (in the following referred to as "coincidences"). In order to assess the significance of the associated normalized coincidence rate κ_{obs}, we compare K_{obs} with the probability distribution of the number of coincidences that would result from two independent Poisson processes with the same event rate as the series under study (see the Supplement accompanying this paper for further information). Further details on this significance test, its limitations and possible alternatives can be found in Donges et al. (2016); Siegmund et al. (2016b).

By performing event coincidence analysis between flowering time and window-mean temperature/precipitation for different time windows before the typical flowering date, we can take possible lagged responses of the plants into account. In turn, studying coincidences between extremes of, e.g., flowering dates and future temperatures (which cannot causally be linked to the flowering), provides a simple test of the reliability and robustness of the obtained results (see Figs. 4 and 5).

3.3.2 Differences with respect to correlation analysis

It is important to highlight that there are several fundamental differences between event coincidence analysis and classical correlation analysis as employed in most recent studies on the impact of climate change on terrestrial ecosystems. While we only provide a brief discussion here, more details

can be found in the Supplement. In the latter, we also provide some numerical examples using artificial data sets as well as selected records studied in this work to support the complementary nature and added value of the methodology used in this work.

The most notable differences between event coincidence analysis and correlation analysis are as follows:

Conceptual viewpoint There are two fundamental differences between correlation analysis and event coincidence analysis already at the conceptual level. Correlation analysis generally takes all observations of two data sets (with the exception of preprocessing for removing possible outliers) with the explicit values of the two variables under study (after possible normalization) into account to provide an estimate of the strength of the statistical interrelationship. In turn, event coincidence analysis considers a distinctively different aspect of a possible statistical interrelationship by making use of preselected data points only (in our case, values in the uppermost/lowermost percentiles of the distributions of the variables under study) and does not use explicit values of the respective observables, but only information about the timing of these values. In this regard, event coincidence analysis reduces the effective sample size by considering only subsets of observations with distinct features, which may help to focus on a specific research problem where only this subset is of particular interest.

Linearity/monotonicity assumption The basic idea beyond correlation analysis in the classical (Pearson) sense is estimating the strength of a statistical interrelationship between two variables by considering the goodness of fit of a linear regression model linking both variables, commonly relying on a Gaussianity assumption that can only be relaxed in the case of sufficiently large sample sizes. The linearity assumption can be relaxed to a monotonicity condition when replacing the explicit time series values by rank numbers, leading to the well-known Spearman rank-order correlation. However, fully non-linear statistical interrelationships (like simple quadratic dependencies) cannot be properly captured by correlation analysis, but require the utilization of more general concepts of statistical interrelationship like mutual information, the estimation of which, however, requires much larger sample sizes. In turn, event coincidence analysis does not make any assumption about the actual functional shape of the interrelationship between two variables beyond two specifically defined "classes" of observations coinciding in terms of their timing. This is commonly the case if a strong linear relationship is present; however, due to the reduction of the effective sample size, one may also find statistically insignificant event coincidence rates in the case of relatively large correlation coefficients or, in turn, observe high coincidence rates when correlation coefficients indicate negligible statistical dependence. We provide numerical examples for both cases in the Supplement accompanying this paper.

Statistical significance Finally, the notion of statistical significance used by both methods is distinctively different due to the very different types of null hypothesis and test statistics derived from the statistical quantity of interest. For correlation analysis, a t test (or Mann–Kendall test in the case of rank-order correlations) is the most common tool of choice, whereas these tests are not applicable in the event coincidence analysis framework. Instead, the test statistic of the latter method is based on a binomial distribution (see the Supplement and Donges et al., 2016, and Siegmund et al., 2016b, for details), the critical values of which are either analytically computed or numerically estimated by means of bootstrapping approaches. In the end, since event coincidence analysis focuses on small subsets of the data under study and thus operates on a much smaller sample size than correlation analysis, its significance statements are more restrictive but also more uncertain (i.e. we have both a lower specificity and lower sensitivity of the associated significance test).

In summary, these three major differences raise the expectation that information on significant event coincidence rates cannot be directly inferred from the presence of significant linear correlations. Following this, event coincidence analysis may actually provide additional information on the emergence of extraordinary reactions of wildlife plant flowering on meteorological stressors that could be discarded by correlation analysis. In the Supplement, we provide some examples highlighting the differences between the results obtained using both methods for the given data sets.

3.4 Multiple testing

Our sliding window approach using mutually overlapping time intervals with evident serial correlations of the meteorological variables of interest leads to a multiple testing problem. The standard approach for dealing with such problems would be a Bonferroni adjustment of the significance level (Shaffer, 1995). Although being aware of this approach, in this study such an adjustment is not considered since the analysis modified in this way would not provide practically useful results in the context of our research agenda. Specifically, our decision against a Bonferroni adjustment to be used in this study follows the arguments raised by Perneger (1998):

- The Bonferroni adjustment is based on one general null hypothesis, i.e. that all individual null hypotheses are true simultaneously. In our present study, it is not intended to state that all shrub stands of one species are

prone to climate impacts in the same manner, which cannot be expected realistically. In turn, our analysis rather seeks to identify general tendencies, which may have multiple individual exceptions. In a similar spirit, our sliding window approach with respect to the meteorological conditions is used as a purely exploratory tool for identifying time windows during which extraordinary meteorological conditions have the strongest relevance for the timing of subsequent plant flowering. In turn, we do not intend to primarily interpret the performed statistical tests in a confirmatory sense.

– Using a Bonferroni adjusted significance level implies that the interpretation of a finding depends on the number of other tests performed. Since the number of phenological stations and, hence, the number of significance tests in this study is larger than 1000 for almost all shrub species, the Bonferroni adjusted significance level would be very close to 0. Thus, such an adjustment cannot be of practical interest for the interpretation of the results of our analysis, since all interdependencies would be discarded by a test with the accordingly corrected significance levels. Or, put differently, "The likelihood of type II errors is also increased, so that truly important differences are deemed non-significant" (Perneger, 1998).

4 Results

4.1 General relationship between flowering dates and meteorological conditions

Figure 3 illustrates the distribution of standardized flowering dates (z scores) of all four shrub species for the twenty 5 % intervals of the two considered meteorological variables. Here, the time span taken for the definition of a "mean spring temperature" and "spring precipitation sum" is related to the typical flowering dates of each species: Julian days (JDs) 59–119 for lilac and hawthorn, JDs 89–149 for elder, and JDs 39–99 for blackthorn. As expected, our results demonstrate a generally very strong negative temperature effect on flowering (i.e. higher spring temperatures foster earlier flowering). A more detailed inspection also reveals that the dependency between spring temperature and flowering is monotonic but slightly non-linear. Specifically, the slope of the estimated statistical relationship increases markedly for spring temperatures above the 90th percentile for all four species. Besides this, the delaying effect of particularly cold spring temperatures on flowering times is slightly stronger than the average dependency (slope) for lilac and hawthorn. In contrast to the findings for temperature impacts, precipitation has hardly any systematically positive or negative influence on the flowering dates, only elder flowering dates seem to be delayed in years with a high spring precipitation amount.

From the above results, we expect that extremely wet or dry conditions during spring may not have a marked influence on the timing of flowering of the four considered shrub species, while extraordinarily high or low spring temperatures could have a stronger effect on the flowering dates than could simply be expected from the outcomes of correlation analysis. In the following, we will examine the validity of these expectations in more detail by means of event coincidence analysis.

4.2 Coincidences with positive temperature extremes

We start our detailed investigations on the impact of extraordinary warm spring temperatures by considering lilac as an example for illustrating the performance of our method in practice. Figure 4 demonstrates the existence of significant coincidence rates between very early lilac flowering and extremely warm window-mean temperatures for three different window sizes and all windows from 1 January of the preceding year to 1 December of the year of flowering. Significant coincidences at a confidence level of $\alpha = 0.05$ are displayed in red, those that are also significant at $\alpha = 0.01$ in black.

For all three window sizes, a maximum number of stations with significant coincidence rates is found during the spring months, especially around March and April. For time windows after the typical flowering time in May, there are generally much fewer indications of corresponding interrelationships than for windows before May. Note that due to the statistical nature of the employed analysis methodology, there are always individual stations exhibiting a significant number of coincidences just by chance, even if there cannot be a causal link between the considered events. This is due to the very small number of events the analysis for each individual station is based upon, i.e. the significance of the results for a single given station is practically irrelevant and becomes only statistically meaningful if the whole ensemble of stations (or a sufficiently large subset thereof) is considered. For example, at a 5 % confidence level, we may expect that at most 5 % of the stations show false positive results (i.e. individually significant results that occur simply due to chance only; same at 1 % level), which is about the order of the maximum numbers of stations with significantly many coincidences observed after May. Hence, this behaviour is to be expected.

Regarding the spatial distribution of stations with significant coincidence rates, we do not observe any systematic latitudinal trend, with one exception: at the northernmost stations, the timing of significant coincidence rates between early flowering and extreme positive temperature anomalies tends to extend further into the late winter than for the more southern stations.

Considering time windows from the previous year, we find some indications of summer (60-day windows) and autumn (15- and 60-day windows) temperature extremes to significantly coincide with early flowering in more cases than is to

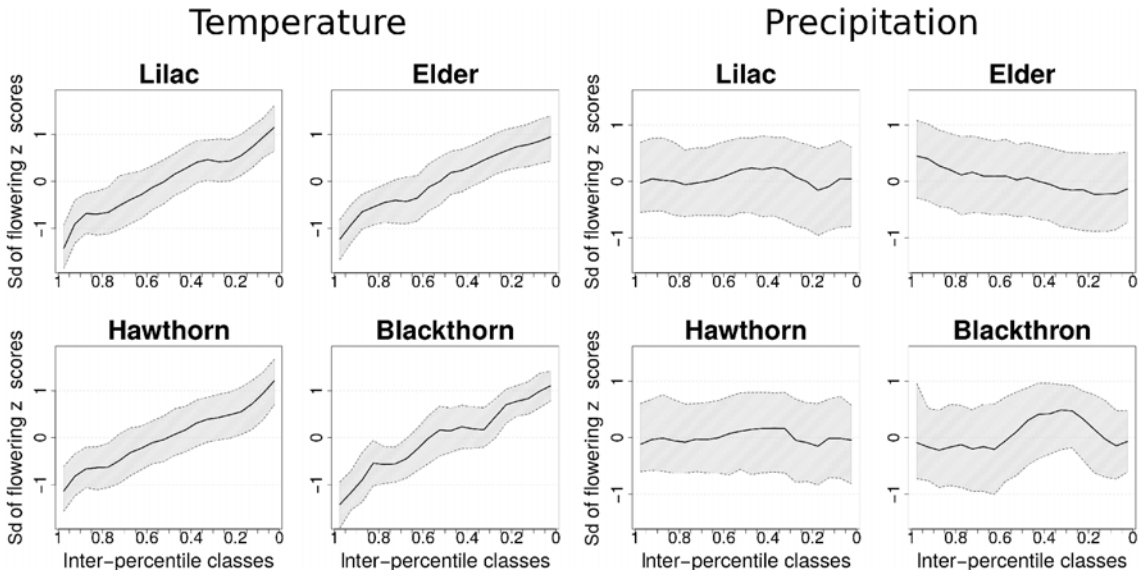

Figure 3. Distribution of standardized flowering dates (median plus 25 %/75 % interquartile range) of the four shrub species in dependence on spring mean temperature and spring precipitation sum. Note the inverted direction of the x axes.

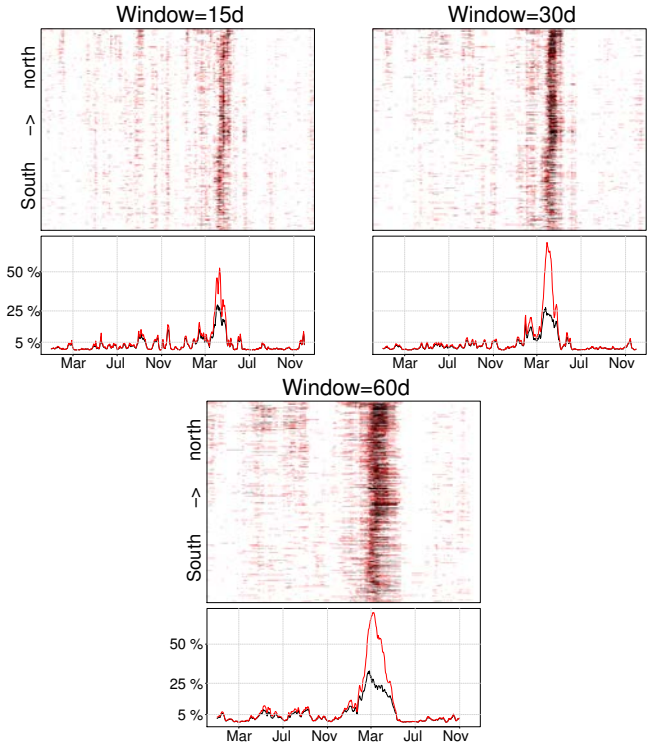

Figure 4. Latitudinal distribution (top panels) and total fraction (bottom panels) of stations with significant coincidence rates (red: $\alpha = 0.05$; black: $\alpha = 0.01$) between very early lilac flowering and extremely high window-mean temperatures for three different window sizes. The x axes refer to the starting date of a window. The dashed horizontal lines at 5 % in the lower panels highlight the employed group-significance criterion.

be expected from the tolerable number of false positives in our testing procedure (Fig. 4).

This effect is mainly present at the more northern stations. We will further discuss possible explanations of these findings in Sect. 5.

Following upon the previous findings for lilac, Fig. 5 summarizes the corresponding results for the flowering of the other three species (red lines). For convenience, we only show the results for two window sizes and without further latitudinal resolution (the corresponding, more detailed results can be found in the Supplement). For elder the maximum fraction of stations with significant coincidence rates arises (due to the generally later flowering of elder) between March and May. Later windows also show a few stations with significant coincidence rates due to the previously discussed test design. A clear latitudinal gradient is absent in the significance profile (see the Supplement). As an exception, for the windows between January and March with a window size of 60 days, again mainly the more northern stations show significant coincidence rates, exhibiting 1–2 peaks in the corresponding temporal profile around the previous year's May and September. The latter peak is especially pronounced for the 15-day windows.

The results for hawthorn closely resemble those obtained for elder, including a clear maximum in the fraction of stations with significant coincidence rates in late spring and no clear influence of latitude. However, the corresponding signal during May and September of the preceding year is less pronounced or not even visible at all. Only for the 15-day windows, significant coincidence rates with September temperatures at the northern stations are clearly beyond the expected number of false positives.

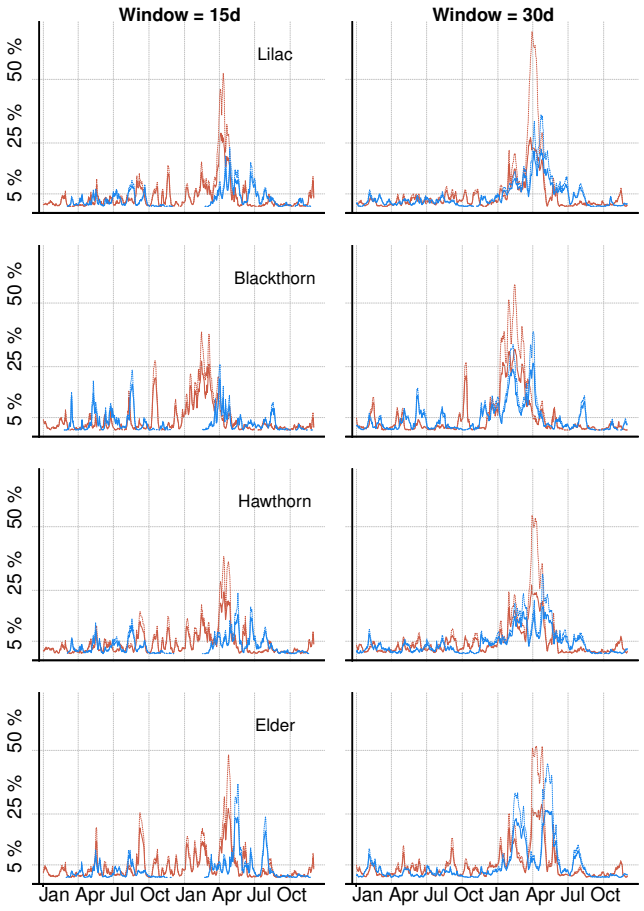

Figure 5. Fraction of stations with significant coincidence rates between extreme flowering dates and extreme window-mean temperature for the four shrub species and two different window sizes. The x axes refer to the starting date of a window; the y axes denote the percentage of stations that show significant coincidence rates for the specific window. Red (blue) lines refer to coincidences of extreme warm (cold) temperatures with extreme early (late) flowering at confidence levels of $\alpha = 0.05$ (solid) and $\alpha = 0.01$ (dotted), respectively.

Finally, the results for blackthorn are markedly shifted towards early spring, consistent with the generally earlier flowering of blackthorn in comparison to the three other shrub species. In contrast, the pertaining signal in the previous autumn is distinctively stronger in the 30-day window than for the other species.

4.3 Coincidences with negative temperature extremes

The blue lines in Fig. 5 display the results of event coincidence analysis between negative (cold) temperature extremes and late flowering. The general shape and intensity of the temporal profile of the number of stations with significant coincidence rates are similar to the results reported above for extremely positive seasonal temperature anomalies, yet slightly shifted towards later time windows. Our results do not show any significant peaks in the number of stations with statistically significant coincidence rates in the previous year for lilac, hawthorn and elder, while for blackthorn, even more distinct peaks in the previous year can be seen than for positive temperature extremes (at least for small windows). Likewise, the tendency of coincidences with temperature extremes in the previous year to be more pronounced at more northern latitudes (as observed for warm extremes) is not visible at all within the results for cold temperatures (see the Supplement). In turn, there is even an opposite tendency: for blackthorn, peaks in the previous year almost completely result from stations south of 50° N. It is notable that this latitudinal distribution has the opposite direction in comparison with that observed for the latitudinal distribution of significant coincidence rates between very warm autumns and very early flowering dates.

4.4 Coincidences with precipitation extremes

As described in the Introduction, the impact of heavy or low rainfall amounts on flowering dates is not yet a fully understood topic. To contribute to this ongoing field of research, we have performed event coincidence analysis between extremely high/low precipitation amounts and extremely early/late flowering. For all four shrub species and all four possible extreme event combinations, we hardly ever find more than 5 % of the stations showing significant coincidence rates (see the Supplement). Only two small exceptions are observed for blackthorn, but these are probably a result of the fact that very warm spring conditions normally originate from intense westerly circulation patterns, which are characterized by relatively high precipitation amounts in central Europe. For an explicit study of the latter relationship, multivariate extensions of event coincidence analysis would be required, the development of which is a subject of ongoing studies (Siegmund et al., 2016a). To this end, we conclude that there is no significant indication of a marked impact of precipitation extremes on the flowering of the four considered shrub species in Germany. Note that the productivity of German terrestrial ecosystems is commonly not limited by water availability. Hence, this result does not necessarily imply a similar absence of relationships for other species and/or regions, especially in situations where water stress can be a problem. We plan to address this question further in our future work.

4.5 Combined effects of temperature and precipitation extremes

Figure 6 illustrates the distribution of flowering dates for years that exhibit different combinations of early spring temperature and precipitation extremes (with early spring being defined here as the same time windows as before). Specifically, we consider “warm” (“cold”) as a situation with the mean spring temperature (as in Fig. 3) being higher (lower)

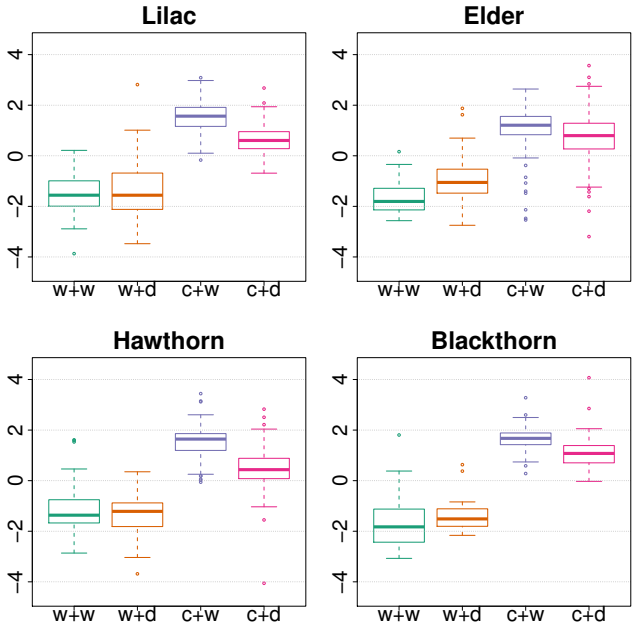

Figure 6. Distribution of flowering dates (standard box plots) for years that exhibit four different combinations of extreme meteorological conditions during early spring (w + w: warm and wet; w + d: warm and dry; c + w: cold and wet; c + d: cold and dry).

than the 90th (10th) percentile. Similarly, "wet" ("dry") conditions are defined as years with spring precipitation sums higher (lower) than the respective percentile.

The results obtained in this way are very similar for all four shrub species. Warm and wet as well as warm and dry spring conditions generally lead to similarly early flowering dates (with exception of elder, where warm and wet conditions have a clearly stronger impact than warm and dry years). Following cold and wet spring conditions, the flowering dates of all four species are heavily delayed, with the effect being somewhat stronger than for very cold and dry conditions. Taken together, this analysis again confirms the minor-to-negligible influence of extremes in water availability on flowering dates in the study region. It should be noted, however, that in each individual combination of temperature and precipitation extremes, we also find cases where the flowering dates show a deviation from normal that is the opposite of what would be expected. The latter is particularly evident for elder and indicates that early spring mean temperature and precipitation sum alone cannot fully describe the plant's flowering dates, but it calls for the consideration of further covariates (like temperature/precipitation in different time windows as well as other meteorological factors not available in the studied data set). The latter observation has a potential relevance for developing improved statistical models for anticipating flowering dates but possibly also other phenological phases. A further detailed investigation of this problem is, however, beyond the scope of the present work.

5 Discussion

The results displayed in Figs. 4 and 5 suggest that event coincidence analysis is (in combination with a sliding window approach) indeed an appropriate technique to identify periods during or prior to the growing season, where extreme temperatures or precipitation sums are statistically related to extreme flowering dates. To our best knowledge, no similar analysis has been performed so far. In turn, all previous studies on possible relations between climate variables and flowering times have been based on linear correlation (Ahas et al., 2000; Sparks et al., 2000; Menzel, 2003). While correlations take all parts of the distributions of the two considered observables into account, event coincidence analysis exclusively focuses on the extremes, ignoring all other values. Although it is widely known that early spring temperatures strongly influence flowering dates, the specific validity of such a relationship for extreme values cannot be concluded from classical correlation analysis (see the Supplement for a detailed discussion). In turn, our methodological approach showed that the relationship does indeed also apply to the extreme values of temperature and flowering time for a significant subset of the investigated stations.

Another notable observation of this study is that positive temperature extremes (warm periods) that coincide with early flowering do not occur arbitrarily early in the year. This general finding is valid for all four analysed shrub species. However, an important exception can be seen at some stations in the very north of the study region and thus close to the North and Baltic seas. For these stations, the time windows for which significant coincidence rates between temperature and flowering date are evident, reach much further into late winter. This observation could result from the regulating effect of these two large water bodies, the large heat capacity of which allows maintaining relatively warm but not necessarily extreme air temperatures (especially during night-time, i.e. suppressing freezing conditions during winter time) for a considerable period of time. As a consequence, an extremely warm period in, for example, January can have a persistent effect on terrestrial ecosystems in coastal regions over the following weeks, resulting in coincidences between positive January window-mean temperature extremes and early flowering. This effect also explains why the prolonged significance peaks (late winter until late spring) of the northernmost stations in Fig. 4 are mainly visible for the longer time windows, since only long-lasting unusually warm conditions are stored for a substantial amount of time. A similar time-lagged regulatory effect of large water bodies on air temperatures (mediated via the long-term memory of sea-surface temperatures) is well known for El Niño events (Kumar and Hoerling, 2003). It was also found that North Atlantic temperature anomalies can influence atmospheric conditions in the following seasons with time lags of up to several months (Wedgbrow et al., 2002; Iwi et al., 2006).

Our analysis also reveals another important observation: for lilac, elder, hawthorn and blackthorn (Fig. 4), we find a small but noticeable signature of coincidences between very warm 15-day windows during early September and very early flowering in the following year. This feature is relatively weakly expressed in comparison to the effect of spring temperature anomalies directly preceding the flowering but still far larger than the expected tolerable false positive rate of our test setting. Indications of the existence of such significant statistical relationships between flowering and temperatures of the previous growing season have already been found by, e.g., Sparks et al. (2000) for autumn crocus and by Fitter et al. (1995), Luterbacher et al. (2007) and Crimmins et al. (2010) for various other plant species. Heide (2003) reported that autumn temperatures were significantly correlated with the number of days to bud burst in the subsequent spring in field experiments with a range of latitudinal birch populations at 60° N. However, the direction of the influence of warm autumn temperatures on the timing of flowering seems to strongly depend on plant species and geographical conditions like elevation (Crimmins et al., 2010). Cook et al. (2012) reported divergent responses of different plant species to spring and winter warming: "(i) apparent nonresponders are indeed responding to warming, but their responses to fall/winter and spring warming are opposite in sign and of similar magnitude; (ii) observed trends in first flowering date depend strongly on the magnitude of a given species' response to fall/winter vs. spring warming; and (iii) inclusion of fall/winter temperature cues strongly improves hindcast model predictions of long-term flowering trends compared with models with spring warming only". In the context of our present study, this accumulated evidence raises confidence that the findings reported here are not just statistical artifacts resulting from the auto-correlation of temperature time series but plant physiologically meaningful. In order to further address this question, future studies should explicitly address the potential influence of auto-correlations in more detail, calling for a methodological extension of event coincidence analysis conditioning on previous events (in a similar spirit as partial correlations or conditional mutual information; see, e.g., Balasis et al., 2013; Siegmund et al., 2016a).

We have also considered the combined effects of very cold/warm and wet/dry conditions. Notably, the delaying impact of very cold conditions appears more effective in combination with very wet than with very dry conditions. This finding was not to be expected from independent analyses of temperature and precipitation influences as commonly considered in the literature (Zscheischler et al., 2014), where in our case precipitation was found not to have any statistically significant effect. However, it may act as a potentially relevant modulator of the effect of extreme temperature on plant phenology. In the specific case of shrub flowering studied in this work, we hypothesize that the additionally delaying effect of wet conditions could be related to snow cover. In fact, prolonged snow cover has widely been found to delay plant development including flowering dates for several species in the Arctic (Cooper et al., 2011; Semenchuk et al., 2013) and alpine regions (Inouye, 2008; Dunne et al., 2003).

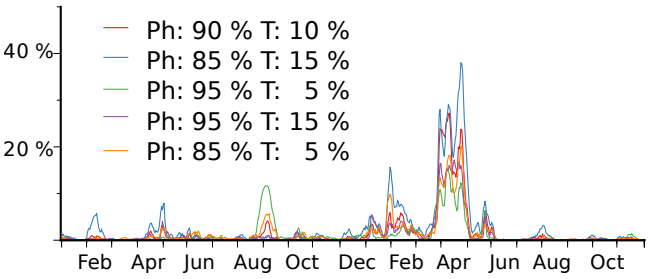

Figure 7. Fraction of stations with significant coincidence rates ($\alpha = 0.05$) among all phenological stations for 30-day windows and five different threshold combinations of extremely warm window-mean temperature and extremely early elder flowering. Note that the red line is the same as the bold red line displayed in Fig. 5, lower right panel.

In contrast, for very warm spring conditions, very high or very low precipitation sums have little additional effect for lilac, hawthorn and blackthorn, while the effect of warm conditions appears to be slightly reduced during years with dry springs for elder. In all cases, it has to be noted that for all four possible combinations of temperature and precipitation extremes, the distribution of flowering dates of the respective years has been very broad and includes in most cases also situations that appear to contradict the previously reported mean effect. Further work should clarify to what extent this observation can be related to site-specific effects.

A potential drawback of event coincidence analysis applied to non-binary data could be a dependence of the results on the threshold used for the definition of an extreme. In this study, we used the 90th and 10th percentiles for temperature, precipitation and flowering time. In order to further demonstrate the qualitative robustness of our results, Fig. 7 recalls the results of Fig. 5 (right panel, second row) with five different threshold definitions. The obtained results show that although the absolute number of stations with significant coincidence rates varies among the different threshold combinations (as expected from the definitions of events and coincidences), the general temporal profile qualitatively remains the same for most windows. In most cases the observed numbers of stations with significant coincidence rates are larger for less restrictive thresholds. As a notable exception, regarding the relevance of warm autumn temperature in the previous year, we find an opposite behaviour, i.e. the event coincidence analysis using a more restrictive threshold (green line in Fig. 7) results in a higher number of stations with significant coincidence rates than the same analysis employing more conservative thresholds (e.g. red line in Fig. 7), indicating that this observation could have been caused by only a few events per station within the considered window of observations. Hence, whereas the relationship between ex-

tremely positive temperature anomalies in spring and early flowering appears to consistently apply for different event magnitudes, for the previous autumn, the strongest positive anomalies could have an over-proportional relevance for the emergence of very early elder flowering.

6 Conclusions

In summary, the first-time application of the modern statistical concept of event coincidence analysis to phenological data revealed a clear statistical relationship between extremely warm spring temperatures and very early flowering dates of lilac, elder, hawthorn and blackthorn, as well as between extremely cold temperatures in spring and extremely late flowering dates. Although this relationship is not evident for all investigated study sites individually, the observed coincidences are quite homogeneously distributed over the study area (see the Supplement).

In addition to the expected relevance of spring temperatures, we identified a period during the previous year's autumn, where extremely warm temperatures significantly coincide with an extremely early flowering in the subsequent year. Although the signatures of this period are not very strong, they are clearly visible. Our study revealed that this effect becomes even stronger when more restrictive threshold definitions are used. In contrast to the confirmed dependence of early and late flowering events on temperature extremes, our analysis did not identify similar marked statistical relationships between extreme precipitation amounts and the timing of flowering unless the precipitation anomalies (in both directions) co-occur with very cold temperatures.

To answer the research questions formulated in the Introduction, we conclude that extremely high (low) temperatures do significantly coincide with extremely early (late) flowering, especially if the extreme period appears during early spring. All four analysed shrub species show the same qualitative behaviour and only differ in the timing, according to their typical flowering time. The specific findings differ somewhat by region, but an easily explainable pattern or spatial clustering of stations with significant coincidence rates could not be found. Our results further support the outcomes of previous studies by underlining the fact that known interdependencies between meteorological variables and flowering dates do not only cover the bulk of their corresponding empirical distributions (as highlighted by studies using linear correlation analysis) but for the tails (i.e. extreme conditions).

To this end, our work presented here has served as a pilot study demonstrating the application of event coincidence analysis in the context of plant phenology. A systematic extension of the obtained results to more species, more phenological phases and more meteorological covariates appears reasonable. In order to cope with data from study sites where even fewer years of observations are available, recently developed group-significance tests for event coincidence analysis (Donges et al., 2016) are ready for application. In a similar spirit, multivariate extensions of this approach (Siegmund et al., 2016b) allow the systematic study of combined impacts of (simultaneous or mutually time-shifted) extremes in different meteorological variables. For the latter purpose (especially the consideration of effects of water availability), the meteorological data set used in this work needs to be systematically extended.

We emphasize that besides providing directly usable information for forest and agricultural management purposes, future extended studies along the lines of the present work do also have great potential value for biogeographical model development. To date, the usability of information about extreme weather impacts on flowering dates for numerical ecosystem models like the Lund–Potsdam–Jena Dynamic Global Vegetation Model (LPJ; Sitch et al., 2003) is strongly limited by the fact that in most cases, these models use growing degree days and corresponding temperature sums for the calculation of phenological phases. Specific extreme events of limited temporal extent like those investigated in our study can commonly not be considered. Furthermore, the parameterizations of shrubs normally does not distinguish between different species. Here, further systematic empirical analyses may provide valuable input to refining these parameterizations.

The findings of this study underline the risk of potential phenological mismatches due to temperature extremes, at least from the plant-ecological perspective. In future studies, it will be especially important to further investigate possible delayed influences of extremely warm temperatures on flowering dates of the following growing season.

7 Data availability

The phenology data used in this study are provided by the German weather service DWD and are available at http://www.dwd.de/phaenologie. For meteorological information we used temperature and precipitation time series produced and provided by Österle et al. (2006), which are available upon request to peterh@pik-potsdam.de.

The Supplement related to this article is available online at doi:10.5194/bg-13-5541-2016-supplement.

Acknowledgements. This study was conducted within the framework of the BMBF Young Investigators Group "CoSy-CC^2: Complex Systems Approaches to Understanding Causes and Consequences of Past, Present and Future Climate Change" (grant no. 01LN1306A) funded by the German Federal Ministry for Education and Research (BMBF). J. F. Siegmund additionally acknowledges the Evangelisches Studienwerk Villigst for providing

financial support. J. F. Donges has been funded by the Stordalen Foundation (via the Planetary Boundary Research Network PB.net), the Earth League's EarthDoc program and the BMBF via the project GLUES. Stimulating discussions with Diego Rybski are gratefully acknowledged. Event coincidence analysis was performed using the R package CoinCalc (Siegmund et al., 2016b) available at https://github.com/JonatanSiegmund/CoinCalc.git.

Edited by: M. Weintraub
Reviewed by: two anonymous referees

References

Ahas, R., Jaagus, J., and Aasa, A.: The phenological calendar of Estonia and its correlation with mean air temperature, Int. J. Biometeorol., 44, 159–166, 2000.

Atkinson, M. and Atkinson, E.: Sambucus nigra L., J. Ecol., 90, 895–923, 2002.

Augspurger, C.: Spring 2007 warmth and frost: phenology, damage and refoliation in a temperate deciduous forest, Funct. Ecol., 23, 1031–1039, 2009.

Balasis, G., Donner, R., Potirakis, S., Runge, J., Papadimitriou, C., Daglis, I., Eftaxias, K., and Kurths, J.: Statistical Mechanics and Information-Theoretic Perspectives on Complexity in the Earth System, Entropy, 15, 4844–4888, 2013.

Barriopedro, D., Fischer, E., Luterbacher, J., Trigo, R., and Garcia-Herrera, R.: The Hot Summer of 2010: Redrawing the Temperature Record Map of Europe, Science, 332, 220–224, 2011.

Burkle, L., Marlin, J., and Knight, T.: Plant-Pollinator Interactions over 120 Years: Loss of Species, Co-Occurrence, and Function, Science, 339, 1611–1615, 2013.

Cleland, E., Chuine, I., Menzel, A., Mooney, H., and Schwartz, M.: Shifting plant phenology in response to global change, Trends Ecol. Evol., 22, 357–365, 2007.

Cook, B., Wolkovich, E., and Parmesan, C.: Divergent responses to spring and winter warming drive community level flowering trends, P. Natl. Acad. Sci. USA, 109, 9000–9005, 2012.

Cooper, E., Dullinger, S., and Semenchuk, P.: Late snowmelt delays plant development and results in lower reproductive success in the High Arctic, Plant Sci., 180, 157–167, 2011.

Coumou, D. and Rahmstorf, S.: A decade of weather extremes, Nature Climate Change, 2, 491–496, 2012.

Crimmins, T., Crimmins, M., and Bertelsen, C.: Complex responses to climate drivers in onset of spring flowering across a semi-arid elevation gradient, J. Ecol., 98, 1042–1051, 2010.

Deutscher Wetterdienst, Offenbach: DWD Klimastationen: Daten der Klimastationen des Deutschen Wetterdienstes, 2009.

Donges, J., Donner, R., Trauth, M., Marwan, N., Schellnhuber, H.-J., and Kurths, J.: Nonlinear detection of paleoclimate-variability transitions possibly related to human evolution, P. Natl. Acad. Sci. USA of the USA, 108, 20422–20427, 2011.

Donges, J., Schleussner, C.-F., Siegmund, J., and Donner, R.: Event coincidence analysis for quantifying statistical interrelationships between event time series: on the role of flood events as triggers of epidemic outbreaks, Eur. Phys. J.-Spec. Top., 225, 471–487, 2016.

Duffey, E., Morris, M., Sheail, J., Ward, L., Wells, D., and Wells, T.: Grassland Ecology and Wildlife Management, Chapman and Hall, 1974.

Dunne, J., Harte, J., and Taylor, K.: Subalpine meadow flowering phenology responses to climate change: Integrating experimental and gradient methods, Ecol. Monogr., 73, 69–86, 2003.

Easterling, D., Meehl, G., Parmesan, C., Changnon, S., Karl, T., and Mearns, L.: Climate extremes: observations, modeling, and impact, Science, 289, 2069–2074, 2000.

Fischer, E., Seneviratne, S., Luethi, D., and Schaer, C.: Contribution of land-atmosphere coupling to recent European summer heat waves, Geophys. Res. Lett., 34, L0607, doi:10.1029/2006GL029068, 2007.

Fitter, A., Fitter, R., Harris, I., and Williamson, M.: Relationships between first flowering date and temperature in the flora of a locality in central England, Funct. Ecol., 9, 55–60, 1995.

Frank, D., Reichstein, M., Bahn, M., Thonicke, K., Frank, D., Mahecha, M., Smith, P., Van der Velde, M., Vicca, S., Babst, F., Beer, C., Buchmann, N., Canadell, J., Ciais, P., Cramer, W., Ibrom, A., Miglietta, F., Poulter, B., Rammig, A., Seneviratne, S., Walz, A., Wattenbach, M., Zavala, M., and Zscheischler, J.: Effects of climate extremes on the terrestrial carbon cycle: concepts, processes and potential future impacts, Glob. Change Biol., 21, 7861–2880, 2015.

Garcia-Herrera, R., Diaz, J., Trigo, R., Luterbacher, J., and Fischer, E.: A Review of the European Summer Heat Wave of 2003, Critical Reviews in Environmental Science and Technology, 40, 267–306, 2010.

Gudmundsson, L. and Seneviratne, S. I.: European drought trends, Proc. IAHS, 369, 75–79, doi:10.5194/piahs-369-75-2015, 2015.

Haylock, M. and Goodess, C.: Interannual variability of european extreme winter rainfall and links with mean large-scale circulation, Int. J. Climatol., 24, 759–776, 2004.

Heide, O.: High autumn temperature delays spring bud burst in boreal trees, counterbalancing the effect of climatic warming, Tree Physiol., 23, 931–936, 2003.

Inouye, D.: Effects of climate change on phenology, frost damage, and floral abundance of montane wildflowers, Ecology, 89, 353–362, 2008.

IPCC: Climate Change 2013: The Physical Science Basis. Contribution of Working Group I to the Fifth Assessment Report of the Intergovernmental Panel on Climate Change, Cambridge University Press, Cambridge, United Kingdom and New York, NY, USA, 2013.

Iwi, A., Sutton, R., and Norton, W.: Influence of May Atlantic Ocean initial conditions on the subsequent North Atlantic winter climate, Q. J. Roy. Meteorol. Soc., 132, 2977–2999, 2006.

Jacobs, J., Clak, S., Denholm, I., Goulson, D., Stoate, C., and Osborne, J.: Pollination biology of fruit-bearing hedgerow plants and the role of flower-visiting insects in fruit-set, Ann. Bot., 104, 1397–1404, 2009.

Jentsch, A., Kreyling, J., and Beierkuhnlein, C.: A new generation of climate change experiments: events not trends, Front. Ecol. Environ., 5, 365–374, 2007.

Jentsch, A., Kreyling, J., Boettcher-Treschkow, J., and Beierkuhnlein, C.: Beyond gradual warming: extreme weather events alter flower phenology of European grassland and heath species, Glob. Change Biol., 15, 837–849, 2009.

Kudo, G. and Ida, T.: Early onset of spring increases the phenological mismatch between plants and pollinators, Ecology, 94, 2311–2320, 2013.

Kumar, A. and Hoerling, M.: The nature and causes for the delayed atmospheric response to El Nino, J. Climate, 16, 1391–1403, 2003.

Kundzewicz, Z., Radziejewski, M., and Pinskwar, I.: Precipitation extremes in the changing climate of Europe, Clim. Res., 31, 51–58, 2006.

Kysely, J., Gaal, L., Beranova, R., and Plavcova, E.: Climate change scenarios of precipitation extremes in Central Europe from ENSEMBLES regional climate models, Theor. Appl. Climatol., 104, 529–542, 2011.

Law, B., Mackowski, C., Schoer, L., and Tweedie, T.: Flowering phenology of myrtaceous trees and their relation to climatic, environmental and disturbance variables in northern New South Wales, Aust. Ecol., 25, 160–178, 2000.

Lupikasza, E., Hansel, S., and Matschullat, J.: Regional and seasonal variability of extreme precipitation trends in southern Poland and central-eastern Germany 1951–2006, Int. J. Climatol., 31, 2249–2271, 2011.

Luterbacher, J., Dietrich, D., Xoplaki, E., Grosjean, M., and Wanner, H.: European seasonal and annual temperature variability, trends, and extremes since 1500, Science, 303, 1409–1503, 2004.

Luterbacher, J., Lininger, M., Menzel, A., Estrella, N., Della-Marta, P., Pfister, C., Rutishauser, T., and Xoplaki, E.: Exceptional European warmth of autumn 2006 and winter 2007: Historical context, the underlying dynamics, and its phenological impacts, Geophys. Res. Lett., 34, L12704, doi:10.1029/2007GL029951, 2007.

McKinney, A., CaraDonna, P., Inouye, D., Barr, B., Bertelsen, C., and Waser, N.: Asynchronous changes in phenology of migrating Broad-tailed Hummingbirds and their early-season nectar resources, Ecology, 93, 1987–1993, 2012.

Menzel, A.: Plant phenological anomalies in Germany and their relation to air temperature and NAO, Climatic Change, 57, 243–263, 2003.

Menzel, A., Seifert, H., and Estrella, N.: Effects of recent warm and cold spells on European plant phenology, Int. J. Biometeorol., 55, 921–932, 2011.

Nagy, L., Kreyling, J., Gellesch, E., Beierkuhnlein, C., and Jentsch, A.: Recurring weather extremes alter the flowering phenology of two common temperate shrubs, Int. J. Biometeorol., 57, 579–588, 2013.

Österle, H., Werner, P., and Gerstengarbe, F.: Qualitätsprüfung, Ergänzung und Homogenisierung der täglichen Datenreihen in Deutschland, 1951-2003: ein neuer Datensatz, in: 7. Deutsche Klimatagung, Klimatrends: Vergangenheit und Zukunft, 9–11 Oktober 2006, 2006.

Parmesan, C.: Ecological and evolutionary responses to recent climate change, Annual Review of Ecology, Evolution and Systematics, 37, 637–669, 2006.

Parmesan, C., Root, T., and Willig, M.: Impacts of Extreme Weather and Climate on Terrestrial Biota, B. Am. Meteorol. Soc., 81, 444–449, 2000.

Perneger, T.: What's wrong with Bonferroni adjustments, British Medical Journal, 316, 1236–1238, 1998.

Petoukhov, V., Rahmstorf, S., Petri, S., and Schellnhuber, H.-J.: Quasiresonant amplification of planetary waves and recent Northern Hemisphere weather extremes, P. Natl. Acad. Sci. USA of the USA, 110, 5336–5341, 2013.

Post, E. and Stenseth, N.: Climate Variability, Plant Phenology and Northern Ungulates, Ecology, 80, 1322–1339, 1999.

Prieto, P., Penuelas, J., Ogaya, R., and Estiarte, M.: Precipitation-dependent flowering of Globularia alypum and Erica multiflora in Mediterranean shrubland under experimental drought and warming, and its inter-annual variability, Ann. Bot., 102, 275–285, 2008.

Rafferty, N., CaraDonna, P., and Bronstein, J.: Phenological shifts and the fate of mutualisms, Oikos, 124, 14–21, 2015.

Rahmstorf, S. and Coumou, D.: Increase of extreme events in a warming world, P. Natl. Acad. Sci. USA, 108, 17905–17909, 2011.

Rajczak, J. P. P. and Schar, C.: Projections of extreme precipitation events in regional climate simulations for Europe and the Alpine Region, J. Geophys. Res.-Atmos., 118, 3610–3626, 2013.

Rammig, A., Wiedermann, M., Donges, J. F., Babst, F., von Bloh, W., Frank, D., Thonicke, K., and Mahecha, M. D.: Coincidences of climate extremes and anomalous vegetation responses: comparing tree ring patterns to simulated productivity, Biogeosciences, 12, 373–385, doi:10.5194/bg-12-373-2015, 2015.

Reichstein, M., Bahn, M., Ciais, P., Frank, D., Mahecha, M., Seneviratne, S., Zscheischler, J., Beer, C., Buchmann, N., Frank, D., Papale, D., Rammig, A., Smith, P., Thonicke, K., van der Velde, M., Vicca, S., Walz, A., and Wattenbach, M.: Climate extremes and the carbon cycle, Nature, 500, 287–295, 2013.

Reyer, C., Leuzinger, S., Rammig, A., Wolf, A., Bartholomeus, R., Bonfante, A., Lorenz, F., Dury, M., Glonning, P., Jaoude, R., Klein, T., Kuster, T., Martinis, M., Niedrist, G., Riccardi, M., Wohlfahrt, G., Angelis, P., DeDato, G., Francous, L., Menzel, A., and Pereira, M.: A plant's perspective of extremes: terrestrial plant responses to changing climatic variability, Glob. Change Biol., 19, 75–89, 2013.

Rutishauser, T., Luterbacher, J., Defila, C., Frank, D., and Wanner, H.: Swiss spring plant phenology 2007: Extremes, a multicentury perspective, and changes in temperature sensitivity, Geophys. Res. Lett., 35, L05703, doi:10.1029/2007GL032545, 2008.

Rybski, D., Holstern, A., and Kropp, J.: Towards a unified characterization of phenological phases: Fluctuations and correlations with temperature, Physica A, 390, 680–688, 2011.

Schaer, C., Vidale, P., Luethi, D., Frei, C., Haeberli, C., Liniger, M., and Appenzeller, C.: The role of increasing temperature variability in European summer heatwaves, Nature, 427, 332–336, 2004.

Schleip, C., Ankerst, D., Bock, A., Estrella, N., and Menzel, A.: Comprehensive methodological analysis of long-term changes in phenological extremes in Germany, Glob. Change Biol., 18, 2349–2364, 2012.

Semenchuk, P., Elberling, B., and Cooper, E.: Snow cover and extreme winter warming events control flower abundance of some, but not all species in high arctic Svalbard, Ecol. Evol., 3, 2586–2599, 2013.

Seneviratne, S. I., Nicholls, N., Easterling, D., Goodess, C. M., Kanae, S., Kossin, J., Luo, Y., Marengo, J., McInnes, K., Rahimi, M., Reichstein, M., Sorteberg, A., Vera, C., and Zhang, X.: Changes in climate extremes and their impacts on the natural physical environment, in: Managing the Risks of Extreme Events and Disasters to Advance Climate Change Adaptation edited by: Field, C. B., Barros, V., Stocker, T. F., Qin, D., Dokken, D. J.,

Ebi, K. L., Mastrandrea, M. D., Mach, K. J., Plattner, G.-K., Allen, S. K., Tignor, M., and Midgley, P. M., A Special Report of Working Groups I and II of the Intergovernmental Panel on Climate Change (IPCC), Cambridge University Press, Cambridge, UK, and New York, NY, USA, 109–230, 2012.

Shaffer, J.: Multiple Hypothesis Testing, Annu. Rev. Psychol., 46, 561–584, 1995.

Siegmund, J., Sanders, T., Heinrich, I., van der Maaten, E., Simard, S., Helle, G., and Donner, R.: Meteorological Drivers of Extremes in Daily Stem Radius Variations of Beech, Oak, and Pine in Northeastern Germany: An Event Coincidence Analysis, Front. Plant Sci., 7, 733, 2016a.

Siegmund, J., Siegmund, N., and Donner, R.: CoinCalc - A new R package for quantifying simultaneities of event (time) series, arXiv:1603.05038, 2016b.

Sitch, S., Smith, B., Prentice, I., Arneth, A., Bondeau, A., Cramer, W., Kaplan, J., Levis, S., Lucht, W., Sykes, M., Thonicke, K., and Venevsky, S.: Evaluation of ecosystem dynamics, plant geography and terrestrial carbon cycling in the LPJ dynamic global vegetation model, Glob. Change Biol., 9, 161–185, 2003.

Southwood, T.: The Number of Insect Species Associated with Various Trees, J. Animal Ecol., 30, 1–8, 1961.

Sparks, T. and Menzel, A.: Observed changes in seasons: an overview, Int. J. Climatol., 22, 1715–1725, 2002.

Sparks, T., Jeffree, E., and Jeffree, C.: An examination on the relationship between flowering times and temperature at the national scale using long-term phenological records from the UK, Int. J. Biometeorol., 44, 82–87, 2000.

Spinoni, J., Naumann, G., and Vogt, J.: Spatial patterns of European droughts under a moderate emission scenario, Adv. Sci. Res., 12, 179–186, 2015a.

Spinoni, J., Naumann, G., Vogt, J., and Barbosa, P.: European drought climatologies and trends based on a multi-indicator approach, Global Planet. Change, 127, 50–57, 2015b.

Stott, P., Stone, D., and Allen, R.: Human contribution to the European heatwave of 2003, Nature, 432, 610–614, 2004.

Tank, K. and Konnen, G.: Trends in indices of daily temperature and precipitation extremes in Europe, 1946–99, J. Climate, 16, 3665–3680, 2003.

Trenberth, K. and Fasullo, J.: Climate extremes and climate change: The Russian heat wave and other climate extremes of 2010, J. Geophys. Res.-Atmos., 117, D17103, doi:10.1029/2012JD018020, 2012.

Wedgbrow, C., Wilby, R. L., Fox, H., and O'Hare, G.: Prospects for seasonal forecasting of summer drought and low river flow anomalies in England and Wales, Int. J. Climatol., 22, 219–236, 2002.

WMO: Standardized Precipitation Index User Guide, Geneva, 2012.

Zimmermann, N., Yoccoz, N., Edwards, T., Meier, E., Thuiller, W., Guisan, A., Schmatz, D., and Pearman, P.: Climatic extremes improve predictions of spatial patterns of tree species, P. Natl. Acad. Sci. USA, 17, 19723–19728, 2009.

Zscheischler, J., Michalak, A., Schwalm, C., Mahecha, M., Huntzinger, D., Reichstein, M., Berthier, G., Ciais, P., Cook, R., El-Masri, B., Huang, M., Ito, A., Jain, A., King, A., Lei, H., Lu, C., Mao, J., Peng, S., Poulter, B., Ricciuto, D., Shi, X., Tao, B., Tian, H., Viovy, N., Wang, W., Wei, Y., Yang, J., and Zeng, N.: Impact of large-scale climate extremes on biospheric carbon fluxes: An intercomparison based on MsTMIP data, Global Biochem. Cy., 28, 585–600, 2014.

Abstract. This document provides supplementary material to the contents of **Siegmund et al. (2016a): Impact of temperature and precipitation extremes on the flowering dates of four German wildlife shrub species, Biogeosciences, 13, 55415555**

S1 Introduction

In the following, we first provide additional methodological details on the application of event coincidence analysis. Then, we further elaborate on the differences between event coincidence analysis and correlation analysis based on the consideration of artificial numerical examples as well as the results obtained for the data studied in our main paper. Finally, we provide further results on the spatial distribution of study sites with statistically significant coincidence rates, which may yield initial information on this aspect which could be potentially useful for planning purposes in terms of agricultural and forest management.

S2 Event coincidence analysis

S2.1 Analytical significance test

Under the assumption of mutually independent events and, hence, independent exponentially distributed waiting times between subsequent events (corresponding to the null hypothesis of Poisson processes generating the event series), the probability that exactly K coincidences are observed just by chance can be expressed as Donges et al. (2016)

$$P(K) = \binom{N}{K} \left[1 - \left(1 - \frac{1}{T}\right)^M\right]^K \cdot \left[\left(1 - \frac{1}{T}\right)^M\right]^{N-K} . \quad (1)$$

In the present case, N and M denote the numbers of extreme events in temperature/precipitation (N) and phenology (M) (where we have restricted most of the analyses in our main paper – with the exception of Fig. 7 – to the case of $N = M$) and T the length of the time series (number of years of observation). Note that Eq. (S1) takes the discrete nature of time steps in the phenological records (one year) into account and requires the sparseness of events, a criterion met by the definition of our event thresholds.

Equation (S1) allows defining a simple significance test for the observed number of coincidences (K_{obs}) in two paired event series. For this purpose, we consider pairs of event series with

$$\sum_{K \geq K_{\text{obs}}} P(K) < \alpha \quad (2)$$

with $\alpha = 0.05$ (0.01) to exhibit a significantly non-random coincidence rate at 5 % (1 %) confidence level.

We note that the Poissonian assumption is only valid in case of sufficiently rare and temporally uncorrelated events in the two series under study. If the latter are not fulfilled, the expectation value and standard deviation computed from Eq. (S1) are systematically biased. In such cases, we recommend application of Monte Carlo methods for obtaining a constrained resampling estimate of the probability density function of the test statistic K used by event coincidence analysis. For a detailed discussion of these aspects together with different types of event surrogates that can be used for this purpose, we refer to Donges et al. (2016).

S2.2 Trigger and precursor tests

We emphasize that under general conditions, there are two basic modes to perform event coincidence analysis (Donges et al. (2016)): a "precursor test" (studying the appearance of a preceding climate extreme conditional on that of an extreme flowering date) and a "trigger test" (conditioning the timing of extreme flowering dates on previous extreme climatic events). Since we consider only climatic events at fixed points (windows) in time (instead of allowing for their appearance within a certain period potentially covering several subsequent windows) and have $N = M$, both tests are equivalent in the setting used in this study.

S3 Event coincidence analysis vs. correlation analysis

In our main paper, we have already discussed the conceptual differences between event coincidence analysis and linear correlation analysis as the statistical approach most commonly used in previous phenological studies. Recall that event coincidence analysis solely takes the timing of well-defined events in each pair of time series into account (in our case, these events have been defined as the extreme values in the upper and lower tails of the distribution of our variables of interest), whereas correlation analysis uses all explicit values in all parts of the distributions of the variables under study. Accordingly, significant coincidence rates mean "significantly simultaneous events in both time series", while significant correlation coefficients imply "significant co-variability of the two series". Moreover, correlation analysis only captures linear interrelationships between two observables, whereas this restriction is (partially) relieved in the case of event coincidence analysis.

Following these differences, a strong correlation does *not* necessarily imply the co-occurrence of extreme values (i.e., rare events) in two data sets (and vice versa). The latter would only be valid if the two variables of interest exhibit a monotonic relationship across all parts of the distributions. Such a monotonic relationship between phenological phases and meteorological parameters could be questioned, since the correlation coefficients found in related studies in the past typically ranged between 0.5 and 0.85. For example, Ahas

et al. (2000) reported an r^2 value between spring temperature and Lilac pollination of 0.52, i.e., only 52% of the pollination time variance could be explained by a linear model, whereas almost half of it remained unexplained by this approach. Even in cases where the variance of a phenological phase is much better explained by a linear regression model using a certain meteorological variable as predictor (e.g., $r^2 = 0.75$ for apple pollination and spring temperature, Ahas et al. (2000)), the remaining unexplained variance can still be relevant. Among other possibilities, the extreme values could play an important role for that part of the total covariability that cannot be explained by a linear model.

In this Section, we will provide further evidence that the results of event coincidence analysis cannot be directly inferred from those of correlation-based studies. We first exemplify this claim based on some artificial data sets before proceeding to an inter-comparison between the results of correlation and event coincidence analysis for the data sets under study in our main paper.

S3.1 Numerical examples

As discussed in our main paper, high (low) correlation coefficients between two time series do not necessarily imply high (low) coincidence rates between the uppermost/lowermost values of these series, especially if the variables of interest exhibit a nonlinear relationship or large noise level. Here, we provide some numerical examples supporting these claims.

S3.1.1 Critical values of test statistics

To begin with, let us address the different sensitivity and specificity of the resulting statistical tests, which can trigger marked differences between the outcomes of both methods even in the presence of a completely linear relationship between two variables in all parts of their respective distributions. For example, let us suppose a sample size of $T = 100$ data points in both variables of interest, and a threshold for defining extremes corresponding to the respective 10th or 90th percentile, i.e., resulting in $N = 10$ events in each series. In the case of the linear correlation coefficient r, we apply a classical t-test with the test statistics

$$t = \frac{r}{\sqrt{(1-r^2)/(T-2)}}, \tag{3}$$

which asymptotically follows a t distribution with $T-2$ degrees of freedom. At a confidence level of $\alpha = 0.05$, this corresponds to a critical value of $r_{crit} = 0.197$ above which an empirical correlation is deemed significant. In turn, under the Poissonian assumption, the probability to find more than 3 (4) coinciding extremes out of 10 within a sample of 100 points is $p(K \geq 3) = 0.063$ ($p(K \geq 4) = 0.011$), so that we would consider a critical value of the coincidence rate $\kappa = K/N$ of $\kappa_{crit} = 0.4$. From this, it is evident that a simple scatter plot of correlation coefficient versus coincidence rate might lead to misleading interpretations, since the distributions of both statistics are (beyond exhibiting continuous versus discrete values) not directly inter-comparable.

S3.1.2 Coincidence rates for nonlinear dependencies

Next, we will discuss a numerical example for which coincidence rates cannot be directly derived from linear correlation values. For this purpose, let us consider one time series $\{x_t\}$ of length $T = 100$ being given by simple Gaussian white noise and a second one $\{y_t\}$ generated by the deterministic function $y_t = 0.3x_t^3 - bx_t$ with a tunable parameter b. In Fig. S1, we show the respective medians and 5%/95% quantiles of Pearson correlation coefficients and coincidence rates (for the uppermost/lowermost 10 values of each sequence) estimated from 100 independent realizations of the noise process $\{x_t\}$. For large b, the linear part in the definition of $\{y_t\}$ dominates, and we observe a linear correlation coefficient of $r \to -1$ and, consequently, coincidence rates between the upper 10% of x-values and the lower (upper) 10% of y-values of $\kappa \to 1$ ($\kappa \to 0$). In turn, for $b \to 0$, only the cubic term contributes effectively, and for values of x_t close to zero (i.e., the majority of values), this cubic term can be roughly approximated by a linear dependence with positive shape, implying that $r \to 1$ and the coincidence rates behave according to the expectations. The most interesting behavior is found at intermediate values of b, where the correlation coefficient between x and y is close to zero, but the coincidence rates differ clearly from zero in many cases. In this regime, the nonlinearity of the function interrelating both variables fully pays out, and the coincidence rates cannot be estimated from the correlation coefficients.

S3.2 Correlations and event coincidences between plant flowering and temperature/precipitation

We next illustrate the difference between correlation and event coincidence analysis based upon flowering dates and mean spring temperatures for a single randomly selected study site taken from the data set studied in our main paper. Figure S2 shows that in the considered example, in four out of six cases with the highest spring temperatures, we also observe four out of the top six earliest flowering dates, i.e., we have a significant coincidence rate of $\kappa = 4/6$. In turn, each of the two variables exhibits two extreme cases with do not coincide with those of the other despite a clearly visible negative correlation.

In order to further underline the necessity of an event-based statistical approach for studying extreme flowering dates in the study area, we proceed with a corresponding analysis for the whole data set. Figures S3 and S4 show scatter plots between correlation coefficients and coincidence rates for all stations. The calculation of the mean spring temperatures was performed in the same manner as for Figs. 3 and 6 in the main paper. The two figures clearly illustrate

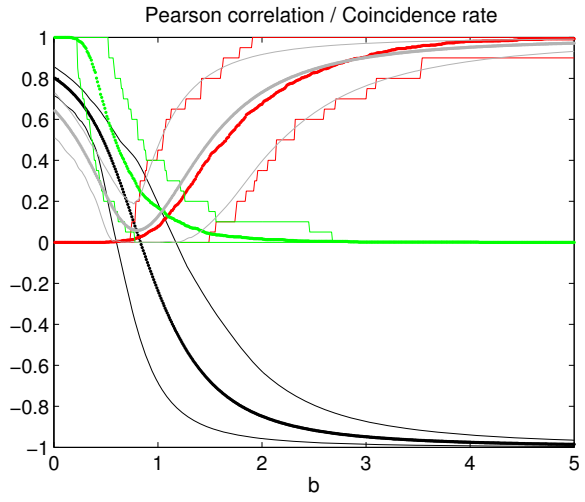

Figure S1. Behavior of Pearson correlation coefficient r (black) and coincidence rates κ (green: upper/upper 10% of values, red: upper/lower 10% of values) for ensembles of realizations of the numerical example with cubic dependence for different values of the parameter b. Thick lines indicate the median, thin lines the 5%/95% quantiles of the respective values obtained from 100 independent realizations of the noise. The gray lines indicate the corresponding results for r^2, which coincide remarkably well with those of the coincidence rates in the linearly dominated regime $b \gg 1$.

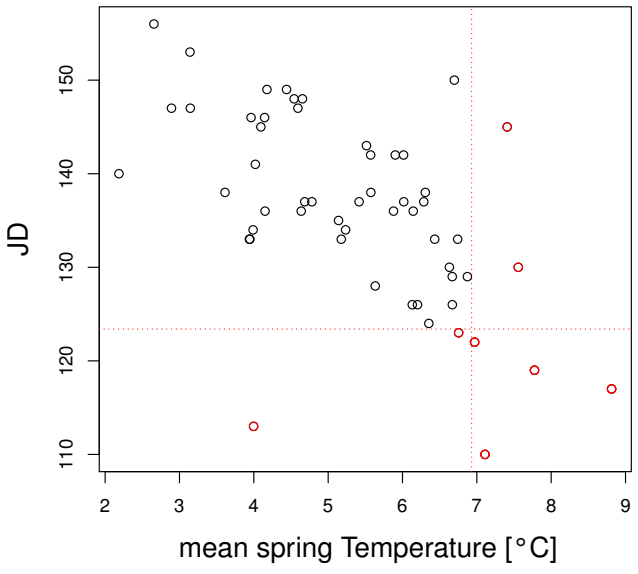

Figure S2. Scatter plot between the flowering dates and mean spring temperatures for a randomly selected case from the considered phenology data set. Red dots highlight cases with very high mean spring temperatures and/or very early flowering.

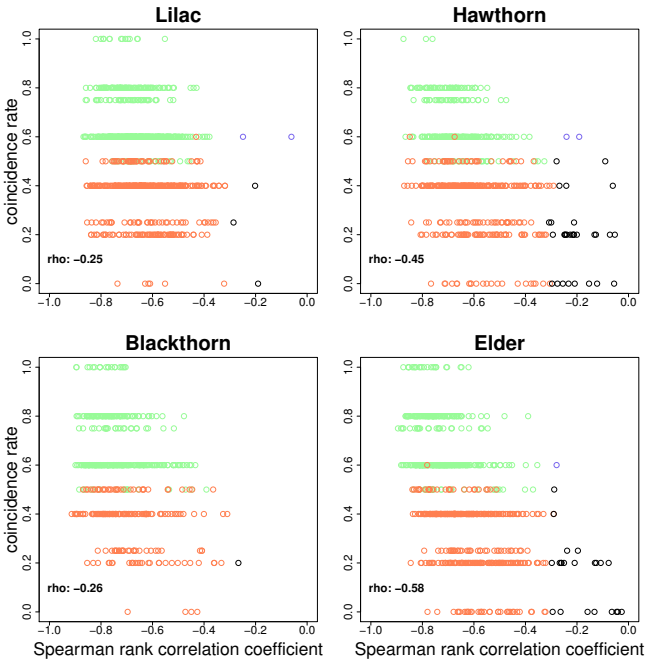

Figure S3. Scatter plot between Spearman's rank-order correlation coefficient and precursor coincidence rate (very warm conditions (>90%) versus very early flowering (<10%)) of each pair of mean spring temperature and flowering date time series. The time span for the calculation of the mean spring temperature is related to the typical flowering dates of each species: temperature is averaged for the time interval of JD 59-119 for Lilac and Hawthorn, JD 89-149 for Elder and JD 39-99 for Blackthorn. Bold numbers in the lower left corner of each panel give the values of Spearman's rho between rank-order correlation coefficients and coincidence rates for all study sites.

that only for roughly half of the stations the correlation coefficient *and* the coincidence rate are both significant (green circles). In turn, there is a large number of stations where, although the correlation is found statistically significant, the coincidence rate for the extremes is very low and/or not significant (red circles). This effect mainly originates from the much smaller effective sample size utilized by event coincidence analysis which makes the associated statistical tests less powerful. Furthermore, stations with significant coincidence rates (here, commonly above 0.5) show a large variability of correlations coefficients ranging from -0.3 to -0.9, and there are even some stations that show significant coincidence rates without a significant correlation (blue circles). Even though the small event sample size necessarily increases the false positive rate of statistical tests based on event coincidence analysis, the latter finding illustrates again that a high correlation value does not always result in a high coincidence rate for the extremes.

In order to further highlight the importance of the different types of significance tests together with different sample

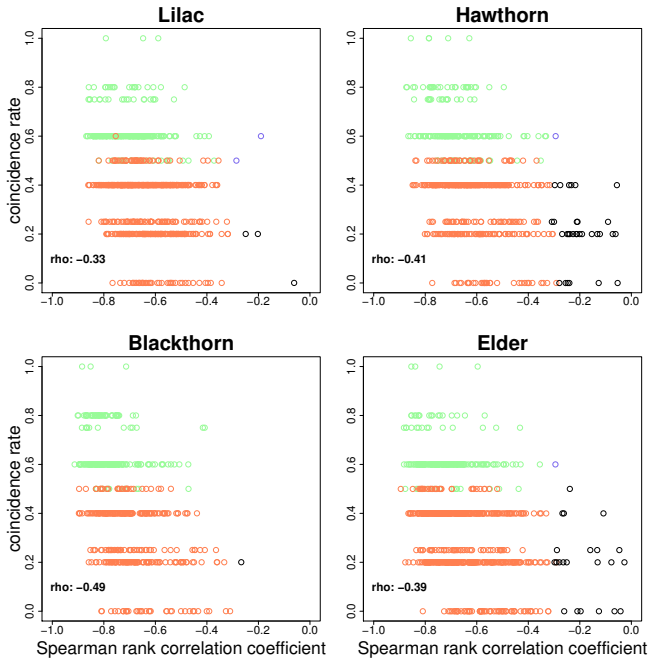

Figure S4. As in Fig. S3 for very cold conditions (<10%) versus very late flowering (>90%).

sizes for correlation and event coincidence analysis, Fig. S5 provides a corresponding example showing the fraction of study sites with significant coincidence rates and correlation coefficients between flowering dates and window-mean temperature and precipitation. One clearly recognizes that coincidence rates provide much more conservative indications of interdependencies between the respective variables than correlations.

S3.3 Correlation analysis based on event data

So far, we have considered correlation analysis and event coincidence analysis as two antagonist methods providing complementary information on the time series under study – one being based on the exclusive consideration of information on whether or not a given data point constitutes an extreme situation and the other explicitly utilizing all data points in the time series under study. However, there are methodological alternatives that could provide a reasonable trade-off between both viewpoints. Specifically, we emphasize that the transformation of explicit time series values to event sequences practically corresponds to the generation of a binary time series with values 1 (0) indicating an event (non-event). Even though the direct application of the classical Pearson correlation coefficient (and even more Spearman's rank-order correlation coefficient) to such data is not meaningful, there are powerful alternatives for the analysis of dichotomous variables, such as the ϕ-coefficient or Cramer's V. In the present study, however, the number of events is very small by definition (i.e., the binarized time series include far more zeros than ones), which can be expected to result in values of the latter statistics that are similarly unstable as those of the coincidence rates. In this spirit, we do not expect that the application of these methods provides a significant improvement of our event-based analysis of statistical interdependencies between flowering dates and meteorological conditions. However, this assumption may be challenged and needs further justification by systematic analysis, which we outline as a subject of future research.

S4 Geographical distributions of significant interdependencies

S4.1 Latitudinal distribution of significant coincidences for different time windows

S4.1.1 Warm temperatures and early flowering

Figure 3 of our main paper has already shown the temporal and latitudinal distribution of study sites with significant coincidence rates between high early-spring temperatures and very early flowering for the case of Lilac. Here, we show the corresponding results for the other three considered shrub species in Figs. S6-S8.

S4.1.2 Cold temperatures and late flowering

In order to complement the results shown above for warm spring temperatures and early flowering, Figs. S9-S12 show the corresponding results for cold temperatures and late flowering for all four shrub species.

S4.2 Precipitation effect on flowering dates

In our main paper, we have already described the absence of a statistically significant precipitation effect on the flowering dates of the four considered shrub species. Figure S13 shows the corresponding results for the four possible combinations between extremely wet/dry spring conditions and extremely early/late flowering for all four species, indicating that the fraction of study sites showing a significant coincidence between any pair of extremes hardly ever exceeds the statistical tolerance level of 5% – the number of false positives to be expected with our test design at an individual confidence level of $\alpha = 0.05$.

S4.3 Spatial distribution of significant coincidences with positive temperature extremes

As discussed in our main paper, we have observed significant coincidence rates especially between early flowering and positive temperature extremes. Specifically, the analyses presented there revealed two time intervals of particular interest: late winter / early spring and the previous year's early to mid-autumn. In this section, we further examine the spatial

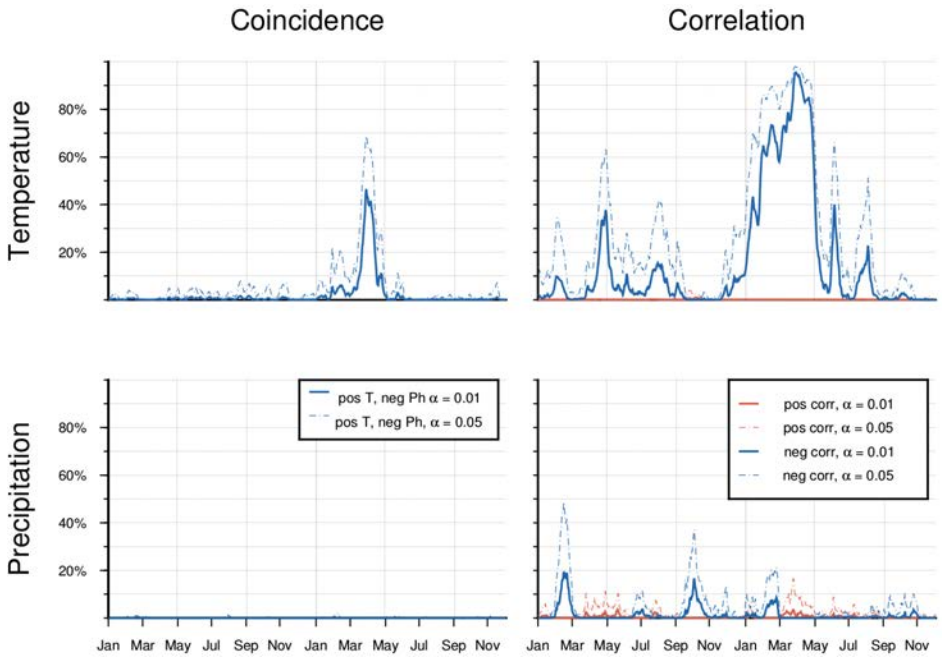

Figure S5. Fraction of stations with significant coincidence rates (left) and Pearson correlations (right) for Lilac flowering with a window site of 30 days. The significance has been assessed with the binomial test statistic under the assumption of two independent Poissonian processes and a classical t-test, respectively.

distribution of records with significantly coincident extremes for both time windows.

Figures S14 and S15 show maps with the corresponding results. In order to condensate the potentially large amount of information provided by this analysis, we only plot two maps per plant species representing the two different time intervals. Black (red) signatures mark those stations, which show at least one window with significant coincidences at $\alpha = 0.01$ ($\alpha = 0.05$) significance level within the time intervals indicated in the respective figure captions. The obtained results allow not only studying the latitudinal distribution of significant coincidences as shown in Fig. 3 of the main paper and Figs. S6-S8 of this Supplementary Material, but also possible patterns or regional clustering of significant results. However, for the 30-days period in spring (Fig. S14), neither a clear pattern nor geographical clusters of stations with significant coincidences are visible.

In contrast to the latter findings, at least the maps for Lilac and Hawthorn in Fig. S15 show a weak tendency towards a spatial accumulation of stations with significant coincidences in Northern Germany. In turn, the signatures for Blackthorn concentrate more in the southern part of Germany. However, this observation could also be an artifact of the missing data for most of Northeastern Germany.

S5 Conclusions

The additional results presented in this Supplementary Material may be used as starting points for further in-depth investigations on various aspects related to both the meteorological drivers of plant flowering as well as methodological aspects. For example, from the visual inspection of the spatial distribution of study sites with statistically significant coincidence rates, it is not obvious if the latter have any statistically relevant underlying pattern. In order to test for the presence of spatial clustering, we outline the application of join-count statistics as a corresponding further research avenue.

References

Ahas, R., Jaagus, J., and Aasa, A.: The phenological calendar of Estonia and its correlation with mean air temperature, International Journal of Biometeorology, 44, 159–166, 2000.

Donges, J., Schleussner, C.-F., Siegmund, J., and Donner, R.: Coincidence analysis for quantifying statistical interrelationships between event time series, European Physical Journal ST, 225, 471–487, 2016.

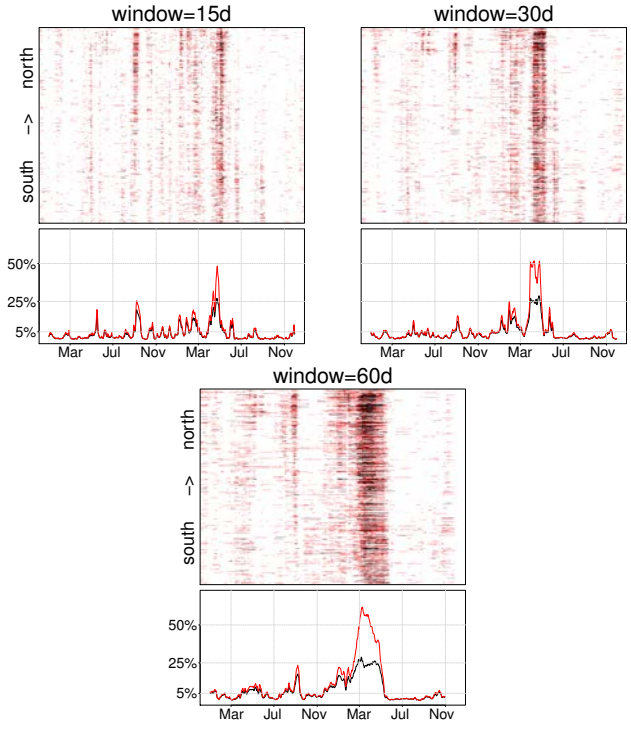

Figure S6. Latitudinal distribution (top panels) and total fraction (bottom panels) of stations with significant coincidence rates (red: $\alpha = 0.05$, black: $\alpha = 0.01$) between very early Elder flowering and extremely high window-mean temperatures for three different window sizes. The x axes refer to the starting date of a window. The dashed horizontal lines at 5 % in the lower panels highlight the employed group-significance criterion.

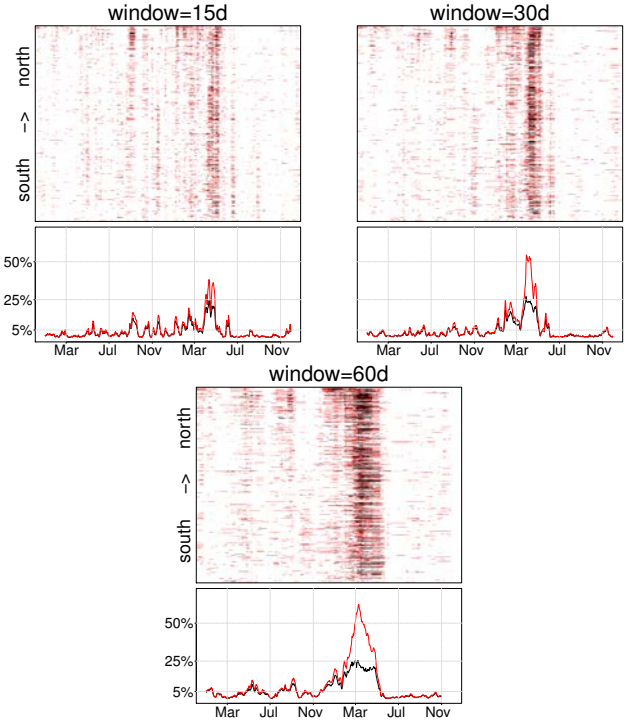

Figure S7. As in Fig. S6 for Hawthorn.

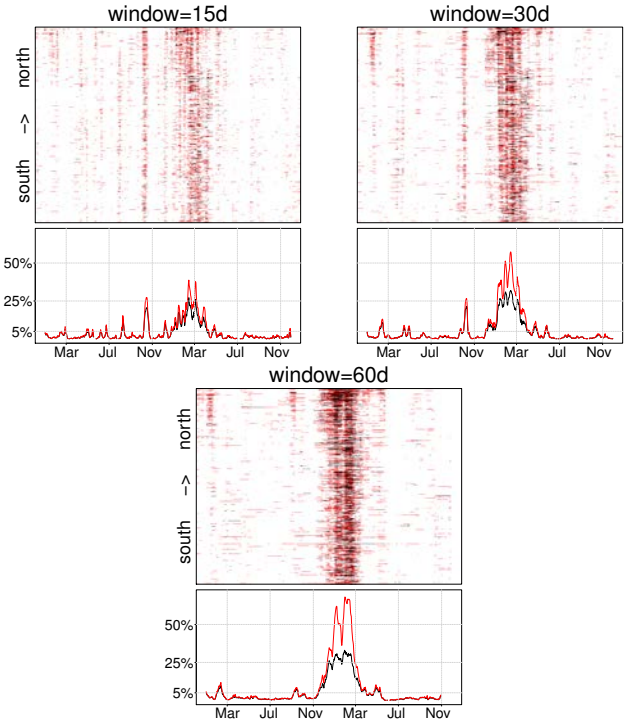

Figure S8. As in Fig. S6 for Blackthorn.

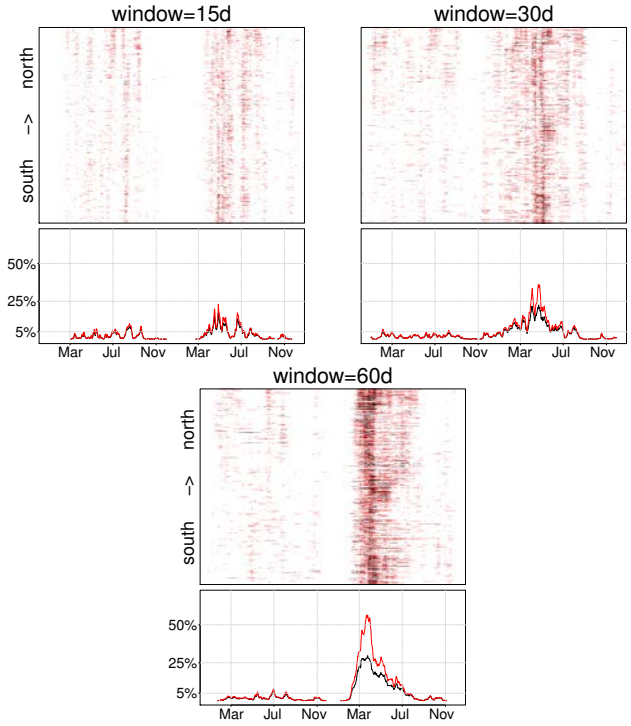

Figure S9. As in Fig. S6 for coincidences between cold spring temperatures and late flowering for Lilac.

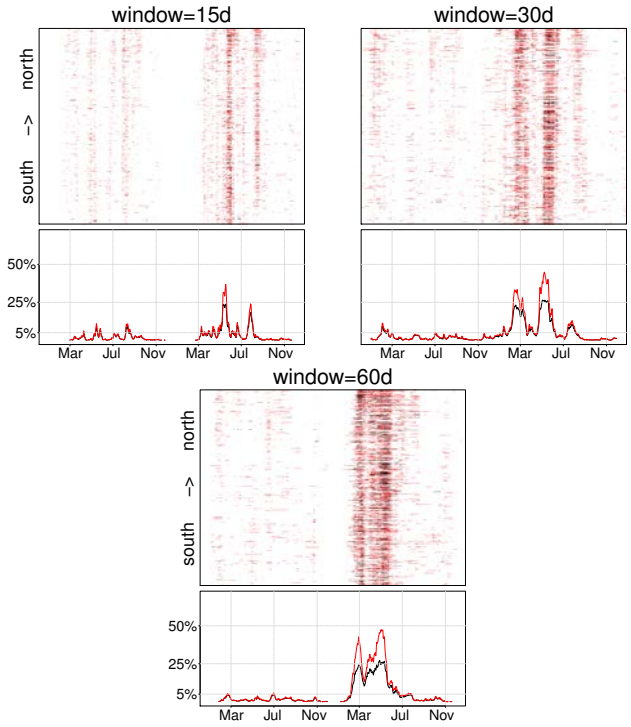

Figure S10. As in Fig. S9 for Elder.

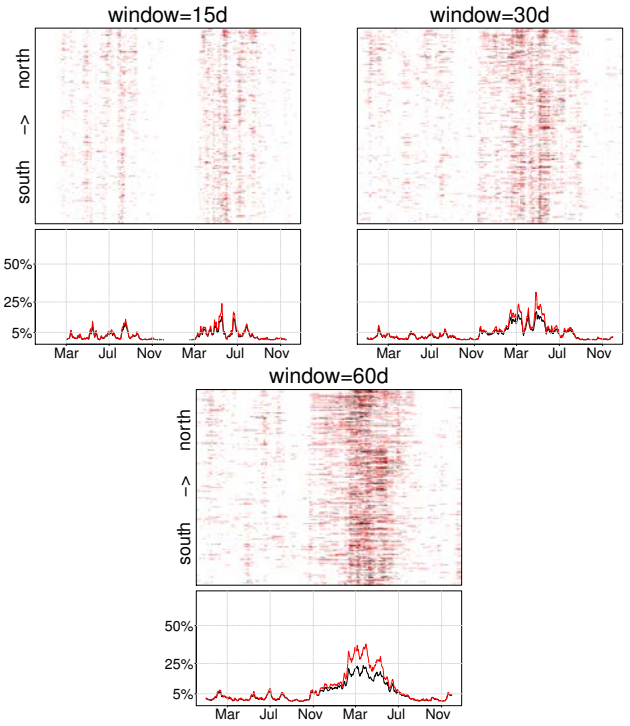

Figure S11. As in Fig. S9 for Hawthorn.

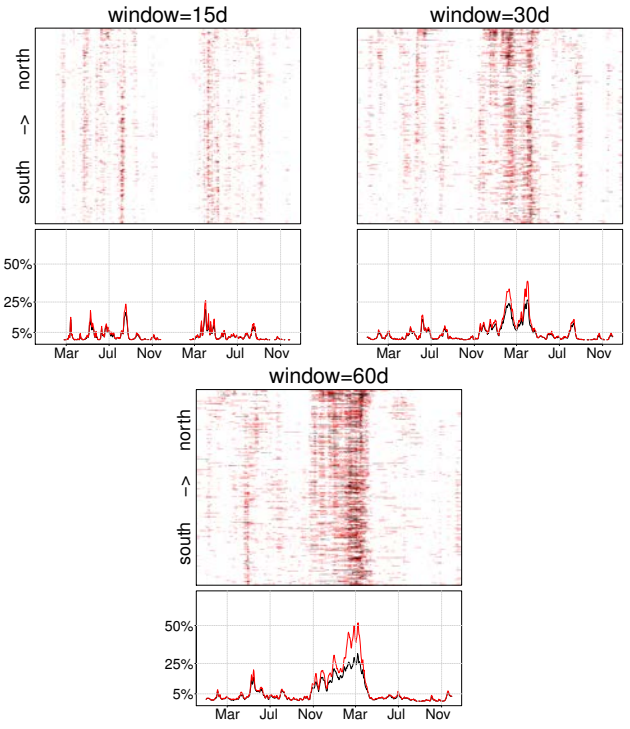

Figure S12. As in Fig. S9 for Blackthorn.

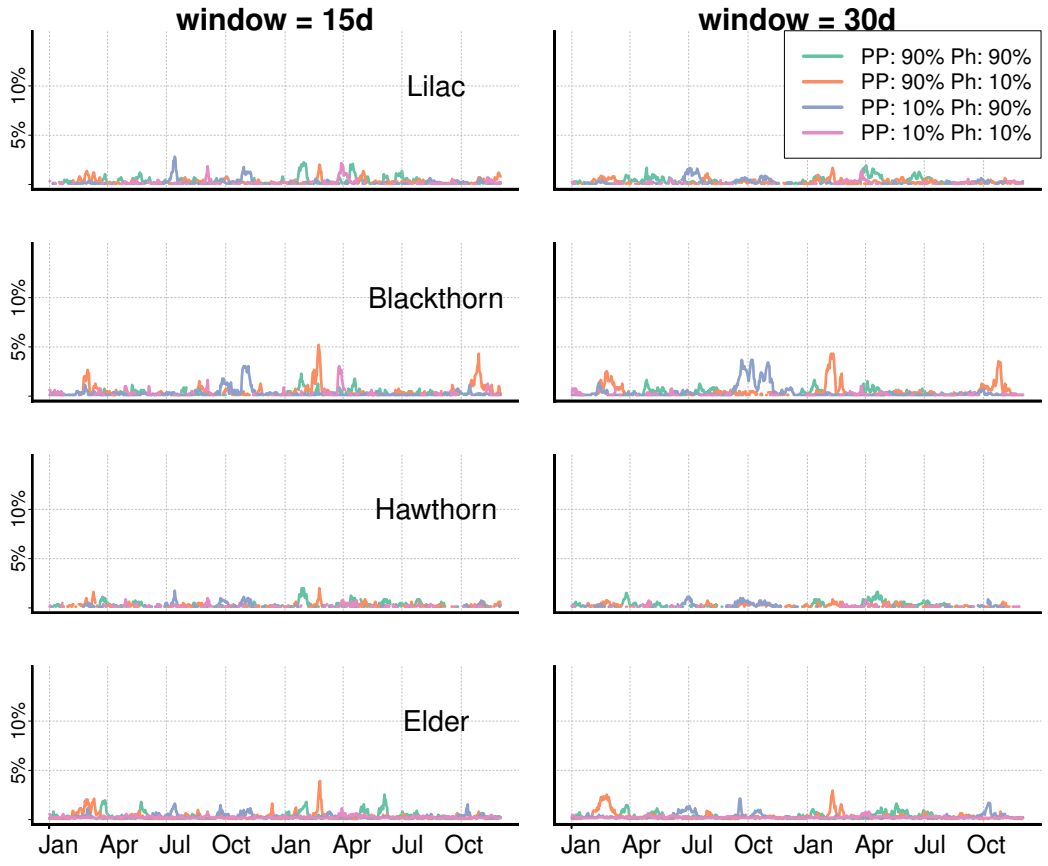

Figure S13. Fraction of study sites with significant coincidence rates between extremly wet/dry spring conditions and extremely early/late flowering dates for all four shrub species. As before, extremes are defined as events outside the upper/lower decile of the empirical distribution of each variable.

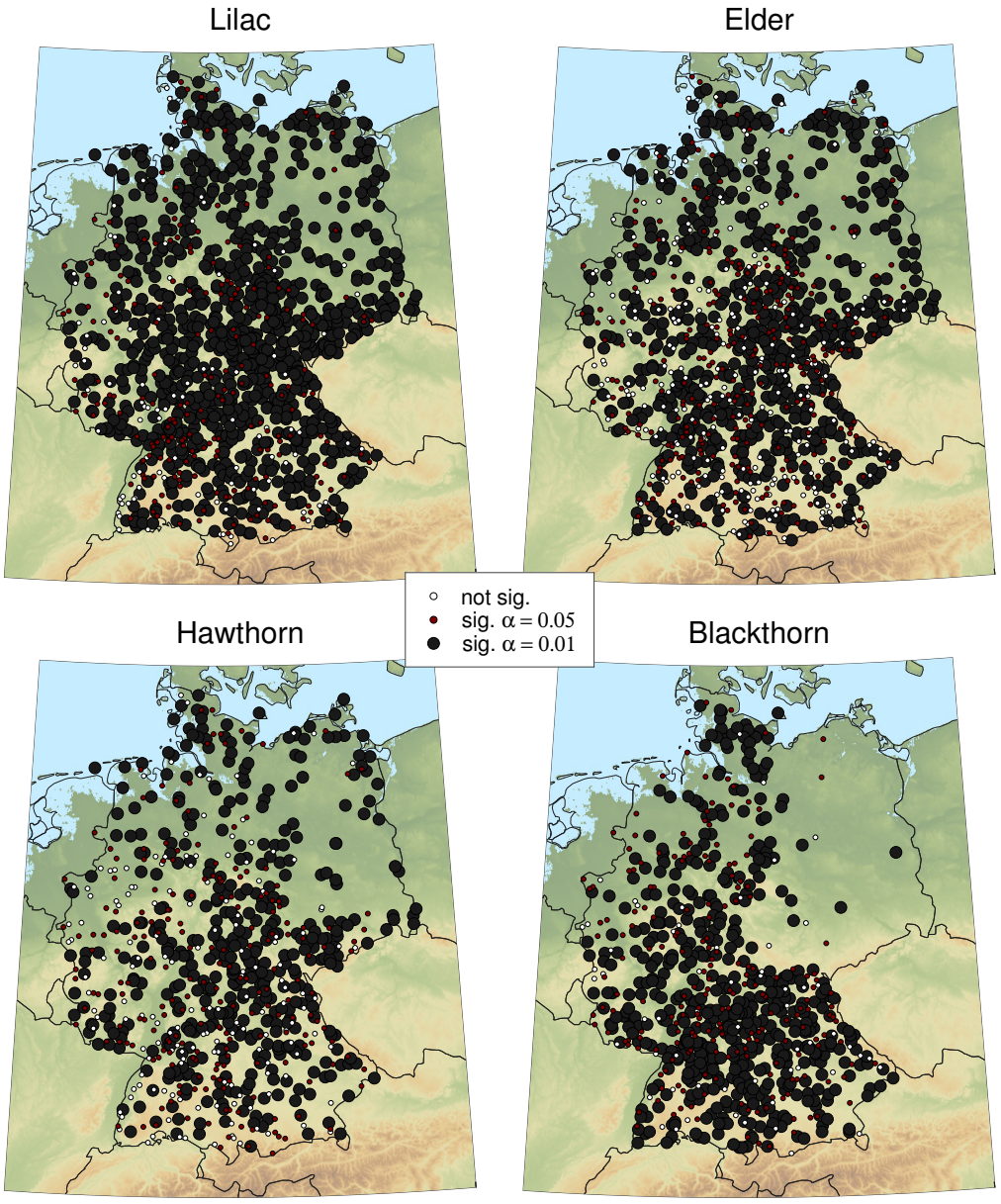

Figure S14. Stations with statistically significant coincidence rates between very early flowering and very warm 30-days window-mean temperatures in the time span from 15 March to 30 April (Lilac, Elder and Hawthorn) and 15 January to 15 March (Blackthorn), respectively. Filled black (red) circles mark those stations that show significant coincidences at $\alpha = 0.01$ ($\alpha = 0.05$) confidence level for at least one window during the aforementioned interval. White circles mark stations that have no significant coincidence for any of the windows.

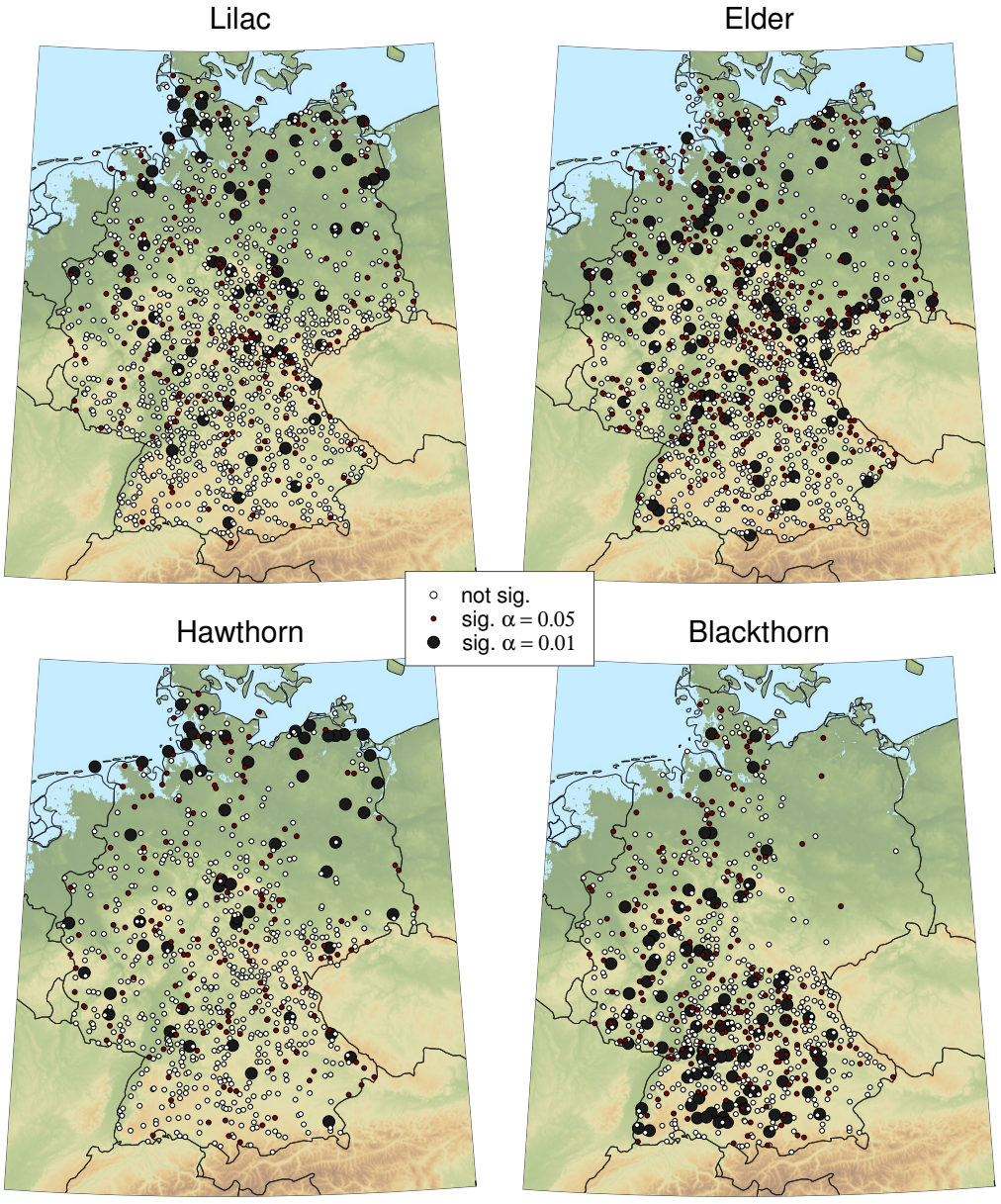

Figure S15. Stations with statistically significant coincidence rates between very early flowering and very warm 15-days window-mean temperatures in the period from 1 to 15 September (Lilac, Elder and Hawthorn) and 10 to 20 October (Blackthorn) of the previous year, respectively. Filled black (red) signatures mark those stations, that show significant coincidences at $\alpha = 0.01$ ($\alpha = 0.05$) confidence level for at least one window during the aforementioned interval. White circles indicate stations that have no significant coincidence for any of the windows.

2.3 Meteorological Drivers of Extremes in Daily Stem Radius Variations of Beech, Oak, and Pine in Northeastern Germany: An Event Coincidence Analysis

frontiers in Plant Science

ORIGINAL RESEARCH
published: 03 June 2016
doi: 10.3389/fpls.2016.00733

Meteorological Drivers of Extremes in Daily Stem Radius Variations of Beech, Oak, and Pine in Northeastern Germany: An Event Coincidence Analysis

Jonatan F. Siegmund[1,2], Tanja G. M. Sanders[3], Ingo Heinrich[4], Ernst van der Maaten[5], Sonia Simard[4], Gerhard Helle[4] and Reik V. Donner[1]*

[1] Research Domain IV—Transdisciplinary Concepts and Methods, Potsdam Institute for Climate Impact Research, Potsdam, Germany, [2] Institute of Earth and Environmental Science, University of Potsdam, Potsdam, Germany, [3] Thünen Institute of Forest Ecosystems, Eberswalde, Germany, [4] Department 5 Geoarchives, Helmholtz Centre Potsdam, GFZ German Research Centre for Geosciences, Potsdam, Germany, [5] Institute of Botany and Landscape Ecology, University of Greifswald, Greifswald, Germany

OPEN ACCESS

Edited by:
Cristina Nabais, University of Coimbra, Portugal

Reviewed by:
Walter Oberhuber, University of Innsbruck, Austria
Alicia Forner Sales, Museo Nacional de Ciencias Naturales-CSIC, Spain

***Correspondence:**
Jonatan F. Siegmund
siegmund@pik-potsdam.de

Specialty section:
This article was submitted to Functional Plant Ecology, a section of the journal Frontiers in Plant Science

Received: *27 February 2016*
Accepted: *12 May 2016*
Published: *03 June 2016*

Citation:
Siegmund JF, Sanders TGM, Heinrich I, van der Maaten E, Simard S, Helle G and Donner RV (2016) Meteorological Drivers of Extremes in Daily Stem Radius Variations of Beech, Oak, and Pine in Northeastern Germany: An Event Coincidence Analysis. Front. Plant Sci. 7:733. doi: 10.3389/fpls.2016.00733

Observed recent and expected future increases in frequency and intensity of climatic extremes in central Europe may pose critical challenges for domestic tree species. Continuous dendrometer recordings provide a valuable source of information on tree stem radius variations, offering the possibility to study a tree's response to environmental influences at a high temporal resolution. In this study, we analyze stem radius variations (SRV) of three domestic tree species (beech, oak, and pine) from 2012 to 2014. We use the novel statistical approach of event coincidence analysis (ECA) to investigate the simultaneous occurrence of extreme daily weather conditions and extreme SRVs, where extremes are defined with respect to the common values at a given phase of the annual growth period. Besides defining extreme events based on individual meteorological variables, we additionally introduce conditional and joint ECA as new multivariate extensions of the original methodology and apply them for testing 105 different combinations of variables regarding their impact on SRV extremes. Our results reveal a strong susceptibility of all three species to the extremes of several meteorological variables. Yet, the inter-species differences regarding their response to the meteorological extremes are comparatively low. The obtained results provide a thorough extension of previous correlation-based studies by emphasizing on the timings of climatic extremes only. We suggest that the employed methodological approach should be further promoted in forest research regarding the investigation of tree responses to changing environmental conditions.

Keywords: dendrometer measurements, event coincidence analysis, climate extremes, growth response

1. INTRODUCTION

During the past 15 years the systematic installation and operation of dendrometers and analysis of the obtained data has received increasing interest in forestry sciences. While the first attempts (Friedrichs, 1897) to use dendrometer data to analyze tree response to environmental conditions were clearly limited by the technical conditions of early instruments, recent developments in the production of modern automated high-precision dendrometers offer the ability to generate dendrometer time series at very high temporal and spatial resolution (Drew and Downes, 2009). The detailed representations of activity in the tree stem—shrinkage, recovery, and swelling cycles—allow for a high-temporal investigation of the tree stem as well as long-term morphological and short-term physiological dynamics (Zweifel and Häsler, 2001; Deslauriers et al., 2003; McLaughlin et al., 2003; Bouriaud et al., 2005; Daudet et al., 2005; Vieira et al., 2013). Where additional environmental information is available, dendrometer data can provide information on the tree stems response to external factors, especially meteorological conditions (McLaughlin et al., 2003; Denneler et al., 2010; Miralles-Crespo et al., 2010; Oberhuber and Gruber, 2010; Jezik et al., 2011; Butt et al., 2014). Investigations such as these are also important in order to better understand the diurnal cycle of sap flow and leaf water potential (Drew and Downes, 2009).

Beyond the fundamental understanding of tree functioning, dendrometer data can also indirectly provide important information on the carbon cycle at the local, regional or global level. Even though stem radius does not allow estimates of total cell numbers, it is an important proxy for a forest's above ground biomass (Schulte-Bisping et al., 2012), because it can help to determine the wood volume available for the fixation of carbon (Cuny et al., 2015).

To the authors' best knowledge, almost all above-mentioned studies have investigated dendrometer data using classical statistical tools like linear correlation analysis or linear multiple regression. These powerful methodological approaches have led to an understanding of the relationship between stem size changes and various environmental parameters. Yet, correlation-based approaches generally take all parts of the distributions of two variables of interest into account and therefore describe the joint behavior of these variables. A crucial question only sporadically addressed so far is how tree stem radius variations (SRVs) are linked to extreme weather conditions. This question gains special importance, since recent climate projections suggest a rising frequency and severity of meteorological extreme events for many parts of the world (Barriopedro et al., 2011; IPCC, 2013; Petoukhov et al., 2013). Consequently, analyzing the impact of such extremes on tree SRVs, on the one hand can help to better understand an event's impact on tree functionality and carbon cycle, and on the other hand, because different tree species may be impacted differently, to generate recommendations for future forest management (Spathelf et al., 2014). New findings concerning the response of stem radius to extreme meteorological conditions would also help to improve existing climate-growth-models like TREERING (Fritts et al., 1999) or CAMBIUM (Drew, 2007).

An important study addressing the response of stem-size fluctuations and tree radius growth to climatic extremes using a large number of dendrometer data sets was recently published by Butt et al. (2014). However, this study did not report explicit results regarding the response of the tree stem to extreme meteorological conditions, due to the fact that they have only used ordinary linear regression to analyze the data.

In this study, we employ the novel methodological approach of event coincidence analysis (ECA) to quantify possible simultaneities between extraordinary daily stem variations and extraordinary meteorological conditions. Here, the commonly used term *extreme* is replaced by *extraordinary*, referring to the upper and lower tails of the empirical distributions of the variables of interest. Due to the comparatively short investigation period of 3 years (and only 8 years of climatological data), "real" extreme events are difficult to identify or define and therefore the investigation of extraordinary conditions shall represent a tree's reaction to the tails of the empirical distribution of weather events, which may well be exceeded by future developments under climate change. Therefore, conclusions from this study's results on trees' reaction on weather extremes should be made unter consideration of the used definition of "extraordinary events."

Taking into account the existing literature on SRVs and their relation to meteorological conditions we expect that extraordinary climatic events, specifically temperature events, and extraordinary dendrometer variations should occur simultaneously. Additionally, it can be expected that there are clear inter-species differences concerning the reaction to extraordinary meteorological events.

2. MATERIALS AND METHODS

2.1. Study Area and Data Sampling

2.1.1. Study Area

The study site was close to Lake Hinnensee (53.33°N, 13.19°E) in the northeastern part of Germany. The site is located within the Müritz National Park. Large parts of this protected area have been classified as UNESCO World Natural Heritage in 2011. The park is characterized by 200–300 years old mixed beech, pine and oak stands. The climate is semi-continental, typical for central Europe, with a mean annual temperature of about 8°C and an annual precipitation between 550 and 650 mm. The soil at the study site as well as at the meteorological station (see Section 2.2.2) is a brunic arenosol on sand of outwash plains, characterized by strong hydraulic permeability Müller (2014).

2.1.2. Data Sampling

The dendrometer data were collected for three tree species: European beech (*Fagus sylvatica*), Scots pine (*Pinus sylvestris*), and Sessile oak (*Quercus petraea*). The distances between the individual trees range from ca. 4 to 20 m and the selection of trees was based on the canopy status of the individual trees (i.e., only dominant trees or co-dominant trees were equipped with dendrometers). This study focuses on the species' response to meteorological conditions, hence the dendrometer data are not differentiated according to the relative positions of the individual

trees in landscape (see Section 2.3), but trees were selected along a transect from the lake shore to a terrace ∼15 m above Lake Hinnensee, in order to sample a possibly large variation of individual local stand variations. The equipped trees have an average height of 26 m with diameters between 50 and 70 cm at breast height.

For each tree species, 10 individuals were equipped with Ecomatik DR point radius dendrometers (Ecomatik GmbH, 2015) installed at 1.2 m height. The sensors were installed at the north face of the trunks in order to avoid direct irradiation. They have a temperature coefficient <0.1m/K. Bark was mostly removed from pine and oak trees prior to setup. SRVs were measured at a temporal resolution of 30 min over a 3-years period between 2012 and 2014.

2.2. Data Preprocessing

2.2.1. Dendrometer Data

After a comprehensive quality check, the raw dendrometer data were pre-processed using the following three steps:

(1) In a first step, the 30-min resolution dendrometer data were used to calculate daily SRVs. Rather then using a stem cycle approach (Deslauriers et al., 2003; Köecher et al., 2012; Vieira et al., 2013) which distinguishes between phases of contraction, expansion, and stem radius increment, we calculated day-to-day SRVs as the first-order differences between mean daily dendrometer recordings. Similar methods were used, for example, by Bouriaud et al. (2005) or van der Maaten et al. (2013). This procedure results in positive and negative values following a clear seasonal cycle. In contrast to van der Maaten et al. (2013), the daily residuals were not normalized by the season's total growth due to the age maturity of the investigated trees.

(2) As a second step, a two-sided sliding window mean (window size of 15 days) was subtracted from the resulting daily SRVs in order to account for the seasonal cycle. The resulting residuals represent the daily stem increments of a tree as deviations the from the 15-day mean. Finally, the investigation period was defined from April 1st to September 30th of each year to cover the entire growth period for each species. A sliding window approach (see Section 2.3) was applied to produce comparable results which are not shifted against each other by species or year.

(3) In order to transform the dendrometer time series into event time series, we applied a 90th and 10th percentile threshold to the daily increments. Values exceeding the 90th percentile of all days of the investigation period were defined as extraordinary positive SRV events, whereas days lower than the 10th percentile were defined as negative events. This event definition results in 55 positive and 55 negative events during the 3-years period for each individual tree. Due to the usage of residuals with respect to the "normal" seasonal behavior, these events are approximately homogeneously distributed within each year (not shown) and the specific timings of the individual events are determined by environmental conditions. An important exception is a very dry period during the summer of 2013 during which only a few strong positive precipitation events were observed.

2.2.2. Meteorological Data

In order to define days with extraordinary meteorological conditions, data from a nearby meteorological station in Serrahn (at a distance of less than 2 km from the study site) were used. The soil conditions at the dendrometer site and the meteorological station site are comparable, but not identical. Systematically differing soil temperatures, for example, can not be excluded. In addition to air temperature and precipitation, the station provides information on (relative air) humidity, soil temperature, air pressure and incoming solar radiation. The data set is available starting January 2006 at a temporal resolution of 1 h. Similar to the daily SRVs, the meteorological data were pre-processed in order to identify events of extraordinary daily meteorological conditions:

(1) The hourly information was aggregated to daily minimum, mean, and maximum values. Observations of air pressure and minimum radiation were not used since no meaningful results are expected by using these variables.

(2) The daily meteorological information was transformed to *z-scores*. Since the time series length of the meteorological station spans only 8 years, the z-scores calculation differs slightly from the classical approach: for each day of the year the mean over all 8 years was additionally averaged over sliding windows (with a window length of 45 days for precipitation, 15 days for all other variables). Then, the resulting mean seasonal cycle as well as the estimated seasonal cycle in variance were used for obtaining z-scores.

(3) Finally, the resulting z-scores were transformed to event time series by applying a 90th and 10th percentile threshold as in the case of the dendrometer data. Due to the application of these percentiles for threshold definition, the number of events in each meteorological variable is also 55 (each negative and positive).

The following meteorological variables were used: air temperature at 2 m (T_{min}, T_{mean}, and T_{max}), land surface air temperature at 5 cm (LST_{min}, LST_{mean}, and LST_{max}), soil temperature in 20 cm depth (ST_{min}, ST_{mean}, ST_{max}), relative humidity (rH_{min}, rH_{mean}, rH_{max}), total precipitation (P_{tot}) and incoming solar radiation (RAD_{mean} and RAD_{max}). Many of these variables are highly correlated among each other. Hence, for a study using classical statistical approaches a principal component analysis (as performed by, e.g., Beck et al., 2013) would be appropriate in order to reduce the number of meteorological observables (i.e., to eliminate collinear variables). However, in this study the novel statistical approach of ECA (see Section 2.3) is applied, where the reduction of dimensions based on their common mean behavior (correlation) would not be useful, since the information of interest (timing of extraordinary events) could eventually get lost. Additionally, this study is particularly focused on the different variations of air, surface and soil temperatures, for example. As an alternative, a dimensionality reduction based on event coincidence rates (see Section 2.3) replacing classical linear correlations as

similarity measure could be performed as a preparatory step. The utilization of such a novel approach is, however, beyond the scope of the present study.

2.3. Statistical Analysis

2.3.1. Bivariate Event Coincidence Analysis

In order to investigate the simultaneity of events in meteorological variables and SRV, we apply *event coincidence analysis (ECA)* (Donges et al., 2016), a novel yet conceptually simple statistical concept. In its basic setting, ECA considers two sequences of events of different types (A and B). As the hypothesis to be tested, events of type B are considered to causally influence the timing of events of type A. To cope with realistic scenarios, ECA allows to not only trivially quantify the number of exactly simultaneous occurrences of events of both types, but to consider also lagged as well as time-uncertain responses. For the latter purpose, a time lag parameter τ as well a temporal tolerance window ΔT can be additionally taken into account. Then, ECA counts how often events of types A and B occur with a mutual delay τ in both sequences within a certain temporal tolerance ΔT. The resulting number of "event coincidences," divided by the total number of events in one of the series is called the *coincidence rate r*.

Since the statistical analysis described above is not symmetric, ECA defines two distinct types of coincidence rates, r_p (*precursor coincidence rate*) and r_t (*trigger coincidence rate*). Here, r_p is defined as the number of event coincidences divided by the number N_A of events of type A, describing the fraction of events of type A that have been preceded by at least one event of type B. In turn, r_t is defined as the number of event coincidences divided by the number N_B of events of type B, thereby describing the fraction of events of type B that have been followed by (and, thus, potentially triggered) at least one event of type A. When using $\tau \neq 0$, this differentiation is essential. A schematic illustration of the two different types of coincidence rates can be found in **Figure 1**.

In addition to the simple calculation of coincidence rates, the R package `CoinCalc` used in this work for performing the corresponding analyses provides different possibilities to test whether the empirically found coincidence rates are significantly different from what could result from two independent random event sequences (Siegmund et al., 2016). In this work, we will exclusively utilize an analytical significance test based on the assumption of Poissonian event statistics (Donges et al., 2011, 2016; Siegmund et al., 2015).

2.3.2. Conditional and Joint Event Coincidence Analysis

As a thorough extension of the basic ECA method for two event sequences, in this work, we introduce new multivariate generalizations of ECA termed *conditional event coincidence analysis (CECA)* and *joint event coincidence analysis (JECA)*. While the above formulation of bivariate ECA is sufficient for many applications (e.g., in Donges et al., 2011), in order to analyze the reaction of ecological variables to extraordinary meteorological conditions, it may be important to additionally consider the conditioning of events on specific situations governed by a third observable, i.e., the case that events of type B appear simultaneously with events in series A if and only if also, one or more events of a third type C take place. This conditioning could, for instance, be relevant to account for the interplay between temperature and moisture or between moisture and radiation.

The conditioning of events of type B by events of type C can be described by the precursor coincidence between B and C. Therefore, the *conditional precursor coincidence rate* r_{cp} and the *conditional trigger coincidence rate* r_{ct} between A and B can be defined (in analogy to r_p and r_t as mathematically defined by Equations (3) and (4) in Donges et al., 2016) as:

$$r_{cp}(\Delta T, \tau, \Delta T_{cond}, \tau_{cond}) = \frac{1}{N_A} \sum_{i=1}^{N_A} \Theta \left[\sum_{j=1}^{N_B} \Theta \left[\sum_{k=1}^{N_C} \mathbb{1}_{[0,\Delta T_{cond}]}((t_j^B - \tau_{cond}) - t_k^C) \right] \mathbb{1}_{[0,\Delta T]}((t_i^A - \tau) - t_j^B) \right] \quad (1)$$

and

$$r_{ct}(\Delta T, \tau, \Delta T_{cond}, \tau_{cond}) = \frac{1}{N_{B,cond}} \sum_{j=1}^{N_B} \Theta \left[\sum_{i=1}^{N_A} \Theta \left[\sum_{k=1}^{N_C} \mathbb{1}_{[0,\Delta T_{cond}]}((t_j^B - \tau_{cond}) - t_k^C) \right] \mathbb{1}_{[0,\Delta T]}((t_i^A - \tau) - t_j^B) \right], \quad (2)$$

respectively. Here, $\{t_i^A\}$, $\{t_j^B\}$ and $\{t_k^C\}$ are the timings of the events of types A, B and C, respectively, N_C is the number of events of type C, ΔT_{cond} is an additional tolerance window for the condition, τ_{cond} a time lag parameter for the condition, and $N_{B,cond}$ is the number of conditional events of type B, i.e., the number of events of type B that show a precursor coincidence with at least one event of type C. $\Theta(\cdot)$ denotes the Heaviside function (i.e., takes a value of one whenever the argument is non-negative, and zero otherwise) and $\mathbb{1}_I$ the indicator function of the interval I (i.e., takes a value of one whenever the argument is within I, and zero otherwise), respectively. In order to visualize the basic idea of the corresponding CECA, **Figure 1** illustrates the approach in a conceptional way.

Using the definitions in Equations (1) and (2), the conditional precursor coincidence rate describes the fraction of events in series A, that appear simultaneously with C-conditioned events of type B, and the conditional trigger coincidence rate is the fraction of C-conditioned events of type B that are followed by at least one event in series A. In the special case of a simultaneous occurrence of events of types B and C (i.e., $\tau_{cond} = 0$), we obtain a setting referred to as JECA.

2.3.3. Methodological Setting in the Present Study

For the application of ECA and CECA/JECA, we dissect the 1095 days period from 2012 to 2014 by sliding windows. For the (bivariate) ECA, the window length is chosen as 61 days with a step size of 5 days, resulting in 75 windows per growing season (1 April to 30 September), where each window contains six events

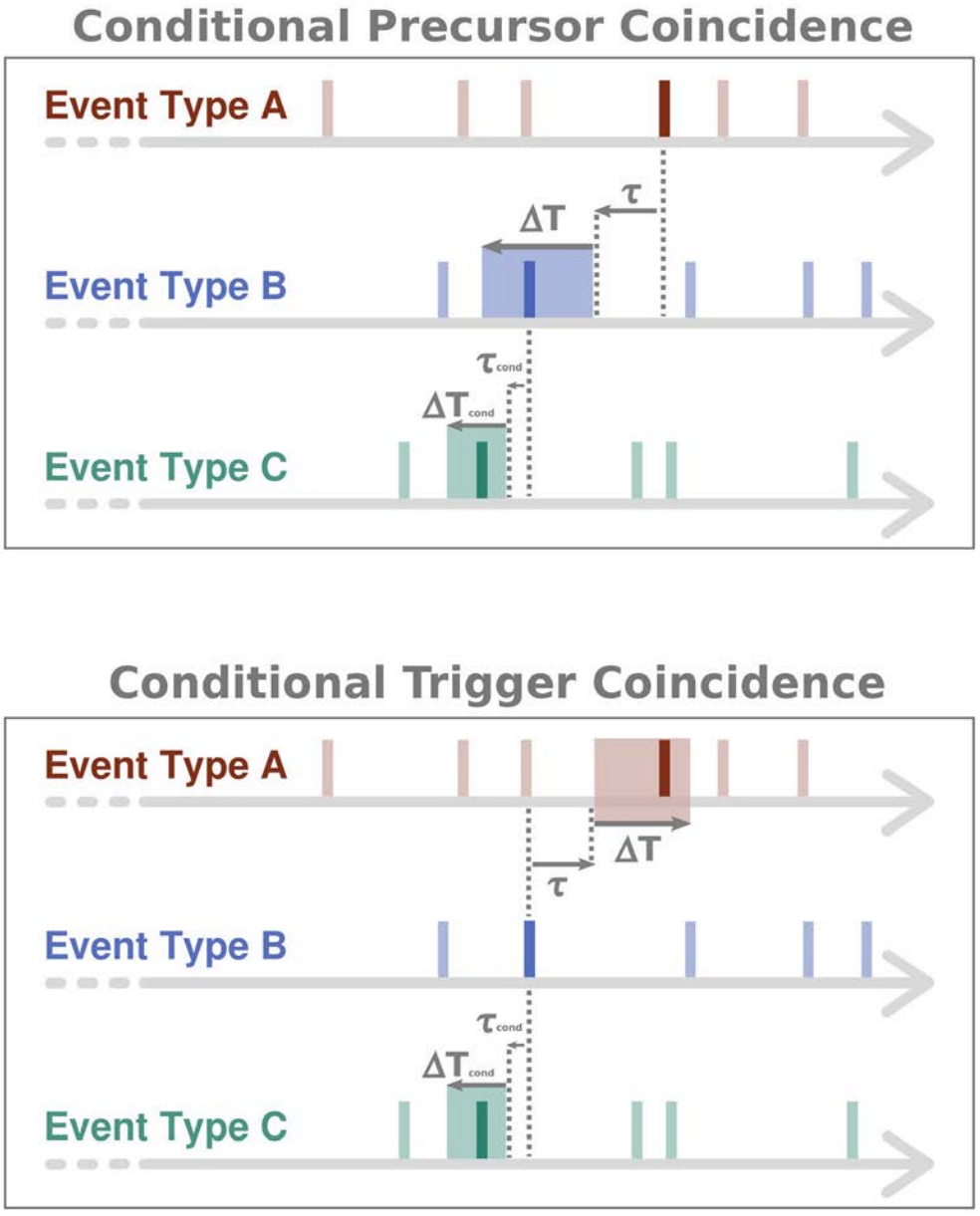

FIGURE 1 | Schematic illustration of (conditional) ECA. In the conditional case, only those events of type B are considered as coinciding with events of type A, that are preceded by at least one event of type C. This conditioning is expressed by a precursor coincidence between events of type B and type C. While ΔT and τ denote the tolerance window and time lag parameter for counting coincidences between events of types A and B, ΔT_{cond} and τ_{cond} are the respective parameters for the conditioning of events of type B on events of type C.

on average. The window length of 61 days is a compromise between a desired high temporal resolution and a possible large window size necessary to produce robust statistics. The step size of 5 days was selected in order to mimimize the computational demand. For the (multivariate) CECA/JECA, the window length is extended to 91 days including nine events on average, since due to the additional conditioning, the number of events in the meteorological variables decreases markedly. In order to cope with the high computational demand of CECA/JECA for 15 variables, the window step size was increased to 10 days, resulting in 15 windows per season.

As a first step, using the sliding window approach, ECA was performed between each of the 15 individual meteorological variables and each tree's SRV series across each window separately. For every window, the fraction of trees with a significant number of coincidences was taken as a proxy describing the reaction of the species to the considered meteorological events. Subsequently, JECA was performed

between the dendrometer data and all pairs of meteorological variables. As a consequence, the chosen analysis setting results in $15 \times 14/2 = 105$ different variable combinations. Note that for $\tau_{cond} \neq 0$, i.e., mutually shifted occurrences of events in the two considered meteorological variables, the number of combinations to be considered in an actual CECA would be twice as large. Therefore, we do not consider mutually conditioned events in this pilot study, but leave a corresponding detailed investigation as a subject of future work. Besides this, we do not consider the possible extension of multivariate conditions (involving different meteorological variables), which would be straightforward yet lead to an even larger combinatorial variety of different cases to be studied.

In all analyses discussed in the remainder of this work only the (conditional) precursor coincidence rates are considered unless stated otherwise.

2.3.4. Cluster Analysis

In order to analyze the simultaneity of event timings between the individual trees, we additionally use the well established approach of hierarchical cluster analysis with complete linkage. Core of the concept of cluster analysis (in this case for dendrometer time series) is a similarity measure, calculated between all possible combinations of individual time series. This similarity measure is, classically, a correlation coefficient. In this study, we additionally introduce the application of event coincidence rate as similarity measure for the cluster analysis. The calculation of the event coincidence rate between each pair of dendrometer event time series follows along the above mentioned approach, using $\tau = \Delta T = 0$. Due to the above described data preprocessing, there is no difference between precursor and trigger event coincidence rate.

3. RESULTS

3.1. Event Coincidence Analysis with Individual Meteorological Variables

Figure 2 shows the fraction of trees with significant precursor coincidence rates between extraordinary positive/negative SRVs and positive/negative events in each of the 15 meteorological variables at the same day ($\Delta T = \tau = 0$).

For positive SRV events (**Figure 2**, left panel), five main observations are made: (i) T_{min} and T_{max} events have an opposite effect in almost all years and for all tree species. Extraordinary positive SRV events mainly coincide with T_{min} values above the 90th percentile and T_{max} values below the 10th percentile. The same observation is also clearly visible for the land surface temperature. (ii) Extraordinary soil temperature generally has a much lower impact on positive SRV events than extraordinary air temperature. Except for 2013 for beech, ST_{mean} and ST_{max} only rarely show coincidences with positive or negative SRV events, while at least extraordinary positive minimum soil temperatures often coincide with positive SRV events. (iii) Extraordinary high values of relative humidity coincide with positive SRV events in all years and for all species. The fraction of trees showing significant coincidences has been slightly reduced in 2014 in comparison with the other 2 years. (iv) Extraordinary high precipitation values do almost continuously coincide with positive SRV events. An important exception is the summer of 2013, where neither tree species showed a corresponding significant relationship. (v) Extraordinary low values of mean and maximum radiation, generally show pronounced coincidences with SRVs above the 90th percentile.

In comparison to positive SRV events, negative events clearly show fewer significant coincidences with extraordinary meteorological conditions (**Figure 2**, right panel). However, two features can be highlighted: (i) For beech, values above the 90th percentile of the maximum temperature strongly coincide with strong negative dendrometer anomalies in 2012, less distinct in 2013, and hardly ever in 2014. In turn, negative oak and pine SRV events do not coincide significantly with maximum temperature events. (ii) Extraordinary low values of relative humidity very often coincide with negative SRV events for all species. This feature is variably expressed during the 3 years of observations but particularly evident in 2012. In contrast, during 2014 maximum relative humidity events (very wet days) significantly coincide with negative beech SRV events.

In addition to the consideration of exactly simultaneous coincidences as described above, **Figure 3** shows the results of precursor ECA using a tolerance window spanning the previous 2 days ($\Delta T = \tau = 1$ day), i.e., this kind of analysis takes into account responses with a time lag of 1 and 2 days. While in this case, positive dendrometer anomalies only show few coincidences with extraordinary meteorological conditions, on the contrary extraordinary negative stem size changes exhibit three major patterns: (i) Maximum land surface and maximum air temperature events show coincidences of their highest values with negative SRV events, which is especially distinct for beech in 2013. (ii) Extraordinary minimum and mean relative humidity values above the 90th percentile show clear coincidences with negative SRV events in 2012 and 2013 for all tree species. (iii) Extraordinary low mean and maximum radiation values coincide with negative SRV events as well. The two last features are mainly visible for beech and pine and are most distinct in 2012 and 2013. Notably, these results are similar to the previous analysis for positive SRV events when using $\Delta T = \tau = 0$ (see **Figure 2**).

3.2. Joint Event Coincidence Analysis for Paired Meteorological Variables

Due to the large number of possible combinations between meteorological variables, the figures showing the results of JECA are provided in the supplementary material. The following analysis concerns *equally directed events* if the values of both meteorological variables under study either both exceed their respective upper threshold value or both fall below their respective lower threshold value used for the definition of events. In the other case where one variable takes extraordinarily high values and the other extraordinarily low ones or vice versa, we will speak of *oppositely directed events*.

3.2.1. Beech

Figure S1 shows the results of JECA between beech SRV events and equally as well as oppositely directed events of each pair

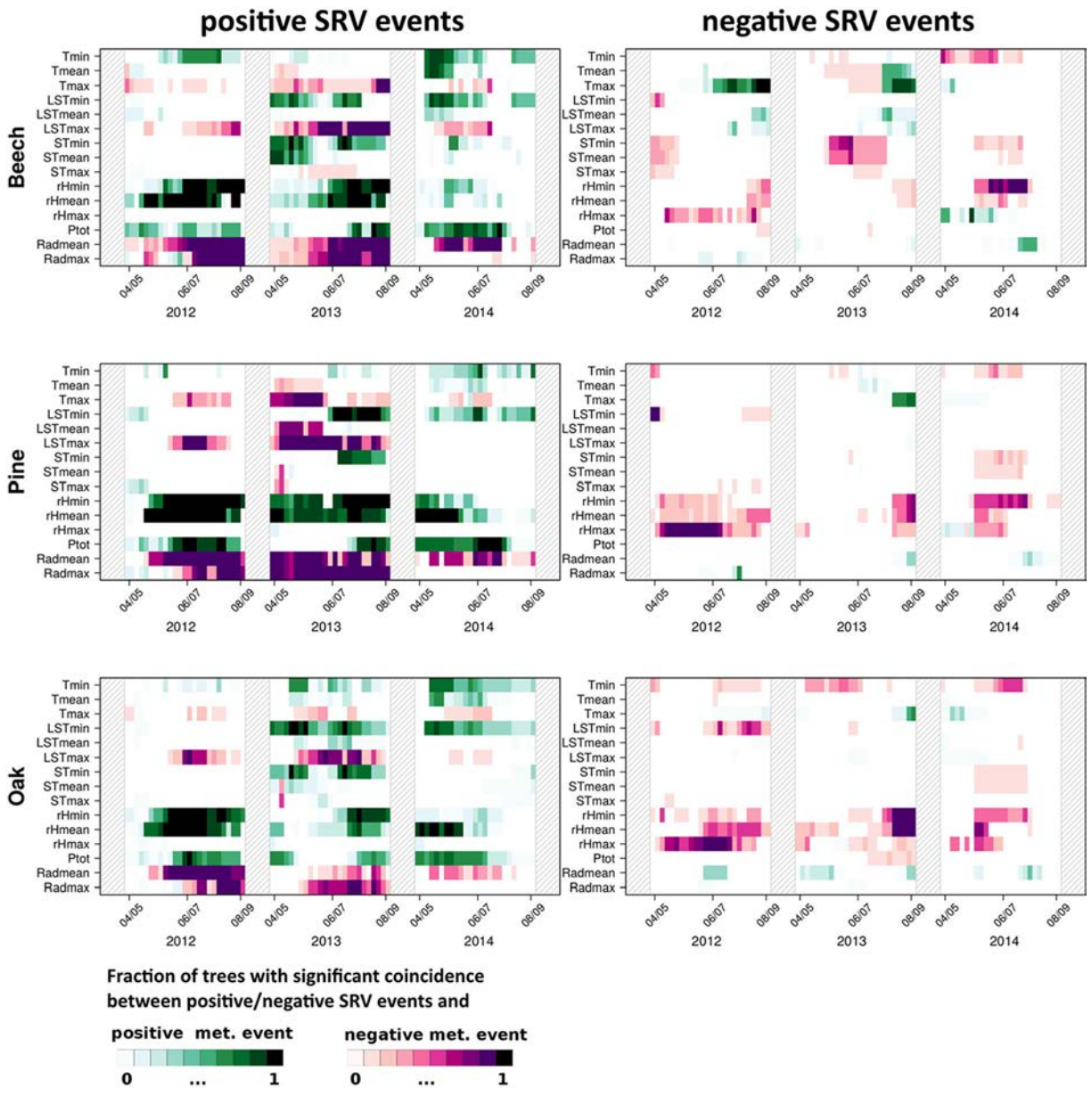

FIGURE 2 | Results of precursor ECA ($\Delta T = 0$ and $\tau = 0$) between positive (left panels) and negative SRV events (right panels) and extraordinarily high (above the 90th percentile, "positive meteorological events") and low (below the 10th percentile, "negative meteorological events") expressions of 15 meteorological variables for beech, oak, and pine during the study period from 2012 to 2014. Colors indicate the fraction of significant coincidences (at $\alpha = 0.05$ confidence level). The dates at the x-axes denote the centers of the sliding windows (61 days).

of meteorological variables, respectively. Six main observations are to be highlighted (which are also evident for the two other tree species but to different degrees): (i) In 2012, extraordinary high minimum temperatures in combination with extraordinary high relative humidity strongly coincide with positive SRV events. (ii) Various combinations of all temperature variables coincide with positive SRV events, but for beech almost only in 2014. (iii) Extraordinary low maximum land surface as well as low maximum air temperature events in combination with extraordinary low mean and maximum radiation coincide with positive SRV events, mainly in 2012 and 2013. (iv) Extreme precipitation plays a rather minor role for beech SRV events when applying JECA for equally directed meteorological extremes. In turn, the combinations of extraordinary low maximum air or land surface temperature with extraordinary high precipitation or extraordinary high air humidity strongly coincide with positive beech SRV events. In addition, (v) extraordinary high minimum temperature values together with extraordinary low radiation, and (vi) extraordinary humid conditions (in terms of strong precipitation or high air humidity) again together with

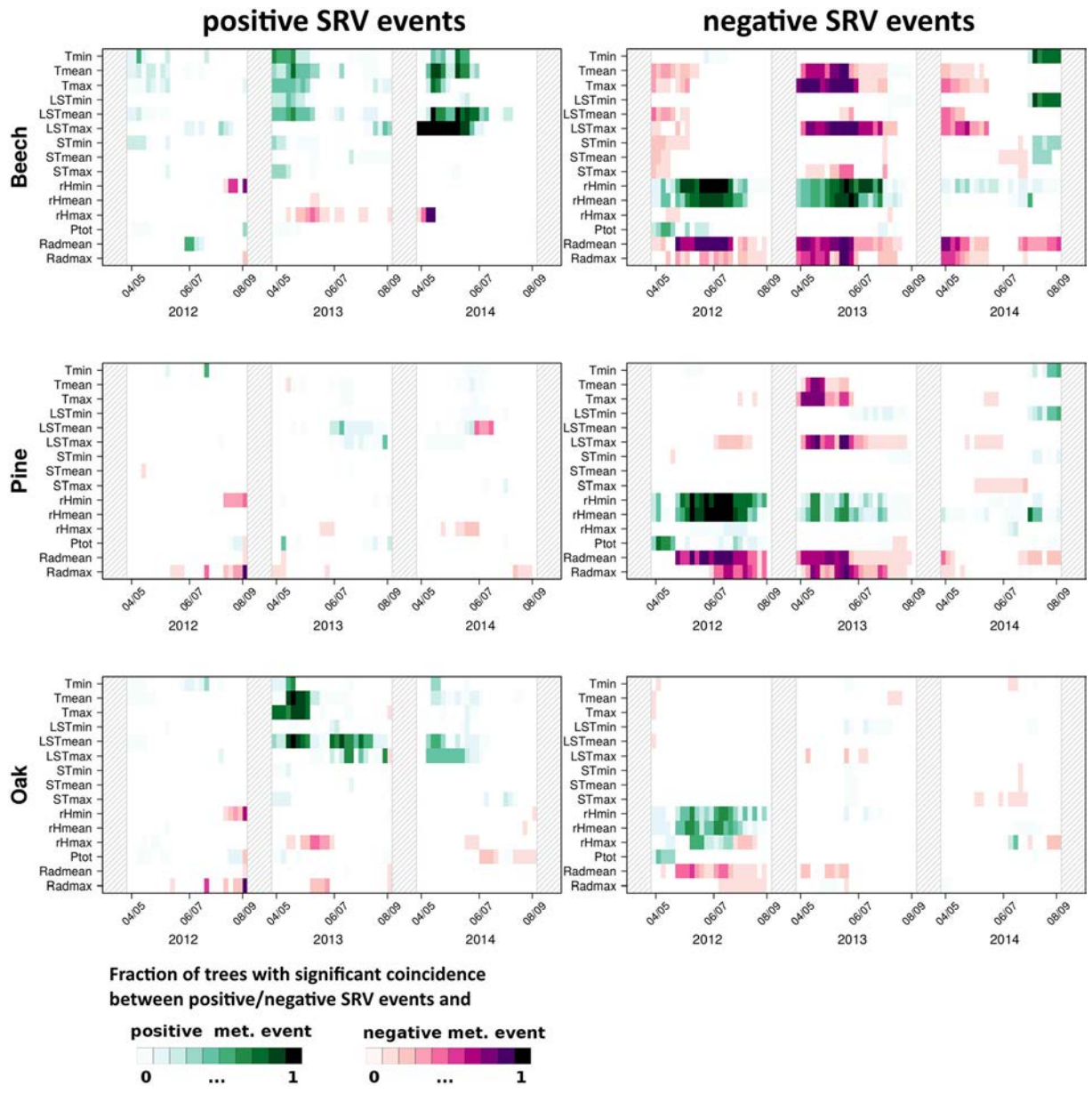

FIGURE 3 | As in Figure 2 but with $\Delta T = 1$ day and $\tau = 1$ day.

extraordinary low radiation also coincide with positive beech SRV events.

The investigation of negative beech SRV events using JECA shows hardly any significant coincidences (see Figure S2). Whenever evident, the behavior is simply opposite to the effects of positive change anomalies and shall therefore not be further detailed here.

3.2.2. Oak

The results of JECA for oak SRV events are provided in Figure S3. The left panel shows again that (i) during a period in early summer 2012 extraordinary high minimum temperatures in combination with extraordinary high air humidity coincide with positive SRV events, and (ii) various combinations of extraordinary high temperatures coincide with positive oak SRV events as well. Unlike beech, oak stem variations also show this feature in 2013. (iii) Additionally, extraordinary low maximum air and land surface temperatures together with extraordinary low radiation coincide with positive SRV events. (iv) Extraordinary high minimum and mean temperatures together with extraordinary precipitation events appear simultaneously with positive SRV events mainly in 2014 and partly in 2013. In contrast to this, similar to beech SRV events, negative maximum temperatures events with co-occuring

extraordinary humid conditions coincide with positive oak SRV events in all 3 years. The features (v) and (vi) are very similar to what has been illustrated in Figure S1 for beech.

For joint coincidences between negative oak SRV events and pairs of meteorological variables (Figure S4), the results are hardly significant in general. However, three specific observations can be made regarding conditions in late summer 2013: (i) Negative SRV events coincide with very dry conditions - indicated by the various combinations of extraordinary low humidity as well as (ii) positive maximum temperature events together with negative humidity events and (iii) negative humidity with positive mean and/or maximum radiation events.

3.2.3. Pine

The features (i), (ii), and (iii) indicated in Figure S5 are very similar to the corresponding features in Figure S1. Yet, feature (i) for positive pine SRV events is additionally visible in 2013. The positive impact of very humid conditions (iv) in terms of combinations of extraordinary high air humidity and extraordinary strong precipitation as well as of low maximum air and land surface temperatures and strong precipitation or high air humidity is clearly visible in all 3 years of observations. The features (v) and (vi) reported above are also clearly visible and in general more distinct than for beech and oak.

Negative pine SRV events (Figure S6) coincide with the same extraordinary meteorological conditions that were observed for oak.

3.3. Positive SRVs and Time Lagged Negative SRVs

As already mentioned in Section 3.1, when comparing the results of ECA without time lag and tolerance window with the results using $\Delta T = \tau = 1$ day, one very important feature is that relative humidity and radiation show coincidences for both, positive ($\Delta T = \tau = 0$) and negative ($\Delta T = \tau = 1$ day) SRV events. A very similar finding was also reported by van der Maaten et al. (2013), based on correlation analysis. The interpretation of this observation leads to the hypothesis that in many cases, after a positive SRV event a negative event occurs during one of the two following days. In order to further test this hypothesis, we also performed ECA between negative SRV events and positive SRV events for previous days. For this purpose, we used negative events (see Section 2) as event series A and positive events as series B with $\Delta T = 2$ days and $\tau = 1$ day. In this analysis a precursor coincidence is found, if a negative event is preceded by a positive event at one of the three previous days, whereas a trigger coincidence is observed if a positive event is followed by a negative event during one of the following 3 days. This analysis was performed for all tree species and for each year separately. **Table 1** summarizes the results which indicate very high rates of both trigger and precursor coincidence. Notably, a very high fraction of positive SRV events (up to 64%) precede negative events at one of the three consecutive days. In all these cases, the observed positive SRV events very likely do not correspond to irreversible growth, but rather reversible swelling. On the other hand, the remaining positive events (40–50%) have not been followed by negative events, i.e., either not followed by stem radius decrease at all or by a gradual decrease that is not identified as extraordinary with the employed event definition.

To further investigate this question, we additionally used JECA with the same setup, where the positive SRV events (series B) have been observed in parallel with extraordinarily high rH values (series C). **Table 2** summarizes the results of this analysis. Notably, the observed joint trigger coincidence rates are clearly higher than the trigger coincidence rates in **Table 1** which implies that positive SRV events induced by high air humidity are more likely to be followed by negative SRV events than other positive SRV events. A possible scenario consistent with this finding would be thunderstorms during relatively dry and/or hot periods, where wet conditions induce positive SRVs and rapid hydrological processes return to dry soil conditions very quickly again. Moreover, we find that the joint trigger coincidence rates are distinctively higher than the joint precursor coincidence rates. This indicates that most of the humidity-induced positive SRV events have triggered negative events, but only a smaller fraction of negative events have been preceded by humidity-induced positive SRV events. This finding suggests, that there are different types of positive SRV events (followed or not followed by negative SRV events events) and different types of negative SRV events events (preceded or not preceded by positive SRV events).

3.4. Coincidences of the Timings of SRV Events between the Individual Trees

When comparing the results of both bi- and multivariate ECA between the three tree species, the differences are relatively small. Altogether, oak seems to not favor wet conditions as strongly as beech and pine, but systematic inter-species differences appear to be absent. In turn, for the mean behavior (of daily as well as

TABLE 1 | Mean precursor and trigger coincidence rates (10 trees per species) between negative (event type A) and positive SRV events (event type B), using $\Delta T = 2$ days and $\tau = 1$ day (i.e., a negative event following a positive events).

	Trigger			Precursor		
	2012	2013	2014	2012	2013	2014
Beech	0.53	0.39	0.44	0.49	0.38	0.55
Pine	0.64	0.54	0.45	0.57	0.58	0.50
Oak	0.60	0.45	0.31	0.51	0.42	0.34

TABLE 2 | Mean joint precursor and joint trigger coincidence rates (10 trees per species) between negative SRV events (series A), positive SRV events (series B) and extraordinarily high rH_{mean} events (series C), using $\Delta T = 2$ days, $\tau = 1$ day, $\Delta T_{cond} = 0$ and $\tau_{cond} = 0$.

	Trigger			Precursor		
	2012	2013	2014	2012	2013	2014
Beech	0.69	0.60	0.58	0.28	0.28	0.25
Pine	0.83	0.66	0.48	0.42	0.40	0.26
Oak	0.77	0.58	0.31	0.35	0.23	0.13

subdaily features), the growth characteristics are widely known to differ markedly between different tree species (Drew and Downes, 2009; Miralles-Crespo et al., 2010; Köecher et al., 2012; Butt et al., 2014). The question, whether there are differences or commonalities regarding the tree species' upper or lower parts of the distribution of SRVs has not been addressed to far. In order to investigate this issue for the three species of this study, we performed a hierarchical cluster analysis as described in Section 3. **Figure 4** shows the results of this analysis and reveals that although the mutual correlations between the individual trees are quite high, the coincidence rates between days with positive SRV events are comparatively low. Based on correlation, we additionally find that the tree individuals are quite well clustered, while when using coincidence rates as similarity measure, the clusters following the individual species are completely lost. This means that the highest SRV variations of the individual trees vary strongly in their timing (at the daily scale), and that this timing is not generally differing by tree species. Hence, a clear systematic difference of the results between the different species (Section 3) cannot be found.

4. DISCUSSION

4.1. Bivariate Event Coincidence Analysis

The two broadleaved species show a positive response to temperature as well as LST while little positive response is found for pine. This positive growth response is likely due to the sufficient supply of water; possibly by reaching groundwater reservoirs. Similar relationships have been found earlier for the mean values (i.e., using correlation-based analyses) by van der Maaten et al. (2013) and others. In contrast to this, the fact that extraordinary negative T_{max} and/or LST_{max} events also coincide with positive SRV events (for all species) delivers important complementary information to the positive correlation between stem size variations and T_{max} found by van der Maaten et al. (2013) and Deslauriers et al. (2003). Due to the fundamentally different nature of these two statistical approaches, two time series can be positively correlated and simultaneously show significant coincidences between negative and positive events. This is not contradictory, but complementary information. The latter finding is further strengthened by the strong coincidence between positive T_{max} events and negative beech SRV events. Since both van der Maaten et al. (2013) and Deslauriers et al. (2003) performed their analysis for the entire (not subdivided) growing season, it is not possible to compare the seasonal timings of these contradicting behaviors.

Only few coincidences were found between SRV events and soil temperature extremes. It is likely that this observation is due to the location of the meteorological station 2 km from the dendrometer site. Due to the variability in soil type and ground cover throughout in the study area, actual soil temperatures beneath the sampled trees may systematically differ from the values measured at the station.

A positive instantaneous (lag zero) correlation between air humidity and SRV has been observed in previous studies (Downes et al., 1999; Deslauriers et al., 2003; Köecher et al., 2012; van der Maaten et al., 2013). In the present work, it was confirmed that this relationship is also evident for the upper (positive events) and lower (negative events) tails of the distribution of SRVs. As may be expected, a similar positive SRV coincidence is recorded with precipitation. However, the absence of a notable heavy precipitation impact during summer 2013 in all tree species is a result of a 60-days dry period except for one single day (35 mm). This suggests that one single heavy rainfall event is not sufficient to result in a significant coincidence rate even if it coincides with a marked positive or negative dendrometer anomaly (which was the case for almost all 30 trees).

The significant coincidences between low radiation values and positive SRV events can interpreted in a twofold way: One the one hand, low radiation decreases transpiration leading to water replenishment. On the other hand, low radiation days commonly correspond to cloudy and foggy conditions and are therefore often characterized by high relative humidity as well. A general negative dependency in terms of negative correlations between radiation and stem radius variability was reported earlier by Downes et al. (1999) and Köecher et al. (2012).

Our analysis revealed some counter-intuitive significant coincidences between days with extraordinary high air humidity and negative SRV events in beech stems during 2014 (**Figure 2**). One possible cause for this may be the result of high air associated with low soil moisture conditions typical of foggy days during spring. Further support of this theory is provided by Figure S2, where in the upper right panel joint coincidences between low T_{min}, high rH_{max} and negative beech SRV events are evident. In order to understand these joint coincidences in more detail, **Figure 5** illustrates the temperature and air humidity development of 4 days in spring and early summer 2014, where the above mentioned coincidences appeared. Specifically, the figure shows very high air humidity values of up to 99% around 9–10 a.m. which abruptly decrease simultaneously with increasing temperature. This behavior is a common indication of foggy conditions during morning hours—caused by inverted atmospheric stratification—that are relieved by the rapidly increasing temperatures on a cloud-free day. The negative SRV events of these days are caused by the extraordinary high temperature and low humidity values of the mid-day and are not linked with the high air humidity values of the morning hours. Applying a classical linear correlation analysis between daily maximum relative humidity and daily SRVs, these days would produce strong residuals, clearly deviating from the well-known positive statistical interrelationship between these two variables. Therefore, these specific days provide a very good example of how to explain singular large residuals in classically assumed interrelationships between weather conditions and dendrometer variations as concluded from correlation analysis on a daily basis.

The results of bivariate (**Figures 2**, **3**), as well as multivariate (Figures S1–S6) event coincidence analysis show that for a number of variables, coincidences with SRV events are not equally evident during all the 3 years of the investigation period. One example was mentioned in the previous paragraph. Another example is that positive T_{max} events only coincide with negative beech SRV events in 2012 and 2013, but not in 2014 (**Figure 2**, upper right panel). In this case, the reason is, that the positive T_{max} events in 2014 are, in absolute values, lower than the

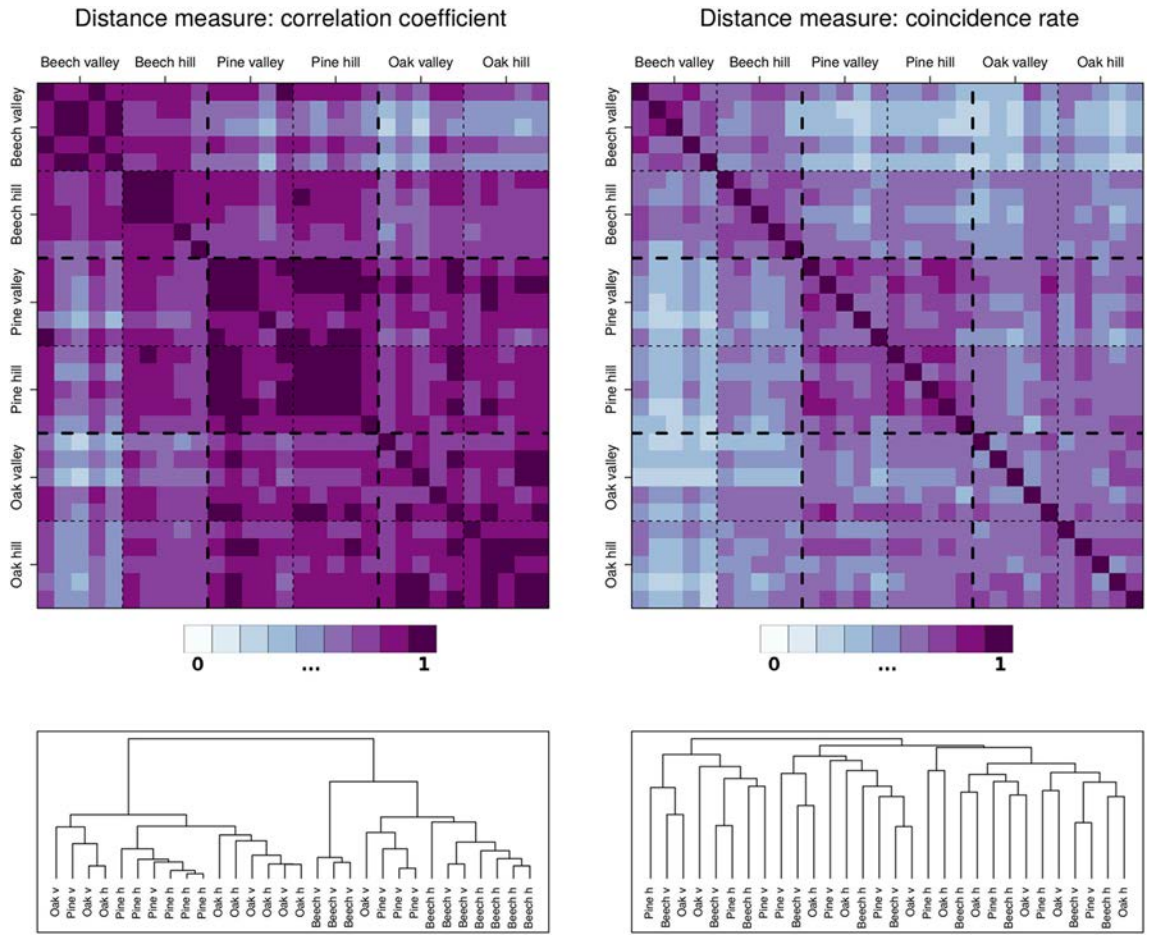

FIGURE 4 | Hierarchical cluster analysis for the 30 dendrometer time series of the growth periods of 2012, 2013, and 2014. Upper panels: Correlation (daily stem increments) and coincidence (values above 90th percentiles) matrices between all pairs of trees used for the cluster analysis. **Lower panels:** Dendrograms of the two cluster analyses. The tree stands can be further subdivided into "hill" and "valley," indicated by *h* and *v*.

positive T_{max} events of the previous 2 years. Even though the events were defined by percentiles over the entire investigation period, a high number of positive T_{max} events in 2012 and 2013 led to this non-uniform distribution of events. In other words: in 2014, the highest T_{max} events were not warm enough to trigger negative SRV events. The same explanation is also valid for the absence of coincidences between positive SRV events (for all species) with LST_{min}, ST_{min} and ST_{mean} in 2012. While in these cases the heterogeneous distribution of coincidences among the years can easily be explained, in other cases the reasons are less obvious. One possible factor leading to inter-year differences in the relation between weather conditions and SRVs could be the effect of the previous year's weather conditions on the current tree growth. Corresponding impacts on earlywood production (especially for oak, but also for the other two species) have been reported by a variety of studies (Lebourgeois, 2000; Rubino and McCarthy, 2000; Lebourgeois et al., 2004, 2005; Drobyshev et al., 2008; Michelot et al., 2012; Latte et al., 2015). Yet, all previous analyses that the authors are aware of, addressed integrated/cumulative stem size rates in terms of total earlywood production. So far, no statistical evidence or physiological explanation has been reported, why and how previous year's conditions should influence the day-to-day SRVs and their reaction to weather extremes.

4.2. Extraordinary Positive vs. Negative Stem Size Variation Events

The counter-intuitive negative beech SRV events found in Figure 2 and discussed in Section 4.1 could also be explained by a statistical artifact due to the co-occurrence between negative SRV events and positive SRV events of the previous day. Such a phenomenon of contradicting climatic signals in tree rings has also been reported for high resolution tree-ring isotope data (Schollän et al., 2013, 2014).

The various cycles of swelling and shrinkage shown by dendrometer data have been addressed in several recent studies (Downes et al., 1999; Köecher et al., 2012; van der Maaten et al., 2013; Vieira et al., 2013). From previous studies like Bouriaud et al. (2005), it is known that stems can shrink over several consecutive days, likely induced by shrinkage of the bark and

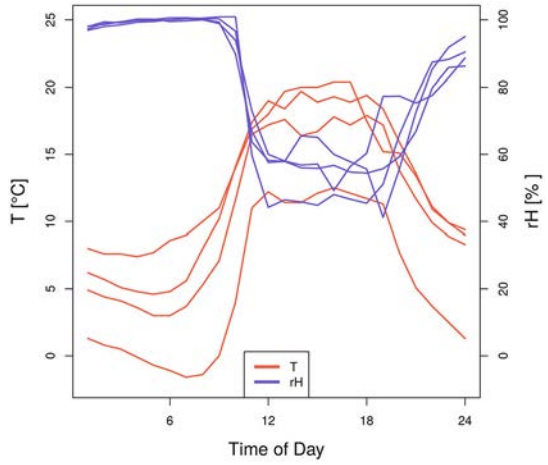

FIGURE 5 | Hourly values of temperature and relative air humidity of four selected days in spring and early summer 2014. These days were all characterized by minimum temperature, maximum relative air humidity and negative SRV events.

relative sap-flow reduction of the stem some time after rain events. Our study refined these findings by pointing out that there are two kinds of strongly positive stem size variations: (1) some that are followed by negative SRV events and (2) some that are not followed by negative stem size changes during consecutive days. For future studies it will be important to investigate how to disentangle the four possible combinations of strong stem size changes defined in this study: There are strong positive SRV events that are followed (i.e., neutralized) by negative SRV events vs. positive SRV events that permanently increase the stem radius, as well as negative SRV events that simply originate from strong positive SRV events during the previous days vs. negative SRV events that have been forced by adverse weather conditions. A first attempt to disentangle these distinct phenomena has been recently published by Chan et al. (2016). The mentioned classical approach do define growth and shrinkage in dendrometer data (Deslauriers et al., 2003; Bouriaud et al., 2005; Köecher et al., 2012; Vieira et al., 2013) does not solve this problem, since (as for the procedures used by van der Maaten et al. (2013) and also in this study) both shrinkage and growth are solely defined based upon the preceding evolution and do not take into account the (short or long-term) following development of the stem radius.

4.3. Joint Event Coincidence Analysis

The JECA revealed six main findings common to all three investigated tree species. (i) The combination of high minimum temperature with high relative humidity events coinciding with positive SRV events describes situations of warm nights followed by moist days. This feature was most clearly visible for pine which is to be explained by pine having the highest potential for water storage due to its larger amount of xylem Pfautsch et al. (2015). (ii) The positive impact of various temperature combinations on stem radius is a logical continuation of the results of bivariate ECA as discussed above. (iii) The combination between low radiation and low maximum temperatures describes very cloudy days. Such days are often also characterized by high air humidity, and this combination (high humidity and low radiation) is highlighted by finding (vi). (iv) Heavy precipitation as an additional event contributing to the aforementioned cloudy and moderately cool days also favors strongly positive SRVs. Such days are often also characterized by high night temperatures (high T_{min}) corresponding to situation (v) highlighted in Section 3.2.

4.4. Differences in the Timing of Stem Size Variation Events between the Species

The observations found in Section 3.4 are in fact not trivial, since very different reactions of the analyzed species to environmental conditions have been well documented by, e.g., Gonzalez-Munoz et al. (2014), Lévesque et al. (2013), Garcia-Suarez et al. (2009), or Kwiaton and Wand (2015). The difference of our analysis to these studies is, that our dendrometer analysis specifically takes into account the timings of SRVs and meteorological extremes on a daily basis, whereas previous studies analyzed relationships between tree stem growth and weather conditions on a seasonal time scale. Therefore, the finding that no clear species-to-species differences are evident in this study does not contradict studies on seasonal scales. In turn, our results suggest, that the species-specific relations on weather conditions are more clearly expressed on longer rather than on shorter time scales. Nonetheless, our study indicates, that the different species do not differ markedly in their susceptibility to climate extremes on a daily scale. General statements or even suggestions to forest management concerning the species' eligibility in the context of ongoing and future climate change should not yet be drawn from this first case study.

5. CONCLUSIONS

We have used high-resolution dendrometer data to investigate tree species-specific responses to extraordinary meteorological conditions. For the first time joint event coincidence analysis as well as a hierarchical clustering analysis based on coincidence rates have been used. This new approach allowed a detailed analysis of the timing of observations falling in the upper and lower tails of the empirical distributions of daily SRVs. This opens new possibilities for interpreting tree-specific responses to meteorological extremes. Our method is able to provide relevant complementary information beyond what has been known from previous correlation-based analyses. Further potential applications of this method include the investigation of dendrochronological data or intra-annual density fluctuations (IADF).

For future investigations, it will be crucial to put additional efforts into disentangling tree stem radius growth from stem swelling, using novel data analysis approaches. Additionally, integrated studies including dendrometer and wood density measurements, as well as an up-scaling across a larger area will be necessary to draw reliable conclusions on tree or forest carbon storage dynamics in relation to meteorological extreme events.

AUTHOR CONTRIBUTIONS

JS Study's Design, Data Analysis, Figures, Writing. TS Study's Design, Proofreading. IH Data Production and Preprocessing, Proofreading. EV Proofreading. SS Data Production and Preprocessing. GH Study's Design, Proofreading. RD Study's Design, Writing, Proofreading.

ACKNOWLEDGMENTS

This study was conducted within the framework of the Young Investigators Group "CoSy-CC^2 : Complex Systems Approaches to Understanding Causes and Consequences of Past, Present and Future Climate Change" (grant no. 01LN1306A) funded by the German Federal Ministry for Education and Research (BMBF), the COST Action FP1106 STReESS supported by COST (European Cooperation in Science and Technology), the Virtual Institute of Integrated Climate and Landscape Evolution Analysis—ICLEA—(grant no. VH-VI-415), and the Terrestrial Environmental Observatories project—TERENO—of the Helmholtz Association. Jonatan Siegmund acknowledges financial support by the Evangelisches Studienwerk Villigst e.V. Ingo Heinrich received support from the Deutsche Forschungs-Gemeinschaft (DFG project number He 7220/1-1). The authors wish to thank Jonathan Bauermann and Jonathan Donges for fruitful discussions on the notation of CECA. Thanks to Daniel Balanzategui for proof-reading the manuscript. All presented analyses have been performed using the R package CoinCalc, available at https://github.com/JonatanSiegmund/CoinCalc. The publication of this article was funded by the Open Access fund of the Leibniz Association.

SUPPLEMENTARY MATERIAL

The Supplementary Material for this article can be found online at: http://journal.frontiersin.org/article/10.3389/fpls.2016.00733

REFERENCES

Barriopedro, D., Fischer, E., Luterbacher, J., Trigo, R., and Garcia-Herrera, R. (2011). The hot summer of 2010: redrawing the temperature record map of europe. *Science* 332, 220–224. doi: 10.1126/science.1201224

Beck, W., Sanders, T., and Pofahl, U. (2013). CLIMTREG: detecting temporal changes in climate growth reactions - a computer program using intra-annual daily and yearly moving time intervals of variable width. *Dendrochronologia* 31, 232–241. doi: 10.1016/j.dendro.2013.02.003

Bouriaud, O., Leban, J.-M., Bert, D., and Deleuze, C. (2005). Intra-annual variations in climate influence growth and wood density of Norway spruce. *Tree Physiology* 25, 651–660. doi: 10.1093/treephys/25.6.651

Butt, N., Bebber, D., Riutta, T., Crockatt, M., Morecroft, M., and Malhi, Y. (2014). Relationships between tree growth and weather extremes: spatial and interspecific comparisons in a temperate broadleaf forest. *For. Ecol. Manage.* 334, 209–216. doi: 10.1016/j.foreco.2014.09.006

Chan, T., Höelttä, T., Beringer, F., Mäekinen, H., Nöejd, P., Mencuccini, M., et al. (2016). Separating water-potential induced swelling and shrinking from measured radial stem variations reveals a cambial growth and osmotic concentration signal. *Plant Cell Environ.* 39, 233–244. doi: 10.1111/pce.12541

Cuny, H. E., Rathgeber, C. B. K., Frank, D., Fonti, P., Maekinen, H., Prislan, P., et al. (2015). Woody biomass production lags stem-girth increase by over one month in coniferous forests. *Nat. Plants* 1:15160. doi: 10.1038/nplants.2015.160

Daudet, F.-A., Améglio, T., Cochard, H., Archilla, O., and Lacointe, A. (2005). Experimental analysis of the role of water and carbon in tree stem diameter variations. *J. Exp. Bot.* 56, 135–144. doi: 10.1093/jxb/eri026

Denneler, B., Bergeron, Y., and Begin, Y. (2010). Flooding effects on tree-ring formation of Riparian Eastern White-Cedar (*Thuja occidentalis* L.), Northwestern Quebec, Canada . *Tree Ring Res.* 66, 3–17. doi: 10.3959/2008-11.1

Deslauriers, A., Morin, H., Urbinati, C., and Carrer, M. (2003). Daily weather response of balsam fir (*Abies balsamea* (L.) Mill.) stem radius increment from dendrometer analysis in the boreal forests of Quebec (Canada). *Trees* 17, 477–484. doi: 10.1007/s00468-003-0260-4

Donges, J. F., Donner, R. V., Trauth, M. H., Marwan, N., Schellnhuber, H.-J., and Kurths, J. (2011). Nonlinear detection of paleoclimate-variability transitions possibly related to human evolution. *Proc. Natl. Acad. Sci. U.S.A.* 108, 20422–20427. doi: 10.1073/pnas.1117052108

Donges, J. F., Schleussner, C. F., Siegmund, J. F., and Donner, R. V. (2016). Coincidence analysis for quantifying statistical interrelationships between event time series: on the role of flood events as possible drivers of epidemic outbreaks. arXiv preprint arXiv:1508.03534.

Downes, G., Beadle, C., and Worledge, D. (1999). Daily stem growth patterns in irrigated *Eucalyptus globulus* and *E. nitens* in relation to climate. *Trees* 14, 102–111. doi: 10.1007/PL00009752

Drew, D. (2007). "Forest growth and timber quality: crown models and simulation methods for sustainable forest management," in *Simulating Daily Xylem Development in Eucalyptus Using Outputs of the Process-Based Model CABALA, IUFRO 4.01.05* (Portland, OR).

Drew, D., and Downes, M. (2009). The use of precision dendrometers in research on daily stem size and wood property variation: a review. *Dendrochronologia* 27, 159–172. doi: 10.1016/j.dendro.2009.06.008

Drobyshev, I., Niklasson, M., Eggertson, O., Linderson, H., and Sonesson, K. (2008). Influence of annual weather on growth of pedunculate oak in southern sweden. *Ann. For. Sci.* 65, 521. doi: 10.1051/forest:2008033

Ecomatik GmbH (2015). *Radius Point Dendrometer*. Available online at: http://www.ecomatik.de/en/radiusdendrometer.php

Friedrichs, J. (1897). Über den Einfluss der Witterung auf den Baumzuwachs. *Mitteilungen Forstlichen Bundes-Versuchsanstalt Wien* 22, 1–160.

Fritts, H., Shaskin, A., and Downes, G. (1999). "TreeRing 3: a simulation model of conifer ring growth and cell structure," in *Tree Ring Analysis: Biological, Methodological and Environmental Aspects*, eds R. Wimmer and R. Vetter (Oxford: CAB International), 3–32.

Garcia-Suarez, A., Butler, C., and Baillie, M. (2009). Climate signal in tree-ring chronologies in a temperate climate: a multi-species approach. *Dendrochronologia* 27, 183–198. doi: 10.1016/j.dendro.2009.05.003

Gonzalez-Munoz, N., Linares, J., Castro-Diez, P., and Sass-Klaassen, U. (2014). Predicting climate change impacts on native and invasive tree species using radial growth and twenty-first century climate scenarios. *Eur. J. For. Res.* 133, 1073–1086. doi: 10.1007/s10342-014-0823-5

IPCC (2013). *Climate Change 2013: The Physical Science Basis*. Contribution of Working Group I to the Fifth Assessment Report of the Intergovernmental Panel on Climate Change. Cambridge University Press, Cambridge, United Kingdom and New York, NY, USA.

Jezik, M., Blazenec, M., Strelcova, K., and Ditmarova, L. (2011). The impact of the 2003-2008 weather variability on intra-annual stem diameter changes of beech trees at a submontane site in central slovakia. *Dendrochronologia* 29, 227–235. doi: 10.1016/j.dendro.2011.01.009

Köecher, P., Horna, V., and Leuschner, C. (2012). Environmental control of daily stem growth patterns in five temperate broad-leaved tree species. *Tree Physiol.* 32, 1–12.

Kwiaton, M., and Wand, J. (2015). Radial growth responses of four deciduous species to climate variables in central Ontario, Canada. *Am. J. Plant Sci.* 6, 2234–2248. doi: 10.4236/ajps.2015.614226

Latte, N., Lebourgeois, F., and Claessens, H. (2015). Increased tree-growth synchronization of beech (*Fagus sylvatica* L.) in response to climate change in northwestern Europe. *Dendrochronologia* 33, 69–77. doi: 10.1016/j.dendro.2015.01.002

Lebourgeois, F. (2000). Climatic signals in earlywood, latewood and total ring width of Corsican pine from western France. *Annu. For. Sci.* 57, 155–164. doi: 10.1051/forest:2000166

Lebourgeois, F., Breda, N., Ulrich, E., and Granier, A. (2005). Climate-tree-growth relationships of European beech (*Fagus sylvatica* L.) in the French Permanent Plot Network (RENECOFOR). *Trees* 19, 385–401. doi: 10.1007/s00468-004-0397-9

Lebourgeois, F., Cousseau, G., and Ducos, Y. (2004). Climate-tree-growth relationships of *Quercus petraea* Mill. stand in the Forest of Berc (Futaie des Clos, Sarthe, France). *Ann. For. Sci.* 61, 1–12. doi: 10.1051/forest:2004029

Lévesque, M., Saurer, M., Siegwolf, R., Eilmann, B. Brang, P., Bugmann, H., et al. (2013). Drought response of five conifer species under contrasting water availability suggests high vulnerability of Norway spruce and European larch. *Glob. Change Biol.* 19, 3184–3199. doi: 10.1111/gcb.12268

McLaughlin, S. B., Wullschleger, S., and Nosal, M. (2003). Diurnal and seasonal changes in stem increment and water use by yellow poplar trees in response to environmental stress. *Tree Physiol.* 23, 1125–1136. doi: 10.1093/treephys/23.16.1125

Michelot, A., Breda, N., Damesin, C., and Dufrene, E. (2012). Differing growth responses to climatic variations and soil water deficits of *Fagus sylvatica*, *Quercus petraea* and *Pinus sylvestris* in a temperate forest. *For. Ecol. Manage.* 265, 161–171. doi: 10.1016/j.foreco.2011.10.024

Miralles-Crespo, J., Snachez-Blanco, M., Navarro, A., Martinez-Sanchez, J., Franco, J., and Banon, S. (2010). Comparison of stem diameter variations in three small ornamental shrubs under water stress. *HortScience* 45, 1681–1689.

Müller, V. (2014). *Landschaftsgeschichtliches Potenzial von Boden-Sediment-Sequenzen am Hinnensee, Müritz-Nationalpark.* Master's thesis, Technische Universität Dresden.

Oberhuber, W., and Gruber, A. (2010). Climatic influences on intra-annual stem radial increment of *Pinus sylvestris* (L.) exposed to drought. *Trees* 24, 887–898. doi: 10.1007/s00468-010-0458-1

Petoukhov, V., Rahmstorf, S., Petri, S., and Schellnhuber, H.-J. (2013). Quasiresonant amplification of planetary waves and recent northern hemisphere weather extremes. *Proc. Natl. Acad. Sci. U.S.A.* 110, 5336–5341. doi: 10.1073/pnas.1222000110

Pfautsch, S., Renard, J., Tjoelker, G., and Salih, A. (2015). Phloem as capacitor: radial transfer of water into Xylem of tree stems occurs via symplastic transport in Ray Parenchyma. *Plant Physiol.* 167, 963–971. doi: 10.1104/pp.114.254581

Rubino, D. L., and McCarthy, B. C. (2000). Dendroclimatological analysis of white oak (*Quercus alba* L., Fagaceae) from an old-growth forest of southeastern Ohio, USA. *J. Torrey Bot. Soc.* 127, 240–250. doi: 10.1016/j.quascirev.2013.05.018

Schollän, K., Heinrich, I., and Helle, G. (2014). UV-laser-based microscopic dissection of tree rings - a novel sampling tool for δ^{13}C and δ^{18}O studies. *New Phytol.* 3, 1045–1055. doi: 10.1111/nph.12587

Schollän, K., Heinrich, I., Neuwirth, B., Krusic, P., D'Arrigo, R., Karyanto, O., et al. (2013). Multiple tree-ring chronologies (ring width, δ^{13}C and δ^{18}O) reveal dry and rainy season signals of rainfall in indonesia. *Quart. Sci. Rev.* 73, 170–181. doi: 10.1016/j.quascirev.2013.05.018

Schulte-Bisping, H., Beese, F., and Dieffenbach-Fries, H. (2012). C-fluxes and C-turnover of a mature mixed beech and pine stand under increasing temperature at ICP Integrated Monitoring site in Neuglobsow (Brandenburg). *Eur. J. For. Res.* 131, 1601–1609. doi: 10.1007/s10342-012-0627-4

Siegmund, J., Donges, J., Wiedermann, M., and Donner, R. (2015). Impact of climate extremes on wildlife plant flowering over Germany. *Biogeosci. Discuss.* 12, 18389–18423. doi: 10.5194/bgd-12-18389-2015

Siegmund, J., Siegmund, N., and Donner, R. (2016). CoinCalc - A new R package for quantifying simultaneities of event (time) series. arXiv:1603.05038.

Spathelf, P., van der Maaten, E., van der Maaten-Theunissen, M., Campioli, M., and Dobrowolska, D. (2014). Climate change impacts in european forests: the expert views of local observers. *Ann. For. Sci.* 71, 131–137. doi: 10.1007/s13595-013-0280-1

van der Maaten, E., Bouriaud, O., van der Maaten-Theunissen, M., Mayer, H., and Spieker, H. (2013). Meteorological forcing of day-to-day stem radius variations of beech is highly synchronic on opposing aspects of a valley. *Agric. For. Meteorol.* 181, 85–93. doi: 10.1016/j.agrformet.2013.07.009

Vieira, J., Rossi, S., Campelo, F., Freitas, H., and Nabais, C. (2013). Seasonal and daily cycles of stem radial variation of pinus pinaster in a drought-prone environment. *Agric. For. Meteorol.* 180, 173–181. doi: 10.1016/j.agrformet.2013.06.009

Zweifel, R., and Häsler, R. (2001). Dynamics of water storage in mature subalpine Picea abies: temporal and spatial patterns of change in stem radius. *Tree Phyiol.* 31, 561–569. doi: 10.1093/treephys/21.9.561

Conflict of Interest Statement: The authors declare that the research was conducted in the absence of any commercial or financial relationships that could be construed as a potential conflict of interest.

Copyright © 2016 Siegmund, Sanders, Heinrich, van der Maaten, Simard, Helle and Donner. This is an open-access article distributed under the terms of the Creative Commons Attribution License (CC BY). The use, distribution or reproduction in other forums is permitted, provided the original author(s) or licensor are credited and that the original publication in this journal is cited, in accordance with accepted academic practice. No use, distribution or reproduction is permitted which does not comply with these terms.

Supplementary Material: Meteorological Drivers of Extremes in Daily Stem Radius Variations of Beech, Oak and Pine in Northeastern Germany: An Event Coincidence Analysis

Jonatan F. Siegmund [1,2,*], **Tanja Sanders** [3], **Ingo Heinrich** [4], **Ernst van der Maaten** [5], **Sonia Simard** [4], **Gerdhard Helle** [4] **and Reik V. Donner** [1]

*Correspondence:
Jonatan F. Siegmund
siegmund@pik-potsdam.de

SUPPLEMENTARY FIGURES

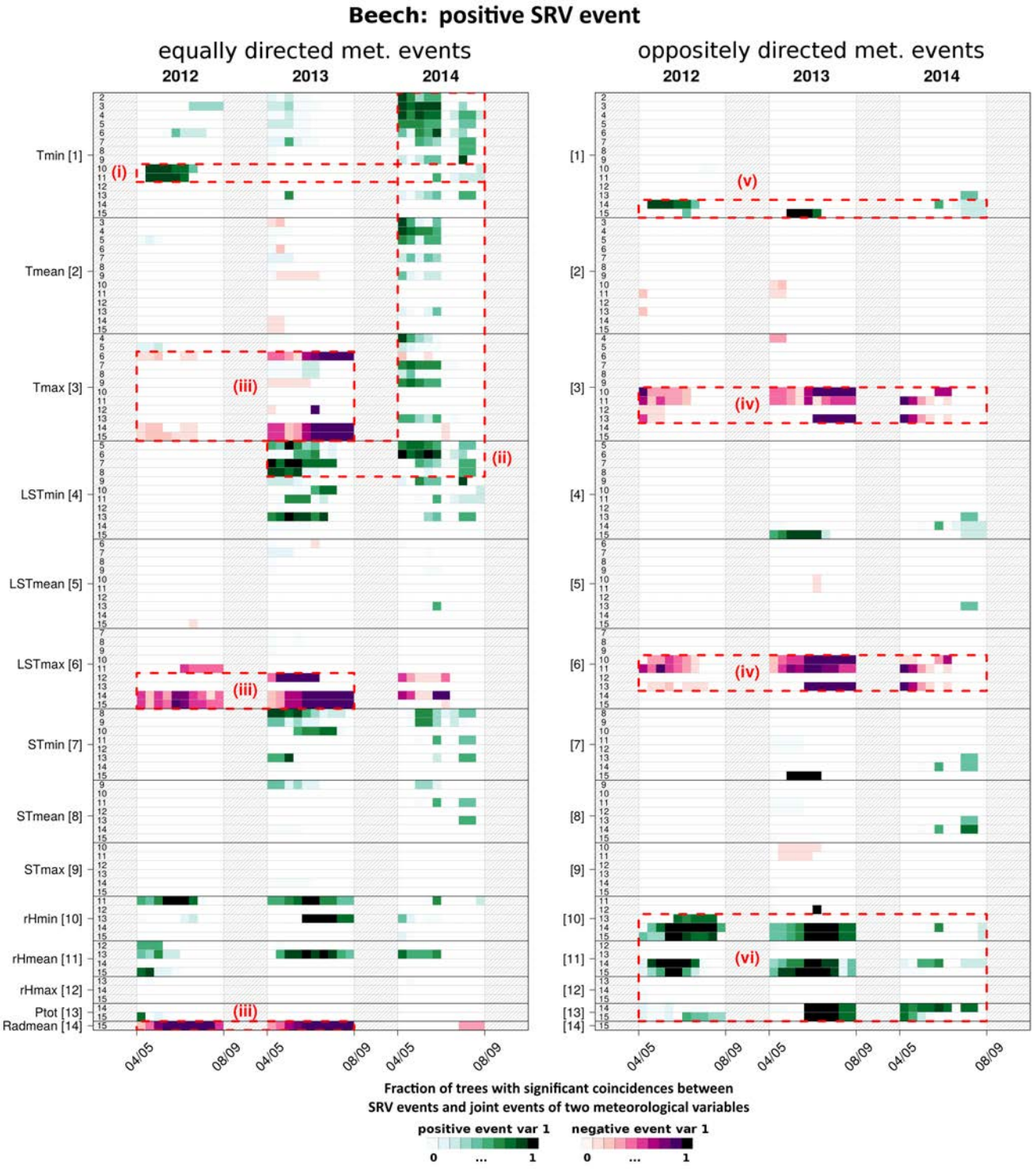

Figure S1. Coincidences between positive daily beech SRV events and joint positive/negative events of pairs of meteorological variables ($\Delta T = \tau = 0$). The left (right) panels show the results for equally (oppositely) directed meteorological events. Colors refer to the direction of the meteorological event in the first variable (indicated at the left) – green colors refer to positive and purple colors to negative events. The respective second variable is indicated by small numbers inside the individual panels (as explained at the left) and has either the same (left panels) or opposite (right panels) directionality of the extreme. Parts of the plots enclosed by dashed red lines highlight the six main findings (i)-(vi) discussed in the main text.

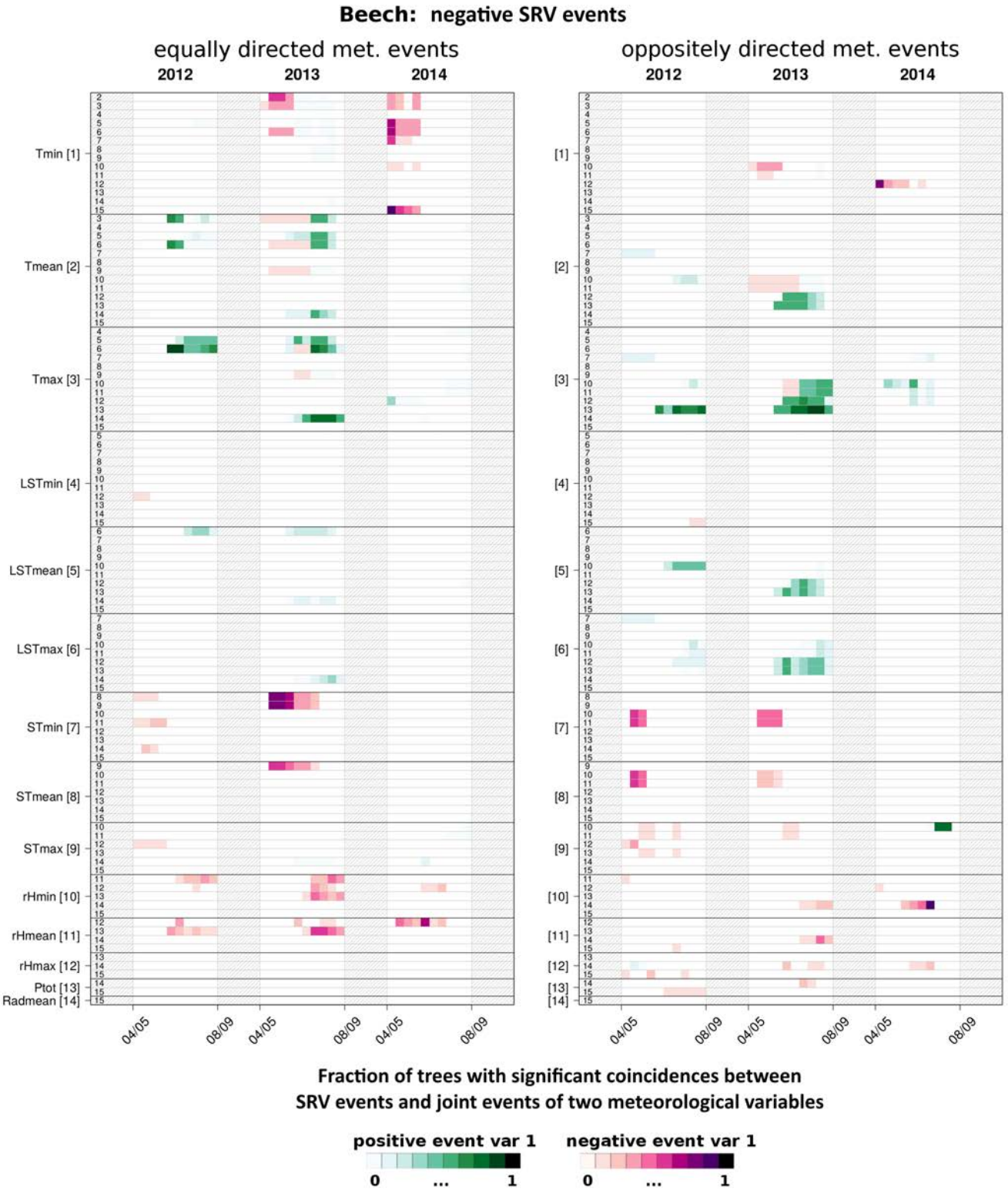

Figure S2. As in Fig. S1 for strongly negative beech SRVs.

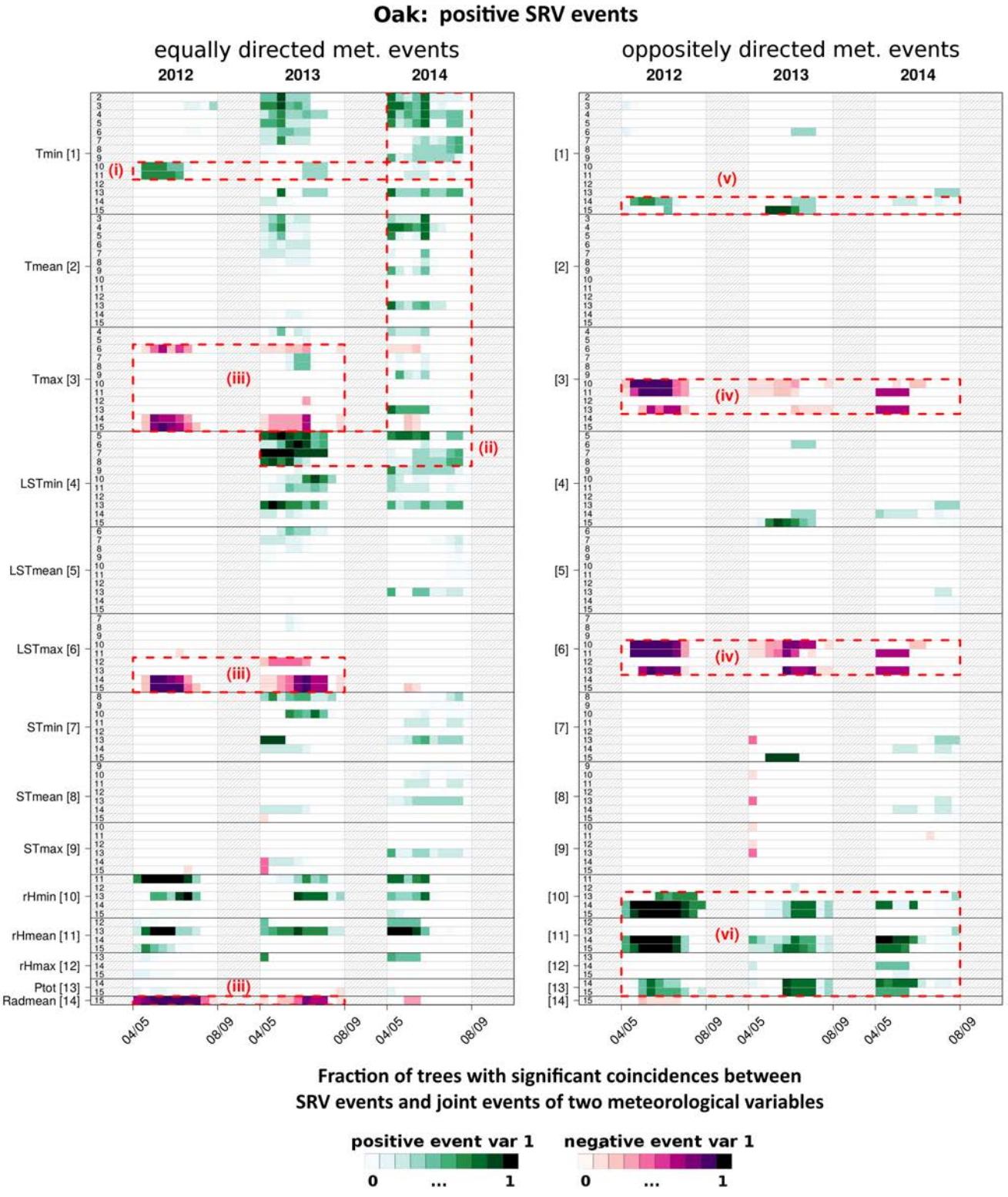

Figure S3. As in Fig. S1 for strongly positive oak SRVs.

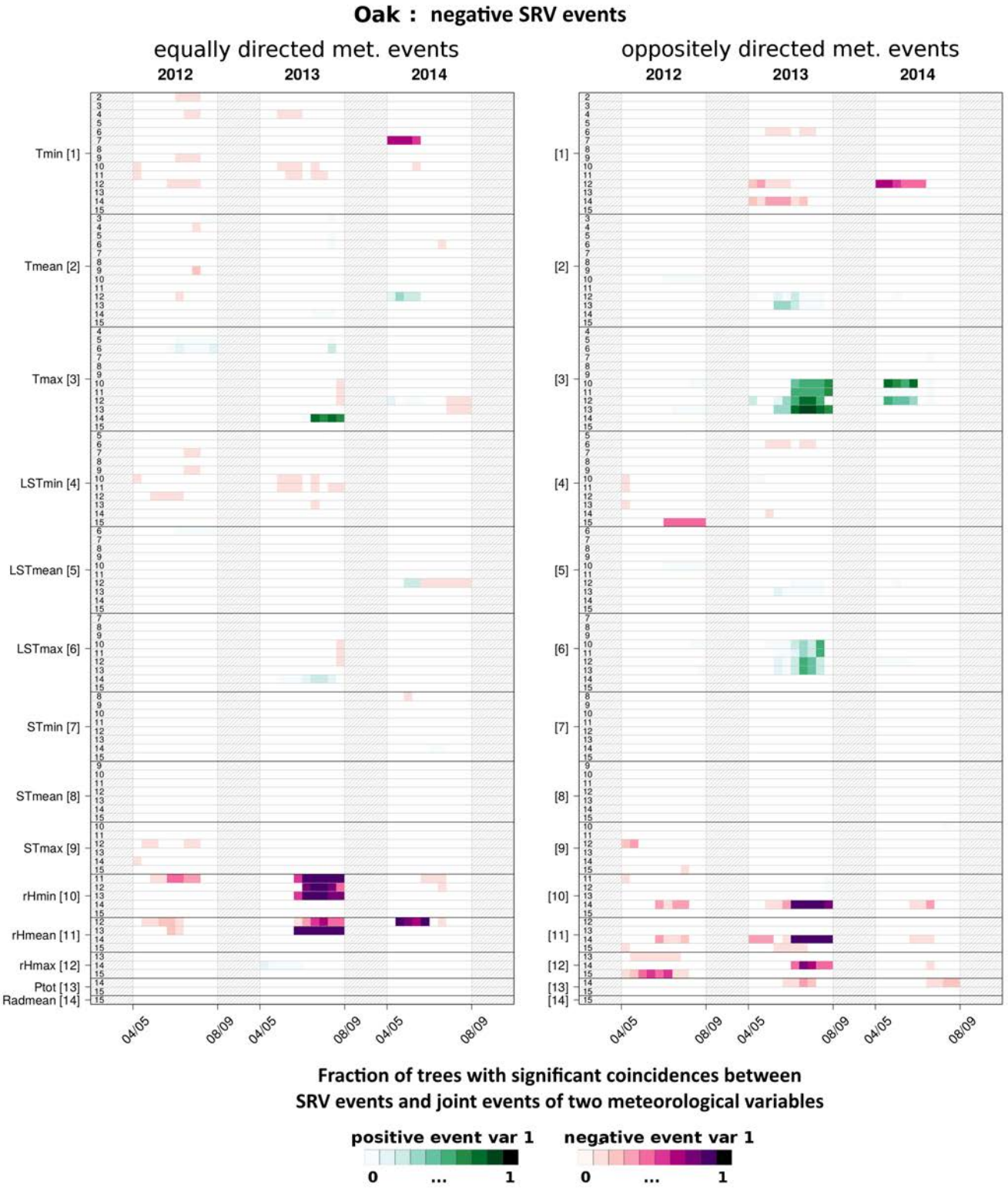

Figure S4. As in Fig. S1 for strongly negative oak SRVs.

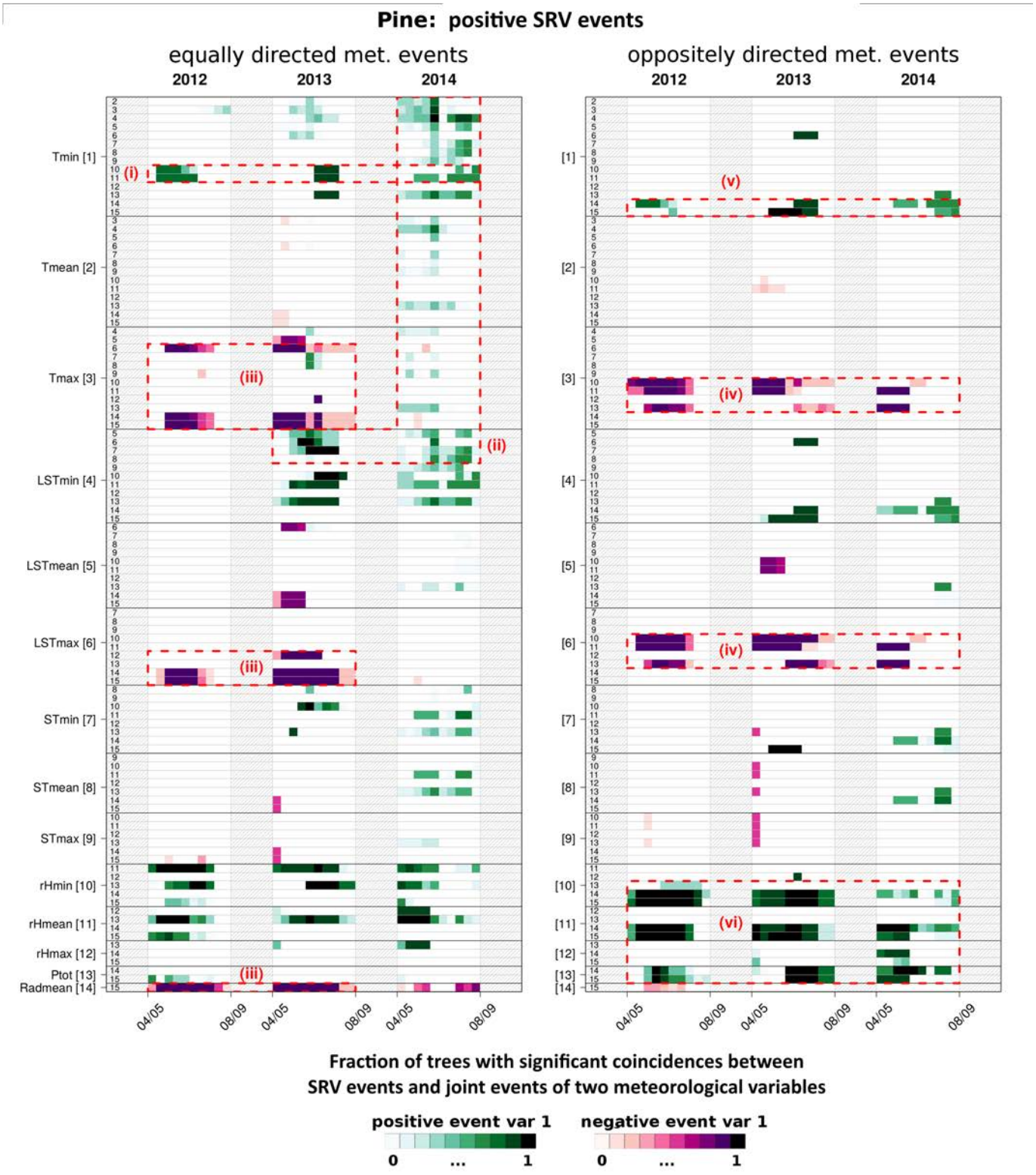

Figure S5. As in Fig. S1 for strongly positive pine SRVs.

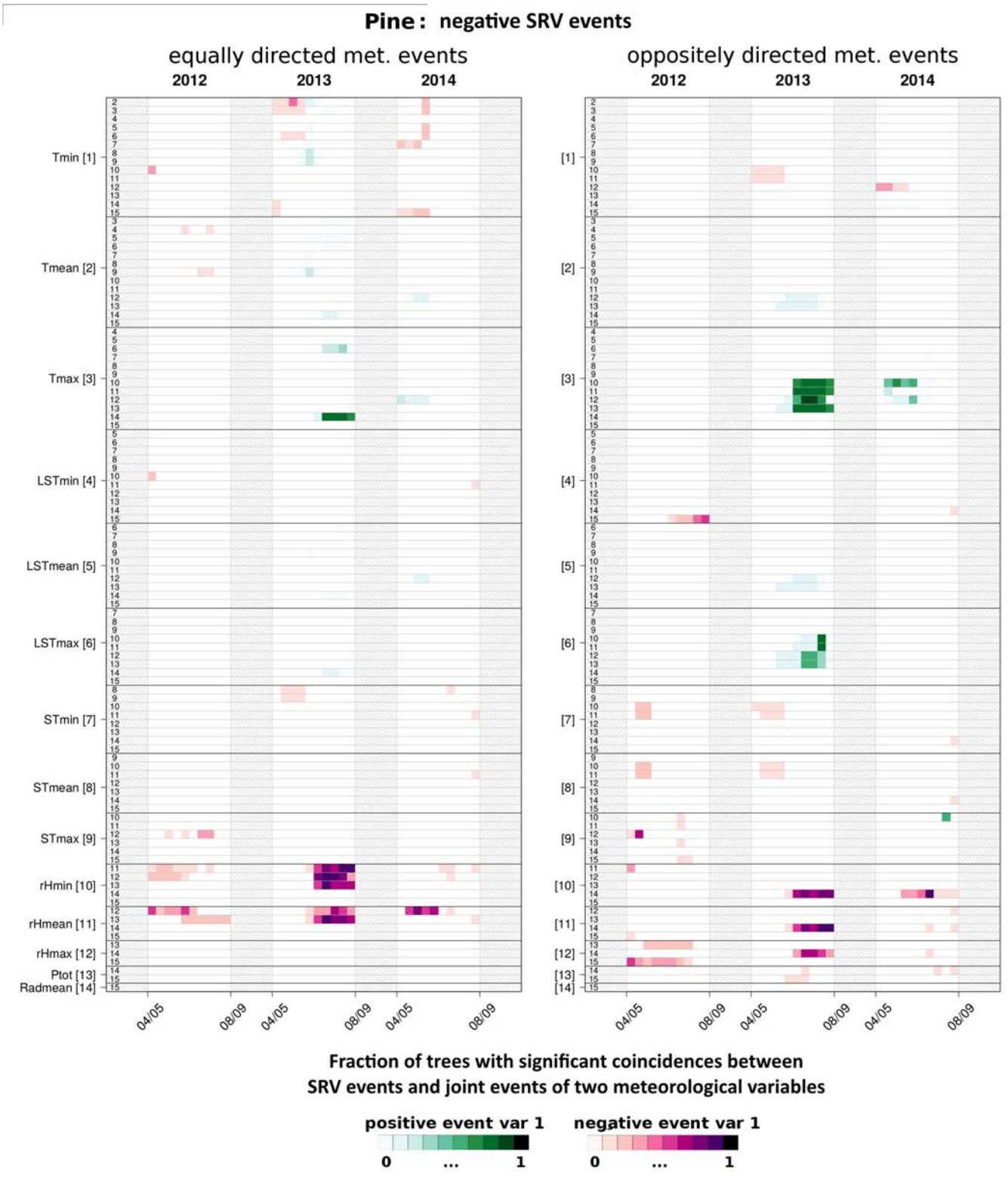

Figure S6. As in Fig. S1 for strongly negative pine SRVs.

2.4 CoinCalc - A new R package for quantifying simultaneities of event series

Computers & Geosciences 98 (2017) 64–72

Contents lists available at ScienceDirect

Computers & Geosciences

journal homepage: www.elsevier.com/locate/cageo

Research paper

CoinCalc—A new R package for quantifying simultaneities of event series

Jonatan F. Siegmund[a,b,*], Nicole Siegmund[b,c,d], Reik V. Donner[a]

[a] Research Domain IV – Transdisciplinary Concepts and Methods, Potsdam Institute for Climate Impact Research, Telegrafenberg A31, 14473 Potsdam, Germany
[b] Institute of Earth and Environmental Science, University of Potsdam, Karl-Liebknecht-Straße 24-25, 14476 Potsdam-Golm, Germany
[c] Leibniz Centre for Agricultural Landscape Research, Department for Soil Landscape Research, Eberswalder Straße 84, 15374 Müncheberg, Germany
[d] Institute of Meteorology and Climate Research, Atmospheric Environmental Research (IMK-IFU), Karlsruhe Institute of Technology, Kreuzeckbahnstraße 19, 82467 Garmisch-Partenkirchen, Germany

ARTICLE INFO

Keywords:
Event coincidence analysis
R
Point processes
Extreme events
Time series analysis

ABSTRACT

We present the new R package CoinCalc for performing event coincidence analysis (ECA), a novel statistical method to quantify the simultaneity of events contained in two series of observations, either as simultaneous or lagged *coincidences* within a user-specific temporal tolerance window. The package also provides different analytical as well as surrogate-based significance tests (valid under different assumptions about the nature of the observed event series) as well as an intuitive visualization of the identified coincidences. We demonstrate the usage of CoinCalc based on two typical geoscientific example problems addressing the relationship between meteorological extremes and plant phenology as well as that between soil properties and land cover.

1. Introduction

In many areas of geosciences, but also other scientific disciplines like neurosciences, there has been a rising interest in inferring information on dynamical interdependencies between different observational series that are not given in the form of continuous or discrete-valued time series, but as sequences of events (e.g., unmarked or marked point processes). Traditional statistical tools like classical (Pearson) correlation analysis are often not directly applicable to such series or of limited explanatory value. While in neurosciences, many methodological developments have been introduced and subsequently applied for studying the statistical interrelationships between event series (e.g., describing sequences of neuronal spiking activity: Brown et al., 2004; Lewicki, 1988; Mulansky et al., 2015), there have been relatively few attempts to transfer corresponding approaches to geoscientific problems (Boers et al., 2013; Malik et al., 2010, 2012).

Event coincidence analysis (ECA) is a recently developed method for studying the statistical interdependency between two event series, which has been originally introduced and applied in a geoscientific context (Donges et al., 2011, 2016; Rammig et al., 2015; Siegmund et al., 2015, 2016). Unlike correlation analysis, this method exclusively takes the timings of certain well-defined events in two series into account and ignores potentially available other information (e.g., underlying explicit time series values) on the gradual variability of related observables. Therefore, it provides a complementary view on data that are either by definition of binary structure (event/no event) or where only certain values (e.g., extreme events) are expected to result in a specific response of interest. Examples include the timings of natural disasters like earthquakes or floods (Donges et al., 2016) or cases where strong deviations from "normal" behavior can result in qualitatively different interdependencies between the variables of interest (e.g., ecosystem responses to extreme environmental conditions like droughts, cold spells or volcanic eruptions) (Reichstein et al., 2013; Zscheischler et al., 2013).

So far, ECA has been successfully applied to studying problems in biogeoscientific (Rammig et al., 2015; Siegmund et al., 2015, 2016), socio-ecological (Donges et al., 2016) and paleoclimatic contexts (Donges et al., 2011). The diversity of research questions discussed in the aforementioned publications suggests a wide range of possible future applications. While Rammig et al. (2015) and Siegmund et al. (2015) used the approach to derive complementary information (beyond classical correlation analysis) by looking at the timing of events in the very tail of the distribution of the underlying continuous variable, the analyses of Donges et al. (2011, 2016) could not have been conducted using standard tools of classical statistics since they addressed series of explicit events.

This paper introduces CoinCalc, an easy-to-handle implementation of ECA in the open statistical software R. We emphasize that the Comprehensive R Archive Network (CRAN) repository already contains the package CNA for performing an entirely different type of analysis

* Corresponding author at: Potsdam Institute for Climate Impact Research, Transdisciplinary Concepts and Methods, 14412, Potsdam, Germany.
E-mail address: jonatan.siegmund@pik-potsdam.de (J.F. Siegmund).

http://dx.doi.org/10.1016/j.cageo.2016.10.004
Received 16 December 2015; Received in revised form 11 June 2016; Accepted 16 October 2016
Available online 21 October 2016
0098-3004/ © 2016 Elsevier Ltd. All rights reserved.

referred to as *coincidence analysis* (Baumgartner and Thiem, 2015), and that the same term is also used in particle physics (Zaborov, 2009) in yet another different context. Within the framework of `CoinCalc`, we exclusively refer to the definition of *event* coincidence analysis as comprehensively described by Donges et al. (2016). We note that there are various conceptually similar yet distinctively different approaches mostly motivated by the neuroscientific problem of analyzing spike train synchrony. Two of the most prominent examples will be briefly discussed in the course of this paper to highlight their similarities and differences as compared to ECA.

The remainder of this paper is organized as follows: In Section 2, the methodological background of ECA is provided together with a brief summary of related methods, followed by a detailed description of the functions provided by `CoinCalc` and their options in Section 3. Finally, two exemplary applications of the package to different geoscientific data sets are discussed in Section 4. The paper concludes with a short summary in Section 5.

2. Methodological background

2.1. Types of event series

Let us consider two sequences of events of distinct types A and B that occur at times t_i^A and t_j^B with $i = 1,\ldots,N_A$ and $j = 1,\ldots,N_B$, where N_A and N_B are the number of events of types A and B, respectively. Here, we exclusively focus on the timing of events and disregard any possibly available information on the magnitudes of these events.

Depending on the specific question under study, event series are commonly provided in the form of one out of two generic data types. On the one hand, we may have just a list of event times (e.g., in Donges et al., 2011) with no continuous data upon which these events have been defined. We will refer to this type of data, where event timings can take arbitrary (real) values on the time axis, as *event sequences* in the following. On the other hand, we may have the situation of a time series containing time-discrete observations of some variable upon which events are defined. The resulting *event time series* is conveniently represented by a binary sequence of a length T equal to the number of underlying observations, where entries 1 (0) correspond to time steps with (without) an event. In contrast to event sequences, event times within an event time series can take only discrete values often conveniently represented by the underlying (integer) time indices of those original observations that have been identified as the events of interest.

To illustrate these two different types of event data, let us suppose a set of 15 equidistant observations, where the 4th, 6th, 7th and 11th values correspond to events. The corresponding event time series reads

(0, 0, 0, 1, 0, 1, 1, 0, 0, 0, 1, 0, 0, 0, 0),

whereas the associated event sequence object would be

{(4, 6, 7, 11), span(1, 15)},

i.e., an object containing a list of event times as well as a vector of length 2 containing the start and end points of observations. As we will detail in Section 3, it is possible to transform one type into the other, at least approximately. When using `CoinCalc`, the choice of the appropriate data type should be guided by the structure of the data to be studied.

2.2. Counting coincidences

ECA essentially counts how often events occur in both series *simultaneously* (referred to as *coincidences*). The notion of *simultaneity* can be further specified by considering two parameters: a user-defined time lag τ and a certain tolerance window ΔT. The consideration of $\tau \neq 0$ can be important in order to study lagged responses of events of type A to such of type B (or vice versa) as known for, e.g., the energy exchange between hydrosphere and atmosphere (Iwi et al., 2006; Kumar and Hoerling, 2003; Wedgbrow et al., 2002) or various ecological systems (Boulton, 2003; Daan et al., 2005; Letnic et al., 2005). In turn, ΔT allows addressing uncertain timings of events in examples like climate reconstructions (Jones et al., 2009; Woodborne et al., 2015), archaeological, paleontological or paleoanthropological records (Donges et al., 2011), or events with an extended duration like climate regime shifts and ecological or social responses to natural disasters (Donges et al., 2011, 2016).

By definition, the notion of event coincidence is not symmetric, i.e., always takes one of the two event series as a reference to which the second is compared. Commonly, in this context events of type B are considered as possibly influencing the timings of events of type A, and *not* vice versa (of course, the roles of both variables can be interchanged). However, there might be applications where such a presumed directional influence cannot be postulated in advance—in this case, ECA can be utilized as an explanatory rather than confirmatory statistical tool to test for the existence, direction and significance of non-random relationships. We note that this setting allows for a naive notion of causality in the physical sense of a cause always preceding (or at most temporally coinciding with) a consequence rather than vice versa. However, assessing causality in the common predictive (e.g., Granger) sense is not possible by means of ECA as formulated here.

Following this conceptual idea, ECA distinguishes between the *precursor coincidence rate*

$$r_p(\Delta T, \tau) = \frac{1}{N_A} \sum_{i=1}^{N_A} \Theta\left(\sum_{j=1}^{N_B} 1_{[0,\Delta T]}((t_i^A - \tau) - t_j^B) \right) \tag{1}$$

and the *trigger coincidence rate*

$$r_t(\Delta T, \tau) = \frac{1}{N_B} \sum_{j=1}^{N_B} \Theta\left(\sum_{i=1}^{N_A} 1_{[0,\Delta T]}((t_i^A - \tau) - t_j^B) \right), \tag{2}$$

where $\Theta(\cdot)$ is the Heaviside function and $1_{[0,\Delta T]}$ is the indicator function of the interval $[0, \Delta T]$. For $\Delta T = 0$, the term in the inner sum will just collapse to $\delta(t_i^A - \tau, t_j^B)$, where $\delta(\cdot,\cdot)$ is the Kronecker delta, providing a value of 1 if and only if both arguments are equal, and zero otherwise. In this context, $r_p(\Delta T, \tau)$ denotes "the fraction of A-type events that are preceded by at least one B-type event", while $r_t(\Delta T, \tau)$ measures "the fraction of B-type events that are followed by at least one A-type event" (Donges et al., 2016). By definition, both coincidence rates can only take values between 0 (complete absence of coincidences) and 1 (all events coincide with events in the reference series).

2.3. Significance tests

Beyond the sole calculation of coincidence rates, `CoinCalc` currently provides three significance tests that can be selected in order to comply with the specific properties of the event series under study.

2.3.1. Analytical test: Poissonian approximation

Under the assumption that the A and B-type events are randomly distributed *and* mutually independent (i.e., follow two independent Poisson processes) and sufficiently rare (specifically, $\Delta T \ll T/N_A \ll T$), the probability of observing a given number of precursor coincidences $K_p = N_A \cdot r_p$ can be approximated by a binomial distribution as

$$P(K_p) = \binom{N_A}{K_p} \left(1 - \left(1 - \frac{TOL}{T - \tau}\right)^{N_B}\right)^{K_p} \times \left(\left(1 - \frac{TOL}{T - \tau}\right)^{N_B}\right)^{N_A - K_p}. \tag{3}$$

Here, all time values are given either in absolute time units (for event sequences) or as discrete numbers of time steps (for event time series), which may, however, be directly identified with specific values on a given time axis. Accordingly, we have $TOL = \Delta T$ for event sequences and $TOL = \Delta T + 1$ for event time series (since the interval $[0, \Delta T]$ used in the definition of the coincidence rates contains $\Delta T + 1$ subsequent

time steps, assuming uniform sampling intervals without gaps). In a similar way, T denotes either the total time span of observations (for event sequences) or the number of observations (for event time series). Note that while *TOL* is a non-negative parameter that can be selected according to the specific problem under study, T is itself part of the necessary information on the event series under study that needs to be known in order to perform ECA.

The p-value of the corresponding *analytical* significance test provided by `CoinCalc` corresponds to the probability that K_P *or more* coincidences occur due to chance according to Eq. (3),

$$p_{K_p} = \sum_{K_{/p} \geq K_p} P(K_{/p}), \tag{4}$$

where K_P is the number of precursor coincidences obtained when comparing the event series A and B. The p-value for the corresponding significance test of the trigger coincidence rate $r_t = K_t/N_B$ is obtained in the same way by interchanging N_A and N_B in Eq. (3) and replacing K_P by K_t (Donges et al., 2016). In both cases, the null hypothesis of the test is that the observed number of coincidences can be explained by two independent series of randomly distributed events. If the given p-value is smaller than a user-defined confidence level α, this null hypothesis can be rejected.

As already mentioned above, an important requirement for the application of the analytical significance test is that the number of events multiplied with the considered tolerance window ΔT must be sufficiently small in comparison with the total period covered by the underlying observations, i.e., the events to be analyzed need to be rare (Donges et al., 2016). This is the case if the conditions $N_A \Delta T$, $N_B \Delta T \ll T$ are fulfilled. In turn, if the latter requirement is not met, a rejection of the null hypothesis resulting from the analytical significance test can also result from the fact that the analytical approximation does not hold, thus not necessarily implying that the two event series are not independent of each other (commonly the desired type of information). In turn, if the rarity condition is violated, `CoinCalc` provides two additional significance tests based on suitably constructed surrogate data as more appropriate alternatives, which are detailed below and also discussed in detail in Donges et al. (2016). Note that the validity of the assumption of rare events should in general be checked *before* the selection of the analytical vs. surrogate data-based significance test.

2.3.2. Surrogate-data based tests

As stated above, beyond the analytical test described in the previous paragraph `CoinCalc` provides two additional significance tests based on surrogates. Here, surrogates denote artificial event series that are compatible with the null hypothesis of mutually independent series but retain certain properties of the original empirical event series. By generating large ensembles of such surrogates independently at random, the distributions of coincidence rates for event data with the desired properties can be approximated numerically, which can then be used for deriving estimates for the desired critical value at a given confidence level.

1. *Random event times* (*shuffle surrogates*): Here, artificial data are generated by constructing two event series of N_A and N_B events (as observed in the empirical data) where the individual event times are drawn independently and uniformly at random from the time period of observations. In the limit $T \to \infty$, the waiting time distribution of such surrogate event series takes an exponential shape as expected for a Poisson process. The empirical distribution $\widehat{P}_{surr}(K_p)$ of the resulting surrogate precursor coincidence rates from all pairs of these "shuffled" surrogate event series approximates the distribution of coincidence rates that would result from two event series with the same length and number of events as the original data sets where the individual events are completely independent of each other. Hence, the p-value for the precursor coincidence rate can be approximated as

$$p_{K_p} = 1 - \widehat{P}_{surr}(K_p). \tag{5}$$

For trigger coincidences, p_{K_t} follows in full analogy.

2. *Prescribed waiting time distributions* (*waiting time surrogates*): Besides the too large number of events in a series already accounted for by the shuffle surrogates described above, another possible reason for the analytical significance test to provide incorrect results can be an empirical distribution of waiting times between subsequent events showing large deviations from the exponential behavior expected for Poisson processes. For such cases, `CoinCalc` provides a third significance test based on another type of surrogate event series that resemble the original data sets in pertaining their series length and waiting time distributions. Specifically, each surrogate event series is produced by iteratively selecting the waiting time until the next event from the empirical distribution of waiting times of the original data sets uniformly at random. The calculation of p-values then follows the same strategy as described above for the shuffle surrogates.

   Unlike analytical and shuffle tests, the latter surrogate-based test does not make any assumption about the Poissonian nature of the event series and is insofar more generally applicable and, hence, less restrictive. Moreover, as the shuffle test, it allows to perform ECA for event series that do not match the condition of rare events. However, it still provides only approximate results for cases in which there is evidence for serial dependence between the events of one of the series. This situation requires the utilization of numerical approximations of the distribution of the considered test statistics making use of even more sophisticated resampling approaches (Donges et al., 2016). A corresponding extension of the currently implemented significance tests is scheduled for future versions of `CoinCalc`.

2.4. Symmetric tolerance windows

Extending upon the methodological setting used by Donges et al. (2016), `CoinCalc` also provides the possibility to define a symmetric tolerance window. The definition of such a window is of specific interest for analyses in which there is evidence for uncertainties in the timing of the events in one or both data sets. In Eqs. (1) and (2) discussed above, ΔT is supposed to define a non-symmetric window, thus either preceding or following the time step of interest, resulting in tolerance windows $[t_i^A - \tau - \Delta T, t_i^A - \tau]$ for a precursor coincidence and $[t_j^B + \tau, t_j^B + \tau + \Delta T]$ for a trigger coincidence.

In turn, for $\tau = 0$, a symmetric tolerance window corresponds to counting coincidences of events in series B falling into a time window including a time interval ΔT both before and after an event in series A. Here, the definition of the time window using this approach is $[t_i^A - \Delta T, t_i^A + \Delta T]$ (i.e., the symmetric tolerance windows are twice as large as their directional counterparts discussed above). For intervals centered around t_j^B and for delayed coincidences with $\tau \neq 0$, the corresponding modifications are straightforward. Hence, Eq. (1) (and similarly Eq. (2)) can be rewritten as

$$r_p(\Delta T, \tau) = \frac{1}{N_A} \sum_{i=1}^{N_A} \Theta\left(\sum_{j=1}^{N_B} 1_{[-\Delta T, \Delta T]}(t_i^A - t_j^B) \right). \tag{6}$$

As a consequence, for the calculation of $P(K_p)$ in Eq. (3) with a symmetric tolerance window, we have $TOL = 2\Delta T$ for event sequences and $TOL = 2\Delta T + 1$ for event time series.

2.5. Related approaches

When reviewing the existing literature on event-based time series analysis, there are several methods serving a similar purpose as ECA. In the following, we detail the similarities and differences between ECA and two of the most common recent approaches in this field:

1. One prominent example is the spike train reliability statistic R proposed by Hunter and Multon (2003). This measure essentially provides a normalized mean exponential temporal distance between each event in one series and the corresponding closest event in a second series, and thus provides large values in case of very similar event timings and low values if both series are essentially unrelated. Unlike ECA, the reliability statistic cannot differentiate between possible directions of mutual influences between the two event series under study, i.e., it provides an undirected similarity measure. Moreover, Hunter and Multon (2003) do not provide a method to assess the statistical significance of possible interrelationships. It should be noted, however, that a corresponding numerical significance test can be easily constructed by adopting the surrogate methods implemented in `CoinCalc` for use together with the coincidence rates within ECA (Donges et al., 2016).
2. Event synchronization (ES) is another method for quantifying the simultaneity between events in two given series (Quiroga et al., 2002), which has gained considerable popularity in the neurosciences and, more recently, climatological applications (Boers et al., 2013, 2014, 2015a, b; Malik et al., 2010, 2012,; Stolbova et al., 2014, 2016). Similar to ECA, ES essentially counts the number of pairs of events of two considered types occur mutually close in time. However, in contrast to ECA, this proximity is defined in some adaptive way to account for the typical waiting times between subsequent events in both series. In this spirit, ES is particularly well suited for events that follow a relatively regular pacing. Due to the more complex definition of temporal closeness, there is no analytical significance test available for ES so far, which is a distinctive difference in comparison to ECA.

   Unlike ECA, ES takes *both* event series individually as references for comparison of the second one and provides two measures—a symmetric one characterizing the overall strength of the mutual relationship and an asymmetric one providing information on the possible directionality. Following these general considerations, ES is commonly used as an exploratory statistics, while ECA can be applied for both explanatory and confirmatory purposes, with a particular emphasis on hypothesis testing.

It may be noted that both ECA and ES are somewhat more complex and more sophisticated than the reliability statistic in that both provide information on the (temporal) directionality of a possible statistical relationship between two event series. ECA and ES are conceptually closely related, but neither contrasting nor redundant, neither better nor worse, but just allow addressing somewhat different scientific questions and approaches. While this manuscript describes the first-time fully operational implementation of ECA in R, both reliability statistic and ES are contained in the recently published R package `mmpp` (Hino et al., 2015). With this implementation and the new package `CoinCalc`, one might perform a thorough inter-comparison of the respective performance of all three methods. However, such an investigation would be clearly beyond the scope of this work.

3. Description of the package

The R package `CoinCalc` provides all necessary functionality to perform the calculation of coincidence rates and the associated significance tests according to the user's specific requirements. Specifically, it is possible to perform ECA for both event sequences (hereafter referred to as `es` format) and event time series (`ts` format) (see Section 2.1). The notation of the `ts` format used throughout the remainder of this paper should not be confused with the common R object type `ts` and shall exclusively indicate a time-ordered binary vector defining an event time series.

Notably, the consideration of the `es` format is particularly useful for large data sets, since the resulting computational demands are considerably lower than for `ts` data. In turn, the disadvantage of the `es` format is that in the current implementation of `CoinCalc`, the data set must be based on continuous observations with no missing periods of recording. In the case of missing observations, the `ts` format should be used instead. Note that in the presence of missing data, only the analytical significance test is available so far. A corresponding extension is planned to be developed and implemented in the next version of the package. In general, performing ECA between two data sets requires the corresponding data being given in the same format. For this purpose, `CoinCalc` provides functions for transforming each of the two formats into the other.

In the following, we give a brief overview on the functions currently provided by the package as well as their usage and possible options:

`CC.binarize()`: This function binarizes a numerical vector (i.e., a time series of an arbitrarily distributed variable) using a given threshold. This threshold can either be a percentile of the variable's empirical distribution or a specific prescribed value. The output object has `ts` format (i.e., is a binary vector of the same length T as the original data). The following arguments and options need to be provided:

- `data (required)`: Numerical vector (time series) to be binarized.
- `ev.def (default="percentile")`: String specifying the event definition method. If "`percentile`", events are defined using the value of `thres` (see below) as percentile threshold. If "`absolute`", events are defined according to an absolute threshold value `thres`.
- `thres (input required)`: Binarization threshold. If `ev.def="percentile"`, `thres` must be a real number within [0,1]. For `ev.def="absolute"`, it can take any real number within the range of `data`.
- `event (default="higher")`: String specifying whether values `"higher"` or `"lower"` than `thres` are to be considered as events.

`CC.ts2es()`: This function converts an event time series (`ts` format) into an event sequence (`es` format). It has only a single argument:

- `data (required)`: Binary event time series to be transformed into an event sequence.

`CC.es2ts()`: This function converts an event sequence (`es` format) object into a binary event time series (`ts` format). It requires the following arguments:

- `data (required)`: Event sequence comprising event positions to be transformed into an event time series.
- `span (required)`: Numerical vector with two elements (`span[1]`: starting point of the data set, `span[2]`: end point of data set).
- `es.round (default=0)`: Number of digits for rounding the given values in `data`. `es.round` additionally defines the temporal resolution (e.g., `es.round=3` leads to a sampling interval of 0.001 time units).

`CC.eca.es()`: This function performs the actual ECA using two event sequences (`es` format). The arguments and options are listed below:

- `seriesA (required)`: Numerical vector specifying the timings of events of type A.
- `seriesB (required)`: Numerical vector specifying the timings of events of type B.
- `spanA (required)`: Numerical vector of length 2 specifying the start and end points of the data set given in `seriesA`.
- `spanB (required)`: Numerical vector of length 2 specifying the start and end points of the data set given in `seriesB`.
- `delT (default=0)`: Non-negative real number for defining the tolerance window ΔT. If `delT=0`, only simultaneous coincidences

are counted.

- `sym (default=FALSE)`: Boolean variable specifying if the temporal tolerance window should be taken symmetrically or not.
- `tau (default=0)`: Non-negative real number specifying the time lag τ.
- `sigtest (default="poisson")`: String specifying the type of significance test. If `sigtest="poisson"`, the analytical significance test based on the assumption of independent and sparse Poisson processes is performed. If `sigtest="shuffle.surrogates"`, the test statistics for randomly located events is numerically approximated. If `sigtest="wt.surrogates"`, the numerical approximation of the test statistics based on coincidence rates for an ensemble of surrogate event sequences with the same waiting time distributions as the original data is utilized.
- `reps (default=1000)`: Positive integer specifying the surrogate ensemble size for the numerical significance test.
- `alpha (default=0.05)`: Desired confidence level for the significance test specified by `sigtest`.

`CC.eca.ts()`: This function performs ECA using two event time series (`ts` format). Missing values are allowed. If NAs are found in one of the input time series, the corresponding time steps (as well as their respective counterparts in the second series) are ignored in the performed analysis. The following arguments and options are required:

- `seriesA (required)`: Binary vector specifying steps with and without events in series A.
- `seriesB (required)`: Binary vector specifying steps with and without events in series B.
- `delT (default=0)`: Non-negative integer for defining the tolerance window ΔT (number of time steps accepted as time difference). For `delT=0`, only simultaneous events are counted as coincidences.
- `sym (default=FALSE)`: see `CC.eca.es()`
- `tau (default=0)`: Non-negative integer specifying the time lag τ.
- `sigtest (default="poisson")`: see `CC.eca.es()`
- `reps (default=1000)`: see `CC.eca.es()`
- `alpha (default=0.05)`: see `CC.eca.es()`

`CC.plot()`: This function creates a visualization of the event series and the results of ECA. The output graphics displays which individual events correspond to coincidences. `CC.plot()` is currently only available for data given as event time series (`ts` format); an extension to general event sequences is planned for a future version of `CoinCalc`. The arguments and options are listed below:

- `seriesA`: see `CC.eca.ts()`
- `seriesB`: see `CC.eca.ts()`
- `delT`: see `CC.eca.ts()`
- `sym`: see `CC.eca.ts()`
- `tau`: see `CC.eca.ts()`
- `dates (default=NA)`: Vector of length T, containing characters or numerical values providing date information for the two series. If specified, event dates are added to the plot.

One example of an illustrative visualization produced by `CC.plot()` can be found in Section 4.

4. Examples

Before illustrating the use of `CoinCalc` for a few real-world geoscientific applications, we emphasize that many recent studies on corresponding problems have been restricted to classical linear correlation analyses so far. Such analyses, however, are not possible for event sequences as considered within `CoinCalc`. Even for event time series, correlation analysis and ECA provide distinctively different views on the same data by considering either the full distribution of the data under study or just the timing of values in certain parts (commonly the tails) of this distribution. Besides being conceptually different, one easily convinces oneself that high correlation values do not need to imply high coincidence rates and vice versa. To see this, let us consider two simple numerical examples, where the first series A is described by Gaussian white noise with zero mean and unit variance, and the second series B is defined as a deterministic cubic function of A. For example, if we take $B = -0.3A^3 + 5A$, we observe the values of A and B being strongly positively correlated, but the coincidence rates between their respective most positive (most negative) values is close to zero. In turn, if we choose $B = 0.3A^3 - A$, the linear correlation coefficient is relatively small (due to the dominance of the nonlinear term) whereas the coincidence rates between values in the upper (lower) tails of the underlying distributions is close to one.

In the following, we will turn to some real-world examples comprising two case studied from biogeography (temperature influence on plant flowering) and the interface of soil science and agriculture. The data sets used for this purpose are included in the R package and can be assessed by executing `data(CC.Example. Data1)` and `data(CC.example. Data2)` for the examples discussed in Sections 4.1 and 4.2, respectively.

4.1. Plant phenology and meteorological extremes

As a first example for the application of the `CoinCalc` package, let us reconsider the problem of identifying time windows during the year within which unusually warm weather conditions can result in (i.e., coincide with) very early flowering of central European shrub species in the same year (Siegmund et al., 2015). The information on flowering dates was provided by the German Weather Service (DWD), and the temperature data were obtained by an area-weighted interpolation of temperature data from DWD-operated meteorological stations (Österle et al., 2006).

Here, we illustrate the utilization of `CoinCalc` by taking one time series of annual Lilac flowering dates and one April mean temperature time series from 1950 to 2010 as an example. Specifically, we use the data from a phenological station located in Niederrimbach, Germany (49.4833°N, 10.000°E). Events in the two considered time series correspond to “very early flowering” and “very warm conditions”, respectively. While the former is defined as a flowering occurring earlier in the year than the empirical 10th percentile of all historical flowering dates in this record, a mean April temperature is considered to be very warm if it exceeds the 90th percentile of all observed April values. Fig. 1 shows the two time series as well as the two thresholds for the definition of events.

In order to conduct ECA for these two time series using `CoinCalc`, let the flowering dates be stored in the vector `Fl.60y` and the temperature data in the vector `TT.60y`. Since a possible lagged effect of spring temperatures on flowering time in a yearly resolved data set is not considered here, τ and ΔT take their default values of 0. Thus, executing

```
Fl.60y.bin <- CC.binarize(data=Fl.60y, ...
... ev.def="percentile", ...
... thres=0.10, event="lower")
TT.60y.bin <- CC.binarize(data=TT.60y, ...
... ev.def="percentile", ...
... thres=0.90, event="higher")
ca.out <- CC.eca.ts(Fl.60y.bin, TT.60y.bin,...
...sigtest="poisson")
```

results in the list `ca.out` containing the following information:

```
NH precursor: FALSE
NH trigger: FALSE
p-value precursor: 0.01777557
p-value trigger: 0.01777557
precursor coincidence rate: 0.5
trigger coincidence rate: 0.5
```

In this example, the null hypotheses of independent random event series can be rejected for both precursor and trigger coincidence rates at a confidence level of $\alpha = 0.05$. In the specific setting considered here, the two coincidence rates and their resulting p-values are identical, since both time series have the same length, no tolerance window is considered ($\Delta T = 0$) and the same number of events ($N_A = N_B = 6$, see Fig. 2) is present in both series due to their definition using the empirical 10th and 90th percentile, respectively. We note again that since the flowering dates contain some missing values, in the present version of `CoinCalc` only the analytical significance test can be used.

It may be worth noting that in the present example, the correlation coefficient between both original time series is already −0.83, suggesting the existence of a strong correlation between the two considered variables. However, as already discussed above, such a strong correlation does not necessarily imply the co-occurrence of extreme values in both records. Hence, even with a generally strong correlation, certain parts of the distribution of the two observables can still completely mismatch in terms of their appearance in the series. Thus, ECA is a prospective complementary tool providing information to understand the relationship between distinct parts of the distribution of two time series.

Fig. 2 shows the plot generated by the function call

```
CC.plot(Fl.60y.bin,TT.60y.bin,dates=FL.dates)
```

where `FL.dates` is a vector containing a sequence from 1951 to 2010. The light blue and light red bars indicate events in the phenological (A)

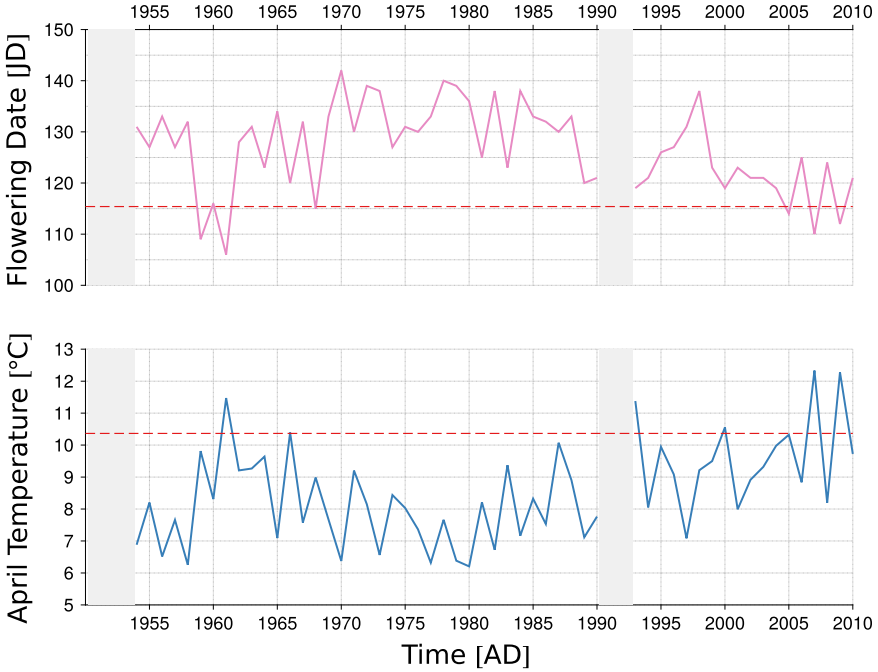

Fig. 1. Time series of Lilac flowering (Julian Day (JD) of the year, upper panel) and April mean temperature (lower panel) in Niederrimbach from 1951 to 2010. The red dashed lines mark the thresholds at the empirical 10th and 90th percentiles, respectively. Events in both time series are defined as those values, that are lower (higher) than the respective threshold. (For interpretation of the references to color in this figure caption, the reader is referred to the web version of this paper.)

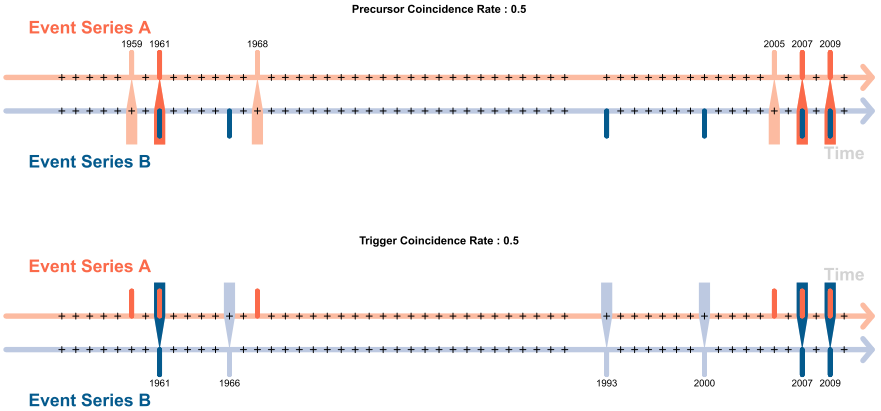

Fig. 2. Graphical output of the `CC.plot` function for the flowering (red) and temperature time series (blue). Blue and red bars mark time steps with events. For the series to be compared with the respective reference sequence, light colors show events without coincidence and dark colors coincidences. For the reference series, no corresponding visual distinction is made. Note that in the present example, $\Delta T = 0$ and $\tau = 0$, i.e., only simultaneous events (referring here to the same year) are considered as coincident. (For interpretation of the references to color in this figure caption, the reader is referred to the web version of this paper.)

and temperature (*B*) time series, respectively, where dark colors highlight those events that correspond to coincidences. It can be seen that in the present example, three of the six early flowering events (series *A*) coincide with warm April temperatures (series *B*) (and vice versa), yielding precursor and trigger coincidence rates of 0.5 as given above.

4.2. Soil organic carbon content and land-use

Our second example illustrates the application of `CoinCalc` to a quite different problem. Here, ECA is not used for studying two time series, but a set of soil samples providing information about the soil organic carbon (SOC) contents of 218 smallhold farmer sites in the Nyando district, Western Kenya. The samples were collected, processed and analyzed in 2013/2014 in the course of the project SAMPLES (http://samples.ccafs.cgiar.org). In addition to the carbon data set, information on the crop types planted on the sampled plot was collected. During field work, two hypotheses were drawn: (i) The plantation of certain crop types (e.g., sorghum) generally leads to very low SOC contents. (ii) Intensive intercropping (i.e., the simultaneous plantation of different crop types) generally leads to very high SOC rates in the top soil layer (0–20 cm).

To test hypothesis (i), carbon contents below the 5th percentile of all samples were defined as events in the SOC data set (event "time" series `carb`), and the cultivation of sorghum was defined as an event in the crop cover data set (event "time" series `crop.sorghum`). In this example, both τ and ΔT are again 0, i.e., we are only interested in "simultaneous" events. Although the given data sets are no time series, the appropriate data format to choose here is that of event time series (`ts`) where individual samples take the role of (temporal) observation points. Executing

```
ca.out <- CC.eca.ts(carb,crop.sorghum,...
... sigtest="poisson")
```

yields the following results contained in the list `ca.out`:

```
NH precursor: FALSE
NH trigger: FALSE
p-value precursor: 0.03824319
p-value trigger: 0.04147892
precursor coincidence rate: 0.2727273
trigger coincidence rate: 0.1875
```

Hence, at the $\alpha = 0.05$ significance level, both null hypotheses can be rejected based on the analytical significance test and, thus, a non-random statistical relationship between sorghum plantation and very low SOC values can be deduced. By definition of the individual "events" as detailed above, the rarity condition for the Poissonian approximation to apply appears to be fulfilled in this case. Moreover, due to the "non-temporal" nature of the data, possible problems due to serial dependencies can be excluded. Note that in contrast to the previous example, precursor and trigger coincidence rates are not equal due to the different numbers of events in both data sets. Here, the precursor coincidence rate corresponds to the fraction of plots with low SOC contents on which sorghum was cultivated, whereas the trigger coincidence rate gives the fraction of plots with sorghum plantation on which low SOC contents were observed. Since both tests indicate statistical significant results, a possible directionality of the studied relationship (i.e., *either* sorghum plantation leading to low SOC *or* plots with low SOC being preferably chosen for sorghum plantation by the farmers) cannot be unambiguously inferred from the present analysis.

Next, in order to investigate whether intercropping systematically co-occurs with very high top-layer SOC contents (hypothesis (ii)), we define crop covers with at least four different crop types (`crop.inter`) and SOC contents larger than the 90th percentile (`carb`) as events and execute

```
ca.out <- CC.eca.ts(carb,crop.inter,...
... sigtest="poisson")
```

resulting in:

```
NH precursor: TRUE
NH trigger: TRUE
p-value precursor: 0.08495326
p-value trigger: 0.07630266
precursor coincidence rate: 0.11
trigger coincidence rate: 0.33
```

In this case, despite the quite high trigger coincidence rate of 0.33, both null hypotheses cannot be rejected at the $\alpha = 0.05$ confidence level. The high trigger coincidence rate in this example means that 33% of the plots characterized by intensive intercropping also show very high SOC values. But since the precursor coincidence rate is rather small, only few plots characterized by high SOC contents have also been cultivated with intercropping. The large difference between trigger and precursor coincidence rate in this example arises again because the numbers of events in the two data sets differ markedly (there are 18 events in the carbon data set and only six events in the crop cover data set). Therefore, to reach a significant p-value at $\alpha = 0.05$, in the present example at least three of the six intercropping fields would have to coincide with events in the carbon data set (i.e. $r_p \geq 0.5$).

For comparison, we apply the shuffle surrogates-based significance test to the same data set using

```
ca.out <- CC.eca.ts(carb,crop.inter,...
... sigtest="shuffle_surrogates",reps=10000)
```

and obtain the following result:

```
NH precursor: TRUE
NH trigger: TRUE
p-value precursor: 0.0621
p-value trigger: 0.0522
precursor coincidence rate: 0.11
trigger coincidence rate: 0.33
```

This example illustrates that in cases where the rejection of the null hypothesis is based on p-values close to the desired confidence level α, the utilization of both significance tests is recommended. Specifically, if we relieve the requested confidence level only slightly (say, $\alpha = 0.06$), the null hypothesis of the trigger test could already be rejected, indicating that high top-layer SOC contents are actually supported by intercropping. Although the numbers of "events" in both data sets (N_A=18 and N_B=6) are relatively small in comparison with the sample size (T=218), the observed changes in the obtained p-values for both precursor and trigger test indicate that the analytical significance test is actually much more conservative than necessary for appropriately testing for the presence of statistical interrelationships between both event series. This suggests that in case of any doubts regarding the validity of the implicit assumptions underlying the analytical significance test, the surrogate-based test should be preferred.

4.3. Further possible applications

As we have detailed in Section 2.5 of the revised paper, ECA can be used as an exploratory as well as confirmatory tool. Since there are other conceptually similar methods (see above) particularly serving the exploratory aspect, the previous examples kept a common focus on the

confirmatory role, i.e., the application of ECA for statistical hypothesis testing, which is distinctively different from what other related existing methods like ES or spike train reliability statistic have been applied for in the past.

In general, the parameters of ECA could also not be considered fixed, but variable, which can provide some interesting insights when applying ECA as an exploratory tool. For example, systematically varying the time delay τ and computing coincidence rates in dependence on this parameter would result in a coincidence function serving a similar purpose as the classical cross-correlation function. We note that Siegmund et al. (2015) have already discussed a corresponding application in the context of plant phenology. Such an analysis can be easily implemented by the user by calling the appropriate function in some `for`-loop using τ as a variable changing with each iteration. In a similar way, one could also explicitly study the dependence of the coincidence rates (respectively the p-values of the associated significance tests) in dependence on the width ΔT of the tolerance window to identify the most appropriate setting in cases where a response occurs with a certain, not exactly constant delay with respect to the triggering event.

Finally, we underline that for continuously valued time series, the method used to define events can be crucial for the results of ECA and needs to be selected based on considerations regarding what kind of (extreme or otherwise rare) event should be studied. It is beyond the scope of `CoinCalc` to serve all corresponding possibilities. To this end, the package contains just the simple function `CC.binarize()` for defining events in the most common case of extremes as time series values exceeding a certain threshold, commonly defined by a certain percentile of the underlying distribution. Beyond this case, the main functions of `CoinCalc` for the execution of ECA can also be used together with any other type of event sequence or event time series defined by the user according to the specific needs of the current analysis. Notably, when working with extreme events, the coincidence rates (and likely the cases identified as significant) can be expected to depend on the specific threshold chosen. However, in the ideal case this dependence should only be weak. Thus, varying this threshold systematically can provide some indication of robustness of the obtained results. One corresponding example can again be found in Siegmund et al. (2015).

5. Conclusions

The new R package `CoinCalc` allows performing event coincidence analysis (ECA), a novel statistical tool for quantifying the degree of simultaneity between two event series (Donges et al., 2011, 2016; Rammig et al., 2015), for different types of event series. The package provides six functions: (i) binarization of continuous time series, (ii) data conversion of binary (event) time series to event sequence format, (iii) conversion of event sequences to binary time series, (iv) ECA for event sequences, (v) ECA for binary event time series, and (vi) a plotting function for visualizing events and coincidences.

Based on two geoscientific example problems, we have illustrated the utilization of the package and interpretation of the obtained results. The current version of `CoinCalc` is freely available at GitHub (https://github.com/JonatanSiegmund/CoinCalc) and shall be additionally released in the CRAN repository (www.r-project.org), including regular future updates and extensions. In its current version, `CoinCalc` already provides all necessary functions for performing ECA under relatively general conditions. Future extensions shall include (among others) a more sophisticated surrogate-based significance test for serially dependent event sequences (i.e., series with correlated waiting times between subsequent events) and functions for multivariate and conditional ECA (Siegmund et al., 2016). Moreover, the package will be expanded in order to handle not only pairs of series of vector format, but to also perform ECA between time series of grid points in spatially extended data sets (e.g., with the dimensions latitude, longitude and time), which are typical for climatological data sets or remote sensing products (Zscheischler et al., 2013). This extension will also allow analyzing coincidences between time series of different regions, opening the package to a further large field of research questions.

Acknowledgements

This work has been financially supported by the German Federal Ministry for Education and Research (BMBF) within the framework of the BMBF Young Investigators Group CoSy-CC^2: Complex Systems Approaches to Understanding Causes and Consequences of Past, Present and Future Climate Change (grant no. 01LN1306A). J.F.S. acknowledges funding by the Evangelisches Studienwerk Villigst e.V. The authors are grateful to the SAMPLES project for providing the framework for the soil sample collection, Gustavo Saiz (IMK-IFU, KIT) for supporting the SOC analysis of the soil samples, and Jonathan Donges and Marc Wiedermann for helpful comments on earlier versions of this manuscript and the software package `CoinCalc` described herein.

References

Österle, H., Werner, P., Gerstengarbe, F., 2006. Qualitätsprüfung, Ergänzung und Homogenisierung der täglichen Datenreihen in Deutschland, 1951–2003: ein neuer Datensatz. In: 7. Deutsche Klimatagung, Klimatrends: Vergangenheit und Zukunft, 9–11 Oktober 2006.

Baumgartner, M., Thiem, A., 2015. Identifying complex causal dependencies in configurational data with coincidence analysis. R J. 7 (1), 176–184.

Boers, N., Bookhagen, B., Marwan, N., Kurths, J., Marengo, J., 2013. Complex networks identify spatial patterns of extreme rainfall events of the South American Monsoon System. Geophys. Res. Lett. 40 (16), 4386–4392.

Boers, N., Rheinwalt, A., Bookhagen, B., Barbosa, H.M.J., Marwan, N., Marengo, J., Kurths, J., 2014. The South American rainfall dipole: A complex network analysis of extreme events. Geophys. Res. Lett. 41 (20), 7397–7405.

Boers, N., Bookhagen, B., Marwan, N., Kurths, J., 2015a. Spatiotemporal characteristics and synchronization of extreme rainfall in South America with focus on the Andes Mountain range. Clim. Dyn. 45 (3), 619–632.

Boers, N., Donner, R.V., Bookhagen, B., Kurths, J., 2015b. Complex network analysis helps to identify impacts of the El Nño Southern Oscillation on moisture divergence in South America. Clim. Dyn. 45 (3), 619–632.

Boulton, A., 2003. Parallels and contrasts in the effects of drought on stream macroinvertebrate assemblages. Freshw. Biol. 48 (7), 1173–1185.

Brown, E., Kass, R., Mitra, P., 2004. Multiple neural spike train data analysis: state-of-the-art and future challenge. Nat. Neurosci. 7 (5), 456–461.

Daan, N., Gislason, H., Pope, J., Rice, J., 2005. Changes in the north sea fish community: evidence of indirect effects of fishing? Ices J. Mar. Sci. 62 (2), 177–188.

Donges, J.F., Donner, R.V., Trauth, M.H., Marwan, N., Schellnhuber, H.-J., Kurths, J., 2011. Nonlinear detection of paleoclimate-variability transitions possibly related to human evolution. Proc. Natl. Acad. Sci. U.S.A. 108, 20422–20427.

Donges, J.F., Schleussner, C.-F., Siegmund, J.F., Donner, R.V., 2016. Coincidence analysis for quantifying statistical interrelationships between event time series. Eur. Phys. J. Spec. Top. 225 (3), 471–487.

Hino, H., Takano, K., Murata, N., 2015. MMPP: a package for calculating similarity and distance metrics for simple and marked point processes. R. J. 7 (2), 237–248.

Hunter, J., Multon, J., 2003. Amplitude and frequency dependence of spike timing: implications for dynamic regulation. J. Neurophysiol. 90, 387–394.

Iwi, A., Sutton, R., Norton, W., 2006. Influence of May Atlantic Ocean initial conditions on the subsequent North Atlantic winter climate. Q. J. R. Meteorol. Soc. 132 (621), 2977–2999.

Jones, P.D., Briffa, K.R., Osborn, T.J., Lough, J.M., van Ommen, T.D., Vinther, B.M., Luterbacher, J., Wahl, E.R., Zwiers, F.W., Mann, M.E., Schmidt, G.A., Ammann, C.M., Buckley, B.M., Cobb, K.M., Esper, J., Goosse, H., Graham, N., Jansen, E., Kiefer, T., Kull, C., Kuettel, M., Mosley-Thompson, E., Overpeck, J.T., Riedwyl, N., Schulz, M., Tudhope, A.W., Villalba, R., Wanner, H., Wolff, E., Xoplaki, E., 2009. High-resolution palaeoclimatology of the last millennium: a review of current status and future prospects. Holocene 19 (1), 3–49.

Kumar, A., Hoerling, M., 2003. The nature and causes for the delayed atmospheric response to El Niño. J. Clim. 16 (9), 1391–1403.

Letnic, M., Tamayo, B., Dickman, C., 2005. The responses of mammals to La Nina (El Nino Southern Oscillation)-associated rainfall, predation, and wildfire in central Australia. J. Mammal. 86 (4), 689–703.

Lewicki, M., 1988. A review of methods for spike sorting: the detection and classification of neural action potentials. Netw.: Comput. Neural Syst. 9 (4), R53–R78.

Malik, N., Marwan, N., Kurths, J., 2010. Spatial structures and directionalities in Monsoonal precipitation over South Asia. Nonlinear Process. Geophys. 17, 371–381.

Malik, N., Bookhagen, B., Marwan, N., Kurths, J., 2012. Analysis of spatial and temporal extreme monsoonal rainfall over South Asia using complex networks. Clim. Dyn. 39, 971–987.

Mulansky, M., Bozanic, N., Sburlea, A., Kreuz, T., 2015. A guide to time-resolved and parameter-free measures of spike train synchrony. In: 2015 International Conference on Event-based Control, Communication, and Signal Processing (EBCCSP), pp. 1–8.

Quiroga, R., Kreuz, T., Grassberger, P., 2002. Event synchronization: a simple and fast method to measure synsynchronic and time delay patterns. Phys. Rev. E 66 (4), 041904.

Rammig, A., Wiedermann, M., Donges, J., Babst, F., von Bloh, W., Frank, D., Thonicke, K., Mahecha, M., 2015. Tree-ring responses to extreme climate events as benchmarks for terrestrial dynamic vegetation models. Biogeosciences 12, 373–385.

Reichstein, M., Bahn, M., Ciais, P., Frank, D., Mahecha, M., Seneviratne, S., Zscheischler, J., Beer, C., Buchmann, N., Frank, D., Papale, D., Rammig, A., Smith, P., Thonicke, K., van der Velde, M., Vicca, S., Walz, A., Wattenbach, M., 2013. Climate extremes and the carbon cycle. Nature 500, 287–295.

Siegmund, J.F., Donges, J.F., Wiedermann, M., Donner, R.V., 2015. Impact of climate extremes on wildlife plant flowering over Germany. Biogeosci. Discuss. 12, 18389–18423.

Siegmund, J.F., Sanders, T.G.M., Heinrich, I., van der Maaten, E., Simard, S., Helle, G., Donner, R.V., 2016. Meteorological drivers of extremes in daily stem radius variations of beech, oak and pine in Northeastern Germany: an event coincidence analysis. Front. Plant Sci. 7, 733.

Stolbova, V., Martin, P., Bookhagen, B., Marwan, N., Kurths, J., 2014. Topology and seasonal evolution of the network of extreme precipitation over the Indian subcontinent and Sri Lanka. Nonlinear Process. Geophys. 21 (4), 901–917.

Stolbova, V., Surovyatkina, E., Bookhagen, B., Kurths, J., 2016. Tipping elements of the Indian monsoon: Prediction of onset and withdrawal. Geophys. Res. Lett. 43 (8), 3982–3990.

Wedgbrow, C., Wilby, R.L., Fox, H., O'Hare, G., 2002. Prospects for seasonal forecasting of summer drought and low river flow anomalies in England and Wales. Int. J. Climatol. 22 (2), 219–236.

Woodborne, S., Hall, G., Robertson, I., Patrut, A., Rouault, M., Loader, N., Hofmeyr, M., *2015*. A 100-year carbon isotope rainfall proxy record from South African Baobab trees (*Adansonia digitata* l.). PLOS ONE *10* (*5*), *e0124202*.

Zaborov, D., 2009. Coincidence Analysis in ANTARES: Potassium-40 and Muons. Phys. At. Nucl. 72 (9), 1537–1542.

Zscheischler, J., Mahecha, M., Harmeling, S., Reichstein, M., 2013. Detection and attribution of large spatiotemporal extreme events in Earth observation data. Ecol. Inform. 15, 66–73.

2.5 Impacts of temperature extremes on European vegetation during the growing season

Biogeosciences, 14, 4891–4903, 2017
https://doi.org/10.5194/bg-14-4891-2017
© Author(s) 2017. This work is distributed under
the Creative Commons Attribution 3.0 License.

Biogeosciences
Open Access
EGU

Impacts of temperature extremes on European vegetation during the growing season

Lukas Baumbach[1,2], **Jonatan F. Siegmund**[1,3], **Magdalena Mittermeier**[1,4], **and Reik V. Donner**[1]

[1]Research Domain IV – Transdisciplinary Concepts and Methods, Potsdam Institute for Climate Impact Research, Telegrafenberg A31, 14473 Potsdam, Germany
[2]Faculty of Environment and Natural Resources, Albert Ludwigs University of Freiburg, Tennenbacherstraße 4, 79016 Freiburg im Breisgau, Germany
[3]Institute of Earth and Environmental Science, University of Potsdam, Karl-Liebknecht-Straße 24–25, 14476 Potsdam, Germany
[4]Department of Geography, Ludwig Maximilians University, Geschwister-Scholl-Platz 1, 80539 Munich, Germany

Correspondence to: Reik V. Donner (reik.donner@pik-potsdam.de)

Received: 15 May 2017 – Discussion started: 19 June 2017
Revised: 28 September 2017 – Accepted: 4 October 2017 – Published: 7 November 2017

Abstract. Temperature is a key factor controlling plant growth and vitality in the temperate climates of the mid-latitudes like in vast parts of the European continent. Beyond the effect of average conditions, the timings and magnitudes of temperature extremes play a particularly crucial role, which needs to be better understood in the context of projected future rises in the frequency and/or intensity of such events. In this work, we employ event coincidence analysis (ECA) to quantify the likelihood of simultaneous occurrences of extremes in daytime land surface temperature anomalies (LSTAD) and the normalized difference vegetation index (NDVI). We perform this analysis for entire Europe based upon remote sensing data, differentiating between three periods corresponding to different stages of plant development during the growing season. In addition, we analyze the typical elevation and land cover type of the regions showing significantly large event coincidences rates to identify the most severely affected vegetation types. Our results reveal distinct spatio-temporal impact patterns in terms of extraordinarily large co-occurrence rates between several combinations of temperature and NDVI extremes. Croplands are among the most frequently affected land cover types, while elevation is found to have only a minor effect on the spatial distribution of corresponding extreme weather impacts. These findings provide important insights into the vulnerability of European terrestrial ecosystems to extreme temperature events and demonstrate how event-based statistics like ECA can provide a valuable perspective on environmental nexuses.

1 Introduction

At a global scale, the year 2016 was the warmest year on record, presenting the third consecutive annual record among more than 100 years of observational data (NOAA National Centers for Environmental Information, 2017). For Europe, it was still the third warmest year after 2014 and 2015. In the context of ongoing anthropogenic greenhouse gas emissions, these general tendencies are likely to continue, resulting in an increasing trend of extreme temperature events (Beniston et al., 2007; Coumou et al., 2013). Particularly, hot days and heat waves have been observed to increase in intensity and frequency in the course of the last few decades – prominent examples include the European summer heat waves of 2003, 2006 and 2010 (De Bono et al., 2004; Rebetez et al., 2009; Barriopedro et al., 2011). Additionally, late spring frost events may pose a threat to plant development due to continuously earlier bud burst of plants in spring (Way, 2011).

Both positive and negative temperature extremes can adversely affect a plant's development and vitality. On the one hand, heat stress leads to changes in plant metabolism and the integrity of cells, causing phenomena such as the inhibition of photosystem II, thermal denaturation of proteins

or the formation of reactive oxygen species (Hasanuzzaman et al., 2013). On the other hand, low temperatures and frosts slow down biochemical processes within the plant cells and may result in the direct damaging or necrosis of new shoots or plant roots as well as indirect damages due to the lack of water access in the frozen soil (frost drought) (Beck et al., 2004). The susceptibility of vegetation to these threats may vary, e.g., depending on the seasonal stage of development (*phenophase*) and vegetation type (see Sect. 3). Foremost, cultivated plants/croplands show high vulnerabilities to extreme temperatures as their optimal climatic niche is relatively narrow (Larcher, 1994). Thus, temperature as a single variable can already have severe impacts and even be of predominant importance for future agricultural production in Europe (Semenov and Shewry, 2011; Deryng et al., 2014). A basic problem related to analyzing such impacts lies in the definition of temperature extremes. One way to identify extraordinary temperatures is to investigate anomalies of long-term average temperatures during specific time intervals. In this work, we focus our attention on land surface temperature anomalies during daytime (LSTAD), which represent a suitable observable, since they integrate temperature information over the daily active time (photo-period) of most plants. However, we emphasize that nighttime temperatures can also have considerable effects on plants in terms of heat stress by stimulating carbon loss by respiration.

At the prospect of increasing frequencies and/or intensities of extreme temperature events in Europe (Coumou and Rahmstorf, 2012; Tank and Konnen, 2003; Luterbacher et al., 2004; IPCC, 2013; Barriopedro et al., 2011; Petoukhov et al., 2013; Seneviratne et al., 2012), plant communities will in general face ever more challenges to resist the stress imposed on them. A widely used measure for identifying plant stress at regional scales based on remote sensing observations is the normalized difference vegetation index (NDVI). While other more recently developed indices for vegetation characteristics (such as the enhanced vegetation index or the net primary productivity) have been shown to yield advantages over the NDVI in terms of stress detection in plants, the NDVI is still in frequent use. Despite its lower sensitivity to changes of the vegetation cover, the NDVI is a conservative, robust measurement tool (Pettorelli, 2013) and has been comprehensively studied regarding its relationship with temperature variability (see, e.g., Schultz and Halpert, 1993, 1995; Kawabata et al., 2001; Karnieli et al., 2010; Kim et al., 2010). The global data availability for a relatively long period of observations has made NDVI easily applicable to remote sensing studies without the need for exhaustive preprocessing. Because of this, we focus in this work on the analysis of NDVI characteristics while outlining refined studies using more sophisticated indices as a subject of future research.

Up to now, research on climatic drivers of NDVI variations has often concentrated on a global scale (e.g., the aforementioned Schultz and Halpert, 1993, 1995; Kawabata et al., 2001; Karnieli et al., 2010; Kim et al., 2010), whereas regional studies like Wang et al. (2003) and Hao et al. (2012) are still rare. In the face of global warming, however, especially inter-regional climate disparities are projected to increase (Ciscar et al., 2011; Iglesias et al., 2012), thus emphasizing the need for regional research.

Moreover, most previous studies on the environmental impacts of changing temperatures have focused on the detection of linear relationships between different variables by means of correlation and regression analysis (see, e.g., Schultz and Halpert, 1995; Los et al., 2001; Ichii et al., 2002; Wang et al., 2003; Stöckli and Vidale, 2004; Hao et al., 2012). Linear correlation analysis is a widely applicable tool allowing us to discover linear statistical relationships between environmental variables. However, corresponding changes associated with global warming cannot a priori be assumed to be of linear nature, but may, for example, only occur when a certain threshold is exceeded (see, e.g., Burkett et al., 2005; Rockström et al., 2009). Liu et al. (2013) took this idea a step further by investigating the sensitivity of vegetation to climate extremes by conducting a pixel-wise regression between extremes in vegetation dynamics subject to a Box–Cox data transformation and extremes of precipitation, Palmer drought severity index and temperature.

While the aforementioned approach explored anomalies in the data distribution and took into account a broad ensemble of drought-related indicators, in this work, we specifically focus on analyzing the impacts of extraordinary warm or cold temperature events by utilizing the novel and straightforward method of event coincidence analysis (ECA; Donges et al., 2016). This method differs from linear correlation analysis in that it does not assess the dependence between two variables as a whole, but focuses on simultaneous occurrences of specific events. The theoretical differences between correlation analysis and ECA, as well as the differences in the interpretations of the outcomes of both methods, have been comprehensively discussed in previous papers (Donges et al., 2016; Siegmund et al., 2016a, b, 2017). In summary, correlation analysis reveals the general common behavior (covariance) between two time series, while ECA addresses the commonality in the timing of occurrences of values in a specific part of the empirical distributions (in our case, the tails) of the variables of interest.

Drawing upon the previous considerations, this study aims to identify regions of Europe with a vegetation cover that is particularly sensitive to temperature extremes. For this purpose, we utilize the land surface temperature anomalies during daytime (LSTAD) as a temperature variable and the NDVI as a proxy for the vegetation condition. By studying the behavior during three distinct periods of the year individually, we will distinguish between different types of temperature–vegetation relations during different parts of the growing season. For each of these periods, we additionally study the distributions of statistically significant event coincidence rates among different classes of land cover and ele-

vation to unveil which types of terrestrial ecosystems may be affected the most by extremal temperature conditions.

The remainder of this paper is organized as follows. The data used in this study and statistical analysis methods employed are introduced in Sects. 2 and 3, respectively. Our main results are described in Sect. 4, followed by a discussion in Sect. 5. The paper concludes with a summary of our main findings.

2 Data

The analyses of this study focus on the region from 33 to 73° N and 25° W to 55° E, encompassing the entire European continent plus some of the surrounding regions of northern Africa and the Levant. For our calculations, the following data sources are used:

- LSTAD and NDVI satellite images from the Moderate Resolution Imaging Spectroradiometer (MODIS) between 2000 and 2015 are retrieved from the NASA Near Earth Observations Program archive (available at http://neo.sci.gsfc.nasa.gov) at a spatial resolution of 0.1°. For both variables, the highest temporal resolution available is chosen – i.e., 16-day intervals for NDVI (NASA, 2017b) and 8-day intervals for LSTAD (NASA, 2017a).

- Land cover data are obtained from the NASA NEO archive (NASA, 2017c) at the same spatial resolution of 0.1°. Here, the data of the most recent available year (2011) are used.

- For topographic information, the ETOPO1 Global Relief data set (Amante and Eakins, 2009) is downloaded at a 1 arcmin resolution and resampled to a resolution of 0.1° by means of spatial averaging.

3 Methods

Since we aim to study statistical relationships between the occurrences of extreme events in LSTAD and NDVI (see Sect. 2) for different periods (Sect. 3.1), we first identify these events for each grid cell (in the following referred to as a *pixel*) individually (Sect. 3.2). We then apply ECA (Sect. 3.3) to the resulting pairs of event sequences for each pixel. The resulting *event coincidence rates* are then presented on maps of the study area and additionally evaluated regarding their dependence on land cover type and elevation (Sect. 3.4).

3.1 Analyzed time periods

We subdivide our analysis into different periods of time during the growing season. This distinction reflects the hypothesis that a plant's vulnerability to temperature extremes strongly depends on its respective stage of development – i.e., its *phenophase* (Hatfield and Prueger, 2015). Strictly speaking, it would be beneficial to define the relevant phenophase for each pixel within our study area separately (reflecting different climatic conditions and predominant plant types). However, an investigation of this kind would also require the consideration of a large number of additional effects influencing local vegetation (e.g., continentality, micro-climate, interannual phenophase shifts). Since such an analysis would extend beyond the limits of the present study, we take here an average continental-scale perspective to identify regional instead of local impact patterns. Therefore, we base the subdivision of the analysis on central European average phenology (Ellenberg and Leuschner, 2010). The chosen time intervals of March–April, May–June and July–September here correspond to the prevernal, vernal and serotinal phases of central European vegetation. Specifically, the prevernal phase (early spring) represents the first development of shoots and usually covers the time from March to April in central Europe. In the subsequent vernal phase (spring) lasting from May to mid-June, leaves are fully proliferated. The time between July and September can be divided into the aestival (mid-June to mid-July) and serotinal phase (mid-July to September), the latter of which is characterized by the aging of the foliage (Tansley, 1993). As most plants are already fully developed at the start of the aestival phase, we extend here our working definition of the serotinal phase to cover all of July and expand the vernal phase up to the end of June for the sake of simplicity. This results in three different parts of the growing season investigated in this study: March–April (prevernal phase), May–June (vernal phase) and July–September serotinal phase). We emphasize that this classification is only accurate for central Europe, while the phenophases differ in onset and length in other parts of Europe. The subdivision should thus be understood as a starting point for differentiating between impacts during different seasons but does not allow for a systematic intercomparison between vegetation responses to climate stress among different parts of Europe from the plant physiological perspective.

3.2 Event definitions

3.2.1 NDVI

The temporal resolution of the available NDVI data already determines a minimum time interval of 16 days that an event would represent. We emphasize that the notion of the term "event" as used in the present work should therefore be understood in a statistical, not a synoptic-scale meteorological sense. While the investigation of shorter intervals may appear desirable, one has to note that the reaction time of the NDVI to temperature changes can strongly depend on the type of ecosystem and its resilience or vulnerability in

the presence of perturbations (Gonzalez et al., 2010). In this context, NDVI responses to climate extremes can either be instantaneous or show time lags of even up to 1 month (Tan et al., 2015). Bearing this fact in mind, in addition to the practical necessity of this strategy, defining extreme NDVI events upon a temporal resolution of 16 days appears a reasonable trade-off to account for both instantaneous and delayed responses at least to a certain degree.

To distinguish between the presence or absence of an extreme event at the given temporal aggregation level, we chose the 10th and 90th percentiles of the available data for each pixel and each time period as upper and lower thresholds for defining extremely low and extremely high NDVI values. This approach already accounts for the diverse nature of the very large study area because, e.g., an "extremely low NDVI value" is always defined in relation to the typical distribution of *local* NDVI values at a given pixel during the time period being analyzed. For example, a "low NDVI event" in a semiarid savanna region might have a very different practical meaning than a "low NDVI event" in a humid temperate forest. Yet, both events are unusual with respect to the local conditions and the current phenophase. By defining the events separately for each time period, the seasonal development cycle is taken into account automatically, and no further preprocessing like (practically rather challenging) deseasonalization of the data prior to further analysis is necessary.

It should also be noted that changes in the NDVI may be attributed to different underlying mechanisms, which may not be distinguished safely through analysis of remote-sensing-based observations. While in this work, we specifically analyze the co-occurrence of very atypical NDVI values with episodes of extraordinary temperature anomalies, other factors including human activities like harvests or land use changes may also lead to NDVI anomalies, which need to be considered for an appropriate interpretation of the results.

Lastly, we note that for regions with a dense vegetation cover and a correspondingly high leaf area index during the vegetation period, NDVI is known to follow a saturation curve and to be insensitive to changes in leaf area or biomass at high levels (see studies by, e.g., Huete et al., 1997; Aparicio et al., 2000). However, this issue mostly applies for high biomass situations like those present in tropical rain forests and is unlikely to affect the results for our study region to a critical extent.

3.2.2 Temperature

The definition of the extreme temperature events is performed in the same way as for the NDVI, with the only difference that the 8-day LSTAD information is averaged to 16-day data first. The temperature values thus obtained do not exhibit any temporal mismatch with respect to the NDVI data. Moreover, as for the NDVI, the pixel-wise approach for different time periods accounts for the spatial and seasonal variability.

3.2.3 Event combinations

The discrimination of the 16-day LSTAD and NDVI data into three time periods results in time series of 64 (March–April and May–June) or 96 (July–September) data points for each pixel. Accordingly, for the time intervals March–April and May–June, the 10 and 90 % threshold definitions identify six low (negative) and six high (positive) events per time series, while for July–September, nine low and nine high events are selected. Takeing these different types of events in both time series (NDVI and LSTAD) leaves us with four possible event combinations to be considered for each part of the growing season:

1. both LSTAD and NDVI are greater than their respective empirical 90 % quantiles (in the following referred to as T90–V90),
2. both LSTAD and NDVI are lower than their 10 % quantile (T10–V10),
3. LSTAD lower than its 10 % and NDVI greater than its 90 % quantile (T10–V90), and
4. LSTAD greater than its 90 % and NDVI lower than its 10 % quantile (T90–V10).

In summary, we emphasize that in the present study, the term *extreme* describes values in the tails of the distributions of both considered types of data set rather than record-like events. The limited time span of available satellite measurements results in these extremes also including potentially still relatively moderate seasonal anomalies. However, in the classical peaks-over-threshold sense, it appears reasonable to consider the identified events as extremes.

3.3 Event coincidence analysis

In order to test for the non-random nature of potential co-occurrences between events in two time series, we apply ECA using the R package `CoinCalc` (Siegmund et al., 2017). ECA computes the empirical fraction of simultaneous events in two series (so-called *coincidences*), which is referred to as the event coincidence rate (ECR). By definition, this ECR takes values between 0 and 1, where 0 indicates that the events in both series never occur simultaneously (indicating the absence of a corresponding instantaneous statistical relationship), whereas an ECR of 1 implies that the events in both series always occur simultaneously. We emphasize that similar approaches have also been used recently by other authors in the context of remote-sensing-based analyses of ecosystem responses to climatic drivers (Zscheischler et al., 2015).

We assess the statistical significance of the ECRs thus obtained using a simple analytical significance test against the null hypothesis of two independent Poisson processes with low event rates (Donges et al., 2016), using a significance

Table 1. Share of each land cover class on the total study area. Pixels classified as "no data" cover 1.23 % of the area.

IGBP land cover units	Areal share (%)
Croplands	25.190
Mixed forest	20.870
Grasslands	14.245
Cropland/natural vegetation mosaic	9.318
Woody savannas	8.279
Open shrublands	7.022
Evergreen needleleaf forest	5.913
Barren or sparsely vegetated	4.118
Deciduous broadleaf forest	1.362
Permanent wetlands	0.826
Urban and built-up	0.819
Permanent snow and ice	0.504
Savannas	0.274
Closed shrublands	0.017
Evergreen broadleaf forest	0.006
Deciduous needleleaf forest	0.002

level of $\alpha = 0.05$. Thereby, we obtain spatial and temporal patterns of statistically significant event coincidence rates (SCRs). Specifically, we apply ECA for each joint pixel of the NDVI and LSTAD data individually, resulting in one ECR for each pixel and time period.

Note that in this work, we do not further account for possible lagged vegetation responses to temperature extremes due to the coarse temporal resolution of our data, which may result in time windows capturing both instantaneous as well as lagged responses. Methodologically speaking, if an additional time lag were included, one would have to consider the ECA as a directional analysis tool that distinguishes between the so-called *precursor rate* and *trigger rate* (Donges et al., 2016). In our setting, however, both rates are always the same by definition.

3.4 Land cover and topography analyses

In addition to the spatially explicit (pixel-wise) analysis described above, we are also interested in the role of elevation and land cover type as possible covariates determining the vegetation response to temperature extremes.

For the possible effects of elevation, the altitude values of all pixels were grouped into six classes defined based on the altitudinal zonation of Frey and Lösch (2014) as follows: planar (below 100 m a.s.l.), colline (100–500 m a.s.l.), submontane (500–1000 m a.s.l.), montane (1000–1600 m a.s.l.), subalpine (1600–2000 m a.s.l.), alpine (2000–3000 m a.s.l.) and nival (above 3000 m). Since only very few pixels fell under the definition of the nival zone, these were combined with the alpine class.

The land cover classification followed the International Geosphere-Biosphere Programme (IGBP) land cover classification scheme (Strahler et al., 1999), excluding the class "water bodies". The shares of the individual land cover classes are summarized in descending order in Table 1. As evergreen broadleaf forests and deciduous needleleaf forests make up a negligibly small fraction of the total study area, these two classes have been excluded from the land cover analysis, effectively leaving 14 classes. Furthermore, due to a discrepancy of land–water masks, the land cover image identified some pixels as water area which the NDVI and LSTAD images does not. To account for this data issue, the affected pixels were classified as "no data" and also excluded from the land cover analysis.

4 Results

4.1 March–April

Figure 1a and b summarize the results of ECA for the time period March–April. The combination of extremely high temperatures with high NDVI values (T90–V90, green pixels in Fig. 1a) results in SCRs on 14.65 % of the terrestrial part of the study area. In central and southern Europe, we find spatially contiguous regions of SCRs over mountain regions such as the Alps, the Caucasus and the Carpathians. Further important patches of SCRs exist in large parts of the lowlands of northeastern Europe (e.g., the East European Plain and Finnish Lakeland) as well as along the southeastern coast of Norway and the coastal regions of Iceland.

In contrast, SCRs between low-temperature extremes and extremely low NDVI values (T10–V10, red pixels in Fig. 1b) are widely spread on disconnected patches across large parts of continental central Europe, the British Isles and southern Scandinavia. The aforementioned mountain ranges do not appear in this analysis. In total, 13.44 % of the study area shows SCRs between low-temperature and low-NDVI events.

The SCRs between low-temperature extremes and extremely high NDVI values (T10–V90, green pixels in Fig. 1b) are sparsely sprinkled across Europe's south, North Africa and northern Scandinavia, covering only about 2.5 % of the total study area. Given the considered confidence level of our significance test, we would accept a false positive rate of 5 % in our detected pixel-wise SCRs, implying that the observed pixels with SCRs barely carry any practically relevant information. A similar conclusion applies to the combination between high-temperature extremes and extremely low NDVI events (T90–V10, red pixels in Fig. 1a), which also reveals only few pixels with SCRs (3.34 % of the study area), mainly within the Fertile Crescent and across the Mediterranean coast of North Africa.

4.2 May–June

Unlike the results for early spring, Fig. 1c only shows a small fraction of SCRs for T90–V90 during May and June (green pixels). As an exception, Scandinavia exhibits a relatively

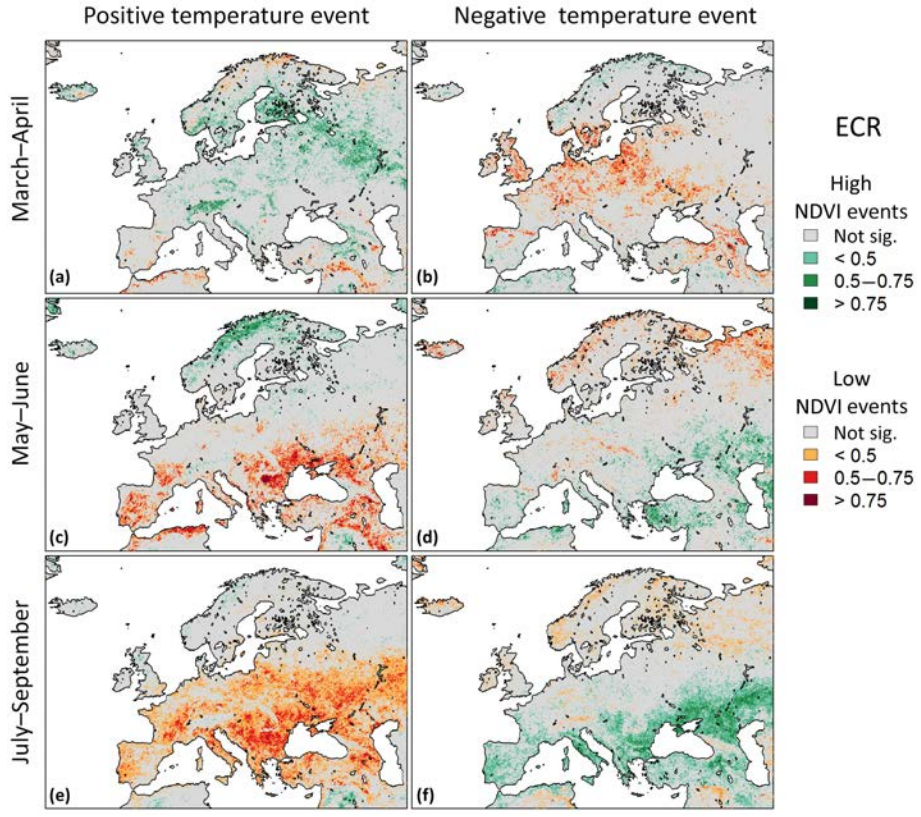

Figure 1. Spatial patterns of significant event coincidence rates (SCRs) between different combinations of low **(a, c, e)** and high **(b, d, f)** temperature and NDVI extremes during the three considered time periods, derived from MODIS satellite measurements from 2000 to 2015. Red colors show SCRs between temperature-related extremes and extremely low NDVI values, green colors such for extremely large NDVI values. Gray areas indicate pixels with non-significant event coincidence rates.

high density of pixels with SCRs, which contribute most to the 5.52 % of pixels with SCRs within the total study area.

The combination T10–V10 (Fig. 1d, red pixels) also shows only a relatively low density of pixels with SCRs with the exception of northwestern Russia along the coastline of the Arctic Ocean (7.80 % of the total study area).

In turn, the analysis of T10–V90 during May and June (Fig. 1d, green pixels) reveals SCRs in 9.37 % of the study area. Here, the most important agglomerations can be found in eastern Europe around the Black Sea, Caspian Sea and Anatolia (especially in its western part).

The most prominent signature of spatially contiguous areas with SCRs during May–June can be observed in Fig. 1c for the analysis of T90–V10 (red pixels). Here, the SCRs cover 16.58 % of the total area and concentrate in five distinct regions: (i) in a belt-like region around the west, north and east of the Black Sea; (ii) along the Fertile Crescent, including more northern regions around Azerbaijan; (iii) in a large patch over southern France north of the Pyrenees; (iv) in more or less the entire Iberian Peninsula (excluding the Pyrenees and the Atlantic coast); and (v) along the Mediterranean coast of the Maghreb regions. We particularly note that over large parts of Wallachia (the flatlands between the Carpathians and the Balkans), the analysis for T90–V10 reveals ECRs of 1.

4.3 July–September

The third considered time period only exhibits a negligible number of SCRs over Europe for T90–V90 (Fig. 1e, green pixels). Only a small agglomeration of SCRs can be found in northwest Mesopotamia, accounting for just 1.79 % of the total study area.

For T10–V10, a broad geographic distribution of SCRs is present (Fig. 1f, red pixels). Notably, these results resemble the observations for the same combination in May–June to a certain degree: the SCRs are loosely spread in the Scandes and northwest Russia (6.88 % of the total study area).

The co-occurrence patterns of T10–V90 (Fig. 1f, green pixels) are concentrated in a latitudinal belt (approximately between 40 and 45° N) from the Caspian Depression via the Kuma-Manych Depression (north of the Caucasus Mountains), the Balkans, almost entire Italy to parts of the Iberian Peninsula. The Caucasus Mountains and the Alps appear to

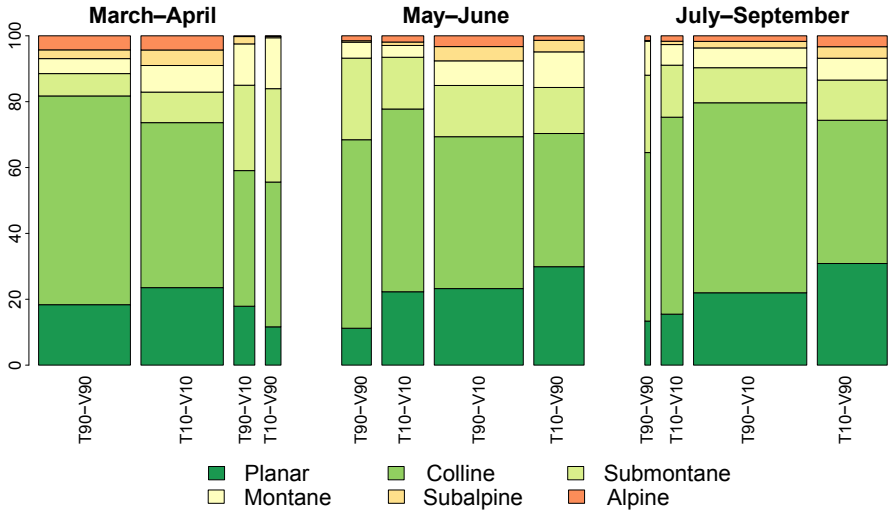

Figure 2. Distribution of pixels with SCRs among the seven altitudinal classes (in percent) for all four event combinations in the three time periods. The width of the columns represents the fraction of pixels with SCRs of the specific event combination within the total study area.

be distinctively excluded from this pattern. In total, 21.93 % of the study area shows SCRs for T10–V90.

Finally, the combination T90–V10 (Fig. 1e, red pixels) exhibits a widespread SCR pattern, which covers almost all of western, central and eastern Europe. Especially high ECRs are found between the Adriatic and the Black Sea, while remarkable areas without SCRs include major mountain ranges like the Alps, the Pyrenees, the northern Carpathians and the Caucasus Mountains. For this combination, 35.52 % of the total study area is covered by SCRs.

4.4 Topographical effects

Figure 2 illustrates the distribution of pixels exhibiting SCRs (for every combination of events and all three time periods) among the six elevation classes. The width of the displayed bars indicates the fraction of pixels with SCRs among the total study area and therefore (to a certain degree) underlines the relevance of this event combination during the respective time period. The SCRs for the two event combinations T90–V90 and T10–V10 during March–April (Fig. 2, left panel) mostly occur on elevation levels of the planar and colline zone, while T10–V10 has a slightly higher tendency towards higher elevations than T90–V90. The alpine zone also exhibits a notable number of pixels with SCRs as compared to the other two event combinations. When comparing this to Fig. 1a, b, the pixels of the alpine zone seem to mainly result from event coincidences in the European Alps for T90–V90 and the Pyrenees and Caucasus Mountains for T10–V10. The few significant pixels of the other two event combinations (T90–V10 and T10–V90) are evenly distributed throughout all elevation classes but the alpine zone.

For the time period May–June (Fig. 2, central panel), the largest differences between the event combinations can be found in the planar zone, where T10–V90 exhibits SCRs at a more than twice as large fraction of pixels as compared to T90–V90. Notably, the event combination T10–V90 shows a clearly higher contribution at the subalpine and alpine zone than the other event combinations, which presumably mainly results from the SCRs in western Anatolia (see Fig. 1d).

The two event combinations showing the most SCRs during the time July–September (T90–V10 and T10–V90, right panel of Fig. 2) again contain the most pixels in the lowest two elevation zones. Yet, T10–V90 has a distinctively larger fraction of pixels with SCRs in the higher four zones than T90–V10, especially in the alpine zone.

4.5 Land cover effects

The results for the analysis of the underlying land cover classes of the SCRs are summarized in Fig. 3. Like for the topographical analyses, the fraction of pixels exhibiting SCRs is plotted in stacked bars, where the width of the bars reflects the share of significant pixels on the entire study area.

Within the time period March–April (Fig. 3, left panel) SCRs of the event combinations T90–V90 and T10–V10 mainly occur on pixels classified as mixed forests and evergreen needleleaf forests as well as the two cropland classes. The fraction of pixels with SCRs on forests is clearly larger for T90–V90 than for T10–V10, which is replaced in T10–V10 by grassland and cropland. The two other event combinations, which exhibit much fewer SCRs in general, are dominated by open shrubland and cropland.

During May–June (Fig. 3, central panel) the SCRs of the event combinations T90–V90 and T10–V10 are relatively evenly distributed among mixed and evergreen needleleaf forests, woody savanna, open shrubland and grassland. In contrast, the SCRs of T90–V10 and T10–V90 almost only

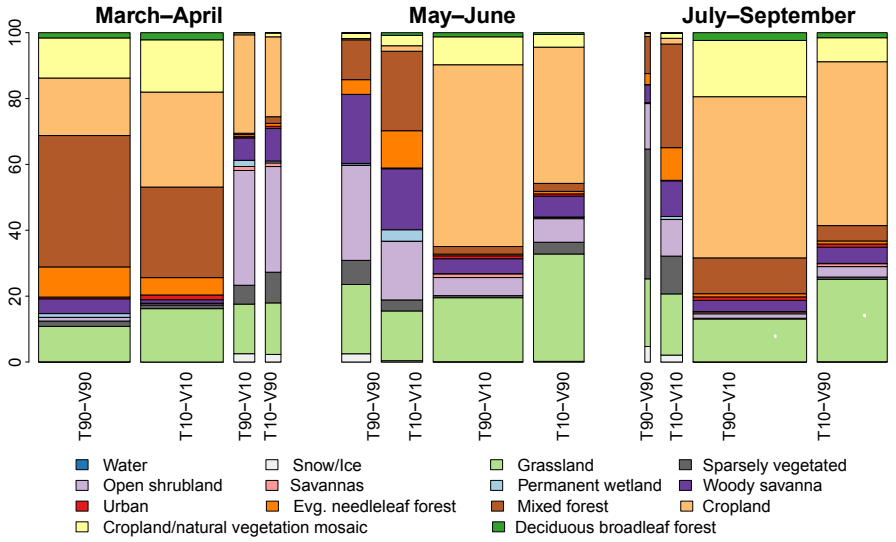

Figure 3. Same as in Fig. 2, for the 14 land cover classes.

occur on pixels classified as cropland or grassland, where for T10–V90 grassland plays a much more important role than for T90–V10.

Finally, for the time from July to September (Fig. 3, right panel) the dominant event combinations T90–V10 and T10–V90 show a picture similar as for May–June, yet with a distinctively higher fraction of SCRs on mixed forests.

5 Discussion

5.1 March–April

The most important finding for the time period March–April is that the strongest impacts of temperature extremes appeared for the two event combinations V90–T90 and V10–T10 (joint positive and negative extreme values, respectively). This suggests a generally positive statistical relationship between LSTAD and NDVI in early spring. Although temperature is widely known to be among the most crucial factors for most plants' physiological regulation during this period of the year (see, e.g., Summerfield and Roberts, 1988; Srikanth and Schmid, 2011), it is surprising that the SCR signatures in Fig. 1a, b only cover comparatively small parts of the study area. In more detail, most SCRs for V90–T90 occur in regions which normally exhibit low temperatures (as compared to the rest of the study area) at that time of the year: northern Europe and high mountain ranges such as the Alps and the Caucasus Mountains. The topographical analysis (Fig. 2) confirms the increased relevance of higher-elevation classes. Similar observations have been made by Cannone et al. (2007), who found fast growth responses of alpine vegetation to increasing temperatures, since the length of the snow cover season decreased. At the same time, earlier bud burst at these altitudes increases the vulnerability of the vegetation to freezing events after a short window of warm conditions (Wheeler et al., 2014).

The land cover analysis suggests that especially croplands, mixed forests, evergreen needleleaf forests and grasslands benefit from extraordinary warm conditions during early spring. On the other hand, also negative effects of cold periods are mainly visible on croplands in the East European Plain (chiefly wheat and corn fields) and central Europe (fruit trees, field crops). Being adapted to a narrow range of climatic conditions, most of these croplands have been reported to be vulnerable to late spring frost events and might be at even larger risk when the growing season extends earlier into the year (Chmielewski et al., 2004; Lavalle et al., 2009; Trnka et al., 2014). For example, in 2007 the wheat belt of the North European Plain (stretching from northern France to the Baltic) experienced a spring backlash after an unusually warm winter followed by a dry and cold spring (USDA, 2007). As a result, heat-advanced crops were damaged throughout northern central Europe, which is also visible in the results of Fig. 1b.

Although the patterns for the other two event combinations are not as pronounced as for the aforementioned two, three distinct regions showed very specific behaviors: the Scandes, the Atlas Mountains and Mesopotamia (see Fig. 1a, b). The dominant land cover class in these three regions is open shrubland (see Fig. 3), which the IGBP classifies as "lands with woody vegetation less than 2 m tall and with shrub canopy cover between 10 and 60 %. The shrub foliage can be either evergreen or deciduous" (Strahler et al., 1999, p. 17). This sparse canopy cover leaves the soil prone to a loss of moisture during high temperature events, which may in the course damage non-perennial grass seedlings that heavily de-

pend on moist conditions in the top soil layer (Harrington, 1991). While this phenomenon can already be observed in spring in these regions, it appears throughout the season and seems to reach its peak in the time period May–June.

Already at this point, it is very important to note that the SCR patterns of T90–V90 and T10–V10 (as well as those of T10–V90 and T90–V10) do not match in many cases. This implies, that in many parts of Europe, a positive or negative relationship between temperature and NDVI is only valid for one tail of the empirical distribution, which presents a finding that could not be deduced based upon classical linear correlation analyses (e.g., Schultz and Halpert, 1995; Los et al., 2001; Ichii et al., 2002; Wang et al., 2003; Stöckli and Vidale, 2004; Hao et al., 2012).

5.2 May–June

For the time between May and June, SCRs for the event combination T90–V90 exhibit a distinct pattern in the northern Scandes. When comparing these results to the same combination during March–April, the observed phenomenon appears to have shifted northwards, presumably due to the later onset of spring in these latitudes. On the other hand, SCRs of T10–V10 are particularly frequent in the northeastern parts of the study area. As mentioned before, this observation may be due to damages induced by cold spells during bud burst or, more likely, late snowfall events that hide the sparse tundric vegetation cover (Dierßen, 1996) from being seen by MODIS.

The largest amount of SCRs appeared for T90–V10. While this heat stress situation is found relevant for vast parts of Europe, croplands and partly grasslands were the most affected land cover types. One reason for this particular sensitivity could be the following. As crops are meant to produce a maximum yield, they often demand high standards in nurturing and water availability and are vulnerable to sudden changes (Semenov and Shewry, 2011; Ma et al., 2015). As already discussed in the Introduction, extreme temperatures can cause substantial losses in crop yields (see, e.g., Schaap et al., 2011; Lesk et al., 2011; Moriondo et al., 2010; Wreford and Adger, 2010). For instance, in 2011 France experienced one of the warmest springs on record which resulted in a 12 % decrease in grain harvest (Coumou and Rahmstorf, 2012; NOAA, 2012). Similarly, based on our results (Fig. 1c), the Wallachia proved to be particularly prone to heat stress. This corroborates observations of Spinoni et al. (2015), who identified almost annually recurring heat waves, with the most extreme cases occurring in 2003 and 2007. However, other lowlands at similar latitudes like the Padan Plain in northern Italy did not exhibit such a behavior. For most parts, we suggest a different water supply situation of these areas (e.g., influenced by continentality, size of the watershed and irrigation) to lead to this finding, while also differing water demands of the vegetation due to different dominating crop types may play a role.

Regarding the repeated appearance of grasslands among the most affected land cover classes for the combination T90–V10, we note that a rapid loss of soil moisture during high temperature events is expected to result in negative NDVI events (Teuling et al., 2010).

5.3 July–September

The combination T90–V10 resulted in the highest fraction of SCRs for the time July–September. This result suggests that extremely high temperatures pose a severe threat to the vegetation particularly during this time of the year. Notably, three of the most severe heat waves on record (in the summers of 2003, 2006 and 2010) occurred during our study period (2000–2015) and most likely constitute a main part of the selected upper 10 % of temperature values. Previous studies from these summers confirm largely adverse effects on vegetation throughout Europe, with regionally higher intensities along the Mediterranean coast (De Bono et al., 2004; Ciais et al., 2005; Fischer and Schär, 2010).

While heat waves themselves already pose a considerable challenge to plants, the meteorological conditions preceding these events also need to be considered as they may exacerbate the impacts of heat on vegetation. The 2003 heat wave provides a good example, as it was preceded by unusually dry conditions between February and August (Fischer et al., 2007), which left the vegetation at severe drought stress even before the actual extreme event. Hence, the high share of pixels with SCRs may also result from vegetation, which had already been stressed in previous months and was thus more vulnerable to repeated temperature extremes.

Interestingly, like in May–June, croplands and grasslands were among the most affected land cover types. These results match well with modeled future crop production (Deryng et al., 2014; Teixeira et al., 2013), which also sees southeastern and eastern Europe at a particularly high risk of crop failure due to extreme temperature events in late spring and summer. Still, it needs to be noted that during this time of the year parts of the extremely low NDVI events may also be the result of harvesting activities (Wardlow et al., 2007). For example, in Ukraine winter wheat harvest usually takes place between the end of June and mid-August (USDA, 2016), which would be compatible with the low NDVI values present in this region during the time periods May–June and July–September.

At the same time, SCRs of T10–V90 were found in large areas around the Black and Mediterranean seas. This could be interpreted as a "pause for breath" for crop species that are under continuous stress during that time period of the year. In contrast, the high fraction of grassland pixels among all SCRs of this event combination contradicts this idea, since the composition of grass species can be assumed not to be anthropogenically influenced and thus to be well adapted to the local climate. Another explanation could be that the cold temperature events during this time period also coincide with

periods of high precipitation, and that the latter (or a combination of both factors) is actually causing the increase in NDVI. This hypothesis shall be further tested in future work.

On a final note, it should be pointed out that the analysis of altitudinal zones yielded no clearly interpretable result. The distribution of SCRs among the different classes more or less represented their parent distributions over the whole study area. This outcome may largely be owing to the fact, that the altitudinal classes were defined uniformly across Europe. That said, especially when looking at the largest European mountain ranges in isolation, the Alps, Carpathians, Pyrenees and Caucasus Mountains indeed showed unique response patterns, which highlights their exceptional position among the European landscape.

6 Conclusions

In the context of projected increasing frequencies of temperature extremes in Europe (Coumou and Rahmstorf, 2012; Tank and Konnen, 2003; Luterbacher et al., 2004; IPCC, 2013; Barriopedro et al., 2011; Petoukhov et al., 2013; Seneviratne et al., 2012), the present study has delivered a spatially resolved statistical assessment of the impacts of very high and very low temperature events on European vegetation. By applying event coincidence analysis to high-resolution remote sensing data, we have investigated the co-occurrences of extremes in daytime land surface temperature anomalies and the normalized difference vegetation index over a period of 16 years (2000–2015). We have analyzed patterns of significant local event coincidence rates, accounting for the type of land cover and altitudinal zone and assessing which regions might be especially vulnerable to possibly rising frequencies and/or intensities of future extreme temperature events.

Our results revealed that the vulnerability to heat stress (particularly between May and June) is very heterogeneously distributed over Europe. The time between July and September displayed the highest densities of significant event coincidence rates for both high- and low-temperature extremes. This was especially true for southern Europe, which emphasizes the vulnerability of this region to climate extremes also in the context of expected increasing frequencies of future heat waves.

Our analysis of the distribution of significant event coincidence rates among altitudinal classes did not reveal clear results. From a geographical point of view, however, high mountain ranges like the Alps and the Caucasus Mountains formed a visible pattern, which points to unique responses of alpine vegetation as compared to the main patterns across Europe. In contrast, the analysis for the different land cover types revealed that the areas suffering from both low- and high-temperature extremes are mostly anthropogenically shaped landscapes. These ecosystems appear to be particularly sensitive to temperature extremes. Another important finding is that forests hardly exhibited significant event coincidences rates, which indicates that these vegetation types are more resilient against temperature extremes than others. Mixed forests are an important exception, which clearly benefit from warm temperature events during spring.

Despite the reported achievements, further research on simultaneous occurrences of climatic extremes with vegetation-related extremes is strongly recommended. First, an explicit consideration of moisture-related variables (like precipitation, soil moisture or drought indices) within the framework of event coincidence analysis would surely yield further valuable insights (for example, for differentiating between heat and drought stress, see also Kogan, 2001). Second, an investigation of the vegetation vitality and atmospheric conditions preceding extreme temperature events could clarify the actual impact of a specific event itself on vegetation. Third, further validation of the obtained results based upon different remote sensing data sets (Scheftic et al., 2014) as well as ground-based observations (Loew et al., 2017) appears necessary. In this context, we particularly highlight the necessity to consider additional observables related to vegetation stress in order to study the robustness of our approach and reveal further details on the associated plant physiological processes. For the latter purposes, we also emphasize the possibility of employing previously developed multivariate extensions of the present analysis methodology (Siegmund et al., 2016b). We outline such investigations as a subject of future work.

Code and data availability. All calculations in this work have been based upon the open-source R package `CoinCalc`, which is available at GitHub (Siegmund, 2017).

All data used in this work are publicly available at the sources described in the main text.

Author contributions. JFS designed the analysis. LB, JFS and MM conducted the analysis. LB and JFS prepared the paper. RVD supervised the analysis and revised the manuscript and the interpretation of the obtained results.

Competing interests. The authors declare that they have no conflict of interest.

Acknowledgements. This work has been financially supported by the German Federal Ministry for Education and Research (BMBF) within the framework of the BMBF Young Investigators Group CoSy-CC^2: Complex Systems Approaches to Understanding Causes and Consequences of Past, Present and Future Climate Change (grant no. 01LN1306A). Jonatan F. Siegmund acknowledges funding by the Evangelisches Studienwerk Villigst e.V. The authors express their gratitude to Catrin Gellhorn and Chiranjit Mitra for giving valuable feedback on this work.

Edited by: Akihiko Ito
Reviewed by: Gerald Moser and two anonymous referees

References

Amante, C. and Eakins, B.: ETOPO1 1 Arc-Minute Global Relief Model: Procedures, Data Sources and Analysis, NOAA Technical Memorandum NESDIS NGDC-24, National Geophysical Data Center, NOAA, available at: https://doi.org/10.7289/V5C8276M (last access: 2 May 2017), 2009.

Aparicio, N., Villegas, D., Casadesus, J., Araus, J. L., and Royo, C.: Spectral vegetation indices as nondestructive tools for determining durum wheat yield, Agron. J., 92, 83–91, https://doi.org/10.2134/agronj2000.92183x, 2000.

Barriopedro, D., Fischer, E. M., Luterbacher, J., Trigo, R. M., and García-Herrera, R.: The hot summer of 2010: redrawing the temperature record map of Europe, Science, 332, 220–224, https://doi.org/10.1126/science.1201224, 2011.

Beck, E. H., Heim, R., and Hansen, J.: Plant resistance to cold stress: mechanisms and environmental signals triggering frost hardening and dehardening, J. Biosci., 29, 449–459, https://doi.org/10.1007/bf02712118, 2004.

Beniston, M., Stephenson, D. B., Christensen, O. B., Ferro, C. A., Frei, C., Goyette, S., Halsnaes, K., Holt, T., Jylhä, K., Koffi, B., Palutikof, J., Schöll, R., Semmler, T., and Woth, K.: Future extreme events in European climate: an exploration of regional climate model projections, Climatic Change, 81, 71–95, https://doi.org/10.1007/s10584-006-9226-z, 2007.

Burkett, V. R., Wilcox, D. A., Stottlemyer, R., Barrow, W., Fagre, D., Baron, J., Price, J., Nielsen, J. L., Allen, C. D., Peterson, D. L., Ruggerone, G., and Doyle, T.: Nonlinear dynamics in ecosystem response to climatic change: case studies and policy implications, Ecol. Complex., 2, 357–394, https://doi.org/10.1016/j.ecocom.2005.04.010, 2005.

Cannone, N., Sgorbati, S., and Guglielmin, M.: Unexpected impacts of climate change on alpine vegetation, Front. Ecol. Environ., 5, 360–364, https://doi.org/10.1890/1540-9295(2007)5[360:UIOCCO]2.0.CO;2, 2007.

Chmielewski, F.-M., Müller, A., and Bruns, E.: Climate changes and trends in phenology of fruit trees and field crops in Germany, 1961–2000, Agr. Forest Meteorol., 121, 69–78, https://doi.org/10.1016/s0168-1923(03)00161-8, 2004.

Ciais, P., Reichstein, M., Viovy, N., Granier, A., Ogée, J., Allard, V., Aubinet, M., Buchmann, N., Bernhofer, C., Carrara, A., Chevallier, F., De Noblet, N., Friend, A. D., Friedlingstein, P., Grünwald, T., Heinesch, B., Keronen, P., Knohl, A., Krinner, G., Loustau, D., Manca, G., Matteucci, G., Miglietta, F., Ourcival, J. M., Papale, D., Pilegaard, K., Rambal, S., Seufert, G., Soussana, J. F., Sanz, M. J., Schulze, E. D., Vesala, T., and Valentini, R.: Europe-wide reduction in primary productivity caused by the heat and drought in 2003, Nature, 437, 529–533, https://doi.org/10.1038/nature03972, 2005.

Ciscar, J.-C., Iglesias, A., Feyen, L., Szabó, L., Van Regemorter, D., Amelung, B., Nicholls, R., Watkiss, P., Christensen, O. B., Dankers, R., Garrotek, L., Goodess, C. M., Hunt, A., Moreno, A., Richards, J., and Sori, A.: Physical and economic consequences of climate change in Europe, P. Natl. Acad. Sci. USA, 108, 2678–2683, https://doi.org/10.1073/pnas.1011612108, 2011.

Coumou, D. and Rahmstorf, S.: A decade of weather extremes, Nat. Clim. Change, 2, 491–496, https://doi.org/10.1038/nclimate1452, 2012.

Coumou, D., Robinson, A., and Rahmstorf, S.: Global increase in record-breaking monthly-mean temperatures, Clim. Change, 118, 771–782, https://doi.org/10.1007/s10584-012-0668-1, 2013.

De Bono, A., Peduzzi, P., Kluser, S., and Giuliani, G.: Impacts of summer 2003 heat wave in Europe, Environ. Alert Bulletin, 2, available at: http://www.unisdr.org/files/1145_ewheatwave.en.pdf, 2004.

Deryng, D., Conway, D., Ramankutty, N., Price, J., and Warren, R.: Global crop yield response to extreme heat stress under multiple climate change futures, Environ. Res. Lett., 9, 034011, https://doi.org/10.1088/1748-9326/9/3/034011, 2014.

Dierßen, K.: Vegetation Nordeuropas: 112 Tabellen, Ulmer, Stuttgart, 1996.

Donges, J. F., Schleussner, C.-F., Siegmund, J. F., and Donner, R. V.: Event coincidence analysis for quantifying statistical interrelationships between event time series, Eur. Phys. J.-Spec. Top., 225, 471–487, https://doi.org/10.1140/epjst/e2015-50233-y, 2016.

Ellenberg, H. and Leuschner, C.: Vegetation Mitteleuropas mit den Alpen: in ökologischer, dynamischer und historischer Sicht, Vol. 8104, Ulmer, Stuttgart, 2010.

Fischer, E. and Schär, C.: Consistent geographical patterns of changes in high-impact European heatwaves, Nat. Geosci., 3, 398–403, https://doi.org/10.1038/ngeo866, 2010.

Fischer, E. M., Seneviratne, S., Vidale, P., Lüthi, D., and Schär, C.: Soil moisture–atmosphere interactions during the 2003 European summer heat wave, J. Climate, 20, 5081–5099, https://doi.org/10.1175/JCLI4288.1, 2007.

Frey, W. and Lösch, R.: Geobotanik: Pflanze und Vegetation in Raum und Zeit, Springer-Verlag, https://doi.org/10.1007/978-3-662-45281-3, 2014.

Gonzalez, P., Neilson, R. P., Lenihan, J. M., and Drapek, R. J.: Global patterns in the vulnerability of ecosystems to vegetation shifts due to climate change, Global Ecol. Biogeogr., 19, 755–768, https://doi.org/10.1111/j.1466-8238.2010.00558.x, 2010.

Hao, F., Zhang, X., Ouyang, W., Skidmore, A. K., and Toxopeus, A.: Vegetation NDVI linked to temperature and precipitation in the upper catchments of Yellow River, Environ. Model. Assess., 17, 389–398, https://doi.org/10.1007/s10666-011-9297-8, 2012.

Harrington, G.: Effects of Soil Moisture on Shrub Seedling Survival in Semi-Arid Grassland, Ecology, 72, 1138–1149, https://doi.org/10.2307/1940611, 1991.

Hasanuzzaman, M., Nahar, K., Alam, M. M., Roychowdhury, R., and Fujita, M.: Physiological, biochemical, and molecular mechanisms of heat stress tolerance in plants, Int. J. Mol. Sci., 14, 9643–9684, https://doi.org/10.3390/ijms14059643, 2013.

Hatfield, J. L. and Prueger, J. H.: Temperature extremes: effect on plant growth and development, Weather Climate Extremes, 10, 4–10, https://doi.org/10.1016/j.wace.2015.08.001, 2015.

Huete, A. R., Liu, H., and van Leeuwen, W. J.: The use of vegetation indices in forested regions: issues of linearity and saturation, in: Proceedings of the 1997 IEEE International Conference on Geoscience and Remote Sensing (IGARSS'97): Remote Sensing – A Scientific Vision for Sustainable Development, 4, 1966–1968, https://doi.org/10.1109/IGARSS.1997.609169, 1997.

Ichii, K., Kawabata, A., and Yamaguchi, Y.: Global correlation analysis for NDVI and climatic variables and NDVI trends: 1982–1990, Int. J. Remote Sens., 23, 3873–3878, https://doi.org/10.1080/01431160110119416, 2002.

Iglesias, A., Garrote, L., Quiroga, S., and Moneo, M.: A regional comparison of the effects of climate change on agricultural crops in Europe, Cli. Change, 112, 29–46, https://doi.org/10.1007/s10584-011-0338-8, 2012.

IPCC: Climate Change 2013: The Physical Science Basis, Contribution of Working Group I to the Fifth Assessment Report of the Intergovernmental Panel on Climate Change, Cambridge University Press, Cambridge, UK, New York, NY, USA, https://doi.org/10.1017/CBO9781107415324, 2013.

Karnieli, A., Agam, N., Pinker, R. T., Anderson, M., Imhoff, M. L., Gutman, G. G., Panov, N., and Goldberg, A.: Use of NDVI and land surface temperature for drought assessment: Merits and limitations, J. Climate, 23, 618–633, https://doi.org/10.1175/2009jcli2900.1, 2010.

Kawabata, A., Ichii, K., and Yamaguchi, Y.: Global monitoring of interannual changes in vegetation activities using NDVI and its relationships to temperature and precipitation, Int. J. Remote Sens., 22, 1377–1382, https://doi.org/10.1080/01431160010028490, 2001.

Kim, Y., Glenn, D. M., Park, J., Ngugi, H. K., and Lehman, B. L.: Hyperspectral image analysis for plant stress detection, American Society of Agricultural and Biological Engineers, Pittsburgh, Pennsylvania, 20–23 June 2010, 1009114, https://doi.org/10.13031/2013.29814, 2010.

Kogan, F. N.: Operational space technology for global vegetation assessment, B. Am. Meteorol. Soc., 82, 1949–1964, https://doi.org/10.1175/1520-0477(2001)082<1949:OSTFGV>2.3.CO;2, 2001.

Larcher, W.: Ökophysiologie der Pflanzen, Ulmer, Stuttgart, 1994.

Lavalle, C., Micale, F., Houston, T. D., Camia, A., Hiederer, R., Lazar, C., Conte, C., Amatulli, G., and Genovese, G.: Climate change in Europe: 3. Impact on agriculture and forestry, A review, Agronomy for sustainable Development, 29, 433–446, https://doi.org/10.1051/agro/2008068, 2009.

Lesk, C., Rowhani, P., and Ramankutty, N.: Influence of extreme weather disasters on global crop production, Nature, 529, 84–87, https://doi.org/10.1038/nature16467, 2011.

Liu, G., Liu, H., and Yin, Y.: Global patterns of NDVI-indicated vegetation extremes and their sensitivity to climate extremes, Environ. Res. Lett., 8, 025009, https://doi.org/10.1088/1748-9326/8/2/025009, 2013.

Loew, A., Bell, W., Brocca, L., Bulgin, C. E., Burdanowitz, J., Calbet, X., Donner, R. V., Ghent, D., Gruber, A., Kaminski, T., Kinzel, J., Klepp, C., Lambert, J.-C., Schaepman-Strub, G., Schröder, M., and Verhoelst, T.: Validation practices for satellite based earth observation data across communities, Rev. Geophys., 55, 779–817, https://doi.org/10.1002/2017RG000562, 2017.

Los, S. O., Collatz, G. J., Bounoua, L., Sellers, P. J., and Tucker, C. J.: Global interannual variations in sea surface temperature and land surface vegetation, air temperature, and precipitation, J. Climate, 14, 1535–1549, https://doi.org/10.1175/1520-0442(2001)014<1535:giviss>2.0.co;2, 2001.

Luterbacher, J., Dietrich, D., Xoplaki, E., Grosjean, M., and Wanner, H.: European seasonal and annual temperature variability, trends, and extremes since 1500, Science, 303, 1409–1503, https://doi.org/10.1126/science.1093877, 2004.

Ma, X., Huete, A., Moran, S., Ponce-Campos, G., and Eamus, D.: Abrupt shifts in phenology and vegetation productivity under climate extremes, J. Geophys. Res.-Biogeo., 120, 2036–2052, https://doi.org/10.1002/2015jg003144, 2015.

Moriondo, M., Bindi, M., Kundzewicz, Z., Szwed, M., Chorynski, A., Matczak, P., Radziejewski, M., McEvoy, D., and Wreford, A.: Impact and adaptation opportunities for European agriculture in response to climatic change and variability, Mitigation and Adaption Strategies on Global Change, 15, 657–679, https://doi.org/10.1007/s11027-010-9219-0, 2010.

NASA: Land Surface Temperature Anomaly [Day] (8 day) Dataset, available at: http://neo.sci.gsfc.nasa.gov/view.php?datasetId=MOD_LSTAD_E, last access: 2 May 2017a.

NASA: Vegetation Index [NDVI] (16 Day – Terra/MODIS) Dataset, available at: http://neo.sci.gsfc.nasa.gov/view.php?datasetId=MOD13A2_M_NDVI, last access: 2 May 2017b.

NASA: Land Cover Classification (1 year) Dataset, available at: http://neo.sci.gsfc.nasa.gov/view.php?datasetId=MCD12C1_T1&date=2011-01-01, last access: 2 May 2017c.

NOAA: 2011 Seasonal Temperature Anomalies, available at: https://www.climate.gov/news-features/featured-images/2011-seasonal-temperature-anomalies (last access: 21 August 2017), 2012.

NOAA National Centers for Environmental Information: State of the Climate: Global Climate Report for Annual 2016, available at: http://www.ncdc.noaa.gov/sotc/global/201613, last access: 13 May 2017.

Petoukhov, V., Rahmstorf, S., Petri, S., and Schellnhuber, H.-J.: Quasiresonant amplification of planetary waves and recent Northern Hemisphere weather extremes, P. Natl. Acad. Sci. USA, 110, 5336–5341, https://doi.org/10.1073/pnas.1222000110, 2013.

Pettorelli, N.: The Normalized Difference Vegetation Index, Oxford University Press, Oxford, https://doi.org/10.1093/acprof:osobl/9780199693160.001.0001, 2013.

Rebetez, M., Dupont, O., and Giroud, M.: An analysis of the July 2006 heatwave extent in Europe compared to the record year of 2003, Theor. Appl. Climatol., 95, 1–7, https://doi.org/10.1007/s00704-007-0370-9, 2009.

Rockström, J., Steffen, W. L., Noone, K., Persson, Å., Chapin III, F. S., Lambin, E., Lenton, T. M., Scheffer, M., Folke, C., Schellnhuber, H. J., Nykvist, B., De Wit, C. A., Hughes, T., van der Leeuw, S., Rodhe, H., Sörlin, S., Snyder, P. K., Costanza, R., Svedin, U., Falkenmark, M., Karlberg, L., Corell, R. W., Fabry, V. J., Hansen, J., Walker, B., Liverman, D., Richardson, K., Crutzen, P., and Foley, J.: Planetary boundaries: exploring the safe operating space for humanity, Ecol. Soc., 14, 32, https://doi.org/10.5751/es-03180-140232, 2009.

Schaap, B., Blom-Zandstra, M., Hermans, C., Meerburg, B., and Verhagen, J.: Impact changes of climatic extremes on arable farming in the north of the Netherlands, Reg. Environ. Change, 11, 731–741, https://doi.org/10.1007/s10113-011-0205-1, 2011.

Scheftic, W., Zeng, X., Broxton, P., and Brunke, M.: Intercomparison of Seven NDVI Products over the United States and Mexico, Remote Sens., 6, 1057–1084, https://doi.org/10.3390/rs6021057, 2014.

Schultz, P. and Halpert, M.: Global correlation of temperature, NDVI and precipitation, Adv. Space Res., 13, 277–280, https://doi.org/10.1016/0273-1177(93)90559-t, 1993.

Schultz, P. and Halpert, M.: Global analysis of the relationships among a vegetation index, precipitation and land surface temperature, Remote Sens., 16, 2755–2777, https://doi.org/10.1080/01431169508954590, 1995.

Semenov, M. A. and Shewry, P. R.: Modelling predicts that heat stress, not drought, will increase vulnerability of wheat in Europe, Sci. Rep.-UK, 1, 66, https://doi.org/10.1038/srep00066, 2011.

Seneviratne, S. I., Nicholls, N., Easterling, D., Goodess, C. M., Kanae, S., Kossin, J., Luo, Y., Marengo, J., McInnes, K., and Rahimi, M.: Changes in climate extremes and their impacts on the natural physical environment, Managing the risks of extreme events and disasters to advance climate change adaptation, Cambridge University Press, 109–230, https://doi.org/10.1017/cbo9781139177245.006, 2012.

Siegmund, J. F.: Open-source R package `CoinCalc`, available at: https://github.com/JonatanSiegmund/CoinCalc, last access: 3 November 2017.

Siegmund, J. F., Wiedermann, M., Donges, J. F., and Donner, R. V.: Impact of temperature and precipitation extremes on the flowering dates of four German wildlife shrub species, Biogeosciences, 13, 5541–5555, https://doi.org/10.5194/bg-13-5541-2016, 2016a.

Siegmund, J. F., Sanders, T. G. M., Heinrich, I., van der Maaten, E., Simard, S., Helle, G., and Donner, R. V.: Meteorological Drivers of Extremes in Daily Stem Radius Variations of Beech, Oak, and Pine in Northeastern Germany: An Event Coincidence Analysis, Front. Plant Sci., 7, 733, https://doi.org/10.3389/fpls.2016.00733, 2016b.

Siegmund, J. F., Siegmund, N., and Donner, R. V.: CoinCalc – A new R package for quantifying simultaneities of event series, Comput. Geosci., 98, 64–72, https://doi.org/10.1016/j.cageo.2016.10.004, 2017.

Spinoni, J., Lakatos, M., Szentimrey, T., Bihari, Z., Szalai, S., Vogt, J., and Antofie, T.: Heat and cold waves trends in the Carpathian Region from 1961 to 2010, Int. J. Climatol., 35, 4197–4209, https://doi.org/10.1002/joc.4279, 2015.

Srikanth, A. and Schmid, M.: Regulation of flowering time: all roads lead to Rome, Cell. Mol. Life Sci., 68, 2013–2037, https://doi.org/10.1007/s00018-011-0673-y, 2011.

Stöckli, R. and Vidale, P. L.: European plant phenology and climate as seen in a 20-year AVHRR land-surface parameter dataset, Int. J. Remote Sens., 25, 3303–3330, https://doi.org/10.1080/0143116031000161814 9, 2004.

Strahler, A., Muchoney, D., Borak, J., Friedl, M., Gopal, S., Lambin, E., and Moody, A.: MODIS Land Cover Product Algorithm Theoretical Basis Document (ATBD) Version 5.0, Tech. rep., Boston University, 1999.

Summerfield, R. J. and Roberts, E. H.: Photo-thermal regulation of flowering in pea, lentil, faba bean and chickpea, Springer the Netherlands, 911–922, https://doi.org/10.1007/978-94-009-2764-3_72, 1988.

Tan, Z., Tao, H., Jiang, J., and Zhang, Q.: Influences of Climate Extremes on NDVI (Normalized Difference Vegetation Index) in the Poyang Lake Basin, China, Wetlands, 35, 1033–1042, https://doi.org/10.1007/s13157-015-0692-9, 2015.

Tank, K. and Konnen, G.: Trends in indices of daily temperature and precipitation extremes in Europe, 1946-99, J. Climate, 16, 3665–3680, https://doi.org/10.1175/1520-0442(2003)016<3665:tiiodt>2.0.co;2, 2003.

Tansley, A. G.: An Introduction to Plant Ecology, Discovery Publishing House, 1993.

Teixeira, E., Fischer, G., van Velthuizen, H., Walter, C., and Ewert, F.: Global hot-spots of heat stress on agricultural crops due to climate change, Agr. Forest Meteorol. 170, 206–215, https://doi.org/10.1016/j.agrformet.2011.09.002, 2013.

Teuling, A. J., Seneviratne, S. I., Stöckli, R., Reichstein, M., Moors, E., Ciais, P., Luyssaert, S., Van Den Hurk, B., Ammann, C., Bernhofer, C., Dellwik, E., Gianelle, D., Gielen, B., Grünwald, T., Klumpp, K., Montagnani, L., Moureaux, C., Sottocornola, M., and Wohlfahrt, G.: Contrasting response of European forest and grassland energy exchange to heatwaves, Nat. Geosci., 3, 722–727, https://doi.org/10.1038/ngeo950, 2010.

Trnka, M., Rötter, R. P., Ruiz-Ramos, M., Kersebaum, K. C., Olesen, J. E., Žalud, Z., and Semenov, M. A.: Adverse weather conditions for European wheat production will become more frequent with climate change, Nat. Clim. Change, 4, 637–643, https://doi.org/10.1038/nclimate2242, 2014.

USDA: Spring Dryness and Freeze Lowers Europe's 2007/08 Winter Crop Prospects, availabe at: https://www.pecad.fas.usda.gov/highlights/2007/05/EU_21May07/ (last access: 22 August 2017), 2007.

USDA: Ukraine: 2016/17 Crop Production Forecasts, availabe at: http://pecad.fas.usda.gov/highlights/2016/05/ukraine_16may2016/, last access: 19 July 2016.

Wang, J., Rich, P., and Price, K.: Temporal responses of NDVI to precipitation and temperature in the central Great Plains, USA, Int. J. Remote Sens., 24, 2345–2364, https://doi.org/10.1080/01431160210154812, 2003.

Wardlow, B. D., Egbert, S. L., and Kastens, J. H.: Analysis of time-series MODIS 250 m vegetation index data for crop classification in the US Central Great Plains, Remote Sens. Environ., 108, 290–310, https://doi.org/10.1016/j.rse.2006.11.021, 2007.

Way, D. A.: Tree phenology responses to warming: spring forward, fall back?, Tree Physiol., 31, 469–471, https://doi.org/10.1093/treephys/tpr044, 2011.

Wheeler, J., Hoch, G., Cortés, A. J., Sedlacek, J., Wipf, S., and Rixen, C.: Increased spring freezing vulnerability for alpine shrubs under early snowmelt, Oecologia, 175, 219–229, https://doi.org/10.1007/s00442-013-2872-8, 2014.

Wreford, A. and Adger, N.: Adaptation in agriculture: historic effects of heat waves and droughts on UK agriculture, Int. J. Agr. Sustain., 8, 278–289, https://doi.org/10.3763/ijas.2010.0482, 2010.

Zscheischler, J., Orth, R., and Seneviratne, S. I.: A submonthly database for detecting changes in vegetation-atmosphere coupling, Geophys. Res. Lett., 42, 9816–9824, https://doi.org/10.1002/2015GL066563, 2015.

2.6 Differential imprints of distinct ENSO flavors in global extreme precipitation patterns

Noname manuscript No.
(will be inserted by the editor)

Differential imprints of distinct ENSO flavors in global extreme precipitation patterns

Marc Wiedermann · Jonatan F. Siegmund · Jonathan F. Donges · Jürgen Kurths · Reik V. Donner

Received: date / Accepted: date

Abstract The specific impacts of El Niño's two flavors, East Pacific (EP) and Central Pacific (CP) El Niño, have been studied intensively in recent years, mostly by applying linear statistical or composite analyses. These techniques, however, focus on average spatio-temporal patterns of climate variability and do not allow for a specific assessment of related extreme impacts. Here, we use event coincidence analysis to study the differential imprints of EP and CP types of both, El Niño and La Niña on global extreme precipitation patterns, which have already been shown to severely affect, among others, agricultural and biomass production or human health. We demonstrate that EP events usually coincide with spatially coherent patterns of seasonal hydro-metereological extremes, while more spatially dispersed patterns emerge for respective CP phases. Our analysis recaptures previously reported interrelations and uncovers further regional extremes arising along with different ENSO phases that have not been reported so far. Ultimately, our results imply that a proper discrimination of El Niño and La Niña into its distinct phases are crucial for anticipating metereological as well as related socio-ecological impacts.

Keywords El Niño Southern Oscillation · El Niño Modoki · Extreme precipitation · Central Pacific El Niño

M. Wiedermann
Potsdam Institute for Climate Impact Research — Telegrafenberg A 31, 14473 Potsdam, Germany, EU

Department of Physics, Humboldt University — Newtonstraße 15, 12489 Berlin, Germany, EU · J. F. Siegmund
Potsdam Institute for Climate Impact Research — Telegrafenberg A 31, 14473 Potsdam, Germany, EU

Institute of Earth and Environmental Science, University of Potsdam, Karl-Liebknecht-Straße 24-25, 14476 Potsdam-Golm, Germany · J.F. Donges
Potsdam Institute for Climate Impact Research — Telegrafenberg A 31, 14473 Potsdam, Germany, EU

Stockholm Resilience Centre, Stockholm University — Kräftriket 2B, 114 19 Stockholm, Sweden, EU · J. Kurths
Potsdam Institute for Climate Impact Research — Telegrafenberg A 31, 14473 Potsdam, Germany, EU

Department of Physics, Humboldt University — Newtonstraße 15, 12489 Berlin, Germany, EU · R. V. Donner
Potsdam Institute for Climate Impact Research — Telegrafenberg A 31, 14473 Potsdam, Germany, EU

1 Introduction

The El Niño Southern Oscillation (ENSO) with its positive (El Niño) and negative phase (La Niña) is known to trigger climatic responses in various parts of the Earth, an effect that is often referred to as teleconnectivity Trenberth (1997); Neelin et al (2003). Specifically, it has been observed in recent years that El Niño further exhibits two distinct types, usually referred to as the East Pacific or canonical El Niño and the Central Pacific El Niño or El Niño Modoki, respectively (Ashok et al, 2007; Kao and Yu, 2009). A similar proposition regarding the existence of two distinct flavors was made recently for La Niña as well (Kug and Ham, 2011), but is a subject of ongoing discussions (Kao and Yu, 2009; Ren and Jin, 2011). For El Niño, it has been shown that its two types may cause different climatic responses in certain regions, such as reduced rainfall over eastern Australia during EP El Niños (Chiew et al, 1998) contrasted by an increase in precipitation over the same area during CP El Niños (Taschetto and England, 2009).

Most previous studies on El Niño's teleconnective impacts have either applied linear statistical tools, such as correlation analysis (Diaz et al, 2001), or investigated

corresponding composites of the climatic observables under study (Hoell et al, 2014). Both approaches share the limitation that they focus on linear or average interdependencies between ENSO and possible response variables, which do not necessarily hold for extreme values. However, with global climate change projected to increase the strength and frequency of both, extreme climatic events (Jones et al, 2007; Karl and Trenberth, 2003; Easterling et al, 2000) as well as extreme ENSO periods (Cai et al, 2014) it has become a pressing issue to specifically assess possible linkages between these two aspects (Allan and Soden, 2008). Therefore, we devote the present work to quantify and spatially resolve signatures of extreme climatic events that are likely to coincide with an ENSO phase of a certain type. In particular, we focus here on heavy precipitation and dry periods, i.e., hydro-meterological extreme events, as ENSO has been shown to largely affect rainfall patterns at both global and regional scales (Dai and Wigley, 2000; Ropelewski and Halpert, 1987).

The main goal of this study is to quantify the likelihood of simultaneous or time-delayed occurrences of localized seasonal precipitation extremes along with an ENSO phase of a given type. For this purpose, we employ *event coincidence analysis* (ECA) (Donges et al, 2011, 2016) for estimating the probability of co-occurrences between such events. This framework has already been successfully applied to quantifying the likelihood of climatic extreme events triggering certain ecological or social responses, such as extreme annual (Rammig et al, 2015) and daily (Siegmund et al, 2016a) tree growth or flowering dates (Siegmund et al, 2016b) as well as the outbreak of epidemics (Donges et al, 2016) or armed conflicts (Schleussner et al, 2016). Acknowledging the already observed differential impacts of EP and CP El Niños, we aim here to further characterize specific extreme impacts of the two flavors of both, El Niño and La Niña.

Several schemes to distinguish EP from CP events have been proposed in the recent past. One prominent example is the *ENSO Modoki Index* that is computed as the weighted average sea surface temperature in the equatorial Pacific (Ashok et al, 2007). Other studies used empirical orthogonal functions (Graf and Zanchettin, 2012; Kao and Yu, 2009) or combinations of the Nino3 and Nino4 indices (Kim et al, 2011; Hu et al, 2011) to provide the desired discriminations. In contrast to statistics related solely to the dynamics within the equatorial Pacific, Wiedermann et al (2016) recently introduced an index to discriminate different ENSO flavors based on the assessment of global teleconnections in surface air temperature. This index shows a more distinct and sharp discrimination as compared to previously proposed measures based on average temperature observations (Ashok et al, 2007). This particular property is important for our present analysis as ECA relies on the assessment of event sequences, which are easily computed for a spike-like signal in contrast to a smoothly varying one.

We use the index proposed by Wiedermann et al (2016) together with the classical Oceanic Nino Index (ONI) (provided by the Climate Prediction Center of the National Oceanic and Atmospheric Administration, NOAA-CPC) to construct four event series representing EP and CP El Niño and La Niña phases. We then utilize ECA to quantify simultaneous occurrences of either of the four ENSO types with spatially resolved seasonal precipitation extremes (wet and dry) in boreal fall and winter of the same year as the start of a certain ENSO episode, and spring of the following year. The data and methods applied in this work are presented in Sec. 2. Section 3 shows the results of our analysis. We start by evaluating the effects of the canonical El Niño on extreme precipitation and demonstrate the validity of our approach by comparing the obtained spatial patterns with recent studies. We then focus on CP El Niños and highlight differences with their EP counterparts. Ultimately, we study La Niña periods and show that most extreme rainfall responses are attributed to the EP type of ENSO's negative phase. We thus conclude that in the light of recent discussions on the existence of two types of La Niña (Kug and Ham, 2011) it is meaningful to distinguish one type that significantly affects global precipitation signals and one that shows hardly any spatially coherent impact. Wherever appropriate, we also discuss possible socio-ecological consequences of the observed seasonal precipitation extremes. Finally, Sec. 4 provides the conclusions of this work as well as suggestions for future research.

2 Data & Methods

2.1 GPCC rainfall data

We utilize gridded monthly precipitation data provided by the Global Precipitation Climatology Centre (GPCC) at a spatial resolution of $2.5° \times 2.5°$ (Schneider et al, 2015). Since reliable estimations of El Niño and La Niña periods according to the ONI as well as a discrimination into their respective EP and CP flavors are only available for the second half of the 20th century so far, we restrict our analysis to the period from 1951 to 2015. Note that the density of stations from which the data

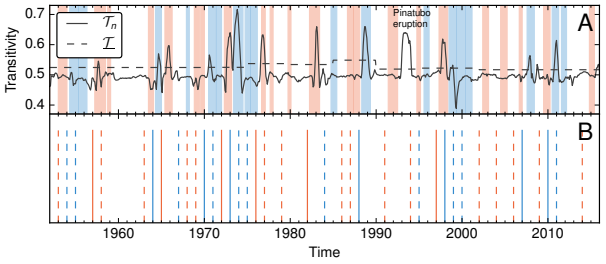

Fig. 1 (A) Network transitivity index indicating EP El Niños or La Niñas if its value exceeds the baseline (dashed line), and CP phases otherwise. Red and blue shaded areas indicate periods of El Niño and La Niña according to the ONI. (B) Corresponding series of EP (solid) and CP (dashed) El Niño (red) and La Niña (blue) events, respectively.

is derived varies between 0 and more than 100 per grid cell and for different years (Lorenz and Kunstmann, 2012), which generally results in a lower accuracy and reliability of the data for those areas with only few stations (Rudolf et al, 1994). We therefore consider only grid cells where the average number of stations between 1951 and 2010 is larger than 1, yielding a total number of $N = 2248$ cells. From the monthly time series, we derive separate records for three seasons s by aggregating the precipitation amounts of the corresponding three-month periods September to November (SON), December to February (DJF) and March to May (MAM). This results in three time series $P_{i,s}(t)$ per grid cell i with $M = 62$ annual values each.

2.2 Network transitivity index of ENSO flavor

Previous approaches to distinguish different flavors of El Niño (Hendon et al, 2009) like empirical orthogonal function (EOF) analysis (Graf and Zanchettin, 2012) or the ENSO Modoki Index (EMI) (Ashok et al, 2007) often yielded ambiguous or mutually inconsistent results (Wiedermann et al, 2016). Radebach et al (2013) were the first to observe that characteristics related to the global correlation structure of surface air temperatures expressed as a complex network can provide sharp discriminators between EP and CP El Niños. Inspired by this approach, Wiedermann et al (2016) recently developed an index based on climate network transitivity $\mathcal{T}$, a measure to quantify the degree of localization of ENSO's global teleconnections, displaying different spatial characteristics for EP and CP flavors of El Niño and La Niña.

The transitivity index is computed upon daily global surface air temperature anomalies (SATA) from the NCEP/NCAR reanalysis (Kistler et al, 2001) used to construct a sequence of 365-days long running-window cross-correlation matrices $\mathbf{C}_n = (C_{n,ij})$ between all pairs of time series in the data set. The most relevant information captured by C_n is contained in the 0.5% of strongest absolute correlations for each window n and expressed using thresholds T_n such that

$$W_{n,ij} = |C_{n,ij}| \cdot \Theta(|C_{n,ij}| - T_n), \tag{1}$$

with $\Theta(\cdot)$ denoting the Heaviside function. One major characteristic of the resulting matrix W_n is the transitivity index

$$\mathcal{T}_n = \frac{\sum_{i,j,k} w_i W_{n,ij} w_j W_{n,jk} w_k W_{n,ki}}{\sum_{i,j,k} w_i W_{n,ij} w_j W_{n,jk} w_k} \in [0,1] \tag{2}$$

with

$$w_i = \cos(\lambda_i). \tag{3}$$

Here, λ_i denotes the latitudinal position of each time series' corresponding grid point on the Earth's surface (Heitzig et al, 2012; Tsonis et al, 2006). A comprehensive description of the above framework is given in Wiedermann et al (2016).

Figure 1A shows the temporal evolution of the transitivity index. In contrast to the EMI, it provides a sharp and distinct discrimination between the two El Niño flavors (and also two corresponding types of La Niña phases), such that a peak in the index indicates an EP type while its absence points to a CP event. A corresponding baseline $\underline{\mathcal{T}}$ (dashed horizontal line in Fig. 1A) above which values of $\mathcal{T}$ are considered a peak is given as well. It is derived as the transitivity computed over the same 30-year periods that are used to determine the base periods for the computation of sea surface temperature anomalies in the definition of the ONI.

2.3 Data preprocessing

We define years with seasons s (DJF, SON, or MAM, see Sec. 2.1) exhibiting extraordinary high or low precipitation amounts from the corresponding time series $P_{s,i}(t)$ for each grid cell i, individually. Specifically, we consider values above (below) the 80th (20th) percentile $p^+_{s,i}$ ($p^-_{s,i}$) in each of the time series $P_{s,i}(t)$ as extraordinary high (low) seasonal precipitation sums. We choose these particular thresholds to ensure the presence of a sufficient number of particularly dry and wet seasons that is comparable with the number of different ENSO phases in the considered time period. It has been checked that the results obtained in the following do not change qualitatively if more restrictive thresholds are applied (not shown).

According to these considerations, we obtain six binary time series $P^{\pm}_{s,i}(t)$ per grid cell,

$$P^{\pm}_{s,i}(t) = \Theta(\pm P_{s,i}(t) \mp p^{\pm}_{s,i}), \tag{4}$$

where $P^{\pm}_{s,i}(t) = 1$ indicates the presence of a seasonal precipitation extreme at grid cell i during season s in year t. By following the above procedure, no further deseasonalisation of the precipitation data is necessary, since the grid cell-specific seasonality of precipitation is already taken into account. Furthermore, the events are defined for each location independent from the others and therefore spatial heterogeneity is taken into account as well.

In addition to the precipitation data set, we create similar binary indicator time series for the different ENSO phases (Fig. 1B), e.g. an EP El Niño series $X_{EPEN}(t)$ with $X_{EPEN} = 1$ if t marks the onset year of an El Niño period (as defined by the ONI) and $\mathcal{T}_n$ exceeds $\underline{\mathcal{T}}$ for at least one month of that considered period. All remaining El Niño periods are classified as CP events, yielding a corresponding event series $X_{CPEN}(t)$ (solid and dashed red lines in Fig. 1B). The same procedure is applied to La Niña periods, yielding event series $X_{EPLN}(t)$ and $X_{CPLN}(t)$, respectively (blue lines in Fig. 1B).

2.4 Event Coincidence Analysis

We apply event coincidence analysis (ECA), a statistical tool to quantify simultaneities between events in two series (Donges et al, 2011; Rammig et al, 2015; Donges et al, 2016). It computes for each grid cell the fraction of EP (CP) El Niño (La Niña) phases that coincide with extreme precipitation sums in SON or DJF of the same year or MAM of the following year, revealing if the timing of precipitation extremes is non-randomly related to the presence of a given type of ENSO phase. Specifically, the event coincidence rate $ECR^{\pm}_{s,i,\bullet}$ for one pair of ENSO and precipitation event series is given by

$$ECR^{\pm}_{s,i,\bullet} = \frac{\sum_t X_\bullet(t) P \pm_{s,i} (t-\tau)}{\sum_t X_\bullet(t)}. \quad (5)$$

Here, $X_\bullet(t)$ represents one of the four time series indicating EP and CP types of El Niño and La Niña. The offset τ reads $\tau = 0$ for SON and DJF and $\tau = 1$ for MAM.

To assess the statistical significance of the obtained event coincidence rates, we assume both involved event sequences to be distributed randomly, independently and uniformly (Donges et al, 2011; Rammig et al, 2015; Siegmund et al, 2016b,a). A corresponding p-value is estimated analytically from the (binomial) probability distribution of event coincidence rates that would occur by chance only. We consider an empirical event coincidence rate as statistically significant if its p-value is smaller than a confidence level of $\alpha = 0.05$ (for mathematical details, see Donges et al (2016)).

3 Results & Discussion

3.1 Seasonal precipitation extremes and EP El Niño

We first investigate event coincidences rates between EP El Niños and the timing of seasonal precipitation extremes. Figures 2A,C,E show locations with significant coincidence rates $ECR^{\pm}_{\bullet,i,ENEP}$ between EP El Niños and extremely dry (red squares) and wet periods (blue squares) in SON, DJF and MAM, respectively.

During SON of EP El Niño years, we find an elevated probability of extremely dry conditions over Indonesia, the Philippines and the southwestern Pacific islands as well as over northern South America and the northern Amazon Basin (Fig. 2A). The latter dry events have been linked to an increased risk of biomass loss in the Amazon which would otherwise serve as a long term carbon sink (Phillips et al, 2009).

For the same season, we also observe an increased likelihood of very wet conditions over the central Pacific islands and the west coast of North America (Fig. 2A). Similarly, wet conditions are found over Ecuador and the South American east coast in SON and DJF (Fig. 2A,B). We further find extremely wet conditions over parts of the Chilean Andes in SON (Fig. 2A) which may result in an increased risk for the occurence of floods in this area (Bookhagen and Strecker, 2012; Boers et al, 2014). All these observations agree well with previous climatological studies (e.g. Diaz et al, 2001). Coinciding with EP El Niños, we also observe more frequent wet extremes over the Mediterranean region (Fig. 2A) in SON, which was partially also reported earlier by Shaman and Tziperman (2010). Furthermore, the wet conditions over East Africa during the same season (Fig. 2A) have previously been described in parts by Camberlin et al (2001). The observed dry conditions in southwestern Africa during DJF (Fig. 2C) were also reported recently by Hoell et al (2014). Finally, we observe significant coincidences between EP El Niños and extremely wet conditions over the Western Caribbean (especially Haiti), which may pose an increased risk for tropical disease outbreaks associated with extreme precipitation (Herrador et al, 2015).

Generally, our ECA results are in good agreement with previously reported interrelations between El Niño and global precipitation, which have mostly been identified using linear correlation analysis. Thus, we conclude that (i) the application of ECA to assess ENSO-related extreme impacts provides valid results, and that (ii) extreme responses to the canonical El Niño display roughly similar spatial patterns as the average statistical interdependency between ENSO-related indices and climatic observables. However, we note that most pre-

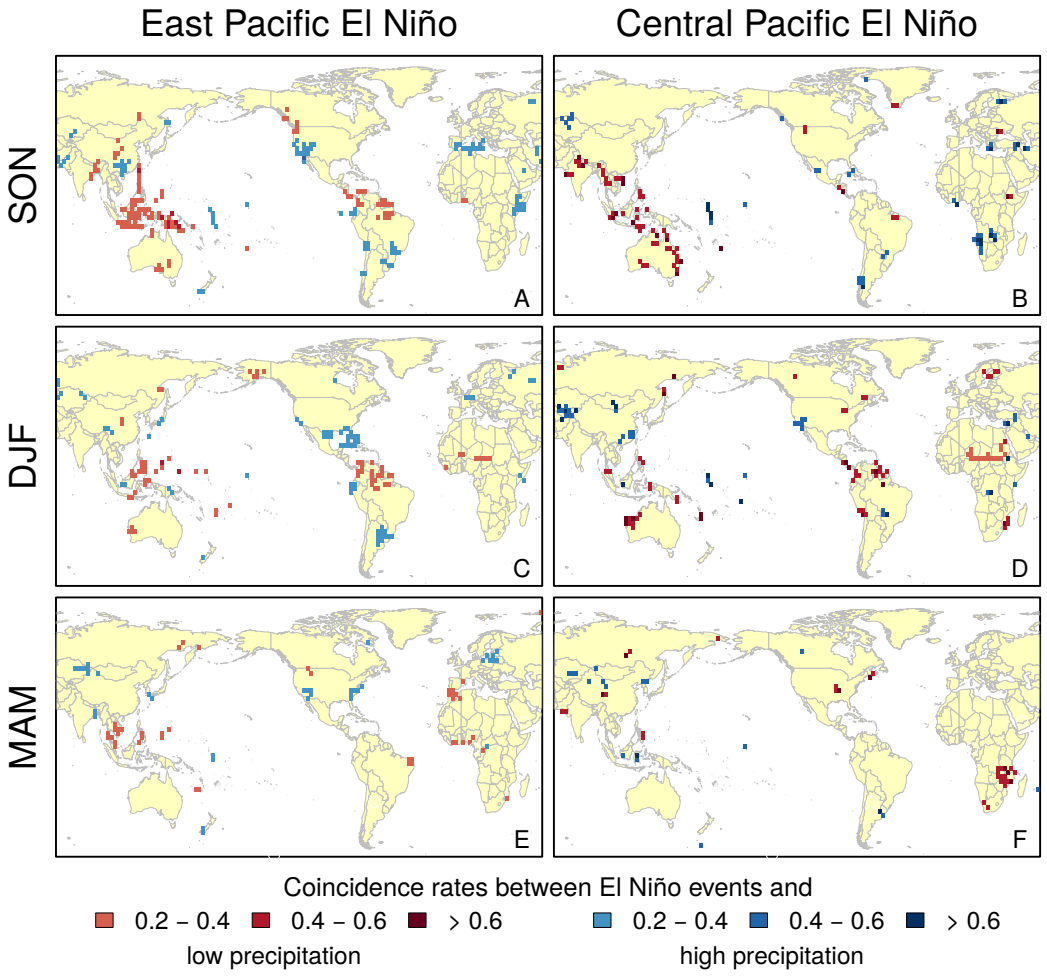

Fig. 2 Statistically significant event coincidence rates between years of EP (left column) and CP (right column) El Niños and very dry or very wet seasons (SON, DJF, MAM). Red (blue) squares represent grid cells with significant event coincidence rates between EP or CP El Niño years and seasonal precipitation sums below (above) the 20th (80th) percentile of all years from 1951 to 2015.

vious studies have not discriminated between the two El Niño flavors. Thus, the agreement between our results for EP El Niños and the recent literature suggests that the previously observed linear effects might just be dominated by the (on average stronger) EP events.

3.2 Seasonal precipitation extremes and CP El Niño

Next, we focus on the specific effects of the less intensively studied CP El Niño and estimate event coincidence rates between these phases and seasons with extreme precipitation sums (Fig. 2B,D,E). We first discuss those regions that display significant coincidence rates for EP El Niños (see Sec. 3.1) but an absence or altered likelihood of seasonal precipitation extremes during CP periods. Notably, the dry events over Central America and the Amazon that frequently occur together with EP El Niños become more likely during DJF (Fig. 2D) but show insignificant coincidence rates in SON (Fig,. 2B). The latter also holds for the wet events along the western coast of Central and North America that have been observed for EP El Niños. In the same manner, the wet SON patterns over Southern China, the Mediterranean, and South-East Africa coinciding with EP El Niños disappear during CP events (Fig,. 2B). We further note, that the large-scale dry events over Indonesia observed along with EP events during SON become less spatially coherent for CP El Niños (Fig. 2B). For MAM, the wet and dry patterns over Europe become insignificant (Fig. 2F). Ultimately, we find that the dry pattern in DJF over the central Sahel in Africa observed in coincidence with EP El Niños increases in its spatial extent (Fig. 2B,D) and is likely to decrease agricultural production (Epule et al, 2014).

While the above observations indicate decreased or weakened impacts of CP El Niños in comparison with the EP type, we also observe the emergence of new

patterns that are not present during EP El Niños but emerge only along with CP phases. Specifically, dry events become more likely along Australia's east coast during SON (Fig. 2B). Such events could thus trigger severe impacts on river ecosystems and agriculture in the area. In particular, dry events in Eastern Australia are likely to cause a cascade of low river inflows, i.e., water scarcity and large scale floodplain forest mortality as well as an increase of toxicity in the surrounding lakes (Leblanc et al, 2012). These natural hazards in turn have large-scale effects on agricultural production in terms of a severe reduction in irrigated crop yields of up to 99% (van Dijk et al, 2013).

In addition to reduced rainfall responses, significant coincidence rates with wet events arise over the south of Chile pointing towards increased rainfall during CP El Niños as compared to their canonical counterparts. In DJF months coinciding with CP events, we observe the emergence of new wet patterns over Central Asia and China as well as a dry pattern over the north of Chile (Fig. 2D). Ultimately, for MAM we observe a pronounced dry pattern over Southeast Africa (Fig. 2F). Generally, we note a decrease in the spatial coherence of seasonal precipitation extremes coinciding with CP El Niños in comparison with EP phases.

3.3 Seasonal precipitation extremes and EP/CP La Niña

We finally perform the same analysis for La Niña periods. For the EP, i.e. canonical, La Niña type (Fig. 3A,C,E) we again find various patterns that were reported in earlier studies. Specifically, during SON coinciding with EP La Niña phases (Fig. 3A) we find the expected wet conditions over Australia and Indonesia (Arblaster et al, 2002) and exceptionally dry conditions in parts of southern Europe (Pozo-Vázquez et al, 2005) and the south of Brazil (Ropelewski and Halpert, 1996). We further observe significant coincidence rates with dry events in the middle East and with extreme rainfall over central Europe. For DJF, our analysis confirms findings by Nicholson and Selato (2000) of wet conditions over South Africa and dry events over West Africa (Fig. 3C), where specifically the latter may cause agricultural losses (Karpouzoglou and Barron, 2014) as well as impose increased health risks (Rataj et al, 2016). We further observe a prominent extreme precipitation dipole with dry conditions over Mexico and increased precipitation in the southwestern part of Canada. The latter has become an important aspect of local water resource management (Lute and Abatzoglou, 2014) but along with other parameters like wind and temperature also poses the threat of landslides in coastal areas (Guthrie et al, 2010).

For MAM seasons associated with EP La Niñas, we observe a tendency towards extreme rainfall over Amazonia (Rogers, 1988) and parts of Northern Australia (Arblaster et al, 2002) (Fig. 3). We further find pronounced significant coincidences between EP La Niñas and very dry conditions in MAM over the Caribbean which may negatively impact rainfed agriculture in the corresponding area (Aladenola et al, 2016).

In contrast to the coherent patterns observed for EP La Niña phases, we find only a few spatially organized structures along with CP events (Fig. 3B, E, F). Most prominently, we recover previously reported wet conditions over parts of Australia in DJF (Arblaster et al, 2002; Cai and Cowan, 2009) (Fig. 3B). Additionally, we uncover strongly reduced rainfall over Florida in DJF, and over Scandinavia and the south of Russia in MAM. Thus, similar as for El Niño, we again observe that CP La Niñas coincide with less spatially coherent extreme precipitation responses.

Following upon the presented findings, we pick up the recently raised question whether it is actually meaningful to distinguish La Niña into two flavors in the same fashion as El Niño (Kug and Ham, 2011). While Kao and Yu (2009) and Ashok and Yamagata (2009) advocated for such a distinction, Kug et al (2009) and Ren and Jin (2011) argued that based on correlation analyses between La Niña related SST patterns no distinct discrimination into two types is evident. Contributing to this discussion, Wiedermann et al (2016) demonstrated that according to the transitivity index characterizing ENSO teleconnectivity it is indeed meaningful to provide a discrimination of La Niño periods analogous to El Niño. The results of our current work demonstrate that seasonal precipitation extremes accompanied by EP La Niñas are generally more likely to arise in a spatially coherent way (Fig. 3) than such observed along with CP phases. The same property also holds for El Niño periods (Sec. 3.2), which highlights again a symmetry not only within the spatial patterns of El Niño and La Niña themselves, but also with respect to their induced extreme precipitation responses. Thus, from an impact-oriented point of view, our work provides further evidence in favor of a distinction between two types of La Niña indicated by the presence or absence of induced seasonal precipitation extremes. In other words, from the viewpoint of extreme events (and thus possibly in contrast to observations based on linear statistical analysis) it seems reasonable to discriminate La Niña into two types in the same way as for El Niño periods.

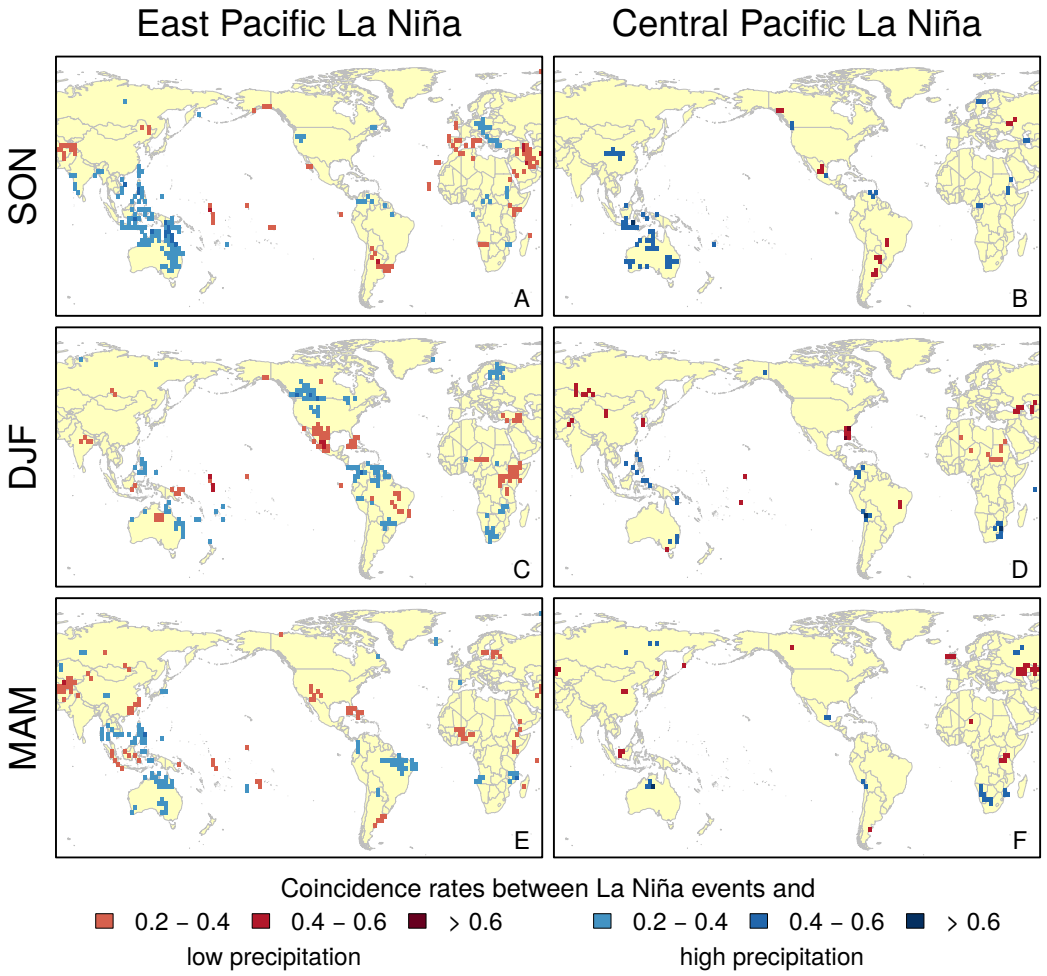

Fig. 3 Same as Fig. 2 for La Niña periods.

4 Conclusion & Outlook

We have carried out a detailed analysis of ENSO imprints in global patterns of seasonal precipitation extremes. Specifically, we discriminated both, El Niño and La Niña into two distinct types (East Pacific and Central Pacific) by utilizing the network transitivity index $\mathcal{T}$ introduced by Wiedermann et al (2016). From $\mathcal{T}$, four distinct event series were defined such that an event in each series corresponds to the presence of the respective type of ENSO event. The globally gridded GPCC rainfall data set was aggregated to grid point-wise seasonal precipitation sums, and corresponding event series were obtained by applying the 80th (20th) percentile to define extremely wet (dry) periods.

We then used event coincidence analysis (Siegmund et al, 2016a; Donges et al, 2016) to identify grid points with significant coincidence rates between different types of ENSO phases and seasonal precipitation extremes. Our analysis confirmed that previously observed interrelationships based on linear correlation or composite analysis also apply to the associated extremes. In addition, we identified further impacts of ENSO episodes, especially of the Central Pacific types of both, El Niño and La Niña, which have to our best knowledge not been described so far. This implies that in these cases, standard analysis methods may not be sufficienct to capture such interrelations. Moreover, it shows that even though a general linear relationship between ENSO and precipitation might be weak or absent for a given region, dry periods or heavy rainfall can still be possible effects of specific types of ENSO phases. At the same time we observe that most previously observed interrelations only hold for events corresponding to East Pacific ENSO flavors. This implies that with a proper discrimination of event types, threats like possible droughts or flooding as well as their socio-ecological consequences could be better anticipated, since for most regions of the Earth, CP types of ENSO events have no or a less

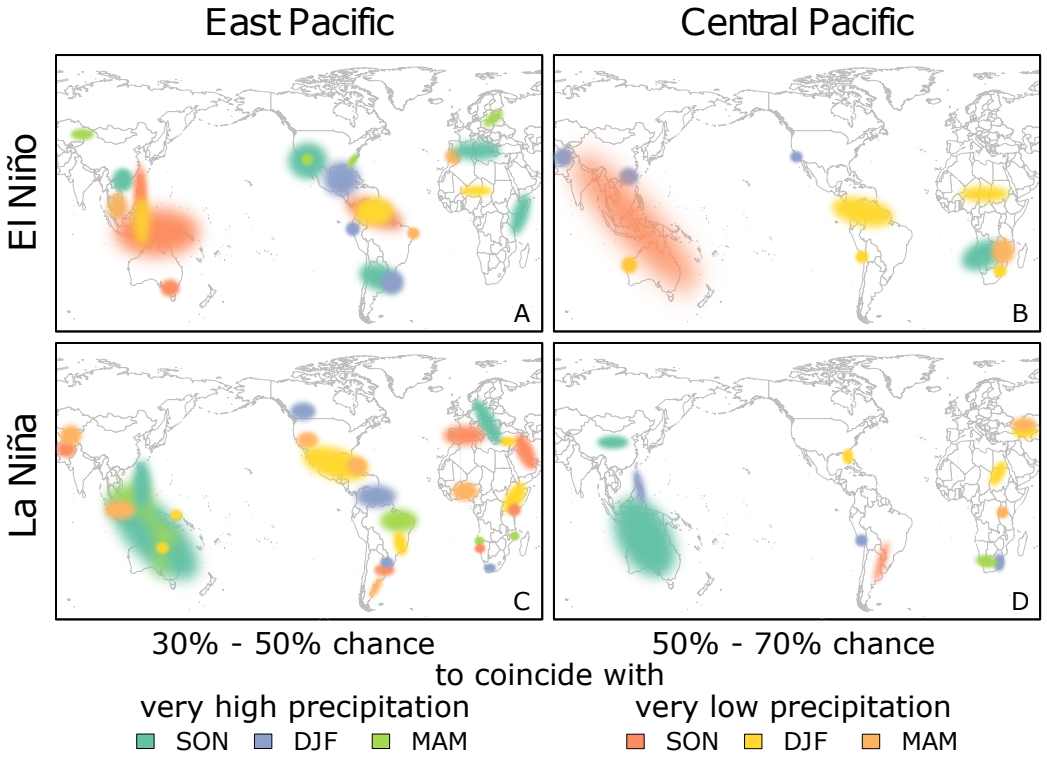

Fig. 4 Schematic summary of the results of this work. Shaded areas indicate geographic locations for which extreme (high or low) seasonal precipitation sums exhibit significant coincidence rates with EP (A,C) or CP (B,D) El Niño (A,B) or La Niña phases (C,D). For all indicated areas related to EP (CP) phases, seasonal precipitation extremes occur with a probability of 30-50% (50-70%), respectively.

spatially organized impact on seasonal precipitation extremes.

Our analysis contributed to the ongoing discourse whether or not it is (statistically and climatologically) meaningful to discriminate La Niña into two flavors in the same way as done for El Niño. The obtained results suggest that such congruence between ENSO's positive and negative phase is meaningful in both ways as (i) the transitivity index clearly distinguishes between two types of events for El Niño as well as La Niña and (ii) event coincidence analysis shows that the EP La Niña displays more spatially coherent seasonal precipitation extremes, while fewer impacts are found for its Central Pacific counterpart.

In conclusion, our analysis provided a detailed and global overview on the large-scale imprints of different ENSO phases and flavors in extreme seasonal precipitation patterns. All findings are ultimately summarized in Fig. 4, which displays schematically all regions for which the four different types of ENSO phases show significant coincidence rates with seasonal precipitation extremes together with the approximate values of these.

Future work shall apply the concepts used in this work to also study ENSO related extreme impacts on further climatic observables, such as temperature. Further, our framework could be applied to directly relate ENSO and its distinct phases more thoroughly to climate impacts, such as those on agricultural yields or water availability. Also, an intercomparison between results obtained from linear and event statistics could prove useful in assessing which regions are most affected in terms of extreme climatic responses to the presence of either type and phase of ENSO. Ultimately, it could be useful to apply the presented framework also to future climate projections in order to assess possible changes in the spatial extent and frequency of ENSO related extreme events.

Acknowledgements MW, JFS and RVD acknowledge funding by the German Federal Ministry for Education and Research (BMBF) via the Young Investigators Group CoSy-CC^2 (grant no. 01LN1306A). JFD thanks the Stordalen Foundation and the Leibniz Society (project DOMINOES) for financial support. JK and RVD acknowledge the IRTG 1740 funded by DFG and FAPESP. JFS has been supported by the Evangelisches Studienwerk Villigst e.V. The authors gratefully acknowledge the European Regional Development Fund (ERDF), the German Federal Ministry of Education and Research and the Land Brandenburg for supporting this project by providing resources on the high performance computer system at the Potsdam Institute for Climate Impact Research.

All computations have been performed using the R package `CoinCalc` (Siegmund et al, 2017).

References

Aladenola O, Cashman A, Brown D (2016) Impact of El Niño and Climate Change on Rainwater Harvesting in a Caribbean State. Water Resourc Manag 30(10):3459–3473, DOI 10.1007/s11269-016-1362-2

Allan RP, Soden BJ (2008) Atmospheric Warming and the Amplification of Precipitation Extremes. Science 321(5895):1481–1484, DOI 10.1126/science.1160787

Arblaster J, Meehl G, Moore A (2002) Interdecadal modulation of Australian rainfall. Clim Dynam 18(6):519–531, DOI 10.1007/s00382-001-0191-y

Ashok K, Yamagata T (2009) Climate change: The El Niño with a difference. Nature 461(7263):481–484, DOI 10.1038/461481a

Ashok K, Behera SK, Rao SA, Weng H, Yamagata T (2007) El Niño Modoki and its possible teleconnection. J Geophys Res 112(C11):C11,007, DOI 10.1029/2006JC003798

Boers N, Bookhagen B, Barbosa H, Marwan N, Kurths J, Marengo J (2014) Prediction of extreme floods in the eastern central andes based on a complex networks approach. Nat Commun 5(5199)

Bookhagen B, Strecker MR (2012) Spatiotemporal trends in erosion rates across a pronounced rainfall gradient: Examples from the southern central andes. Earth Planet Sc Lett 327:97–110

Cai W, Cowan T (2009) La Niña Modoki impacts Australia autumn rainfall variability. Geophys Res Lett 36(12):L12,805, DOI 10.1029/2009GL037885

Cai W, Borlace S, Lengaigne M, van Rensch P, Collins M, Vecchi G, Timmermann A, Santoso A, McPhaden MJ, Wu L, England MH, Wang G, Guilyardi E, Jin FF (2014) Increasing frequency of extreme El Niño events due to greenhouse warming. Nature Clim Change 4(2):111–116, DOI 10.1038/nclimate2100

Camberlin P, Janicot S, Poccard I (2001) Seasonality and atmospheric dynamics of the teleconnection between African rainfall and tropical sea-surface temperature: Atlantic vs. ENSO. Int J Climatol 21(8):973–1005, DOI 10.1002/joc.673

Chiew FHS, Piechota TC, Dracup JA, McMahon TA (1998) El Niño/Southern Oscillation and Australian rainfall, streamflow and drought: Links and potential for forecasting. J Hydrol 204(14):138–149, DOI 10.1016/S0022-1694(97)00121-2

Dai A, Wigley TML (2000) Global patterns of ENSO-induced precipitation. Geophys Res Lett 27(9):1283–1286, DOI 10.1029/1999GL011140

Diaz HF, Hoerling MP, Eischeid JK (2001) ENSO variability, teleconnections and climate change. Int J Climatol 21(15):1845–1862, DOI 10.1002/joc.631

van Dijk AIJM, Beck HE, Crosbie RS, de Jeu RAM, Liu YY, Podger GM, Timbal B, Viney NR (2013) The millennium drought in southeast australia (20012009): Natural and human causes and implications for water resources, ecosystems, economy, and society. Water Resour Res 49(2):1040–1057, DOI 10.1002/wrcr.20123

Donges JF, Donner RV, Trauth MH, Marwan N, Schellnhuber HJ, Kurths J (2011) Nonlinear detection of paleoclimate-variability transitions possibly related to human evolution. Proc Natl Acad Sci 108(51):20,422–20,427, DOI 10.1073/pnas.1117052108

Donges JF, Schleussner CF, Siegmund JF, Donner RV (2016) Event coincidence analysis for quantifying statistical interrelationships between event time series: on the role of flood events as triggers of epidemic outbreaks. Eur Phys J ST 225(3):471–487, DOI 10.1140/epjst/e2015-50233-y

Easterling DR, Evans J, Groisman PY, Karl T, et al (2000) Observed variability and trends in extreme climate events: a brief review. Bull Amer Meteor Soc 81(3):417

Epule ET, Peng C, Lepage L, Chen Z (2014) The causes, effects and challenges of Sahelian droughts: a critical review. Reg Environ Chang 14(1, SI):145–156, DOI 10.1007/s10113-013-0473-z

Graf HF, Zanchettin D (2012) Central Pacific El Niño, the subtropical bridge, and Eurasian climate. J Geophys Res 117(D1), DOI 10.1029/2011JD016493

Guthrie RH, Mitchell SJ, Lanquaye-Opoku N, Evans SG (2010) Extreme weather and landslide initiation in coastal British Columbia. Q J Eng Geol Hydrogeol 43(4):417–428, DOI 10.1144/1470-9236/08-119

Heitzig J, Donges JF, Zou Y, Marwan N, Kurths J (2012) Node-weighted measures for complex networks with spatially embedded, sampled, or differently sized nodes. Eur Phys J B 85(1):1–22, DOI 10.1140/epjb/e2011-20678-7

Hendon HH, Lim E, Wang G, Alves O, Hudson D (2009) Prospects for predicting two flavors of El Niño. Geophys Res Lett 36(19):L19,713, DOI 10.1029/2009GL040100

Herrador BRG, de Blasio BF, MacDonald E, Nichols G, Sudre B, Vold L, Semenza JC, Nygard K (2015) Analytical studies assessing the association between extreme precipitation or temperature and drinking water-related waterborne infections: a review. Environ Health 14, DOI 10.1186/s12940-015-0014-y

Hoell A, Funk C, Magadzire T, Zinke J, Husak G (2014) El Niño-Southern Oscillation diversity and Southern Africa teleconnections during Austral Summer. Clim Dynam 45(5-6):1583–1599, DOI 10.1007/s00382-014-2414-z

Hu ZZ, Kumar A, Jha B, Wang W, Huang B, Huang B (2011) An analysis of warm pool and cold tongue El Niños: air-sea coupling processes, global influences, and recent trends. Clim Dynam 38(9-10):2017–2035, DOI 10.1007/s00382-011-1224-9

Jones P, Trenberth K, Ambenje P, Bojariu R, Easterling D, Klein T, Parker D, Renwick J, Rusticucci M, Soden B, et al (2007) Observations: surface and atmospheric climate change. Climate change 2007: the physical science basis Contribution of Working Group I to the Fourth Assessment Report of the Intergovernmental Panel on Climate Change pp 235–336

Kao HY, Yu JY (2009) Contrasting Eastern-Pacific and Central-Pacific Types of ENSO. J Climate 22(3):615–632, DOI 10.1175/2008JCLI2309.1

Karl TR, Trenberth KE (2003) Modern global climate change. Science 302(5651):1719–1723

Karpouzoglou T, Barron J (2014) A global and regional perspective of rainwater harvesting in sub-Saharan Africa's rainfed farming. Phys Chem Earth 72-75:43–53, DOI 10.1016/j.pce.2014.09.009

Kim W, Yeh SW, Kim JH, Kug JS, Kwon M (2011) The unique 2009-2010 El Niño event: A fast phase transition of warm pool El Niño to La Niña. Geophys Res Lett 38(15):L15,809, DOI 10.1029/2011GL048521

Kistler R, Collins W, Saha S, White G, Woollen J, Kalnay E, Chelliah M, Ebisuzaki W, Kanamitsu M, Kousky V, van den Dool H, Jenne R, Fiorino M (2001) The NCEP-NCAR 50-Year Reanalysis: Monthly Means CD-ROM and Documentation. Bull Amer Meteor Soc 82(2):247–267, DOI 10.1175/1520-0477(2001)082¡0247:TNNYRM¿2.3.CO;2

Kug JS, Ham YG (2011) Are there two types of La Nina? Geophys Res Lett 38(16):L16,704, DOI 10.1029/2011GL048237

Kug JS, Jin FF, An SI (2009) Two Types of El Niño Events: Cold Tongue El Niño and Warm Pool El Niño. J Climate 22(6):1499–1515, DOI 10.1175/2008JCLI2624.1

Leblanc M, Tweed S, Van Dijk A, Timbal B (2012) A review of historic and future hydrological changes in the murray-darling basin. Glob Planet Chang 80:226–246

Lorenz C, Kunstmann H (2012) The hydrological cycle in three state-of-the-art reanalyses: Intercomparison and performance analysis. J Hydrometeorol 13(5):1397–1420, DOI 10.1175/JHM-D-11-088.1

Lute AC, Abatzoglou JT (2014) Role of extreme snowfall events in interannual variability of snowfall accumulation in the western United States. Water Resour Res 50(4):2874–2888, DOI 10.1002/2013WR014465

Neelin JD, Chou C, Su H (2003) Tropical drought regions in global warming and El Niño teleconnections. Geophys Res Lett 30(24):2275, DOI 10.1029/2003GL018625

Nicholson S, Selato J (2000) The influence of La Niña on African rainfall. Int J Climatol 20(14):1761–1776, DOI 10.1002/1097-0088(20001130)20:14¡1761::AID-JOC580¿3.0.CO;2-W

Phillips OL, Aragão LEOC, Lewis SL, Fisher JB, Lloyd J, López-González G, Malhi Y, Monteagudo A, Peacock J, Quesada CA, van der Heijden G, Almeida S, Amaral I, Arroyo L, Aymard G, Baker TR, Bánki O, Blanc L, Bonal D, Brando P, Chave J, de Oliveira ÁCA, Cardozo ND, Czimczik CI, Feldpausch TR, Freitas MA, Gloor E, Higuchi N, Jiménez E, Lloyd G, Meir P, Mendoza C, Morel A, Neill DA, Nepstad D, Patiño S, Peñuela MC, Prieto A, Ramírez F, Schwarz M, Silva J, Silveira M, Thomas AS, Steege Ht, Stropp J, Vásquez R, Zelazowski P, Dávila EA, Andelman S, Andrade A, Chao KJ, Erwin T, Di Fiore A, C EH, Keeling H, Killeen TJ, Laurance WF, Cruz AP, Pitman NCA, Vargas PN, Ramírez-Angulo H, Rudas A, Salamão R, Silva N, Terborgh J, Torres-Lezama A (2009) Drought sensitivity of the amazon rainforest. Science 323(5919):1344–1347, DOI 10.1126/science.1164033

Pozo-Vázquez D, Gámiz-Fortis SR, Tovar-Pescador J, Esteban-Parra MJ, Castro-Díez Y (2005) El Niño–Southern Oscillation events and associated European winter precipitation anomalies. Int J Climatol 25(1):17–31, DOI 10.1002/joc.1097

Radebach A, Donner RV, Runge J, Donges JF, Kurths J (2013) Disentangling different types of El Niño episodes by evolving climate network analysis. Phys Rev E 88(5):052,807, DOI 10.1103/PhysRevE.88.052807

Rammig A, Wiedermann M, Donges JF, Babst F, von Bloh W, Frank D, Thonicke K, Mahecha MD (2015) Coincidences of climate extremes and anomalous vegetation responses: comparing tree ring patterns to simulated productivity. Biogeosciences 12(2):373–385, DOI 10.5194/bg-12-373-2015

Rataj E, Kunzweiler K, Garthus-Niegel S (2016) Extreme weather events in developing countries and related injuries and mental health disorders-a systematic review. BMC public health 16(1):1020

Ren HL, Jin FF (2011) Niño indices for two types of ENSO. Geophys Res Lett 38(4):L04,704, DOI 10.1029/2010GL046031

Rogers JC (1988) Precipitation Variability over the Caribbean and Tropical Americas Associated with the Southern Oscillation. J Climate 1(2):172–182, DOI 10.1175/1520-0442(1988)001¡0172:PVOTCA¿2.0.CO;2

Ropelewski CF, Halpert MS (1987) Global and Regional Scale Precipitation Patterns Associated with the El Niño/Southern Oscillation. Mon Wea Rev 115(8):1606–1626, DOI 10.1175/1520-0493(1987)115¡1606:GARSPP¿2.0.CO;2

Ropelewski CF, Halpert MS (1996) Quantifying Southern Oscillation-Precipitation Relationships. J Climate 9(5):1043–1059, DOI 10.1175/1520-0442(1996)009¡1043:QSOPR¿2.0.CO;2

Rudolf B, Hauschild H, Rueth W, Schneider U (1994) Terrestrial Precipitation Analysis: Operational Method and Required Density of Point Measurements. In: Desbois M, Désalmand F (eds) Global Precipitations and Climate Change, no. 26 in NATO ASI Series, Springer Berlin Heidelberg, pp 173–186

Schleussner CF, Donges JF, Donner RV, Schellnhuber HJ (2016) Armed-conflict risks enhanced by climate-related disasters in ethnically fractionalized countries. P Natl Acad Sci 113(33):9216–9221, DOI 10.1073/pnas.1601611113

Schneider U, Becker A, Finger P, Meyer-Christoffer A, Rudolf B, Ziese M (2015) GPCC Full Data Reanalysis Version 7.0 (at 0.5°, 1.0°, 2.5°): Monthly Land-Surface Precipitation from Rain-Gauges built on GTS-based and Historic Data

Shaman J, Tziperman E (2010) An Atmospheric Teleconnection Linking ENSO and Southwestern European Precipitation. J Climate 24(1):124–139, DOI 10.1175/2010JCLI3590.1

Siegmund JF, Sanders TGM, Heinrich I, van der Maaten E, Simard S, Helle G, Donner RV (2016a) Meteorological Drivers of Extremes in Daily Stem Radius Variations of Beech, Oak, and Pine in Northeastern Germany: An Event Coincidence Analysis. Front Plant Sci 7

Siegmund JF, Wiedermann M, Donges J, Donner RV (2016b) Impact of temperature and precipitation extremes on the flowering dates of four German wildlife shrub species. Biogeosciences 13:5541–5555, DOI 10.5194/bg-13-5541-2016

Siegmund JF, Siegmund N, Donner RV (2017) CoinCalc - A new R package for quantifying simultaneities of event series. Comput and Geosci 98:64–72, DOI 10.1016/j.cageo.2016.10.004

Taschetto AS, England MH (2009) El Niño Modoki Impacts on Australian Rainfall. J Climate 22(11):3167–3174, DOI 10.1175/2008JCLI2589.1

Trenberth KE (1997) The Definition of El Niño. Bull Amer Meteor Soc 78(12):2771–2777, DOI 10.1175/1520-0477(1997)078¡2771:TDOENO¿2.0.CO;2

Tsonis AA, Swanson KL, Roebber PJ (2006) What Do Networks Have to Do with Climate? Bull Amer Meteor Soc 87(5):585–595, DOI 10.1175/BAMS-87-5-585

Wiedermann M, Radebach A, Donges JF, Kurths J, Donner RV (2016) A climate network-based index to discriminate different types of El Niño and La Niña. Geophys Res Lett 43(13):2016GL069,119, DOI 10.1002/2016GL069119

Chapter 3

Discussion

The central theme leading through the publications included into this manuscript is the statistical method of event coincidence analysis and how it can be used to analyze the impacts of extreme (or extraordinary) climate events on parts of terrestrial ecosystems. This new approach is a tool that enables researchers to statistically quantify simultaneities between events of two [e.g. *Siegmund et al.* (2016a)] or more [*Siegmund et al.* (2016b)] time series.

The novelty of this method in comparison to other event statistics like the 'spike train reliability statistic R' [*Hunter and Multon* (2003)] or 'event synchronization' [*Quiroga et al.* (2002)] is the distincty defined directionality (taking into account two possible different temporal orders of the events of interest) with significance tests being performed individually for both directions. Although this statistical framework is not capable to detect causal relationships, the output of ECA and especially of CECA can support the interpretation of possible directed causal interplays between events.

A further advantage of the method is the easy-to-understand concept. This is a very important and not to neglect characteristic of a statistical method, because the maybe most important part of a scientific study - the interpretation of the results - can only be of success if author *and* audience can understand the underlying methodology. Furthermore, a well accessable basic concept fosters the distribution of a method in the scientific community and, thus, supports new scientific contributions. For example, at the time of the writing of this manuscript, ECA and the `CoinCalc` package are already being used at numerous international research institutions like the *German Research Centre for Geoscience (GFZ)*, the *Commonwealth Scientific and Industrial Research Organisation*

(CSIRO), Australia, the *Second University of Naples, Italy*, the *Royal Museum for Central Africa, Belgium*, the *Universidad National de La Pampa, Argentina*, the *University of Texas at Austin* and others.

In difference to the application of ECA on time series with self-defined events like in e.g. *Donges et al.* (2016), *Schleussner et al.* (2016) or partly in *Wiedermann et al.* (2017), the results of ECA on continuous time series where the events have to be defined by thresholding [e.g. *Siegmund et al.* (2016a), *Siegmund et al.* (2016b), *Baumbach et al.* (2017)] can be assumed to be strongly dependent on the specific definition of this threshold. In *Siegmund et al.* (2016a) it was suggested to cope with this problem by performing the analysis with an ensemble of event time series with each member being created using slightly varied event thresholds. While small quantitative differences of the results must be expected in this case, the result can be accepted as robust if the entire ensemble shows results of the same quality and similar magnitude. In contrast, a dependency of ECA results on a specific threshold definition can also be used to systematically investigate critical thresholds. This could easily be achieved by iteratively rising or lowering a certain threshold. Such an explorative data analysis approach could be usable for a large variety of research questions in environmental sciences and other disciplines dealing with nonlinear systems.

The general research questions given in the *Introduction* part of this thesis have been answered by the entity of the contributing publications:

First, the definition of Event Coincidence Analysis [*Donges et al.* (2016)] and it's specifications the Conditional and Joint Event Coincidence Analysis [*Siegmund et al.* (2016b)] deliver quantitative measures of simultaneity for event time series that also allow for deduction of directionality. Second, it could be demonstrated that this new method is well capable to deliver new findings about the impact of extreme weather events on terrestrial ecosystems [*Siegmund et al.* (2016a), *Siegmund et al.* (2016b), *Siegmund et al.* (2017), *Baumbach et al.* (2017), *Wiedermann et al.* (2017)]. Third, in all of these publications some results (sometimes even oppositely) differed from previous findings based on linear correlation analysis and similar approaches.

The specific research questions given in the *Introduction* part of this thesis have comprehensively been investigated and discussed within the contributing publications:

In *Siegmund et al.* (2016a) and *Siegmund et al.* (2016b) it could be shown that the ECA is a very appropriate method to investigate the impact of extraordinary climatic conditions on individual plants. For the relationship between flowering times and temperature,

literature classically assumes a strong negative linear correlation [see e.g. *Ahas et al.* (2000), *Sparks et al.* (2000), *Menzel* (2003)] but so far it had not been shown that this interdependency is also true for the tails of the distribution. In *Siegmund et al.* (2016a) it could be demonstrated that on the one hand the negative relationship also holds for extreme events at many of the sites but on the other hand also many investigated sites do no exhibit significant coincidences for the tails of the distribution. Both findings are new in respect to so far published literature and could not have been obtained by the application of classical linear correlation analysis. Furthermore, we found that unusually warm conditions in autumn occur simultaneously with very early flowering in the following year. Hints to such long range inter-seasonal effects of temperature on flowering had already been given by *Sparks et al.* (2000), *Fitter et al.* (1995), *Luterbacher et al.* (2007) and *Crimmins et al.* (2010), but as a result of our data explorative approach one explicitly defined period in Autumn could be identified for each of the investigated species. Yet, a physiological explanation for this statistical finding is still missing.

In *Siegmund et al.* (2016b) it could be shown that the generally assumed positive correlation between tree diameter variation and temperature [see e.g. *Deslauriers et al.* (2003); *van der Maaten et al.* (2013)] can not be confirmed for the extraordinary warm and cold events on a daily time scale: very warm and very cold days even showed significant coincidence rates with negative and positive stem radius variation (SRV) events, respectively. This finding provides a very good example of how classically assumed relationships (commonly investigated using linear correlation analysis) are not necessarily valid for the entire range of data values and it illustrates how important it is to have a closer look.

Furthermore in the course of this high temporal resolution dendrometer analysis one specific weather situation could be identified where very humid air conditions did coincide with negative SRV events on a daily scale although the interplay between relative humidity and tree ring width is widely accepted to be characterized by clear positive correlations [see e.g. *Deslauriers et al.* (2003); *Koecher et al.* (2012); *van der Maaten et al.* (2013)]. It could be shown that the negative SRV events were not linked to the positive air humidity events, but to positive air temperature events on the same days. This example very well illustrates that deducing a causal relationship from significant coincidence rates is not possible because the analysis also detects non-causal simultaneities.

In *Siegmund et al.* (2016b) it could also be shown that the impact of extraordinary

weather conditions is strongly depending on the time of the year and may even be revers during the growing season. This is an important fact because it illustrates how difficult it is to assess the vulnerability of specific species in the course of ongoing climate change. In order to assess how a tree species might be able to cope with future climate extreme events very detailed knowledge about the temporal variability of the atmospheric avariables would be necessary. Additionally, by using coincidence rates as similarity measure for a hierarchical cluster analysis (an approach that has been suggested in *Siegmund et al.* (2016b) for the first time) it could be shown that the intra-species differences concerning the timing of SRV events on a daily scale are not systematically smaller than the inter-species differences, although clear inter-species differences have been shown on longer time scales [see e.g. *Garcia-Suarez et al.* (2009); *Gonzalez-Munoz et al.* (2014); *Levesque et al.* (2013)]. This finding again makes assessments of the species' susceptibility to more frequent climate extreme events a big challenge, at least when talking about extreme events on very short time scales.

In addition to the cluster analysis on a coincidence basis, in *Siegmund et al.* (2016b) the novel approach of conditioned and joint coincidence analysis (CECA) was presented. In combination with the distinction between trigger and precursor coincidence rate, CECA provides a strong tool to investigate statistical simultaneities in more detail. For example the detection of joint coincidences between positive air humidity events, positive SRV events and negative SRV events on one of the consecutive days delivered valuable new insights in the daily cycles of swelling and shrinkage of tree stems.

The analysis of *Baumbach et al.* (2017) revealed that the well known positive relationship between temperature and NDVI in spring and the negative relationship between both during summer [see e.g. *Hao et al.* (2012); *Stöckli and Vidale* (2004)] can for the tails of the distributions (very high/low temperature, very high/low NDVI) not be confirmed for entire Europe, but rather show very diverse and inhomogeneous patterns. It was shown that especially those regions are effected that are characterized by intensive anthropogenical shaping (e.g. croplands) while less regulated land cover classes like mixed forests are distinctly less effected. Although also other factors like harvesting could have influenced the analysis especially in late summer, the results emphasize the susceptibility of especially eastern European crop production to extreme temperature events and future challenges for argriculture in the course of ongoing climate change. The study also provided an example of how the novel approach of ECA can be used to quantify the impact of climate extremes on a large spacial scale without using the widely used

but somehow circuitous approach of comparing anomaly maps.

The extreme events of the El Niño southern oscillation (ENSO) can also be understood as local extreme (sea surface) temperature events. The impacts of these extreme climate events on the precipitation patterns on a global scale have been investigated in *Wiedermann et al.* (2017). By analyzing two different types ('flavors') of El Niño/La Niña events a comprehensive image of possible ENSO teleconnections could be drawn: besides confirming many individual previously found results that have been published in isolated regional studies, the analysis could also detect so far undocumented possible ENSO teleconnections in terms of significant coincidence rates between El Niño/La Niña events and extraordinary high or low precipitation amounts. Although not providing physical explanations for the found statistical interdependencies, the study revealed the power of the ECA on one of the most intensively investigated issues of climate research.

Chapter 4

Summary

In the course of the publications presented and discussed above it could be shown that the Event Coincidence Analysis (ECA) is a well appropriate tool to investigate the impacts of climate extreme events on different parts of the terrestrial ecosystem. With its quantitative and directed nature ECA enables users to draw statistically robust conclusions about simultaneities of events in two or more time series. The method provides a strong new tool that can reveal new information about the interplay between environmental variables especially when the relationship is not constant over all parts of the empirical distributions. In *Siegmund et al.* (2016a), *Siegmund et al.* (2016b) and *Baumbach et al.* (2017) has been shown that the application of ECA concerning the question of how climate extremes impact terrestrial ecosystems can refine already known relationships based on classical methods and also deliver substantial new findings to the scientific community. In addition *Wiedermann et al.* (2017) illustrated the application of ECA on the investigation of El Niño teleconnections - one of the most classical event time series in environmental sciences - and could (besides identifying new teleconnections) unify the various global ENSO precipitation teleconnections to a distinct El-Niño-event-impact-map. In addition, the manuscripts included in this thesis represented a travel across scales: the analyses presented investigations on impacts of climate extremes from local [*Siegmund et al.* (2016a)] over regional [*Siegmund et al.* (2016b)] over continental [*Baumbach et al.* (2017)] to global [*Wiedermann et al.* (2017)] spacial scale and from subdaily [*Siegmund et al.* (2016b)] over weekly and monthly [*Siegmund et al.* (2016a) and *Baumbach et al.* (2017)] to seasonal [*Wiedermann et al.* (2017)] temporal scale.
Finally, by publishing the R package `CoinCalc`, holding an implementation of the ECA,

this thesis not only provides new findings about the impacts of climate extreme events on terrestrial ecosystems, but also enables other researcher to further investigate on similar research questions by using Event Coincidence Analysis.

Bibliography

Ahas, R., J. Jaagus, and A. Aasa (2000), The phenological calendar of Estonia and its correlation with mean air temperature, *International Journal of Biometeorology*, *44*, 159–166, doi: 10.1007/s004840000069.

Anderson, M., C. Zolin, C. Hain, K. Semmens, M. Tugrul, and Y. Gao (2015), Comparison of satellite-derived LAI and precipitation anomalies over Brazil with a thermal infrared-based Evaporative Stress Index for 2003-2013 , *Journal of Hydrology*, doi: 10.1016/j.jhydrol.2015.01.005.

Arnone, J., R. Jasoni, A. Lucchesi, J. Larsen, E. Leger, R. Sherry, Y. Luo, D. Schimel, and P. Verburg (2011), A climatically extreme year has large impacts of on C 4 species in tallgrass prairie ecosystems but only minor effects on species richness and other plant functional groups, *Journal of Ecology*, *99*, 678–688., doi: 10.1111/j.1365-2745.2011.01813.x.

Baumbach, L., J. Siegmund, M. Mittermeier, and R. Donner (2017), Impacts of temperature extremes on european vegetation during the growing season, *Biogeosciences*, under Review.

Burkett, V. R., et al. (2005), Nonlinear dynamics in ecosystem response to climatic change: case studies and policy implications, *Ecological complexity*, *2*(4), 357–394, doi: 10.1016/j.ecocom.2005.04.010.

Burkle, L., J. Marlin, and T. Knight (2013), Plant-pollinator interactions over 120 years: Loss of species, co-occurrence, and function, *Science*, *339*, 1611–1615, doi: 10.1126/science.1232728.

Coumou, D., and S. Rahmstorf (2012), A decade of weather extremes, *Nature Climate Change*, *2*(7), 491–496.

Crabbe, R., J. Dash, V. Rodriguez-Galiano, D. Janous, M. Pavelka, and M. Mark (2016), Extreme warm temperatures alter forest phenology and productivity in Europe, *Science of the Total Environment*, *563-564*, 486–495, doi: 10.1016/j.scitotenv.2016.04.124.

Cramer, W., et al. (2001), Global response of terrestrial ecosystem structure and function to CO_2 and climate change: results from six dynamic global vegetation models, *Global Change Biology*, *7*, 357–373, doi: 10.1046/j.1365-2486.2001.00383.x.

Crimmins, T., M. Crimmins, and C. Bertelsen (2010), Complex responses to climate drivers in onset of spring flowering across a semi-arid elevation gradient, *Journal of Ecology*, *98*, 1042–1051, doi: 10.1111/j.1365-2745.2010.01696.x.

Deslauriers, A., H. Morin, C. Urbinati, and M. Carrer (2003), Daily weather response of balsam fir (Abies balsamea (L.) Mill.) stem radius increment from dendrometer analysis in the boreal forests of Quebec (Canada), *Trees*, *17*, 477–484, doi: 10.1007/s00468-003-0260-4.

Donges, J., C.-F. Schleussner, J. Siegmund, and R. Donner (2016), Event coincidence analysis for quantifying statistical interrelationships between event time series, *The European Physical Journal Special Topics*, *225*(3), 471–487.

Engels, A., O. Hüther, M. Schäfer, and H. Held (2013), Public climate-change skepticism, energy preferences and political, *Global Environmental Change*, *23*, doi: 10.1016/j.gloenvcha.2013.05.008.

Eurobarometer (2008), *Einstellungen der europischen Brger zum Klimawandel*, Europische Kommission.

Fitter, A., R. Fitter, I. Harris, and M. Williamson (1995), Relationships between first flowering date and temperature in the flora of a locality in central England, *Functional Ecology*, *9*, 55–60, doi: 10.2307/2390090.

Garcia-Suarez, A., C. Butler, and M. Baillie (2009), Climate signal in tree-ring chronologies in a temperate climate: A multi-species approach, *Dendrochronologia*, *27*, 183–198, doi: 10.1016/j.dendro.2009.05.003.

Gonzalez-Munoz, N., J. Linares, P. Castro-Diez, and U. Sass-Klaassen (2014), Predicting climate change impacts on native and invasive tree species using radial growth

and twenty-first century climate scenarios, *European Journal of Forest Research*, *133*, 1073–1086, doi: 10.1007/s10342-014-0823-5.

Hao, F., X. Zhang, W. Ouyang, A. K. Skidmore, and A. Toxopeus (2012), Vegetation NDVI linked to temperature and precipitation in the upper catchments of Yellow River, *Environmental Modeling & Assessment*, *17*(4), 389–398, doi: 10.1007/s10666-011-9297-8.

Haylock, M., and C. Goodess (2004), Interannual variability of european extreme winter rainfall and links with mean large-scale circulation, *International Journal of Climatology*, *24*(6), 759–776, doi: 10.1002/joc.1033/.

Heller, N., and E. Zavaleta (2009), Biodiversity management in the face of climate change: A review of 22 years of recommendations, *Biological Conservation*, *142*, 14–32, doi: 10.1016/j.biocon.2008.10.006.

Hoegh-Guldberg, O., and J. Bruno (2010), The Impact of Climate Change on the Worlds Marine Ecosystems, *Science*, *328*, 1523, doi: 10.1126/science.1189930.

Hunter, J., and J. Multon (2003), Amplitude and Frequency Dependence of Spike Timing:Implications for Dynamic Regulation, *Journal of Neurophysiology*, *90*, 387–394, doi: 10.1152/jn.00074.2003.

IPCC (2013), *Climate Change 2013: The Physical Science Basis. Contribution of Working Group I to the Fifth Assessment Report of the Intergovernmental Panel on Climate Change*, Cambridge University Press, Cambridge, United Kingdom and New York, NY, USA.

Jentsch, A., J. Kreyling, and C. Beierkuhnlein (2007), A new generation of climate change experiments: events not trends, *Frontiers in Ecology and Environment*, *5*(7), 315324, doi: 10.1890/1540-9295(2007)5[365:ANGOCE]2.0.CO;2.

Jentsch, A., J. Kreyling, J. Boettcher-Treschkow, and C. Beierkuhnlein (2009), Beyond gradual warming: extreme weather events alter flower phenology of European grassland and heath species, *Global Change Biology*, *15*, 837–849, doi: 10.1111/j.1365-2486.2008.01690.x.

Koecher, P., V. Horna, and C. Leuschner (2012), Environmental control of daily stem growth patterns in five temperate broad-leaved tree species, *Tree Physiology*, *32*, 1–12.

Kudo, G., and T. Ida (2013), Early onset of spring increases the phenological mismatch between plants and pollinators, *Ecology*, *94*, 2311–2320, doi: 10.1890/12-2003.1.

Kundzewicz, Z., M. Radziejewski, and I. Pinskwar (2006), Precipitation extremes in the changing climate of Europe, *Climate Research*, *31*(1), 51–58.

Kysely, J., L. Gaal, R. Beranova, and E. Plavcova (2011), Climate change scenarios of precipitation extremes in Central Europe from ENSEMBLES regional climate models, *Theoretical and Applied Climatology*, *104*, 529–542, doi: 10.1007/s00704-010-0362-z.

Law, B., C. Mackowski, L. Schoer, and T. Tweedie (2000), Flowering phenology of myrtaceous trees and their relation to climatic, environmental and disturbance variables in northern New South Wales, *Australian Ecology*, *25*, 160–178, doi: 10.1046/j.1442-9993.2000.01009.x.

Levesque, M., M. Saurer, R. Siegwolf, P. Eilmann, B. Brang, H. Bugmann, and A. Rigling (2013), Drought response of five conifer species under contrasting water availability suggests high vulnerability of Norway spruce and European larch, *Globale Change Biology*, *19*, 3184–3199, doi: 10.1111/gcb.12268.

Liu, G., H. Liu, and Y. Yim (2013), Global patterns of NDVI-indicated vegetation extremes and their sensitivity to climate extremes, *Environmental Research Letters*, *8*, 025,009, doi: 10.1088/1748-9326/8/2/025009.

Luterbacher, J., D. Dietrich, E. Xoplaki, M. Grosjean, and H. Wanner (2004), European seasonal and annual temperature variability, trends, and extremes since 1500, *Science*, *303*, 1409–1503, doi: 10.1126/science.1093877.

Luterbacher, J., M. Liniger, A. Menzel, N. Estrella, P. Della-Marta, C. Pfister, T. Rutishauser, and E. Xoplaki (2007), Exceptional European warmth of autumn 2006 and winter 2007: Historical context, the underlying dynamics, and its phenological impacts, *Geophysical Research Letters*, *34*, L12,704, doi: 10.1029/2007GL029951.

Ma, X., A. Huete, S. Moran, G. Ponce-Campos, and D. Eamus (2015), Abrupt shifts in phenology and vegetation productivity under climate extremes, *Journal of Geophysical Research: Biogeosciences*, *120*, 2036–2052, doi: 10.1002/2015JG003144.

Marchand, F., S. Mertens, F. Kockelbergh, L. Beyens, and I. Nijs (2005), Performance of High Arctic tundra plants improved during but deteriorated after exposure to a

simulated extreme temperature event, *Global Change Biology*, *11*, 2078–2089, doi: 10.1111/j.1365-2486.2005.01046.x.

Menzel, A. (2003), Plant phenological anomalies in Germany and their relation to air temperature and NAO, *Climatic Change*, *57*(3), 243–263, doi: 10.1023/A: 1022880418362.

Menzel, A., H. Seifert, and N. Estrella (2011), Effects of recent warm and cold spells on European plant phenology, *International Journal of Biometeorology*, *55*, 921–932, doi: 10.1007/s00484-011-0466-x.

Nagy, L., J. Kreyling, E. Gellesch, C. Beierkuhnlein, and A. Jentsch (2013), Recurring weather extremes alter the flowering phenology of two common temperate shrubs, *International Journal of Biometeorology*, *57*, 579–588, doi: 10.1007/s00484-012-0585-z.

Parmesan, C., T. Root, and M. Willig (2000), Impacts of Extreme Weather and Climate on Terrestrial Biota, *Bulletin of the American Meteorological Society*, *81*, 444–449, doi: 10.1175/1520-0477(2000).

Patz, J., D. Campbell-Lendrum, T. Holloway, and J. Foley (2005), Impact of regional climate change on human health, *Nature*, *438*, 310–317, doi: 10.1038/nature04188.

Quiroga, R., T. Kreuz, and P. Grassberger (2002), Event synchronization: a simple and fast method to measure synsynchronic and time delay patterns, *Physical Review E*, *041904*, doi: 10.1103/PhysRevE.66.041904.

Rafferty, N., P. CaraDonna, and J. Bronstein (2015), Phenological shifts and the fate of mutualisms, *Oikos*, *124*(1), 14–21, doi: 10.1111/oik.01523.

Rahmstorf, S., and D. Coumou (2011), Increase of extreme events in a warming world, *Proceedings of the National Academy of Sciences of the USA*, *108*(44), 17,905, doi: 10.1073/pnas.1101766108.

Rajczak, J., P. P., and C. Schar (2013), Projections of extreme precipitation events in regional climate simulations for Europe and the Alpine Region, *Journal of Geophysical Research - Atmospheres*, *118*, 3610–3626, doi: 10.1002/jgrd.50297.

Rammig, A., M. Wiedermann, J. Donges, F. Babst, W. von Bloh, D. Frank, K. Thonicke, and M. Mahecha (2015), Tree-ring responses to extreme climate events as benchmarks

for terrestrial dynamic vegetation models, *Biogeosciences*, *12*, 373–385, doi: 10.5194/bg-12-373-2015.

Rockström, J., et al. (2009), Planetary boundaries: exploring the safe operating space for humanity, *Ecology and Society*, *14*(32).

Rutishauser, T., J. Luterbacher, C. Defila, D. Frank, and H. Wanner (2008), Swiss spring plant phenology 2007: Extremes, a multi-century perspective, and changes in temperature sensitivity, *Geophysical Research Letters*, *35*, L05,703, doi: 10.1029/2007GL032545.

Schäfer, M. (2016), Climate change communication in germany, *Oxford Research Encyclopedia of Climate Science*, doi: 10.1093/acrefore/9780190228620.013.448.

Schleussner, C.-F., J. Donges, R. Donner, and H.-J. Schellnhuber (2016), Armed-conflict risks enhanced by climate-related disasters in ethnically fractionalized countries, *Proceedings of the National Academy of Sciences USA*, *113*(33), 9216–9221, doi: 10.1073/pnas.1601611113.

Siegmund, J., M. Wiedermann, J. Donges, and R. Donner (2016a), Impact of temperature and precipitation extremes on the flowering dates of four German wildlife shrub species, *Biogeosciences*, *13*, 55415555, doi: 10.5194/bg-13-5541-2016.

Siegmund, J., T. Sanders, I. Heinrich, E. van der Maaten, S. Simard, G. Helle, and R. Donner (2016b), Meteorological Drivers of Extremes in Daily Stem Radius Variations of Beech, Oak, and Pine in Northeastern Germany: An Event Coincidence Analysis, *Frontiers in Plant Sciences*, *7:733*, doi: 10.3389/fpls.2016.00733.

Siegmund, J. F., N. Siegmund, and R. V. Donner (2017), CoinCalc - A new R package for quantifying simultaneities of event series, *Computers and Geosciences*, *98*, 64–72, doi: 10.1016/j.cageo.2016.10.004.

Sparks, T., E. Jeffree, and C. Jeffree (2000), An examination on the relationship between flowering times and temperature at the national scale using long-term phenological records from the UK, *International Journal of Biometeorology*, *44*, 82–87.

Stöckli, R., and P. L. Vidale (2004), European plant phenology and climate as seen in a 20-year AVHRR land-surface parameter dataset, *International Journal of Remote Sensing*, *25*(17), 3303–3330, doi: 10.1080/01431160310001618149.

Tank, K., and G. Konnen (2003), Trends in indices of daily temperature and precipitation extremes in Europe, 1946-99, *Journal of Climate*, *16*, 3665–3680, doi: 10.1175/1520-0442(2003)016⟨3665:TIIODT⟩2.0.CO;2.

van der Maaten, E., O. Bouriaud, M. van der Maaten-Theunissen, H. Mayer, and H. Spieker (2013), Meteorological forcing of day-to-day stem radius variations of beech is highly synchronic on opposing aspects of a valley, *Agricultural and Forest Meteorology*, *181*, 85–93, doi: 10.1016/j.agrformet.2013.07.009.

Walther, G.-R., R. Post, P. Convey, A. Menzel, C. Parmesan, T. Beebee, J.-M. Fromentin, O. Hoegh-Guldberg, and F. Bairlein (2002), Ecological responses to recent climate change, *Nature*, *416*, 389–395, doi: 10.1038/416389a.

Wiedermann, M., J. Siegmund, J. Donges, and R. Donner (2017), Differential imprints of distinct enso flavors in global extreme precipitation patterns, *Climate Dynamics*, under Review.

Xu, X., S. Piao, X. Wang, A. Chen, P. Ciais, and R. Myneni (2012), Spatio-temporal patterns of the area experiencing negative vegetation growth anomalies in china over the last three decades, *Environmental Research Letters*, *7*, 035,701, doi: 10.1088/1748-9326/7/3/035701.

Zscheischler, J., M. Reichstein, S. Harmeling, A. Rammig, E. Tomelleri, and M. Mahecha (2014), Extreme events in gross primary production: a characterization across continents, *Biogeosciences*, *11*, 2909–2924, doi: 10.5194/bg-11-2909-2014.